Noonan and LEOPARD Syndrome in Zebrafish: Molecular Mechanisms and Cardiac Development

ISBN 978-94-6203-663-5

On the cover: a z-stack lightsheet microscopy image of a *Tg(H2B-eGFP)* embryo prior to bud stage expressing wild type Shp2. Courtesy of A.J. Hale

Printing: CPI Koninklijke Wöhrmann B.V. - Zutphen

To Eufrasia

Voor Vera

Noonan and LEOPARD Syndrome in Zebrafish: Molecular Mechanisms and Cardiac Development

Proefschrift

ter verkrijging van
de graad van Doctor aan de Universiteit Leiden,
op gezag van Rector Magnificus Prof.Mr. Carel J.J.M. Stolker
volgens besluit van het College voor Promoties
te verdedigen op woensdag 15 oktober 2014
klokke 10.00 uur

door
Monica Bonetti
geboren te Palizzi Marina (Italië) in 1984

en

klokke 11.15 uur

door

Jeroen Paardekooper Overman
geboren te Hoorn in 1984

Promotiecommissie Monica Bonetti

Promotor:

Prof. Dr. J. den Hertog - Hubrecht Institute, Utrecht

Overige leden:

Prof. Dr. C. J. ten Cate
Prof. Dr. H. P. Spaink
Prof. Dr. M. K. Richardson
Prof. Dr. C. L. Mummery
Prof. Dr. P. ten Dijke
Prof. Dr. M. J. T. H. Goumans
Prof. Dr. A. Elson - Weizmann Institute, Rehovot, Israël
Prof. Dr. A. Ostman - Karolinska Institute, Stockholm, Sweden

Promotiecommissie Jeroen Paardekooper Overman

Promotor:

Prof. Dr. J. den Hertog - Hubrecht Institute, Utrecht

Overige leden:

Prof. Dr. C. J. ten Cate
Prof. Dr. H. P. Spaink
Prof. Dr. M. K. Richardson
Prof. Dr. C. L. Mummery
Prof. Dr. P. ten Dijke
Prof. Dr. M. J. T. H. Goumans
Prof. Dr. A. Elson - Weizmann Institute, Rehovot, Israël
Prof. Dr. A. Ostman - Karolinska Institute, Stockholm, Sweden

Dit betreft een gezamenlijk onderzoek aan het Hubrecht Instituut voor Ontwikkelingsbiologie en Stamcelonderzoek, onderdeel van de Koninklijke Nederlandse Akademie van Wetenschappen (KNAW) waarvan het resultaat heeft geleid tot een gezamenlijk proefschrift.

Table of Contents

Introduction to signaling during early embryonic development

Monica Bonetti and Jeroen Paardekooper Overman

1 Zebrafish gastrulation

The perpetuation of animal life across uncountable generations is dependent on the remarkable fact that from a single cell, a complex organism is formed. How is it possible that from a single cell, then a lump of cells, finally all these dividing cells know where to go and what to do to form a new viable generation? According to Lewis Wolpert, "it is not birth, marriage or death but gastrulation which is truly the most important time in your life". Indeed, gastrulation, the process of cellular arrangements (epiboly, internalization, convergence and extension) after an initial stage of cell division following fertilization is a complex event that sets the stage for further developmentin all vertebrates. Embryonic development is highly predictable and can be studied more easily in some animal models than others. Compared to mammals which develop *in utero*, fish embryos are staged and imaged easily during development [1].

Primary cell divisions

Fish development starts with a large yolk syncytium with the oocyte sitting at the animal pole. After fertilization, the zygote starts to divide and initially forms a large lump of cells on top of the yolk known as the blastoderm. The blastoderm consists of three cell layers: mesenchymal deep cells that will give rise to the embryo *proper*. The deep cells are surrounded by a protective layer of epithelial enveloping layer cells (EVL). The most vegetal cells of blastoderm fuse with the yolk to form a multi-nucleated structure known as the yolk syncytial layer (YSL). The EVL acts as a protective layer for the deep cells, which are tightly attached to it. Likewise, the YSL is attached to the EVL. Initially, messenger RNA is maternally provided, yet after 2.5 hours post fertilization (hpf), zygotic transcription is initiated and maternal mRNA is cleared by miR-430 at 4hpf [2].

Epiboly

At sphere stage, or four hpf, a process called epiboly causes the deep cells to move over the yolk towards the vegetal pole, much like a knitted hat being pulled over your head (figure 1). First, intercalation of the deep cells to more superficial layers cause a thinning and spreading of the tissue. Not only cell migration but also changes in cell shape drive this process. These initial cell movements cause the embryo to shape itself from a 'sphere' towards the 'dome' stage. Further vegetal movement of the deep cells is caused by the pulling of the YSL and the attached EVL. This is partially mediated by microtubuli, which are attached to an actin meshwork at the vegetal pole of the yolk. Additionally, massive endocytosis in the YSL vegetal of the EVL attachment also mediates epiboly independent of microtubuli [3].

Involution

At about 50% epiboly, cells start to move inwardly in a process called internalization or emboly. This will form the germ ring. Notably, at the ventral and medial parts of the embryo this occurs via involution of sheets of cells, while at the dorsal region this occurs via the ingression of individual cells. These processes give rise to the different cell layers endoderm, mesoderm and ectoderm. The internalizing mesendodermal cells move inwardly towards the animal pole, forming the hypoblast. Meanwhile, the overlaying cells that do not move inwardly (epiblast) will form the ectoderm and continue epiboly.

Convergence and extension

At 6hpf, cells accumulate dorsally from the lateral and ventral regions of the embryo in a process called convergence. Meanwhile, lengthening of the embryonic axis occurs by cells intercalating and moving anteriorly in a process called extension. Together, these processes are termed

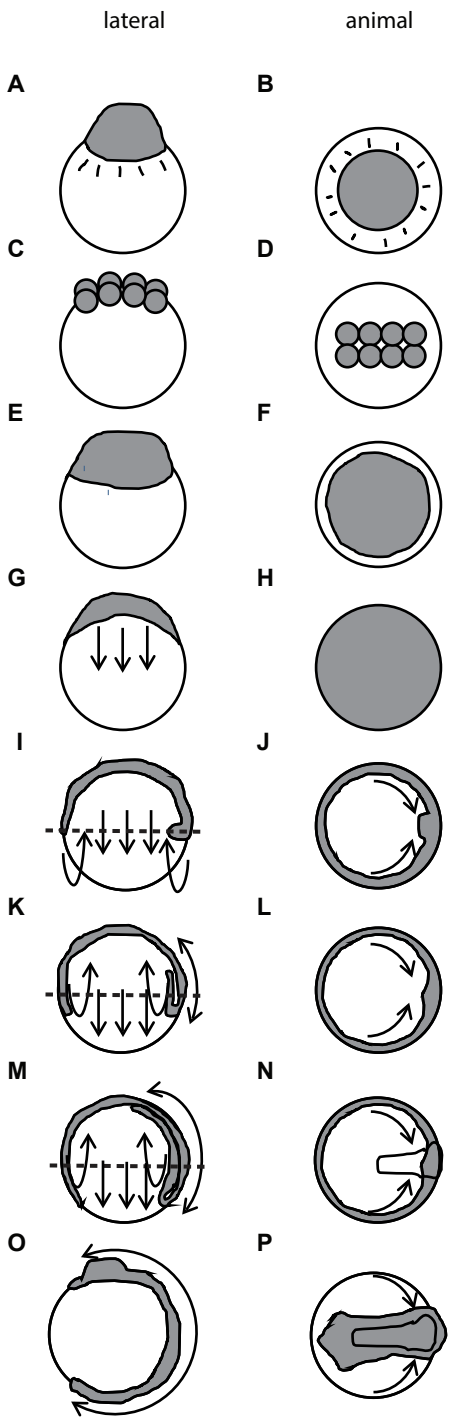

convergence and extension (C&E) which mediates the anterio-posterior lengthening and medio-lateral thickening of the embryo forming the longitudinal axis. Additionally, cells moving inwardly at the dorsal side of the embryo form a thickening called the shield, which functions in a similar way as the Spemann-Mangold organizer in other vertebrates like *Xenopus* and mouse, thus calling this stage the 'shield' stage.

Cells more lateral to the shield move slower than cells close to the shield. Several cellular movements can be distinguished in several areas of the embryo. From more ventral to dorsal these are: 1) vegetal pole migration in the ventral mesoderm, 2) slow dorsal convergence along irregular paths, 3) cell packing (fast and efficient convergence) in the lateral mesoderm, 4) medial planar intercalations and 5) polarized radial intercalations in the medial presomitic mesoderm. Most dorsally in the axial mesoderm, cells show 6) anterior-directed migration and 7) mediolateral intercalations [4].

Figure 1. Schematic representation of zebrafish development from the Zygote Period to the end of the Gastrulation Period.

Following the brief zygote period (a/b), when the embryo is at the single-cell stage, the cleavage period (c-d) runs from the two-cell to the 64-cell stage (i.e. 0.75–2.25 h post-fertilization (h.p.f). (h–p) The blastula period follows the cleavage period and runs from the 128-cell stage to the 50% epiboly stage (i.e. from 2.25 to 5.3 hpf). (e-f) Formation of the enveloping layer (EVL) and yolk syncytial layer (YSL). (g–p) The gastrula period then runs from the end of the blastula period at 50% epiboly (i.e. 5.3 hpf) through to the bud stage at 10 hpf, after which the segmentation period begins. Cell movements of convergence and extension (indicated with the arrows) start during the gastrulation period.

2 Signalling in gastrulation

Non canonical Wnt signalling

Convergence and extension cell movements are mediated by multiple signalling pathways that drive cell migration, adhesion and cell polarization. A principal pathway regulating C&E is the non-canonical Wnt/planar cell polarity (PCP) pathway [5]. The PCP pathway was first discovered in *Drosophila*, where mutants for components of the, then unknown, PCP pathway showed unorganized (unpolarized) wing epithelia. Later, disruption of the PCP pathway showed reduced body axis and neural tube defects in vertebrates [5]. In zebrafish, the core non-canonical Wnt/PCP pathway consists of extracellular Wnt glycoproteins, Wnt5 and Wnt11. Mutants for these Wnts (*pipetail* and *silberblick,* respectively) were identified in the late 90's [6,7] having defects in forebrain development and tail formation, respectively. The Wnts are able to bind the Frizzled 2/7 and the co-receptor glypican 4/Knypek a heparan sulphate proteoglycan [4]. Binding of Wnt to Frizzled causes intracellular recruitment of Dishevelled by its PDZ domain. Dishevelled in turn recruits Daam1, which causes RhoA, a small GTPase, activation. Additionally, Dishevelled activates the other small GTPases Rac1 and Cdc42. RhoA and Rac1 elicit activation of other downstream kinases, ROCKII and Jun kinase, respectively, which cause cytoskeletal rearrangements while Rac1 exerts its function on protein kinase C [4]. Other non-canonical Wnt pathways may regulate gastrulation as well. Ror2, the tyrosine kinase receptor for Wnt5, is able to modulate expression of paraxial protocadherin (PAPC) in *Xenopus* [8]. PAPC is an important regulator of cell adhesion and gastrulation [9]. Convergence and extension cell movements are also mediated through the Src family kinases Fyn and Yes, which are controlled upstream by Csk [10]. Interestingly, Fyn/Yes signalling acts parallel to non-canonical Wnt signalling, both of which act on RhoA downstream [11]. Additionally, maternally contributed canonical Wnt signalling activates Stat3 on the dorsal side of developing embryos [12]. Stat3 morphant embryos show C/E defects without affecting cell fate. More recently, *ofd1*, a gene associated with oral-facial-digital type 1 syndrome, which is required for ciliary motility and function was shown to interact genetically with components of the non-canonical Wnt pathway. Loss of *ofd1* results in shorter and wider embryos, indicating a role for cilia in C/E movements as well [13].

Cell-cell adhesion

Epiboly movements are severely impaired in zebrafish embryos of the E-cadherin mutant half baked. Cells deficient for E-cadherin are able to migrate, but are unable to undergo mesenchymal to epithelial transition necessary for proper intercalation movements during epiboly [14]. The cell adhesion molecule PAPC also regulates C/E by activation of RhoA and JNK [9]. Moreover, the trimeric G-proteins Gα12 and Gα13 mediate Rho activation, and mutants show C/E defects while their cells exhibit a rounder shape [3].

MAPK signalling

The Src family kinases Fyn and Yes not only control non-canonical Wnt signalling, but also control MAPK signalling. Mitogen activated protein kinase (MAPK) signalling is crucial for zebrafish development. For example, while partial knockdown of Erk1 causes convergence defects, partial loss of Erk2 results in extension defects, showing distinct functions of these kinases [15]. Notably, while more complete loss of Erk1 only mildly affects epiboly, Erk2 knockdown results in a developmental arrest at the onset of epiboly. Interestingly, loss of Erk1 is rescued by expression of Erk2, but not *vice versa*, indicating a prerequisite function of Erk2 during gastrulation [15].
Interestingly, also expression of activating forms of NRas, BRaf and Mek induce gastrulation

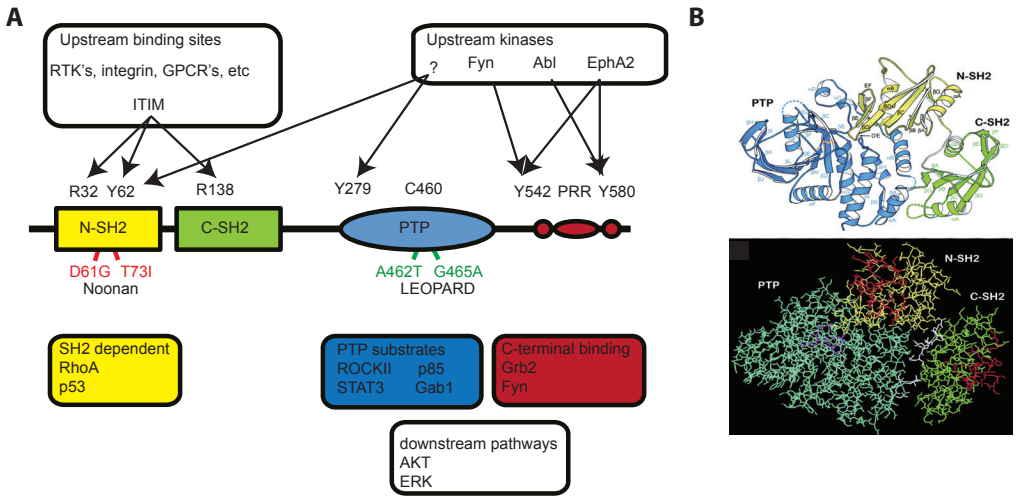

Figure 2. A Schematic representation of the Shp2, its binding sites and disease associated mutations.

A) Schematic representation of Shp2 protein, indicating the N terminal (N-SH2) and C-terminal (C-SH2) SH2 domains (yellow and green respectively), the catalytic protein-tyrosine phosphatase (PTP) domain (blue) and C-terminal tail (red). Many upstream kinases phosphorylate Shp2 on its tyrosines to regulate its activity, including the Src family kinase Fyn, Abl and EphA2. Upstream binding sites of receptors, including receptor tyrosine kinases (RTKs), Integrins and G-Protein Coupled Receptors (GPCRs), bind to the tandem SH2 domains of Shp2 when they are phosphorylated. Of particular note are Immunoreceptor Tyrosine Inhibitory Motifs (ITIMs) which are tyrosine motifs that are aptly spaced for Shp2 tandem SH2 binding. The arginines 32 and 138 are essential for the binding properties of Shp2. SH2 dependent functions of Shp2 include interactions with p53 and RhoA. The catalytic cysteine 460 is essential for the phosphatase function of Shp2, whereby mutation of C460 to serine completely abrogates its activity. Known PTP substrates are ROCKII, p85, Stat3 and Gab1. The C terminus of Shp2 contains two tyrosines and a proline rich region (PRR). Proteins known to associate with Shp2's C-terminus are Grb2 and Fyn. Activation of Shp2 is essential for downstream signaling pathways including the ERK and AKT pathways. Mutations associated with Noonan syndrome have been found mainly in the N-SH2 domain whereas LEOPARD associated mutations are found in the PTP domain, near the catalytic site. Whereas NS associated mutations result in enhanced PTP activity, LS mutations result in decreased PTP activity. In the studies described in this thesis, the NS mutations D61G and T73I, and the LS mutation A462T and G465A are mainly used. See text for further details.B) Crystal structure of Shp2. Structures in top and bottom are in similar orientations. The N- and C-terminal SH2 domains are yellow and green, respectively; the catalytic PTP domain is blue, and interdomain linkers (residues 104–111 and 217–220) are white in both panels. Top: Ribbon diagram showing secondary structure and organization of the domains. Orange, the side chain of Cys459 (the catalytic nucleophile); dashed lines, disordered loops. Bottom: All nonhydrogen atoms of SHP-2 are displayed. Although SH2 domain–bound peptides are not present in the structure, residues of both domains known to contact phosphopeptides are colored red. Note that peptide binding sites of both SH2 domains are exposed on the molecule surface. A distinct surface of the N-SH2 domain occupies the active site of the PTP domain. Magenta, residues of the PTP signature motif, HCSAGIGRS; these residues participate in catalysis and phosphate binding.[25]

defects [16,17]. Hyperactivation of the MAPK pathway results in C/E defects similar to knockdown of Erk1/2, suggesting a tight balance between activation and inactivation of this signalling pathway. Indeed, phenotypes resulting from hyperactive forms of BRaf and Mek are rescued using small molecule inhibitors of Mek, restoring the physiological levels of Erk1/2 activation [16,17]. What is more striking is that a treatment during a temporal window of 1 hour prior to shield formation is sufficient to rescue the gastrulation defect and later phenotypes. This indicates that, during shield stage, a tight balance between activation and inactivation of the MAPK pathway is important for proper development [16,17].

4 Shp2

Several studies have shown that the non-receptor tyrosine phosphatase SHP2 plays a fundamental role during gastrulation [18-20]. In zebrafish, knockdown of Shp2 results in defective gastrulation cell movements, without affecting cell fate specification [18]. In *Xenopus*, Shp2 is required for mesoderm induction and completion of gastrulation [21]. A study in Shp2 homozygous mutant embryonic stem cells showed that Shp2 is required at the initial steps of gastrulation, and that Shp2 mutant cells do not properly respond to signals initiated by fibroblast growth factors [20].
SHP2 is encoded by the *PTPN11* gene in humans. The importance of SHP2 in human genetics arose with the discovery that mutations in the *PTPN11* gene are the main cause of Noonan and LEOPARD syndromes, two autosomal dominant disorders with overlapping clinical features [22,23]. Due to a partial genome duplication in teleosts, the zebrafish genome encodes two Shp2 genes, *ptpn11a* and *ptpn11b* coding for the proteins Shp2a and Shp2b. Both Shp2a and Shp2b are derived from a common Shp2 ancestor [24]. SHP2 consists of two Src homology 2 (SH2) domains in tandem, a tyrosine phosphatase domain and a C-terminal tail [25] (Figure 2).

The SH2 domains of SHP2 are able to bind to phosphorylated tyrosines and thereby mediate binding of Shp2 to its target sites. Under basal conditions, Shp2 is kept in an 'inactive' closed state, whereby the N-terminal SH2 domain blocks the active site of the PTP domain to prevent dephosphorylation of its target sites [25]. The C-terminal SH2 domain however, is able to bind to tyrosyl phosphorylated SHP2-specific binding sequences and promote binding. Since SHP2 contains two SH2 domains in tandem, most SHP2 target proteins have tandem tyrosyl phosphorylation sites. Once the C-SH2 domain engages the target sequence, the tandem N-SH2 domain is prone to bind the other phosphorylation site by which SHP2 adopts an 'open' structure. Opening the structure of SHP2 causes an availability of the PTP domain, which facilitates dephosphorylation of its targets (Figure 3). These do not have to be the binding partner of SHP2 itself, but may also be other proteins in the complex [26].

Dephosphorylation of SHP2 target proteins is one of the mechanisms whereby Shp2 activation exerts its activity to activate downstream signalling pathways [27]. In *Xenopus*, a mutational analysis was performed to study the role of Shp2 in mesoderm induction following basic-fibroblast growth factor (bFGF) induction. Whereas the C-terminal SH2 domain is necessary only for wild-type function of Shp2, the N-SH2 domain and PTP activity are indispensable for Shp2 function [21]. The C-terminal tail, however, appears to be dispensable for Shp2 function. Alternatively, Shp2 may exhibit adaptor like activity, since EGF induced PI3K activation is enhanced by wild type- and phosphatase dead Shp2, but not by a Shp2 mutant that is unable to bind to its target [28].

Other studies suggest a role for the C-terminal domains of SHP2 [29]. The C-terminal tail of SHP2 consists of a proline rich domain, which is able to bind a Src homology 3 (SH3) domain, flanked by two tyrosines (Y542 and Y580 in zebrafish), which may be bound to SH2 domains. This suggests a role for SHP2 as an adaptor protein, while the C-terminus has also been opted to play a role in the conformational 'opening' and 'closing' of the phosphatase [30]. The upstream growth factor signalling pathway seems to have a decisive role in Shp2-mediated signaling, since C-terminal phosphorylation is mediated by FGF and PDGF, but not by EGF and IGF [29].

Despite the crucial role of SHP2 during gastrulation cell movements, little is known about the implication of the gastrulation defects on later development. For example, knockdown zebrafish embryos for Shp2 show defective gastrulation cell movements at 10 hpf and craniofacial/heart defects at 4 dpf [18]. However, it is poorly understood if the gastrulation cell movement defects are the direct cause of the later developmental defects and how the aberrant behavior of cells during gastrulation contribute to the impairment of development of other organs.

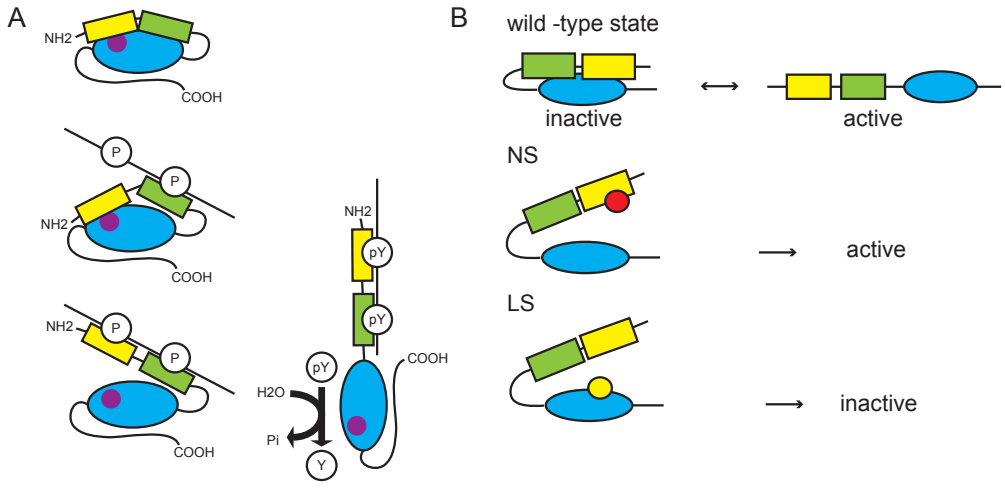

Figure 3. Regulation of Shp2 in the wild-type state and in Noonan and LEOPARD syndrome.

A) In the basal state, Shp2 is largely inactive, because the backside loop of the N-SH2 is inserted into the catalytic cleft. This results in mutual allosteric inhibition, with the N-SH2 inhibiting the PTP domain and the PTP domain contorting the pTyr peptide-binding pocket of the N-SH2 on the opposite surface. Shp2 activation starts when the two pTyr sites (pY), one that binds the C-SH2 and the other that binds the N-SH2, contacts Shp2. The C-SH2 is engaged first by its pTyr ligand. The resultant increase in local concentration of the ligand for the N-SH2 overcomes mutual allosteric inhibition, resulting in binding of the N-SH2 to its pTyr ligand, thus opening the enzyme into an active conformation. This mechanism of activation is strongly supported by crystal structure data and multiple enzymological studies [25]. Activation of Shp2 results in substrate dephosphorylation with release of phosphate. B) Regulation of Shp2 activity is, in part, achieved by an intramolecular interaction between the PTP domain of the protein and the N-SH2 domain leading to a "closed" protein conformation and autoinhibition. In the wild-type situation, "opening" of the N-SH2 and PTP domains is required for the protein to become active. NS mutations affect the interaction between the N-SH2 domain and the PTP domain, resulting in a protein that is in an "open" conformation and always active. LS mutations reside in the PTP domain and impair the catalytic activity of Shp2, resulting in a protein that is catalytically inactive.

Interestingly, not only knockdowns of Shp2 induce gastrulation cell movement defects, but also expression of mutant Shp2 with mutations that were identified in human patients with Noonan Syndrome or LEOPARD syndrome. These embryos show defects at later stages that are a phenocopy of the symptoms observed in human patients, including short stature, hypertelorism and cardiac defects [18]. Moreover, the contribution of Shp2 on gastrulation signaling pathways and its direct substrates still need to be addressed. Detailed analysis of the role of Shp2 during gastrulation may provide insight into the function Shp2 in Noonan and LEOPARD syndrome.

Outline of this thesis

Recent complementary *in vivo, in vitro* and *ex vivo* experiments reveal new insights into the function of Shp2 in NS and LS. However, it remains unclear how GOF and LOF mutants of Shp2 cause overlapping disease. In this thesis we investigate the role of NS and LS Shp2 using zebrafish as an animal model and the cellular and molecular mechanisms by which biochemically opposite Shp2 mutations result in two genetic disorders with overlapping features. The main theme of our projects was on NS and LS Shp2 in zebrafish, with Paardekooper Overman focusing more on the underlying molecular mechanism and Bonetti more on developmental aspects. We have indicated below who of the two of us is the main contributor to the different chapters.

In ***Chapter two*** (Paardekooper Overman) we describe several methods that are used to study phosphatases using zebrafish and techniques that we and others have developed to assess gastrulation defects and to assess changes in the phosphoproteome of developing zebrafish.

Chapter three (Bonetti) is an overview of the genetics of Noonan and LEOPARD syndrome and of molecular mechanisms that regulate these two genetic disorders. Moreover, we introduce the cardiac defects associated with Noonan and LEOPARD syndrome and the use of zebrafish as a model to study heart development.

In ***Chapter four*** (Bonetti) we study the phenotype of knock-out zebrafish embryos for both *ptpn11* genes. Shp2 has an essential role in embryonic development. Homozygous *Ptpn11-/-* mouse embryos die pre-implantation due to defective Erk activation and trophoblast stem cell death, precluding the possibility to study Shp2 function in differentiated cell types in adult animals [20]. Zebrafish embryo development occurs externally and the embryos are transparent, allowing the study of gene function *in vivo.* Due to partial genome duplication in teleosts, the zebrafish genome encodes two genes, *ptpn11a* and *ptpn11b* coding for the proteins Shp2a and Shp2b. We identified stop mutations in the N-terminal SH2 domain of each of the two *ptpn11* genes and we study the phenotype of the single homozygous mutants and of double homozygous mutant embryos.

In ***Chapter five*** (Paardekooper Overman) we describe the identification of Fer kinase as a candidate downstream factor in NS and LS signaling using a phosphotyrosine immunoprecipitation and mass spectrometry approach. Following that, we investigated the role of Fer kinase in the regulation of gastrulation and its role in the pathogenesis of NS and LS in zebrafish.

In ***Chapter six*** (Paardekooper Overman), we identify PZR, an important binding partner and substrate of Shp2 involved in adhesion and cell migration, as a hyperphosphorylated protein in NS and LS in both mouse and zebrafish. We show that PZR is required for normal embryonic development in zebrafish. Moreover, we provide evidence that PZR exerts its effects by changing the flux of Src activation in NS and LS.

Heart defects are the main cause of death in NS and LS patients. In ***Chapter seven*** (Bonetti) we investigate the role of NS and LS Shp2 in zebrafish cardiac development. We found that impaired heart function and morphogenesis are highly similar in NS- and LS-Shp2 expressing embryos. NS and LS-Shp2 both lead to up-regulation of Erk phosphorylation at the end of gastrulation, indicating a common biochemical pathway for NS and LS syndrome in zebrafish development.

The genetic cause of some 25% of all Noonan cases still remains to be determined. In ***Chapter eight*** (Bonetti and Paardekooper Overman), we describe the identification of mutations in Alpha-2-Macroglobulin-Like-1 (*A2ml1*) as cause of a disorder clinically related to NS. We identified *de novo* mutations in *A2ML1* using family-based whole exome sequencing of a case-parent trio with a clinical diagnosis of NS. Moreover, A2ML1 mutants were functionally characterized in zebrafish, showing that disease associated A2ml1 induces developmental defects, reminiscent of the developmental defects induced by a NS-variant of Shp2.
Finally the findings and the implications described in this thesis are discussed in ***Chapter nine*** (Paardekooper Overman and Bonetti).

References:

1. Kimmel CB, Ballard WW, Kimmel SR, Ullmann B, Schilling TF (1995) Stages of embryonic development of the zebrafish. Dev Dyn 203: 253-310.
2. Giraldez AJ, Mishima Y, Rihel J, Grocock RJ, Van Dongen S, et al. (2006) Zebrafish MiR-430 promotes deadenylation and clearance of maternal mRNAs. Science 312: 75-79.
3. Solnica-Krezel L (2006) Gastrulation in zebrafish -- all just about adhesion? Curr Opin Genet Dev 16: 433-441.
4. Roszko I, Sawada A, Solnica-Krezel L (2009) Regulation of convergence and extension movements during vertebrate gastrulation by the Wnt/PCP pathway. Semin Cell Dev Biol 20: 986-997.
5. Tada M, Kai M (2009) Noncanonical Wnt/PCP signaling during vertebrate gastrulation. Zebrafish 6: 29-40.
6. Heisenberg CP, Brand M, Jiang YJ, Warga RM, Beuchle D, et al. (1996) Genes involved in forebrain development in the zebrafish, Danio rerio. Development 123: 191-203.
7. Hammerschmidt M, Pelegri F, Mullins MC, Kane DA, Brand M, et al. (1996) Mutations affecting morphogenesis during gastrulation and tail formation in the zebrafish, Danio rerio. Development 123: 143-151.
8. Schambony A, Wedlich D (2007) Wnt-5A/Ror2 regulate expression of XPAPC through an alternative noncanonical signaling pathway. Dev Cell 12: 779-792.
9. Unterseher F, Hefele JA, Giehl K, De Robertis EM, Wedlich D, et al. (2004) Paraxial protocadherin coordinates cell polarity during convergent extension via Rho A and JNK. EMBO J 23: 3259-3269.
10. Jopling C, Hertog J (2007) Essential role for Csk upstream of Fyn and Yes in zebrafish gastrulation. Mech Dev 124: 129-136.
11. Jopling C, den Hertog J (2005) Fyn/Yes and non-canonical Wnt signalling converge on RhoA in vertebrate gastrulation cell movements. EMBO Rep 6: 426-431.
12. Yamashita S, Miyagi C, Carmany-Rampey A, Shimizu T, Fujii R, et al. (2002) Stat3 Controls Cell Movements during Zebrafish Gastrulation. Dev Cell 2: 363-375.
13. Ferrante MI, Romio L, Castro S, Collins JE, Goulding DA, et al. (2009) Convergent extension movements and ciliary function are mediated by ofd1, a zebrafish orthologue of the human oral-facial-digital type 1 syndrome gene. Hum Mol Genet 18: 289-303.
14. Schier AF, Talbot WS (2005) Molecular genetics of axis formation in zebrafish. Annu Rev Genet 39: 561-613.
15. Krens SF, He S, Lamers GE, Meijer AH, Bakkers J, et al. (2008) Distinct functions for ERK1 and ERK2 in cell migration processes during zebrafish gastrulation. Dev Biol 319: 370-383.
16. Anastasaki C, Estep AL, Marais R, Rauen KA, Patton EE (2009) Kinase-activating and kinase-impaired cardio-facio-cutaneous syndrome alleles have activity during zebrafish development and are sensitive to small molecule inhibitors. Hum Mol Genet 18: 2543-2554.
17. Runtuwene V, van Eekelen M, Overvoorde J, Rehmann H, Yntema HG, et al. (2011) Noonan syndrome gain-of-function mutations in NRAS cause zebrafish gastrulation defects. Dis Model Mech 4: 393-399.
18. Jopling C, van Geemen D, den Hertog J (2007) Shp2 knockdown and Noonan/LEOPARD mutant Shp2-induced gastrulation defects. PLoS Genet 3: e225.
19. Saxton TM, Pawson T (1999) Morphogenetic movements at gastrulation require the SH2 tyrosine phosphatase Shp2. Proc Natl Acad Sci U S A 96: 3790-3795.
20. Saxton TM, Henkemeyer M, Gasca S, Shen R, Rossi DJ, et al. (1997) Abnormal mesoderm patterning in mouse embryos mutant for the SH2 tyrosine phosphatase Shp-2. EMBO J 16: 2352-2364.
21. O'Reilly AM, Neel BG (1998) Structural determinants of SHP-2 function and specificity in Xenopus mesoderm induction. Mol Cell Biol 18: 161-177.
22. Tartaglia M, Mehler EL, Goldberg R, Zampino G, Brunner HG, et al. (2001) Mutations in PTPN11, encoding the protein tyrosine phosphatase SHP-2, cause Noonan syndrome. Nat Genet 29: 465-468.
23. Digilio MC, Conti E, Sarkozy A, Mingarelli R, Dottorini T, et al. (2002) Grouping of multiple-lentigines/ LEOPARD and Noonan syndromes on the PTPN11 gene. Am J Hum Genet 71: 389-394.
24. van Eekelen M, Overvoorde J, van Rooijen C, den Hertog J (2010) Identification and expression of the family of classical protein-tyrosine phosphatases in zebrafish. PLoS One 5: e12573.
25. Hof P, Pluskey S, Dhe-Paganon S, Eck MJ, Shoelson SE (1998) Crystal structure of the tyrosine phosphatase SHP-2. Cell 92: 441-450.
26. Neel BG, Gu H, Pao L (2003) The 'Shp'ing news: SH2 domain-containing tyrosine phosphatases in cell signaling. Trends Biochem Sci 28: 284-293.
27. Zhang SQ, Yang W, Kontaridis MI, Bivona TG, Wen G, et al. (2004) Shp2 regulates SRC family kinase activity and Ras/Erk activation by controlling Csk recruitment. Mol Cell 13: 341-355.
28. Wu CJ, O'Rourke DM, Feng GS, Johnson GR, Wang Q, et al. (2001) The tyrosine phosphatase SHP-2 is required for mediating phosphatidylinositol 3-kinase/Akt activation by growth factors. Oncogene 20: 6018-6025.
29. Araki T, Nawa H, Neel BG (2003) Tyrosyl phosphorylation of Shp2 is required for normal ERK activation in response to some, but not all, growth factors. J Biol Chem 278: 41677-41684.
30. Lu W, Gong D, Bar-Sagi D, Cole PA (2001) Site-specific incorporation of a phosphotyrosine mimetic reveals a role for tyrosine phosphorylation of SHP-2 in cell signaling. Mol Cell 8: 759-769.

Zebrafish as a model to study PTPs during development

Jeroen Paardekooper Overman[1] and Jeroen den Hertog[1,2,3]

1. Hubrecht Institute-KNAW and University Medical Centre Utrecht, the Netherlands
2. Institute of Biology Leiden, Leiden University, the Netherlands
3. Corresponding author: Hubrecht Institute, Uppsalalaan 8, 3584 CT Utrecht, The Netherlands
Tel: +31 30 2121800 e-mail: j.denhertog@hubrecht.eu

Methods. 2014. January 15; 65(2): 247-253

Abstract

Protein-Tyrosine Phosphatases (PTPs) have important roles in signaling, but relatively little is known about their function *in vivo*. We are using the zebrafish as a model to study the function of PTPs at the organismal, cellular and molecular level. The zebrafish is an excellent experimental model for the analysis of gene function. We have developed methods to quantitatively study effects of PTP knockdown or expression of (mutant) PTPs, particularly with respect to gastrulation cell movements. Moreover, we have studied the phosphoproteome of zebrafish embryos. In this review, we will discuss methods to manipulate the zebrafish genome and techniques that we have developed to assess developmental defects during gastrulation and to assess differences in the phosphoproteome.

1. Introduction

Much is known about catalysis and regulation of PTPs [1]. However, to fully understand the function of PTPs, their role in whole organisms *in vivo* needs to be addressed. Several model organisms have been used to investigate the function of PTPs, including the invertebrates *Drosophila* and *C.elegans* and vertebrate models, particularly the mouse. Many mouse knock-outs have been generated that provided important insight into the function of PTPs in development and conditional knock-outs have allowed the analysis of the function of PTPs in particular tissues [2,3]. Generation of mouse models can be laborious however, and *in vivo* imaging is difficult. We and others have used the zebrafish as a model for the analysis of PTP function, because of the many advantages that zebrafish embryos have to offer as an experimental system. Zebrafish are particularly amenable for genetics, intravital imaging and large scale approaches. In addition, we have recently developed a method to derive cell lines from single zebrafish embryos and tumors [4], which complements the wide range of experimental approaches in zebrafish. Here, we will review zebrafish as a model system in general, the genetic tools available, the approaches that we have used to assess PTP function in zebrafish, focusing on *in vivo* cell behavior and phosphoproteomics and we will give an outlook on approaches that may be used in the near future to assess PTP function *in vivo*.

2. Zebrafish as an experimental system

The zebrafish is an excellent model system that was initially used for large scale forward genetic screens [5,6]. Since then, zebrafish are increasingly being used to model human diseases [7]. Major advantages of the zebrafish as an experimental system are that large numbers of embryos can be obtained easily; 100 - 200 embryos per clutch, 1 - 2 clutches per week per adult zebrafish pair. The embryos develop quickly and outside the mother; after 1 – 2 days most organs have formed. The embryos are transparent, facilitating analysis of embryonic development by (time-lapse) microscopy. Many genetic mutants are available and transgenesis is feasible. More and more transgenic lines are becoming available, expressing fluorescent marker proteins under the control of specific promoters, which allows for intravital imaging. Overexpression of genes or proteins of interest can easily be achieved by micro-injection of synthetic mRNA encoding the protein of interest at the one-cell stage. In addition, transient knockdown of target proteins and target-selected gene inactivation are feasible in zebrafish (see below). Finally, chemical compounds can easily be administered to zebrafish embryos by simple addition to the aqueous embryo medium. Medium to large scale screens for bioactive compounds have been done using zebrafish development as read-out [8,9]. Taken together, the zebrafish is an ideal model system for analysis of gene function at the genetic, molecular and cellular level in whole organisms.

3. Zebrafish Protein Tyrosine Phosphatases

The zebrafish genome sequence is available in public databases (http://www.ensembl.org/Danio_rerio/Info/Index)[10]. In general, orthologs of most human genes can be found in the zebrafish genome. In fact, some genes are duplicated in the zebrafish genome, due to a genome duplication in teleosts 320 million years ago [11,12]. In human, PTPs are divided in four classes i.e. classical and VH1-like dual specific protein phosphatases (DSPs) (class I), low molecular weight phosphatases (class II), Cdc25 phosphatases (class III) and Aspartic acid-based pTyr specific phosphatases (IV) (Alonso *et al.* 2004). Class I classical PTPs are further subdivided into receptor and non-receptor PTPs. Class I DSPs are divided into seven groups, namely: mitogen

activated protein kinase (MAPK) phosphatases (MKPs), atypical DSPs, the slingshot phosphatases, PRLs, CDC14s, phosphatase and tensin homologues (PTENs) and myotubularins. Since we focus on on classical PTPs and PTENs, these will be discussed in this review.

The zebrafish genome encodes 51 classical PTPs and all the subtypes that have been identified in the mammalian genomes are represented in the zebrafish genome [13](Table 1). Fourteen PTP genes are duplicated in the zebrafish genome and whether these duplicated genes are all functional remains to be determined. Comparison of the PTP family in the genome of five distinct fish species led to the surprising discovery that *ptpn20*, which was supposed to encode little more than a PTP domain, actually encodes a large PTP with multiple functional domains, resembling PTP-BL. The human and mouse *PTPN20* genes have a similar structure as zebrafish *ptpn20*, and we confirmed this by reverse transcription PCR [14].

To unravel the function of PTPs during zebrafish development, we have compared the expression patterns of all PTP genes in zebrafish by whole mount *in situ* hybridization using standard protocols [13,15]. Most PTP genes are expressed throughout development with broad expression patterns early on, which become more restricted later in development [13]. Interestingly, some of the duplicated PTP genes have overlapping spatio-temporal expression patterns whereas others are mutually exclusive. It is likely that the function of the latter PTPs has diverged since their duplication. For gene specific expression data during embryonic development we refer to [13].

4. Genetic tools to study PTP function in zebrafish

PTP function has been studied in zebrafish by transient, morpholino-mediated knockdown, in genetic loss-of-function mutants and by expression of exogenous PTP genes and mutants thereof.

4.1 Morpholinos

Transient knockdown of target proteins by microinjection of morpholinos is widely used to study gene function [16,17]. Morpholinos are either directed at the start ATG to block translation of the target protein or at splice sites to block splicing of the target RNA (Figure 1). Morpholino-mediated knockdown of Pez (*ptpn14*) results in developmental defects in the heart and somites, which may at least in part be mediated by impaired TGFβ3 signaling-dependent epithelial to mesenchymal transition [18]. Knockdown of PTPσ results in accumulation of synaptic vesicles in the axon terminals of olfactory sensory neurons [19]. PTPσ is related to the LAR receptor tyrosine phosphatases and these guide peripheral sensory axons to the skin in zebrafish embryos [20]. Ve-ptp is required for vascular integrity, due to its role in adherens junctions where it regulates VEGFR-dependent VE cadherin phosphorylation and cell polarity [21,22]. Ptpro is structurally related to Ve-ptp and is required for cerebellar formation [23]. Knockdown of Shp1 (*ptpn6*) hyperactivates the innate immune system [24]. All of the studies above used transient morpholino-mediated knockdown of the PTP target proteins. To study the function of all classical PTPs in development, we have designed two non-overlapping morpholinos against each classical PTP gene in the zebrafish genome and assessed their effects on early development by micro-injection at the one-cell stage. Not all pairs of morpholinos induced the same defects, suggesting off-target effects (van Eekelen, Runtuwene and den Hertog, unpublished results). We have pursued some knockdowns in detail (see below) and rescue of the morpholino-induced defects by co-expression of the respective target RNAs is taken as good evidence that the observed defects are not merely off-target effects.

4.2 Target selected gene inactivation

Off-target effects of morpholinos are a concern and reverse genetics approaches have been developed to generate genetic mutants of target genes. Both mutagenesis and viral insertions are commonly used to disrupt target genes. Many loss-of-function mutations have been identified in PTP genes (www.zfin.org)(Table 1). Mutagenesis-based gene inactivation makes use of reagents such as N-ethyl-N-nitrosourea (ENU) to generate random single nucleotide polymorphisms (SNPs) in adult males. Subsequently, offspring is generated and mutations are identified in target genes by SNP detection or sequencing. Target selected gene inactivation by random mutagenesis and resequencing of the gene of interest in a large number of F1 mutants has led to the identification of nonsense mutations in more than 200 target genes [25] (www.zfin.org). An ongoing project makes use of high-throughput sequencing and is aimed at disrupting every gene in the zebrafish genome. So far potentially disruptive mutations have been identified in 38% of the zebrafish genes [26].

One of the first genes that was disrupted by the original target selected gene inactivation method was zebrafish *pten*. PTEN is a prominent member of the PTP superfamily, even though its catalytic activity is directed at lipids, rather than phosphotyrosine. *PTEN* is one of the most frequently mutated tumor suppressor genes in human cancer and is essential for mammalian development. We identified an early stop in the *pten* gene and much to our surprise, homozygous fish were viable. However, unlike the human genome, the zebrafish genome encodes two *pten* genes, *ptena* and *ptenb*, prompting us to disrupt the second *pten* gene too. Zebrafish embryos without functional Pten (*ptena-/-ptenb-/-*) display various hyperplastic/dysplastic defects and are embryonic lethal [27]. Genetic mutants that lack functional Ptena or Ptenb are viable and fertile, indicating that Ptena and Ptenb have at least partially redundant functions. Yet, adult fish that retain only a single wild type *pten* allele (*ptena+/-ptenb-/-* and *ptena-/-ptenb+/-*) develop hemangiosarcomas, endothelial tumors[28]. These findings illustrate that the duplication of genes in teleosts can be used to study gene function in a way that is not possible in mammalian systems. Future analysis of the pten mutants will provide new insights into Pten function *in vivo.*

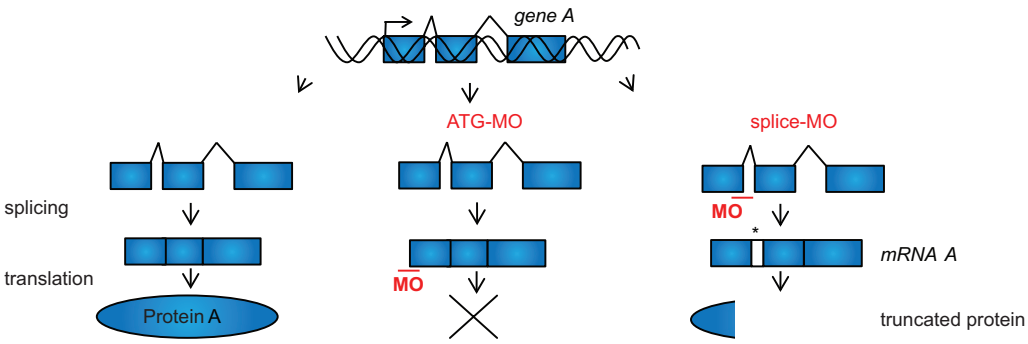

Figure 1. Morpholino method. Both translation initiation and splice- site blocking morpholinos have been used to knockdown expression of target proteins. Gene A is transcribed and the RNA is spliced and translated normally. Translation initiation blocking morpholinos (ATG-MO) are targeted at the start ATG and will interfere with mRNA binding to the ribosome complex thus leading to impaired protein synthesis of Protein A. Splice-site blocking morpholinos (splice-MO) are targeted at splice-donor or –acceptor sites and interfere with splicing, thus leading to inclusion of introns which may contain internal stop sites or lead to a frame shift, resulting in truncated, dysfunctional proteins.

Zebrafish gene	Zebrafish protein	Human protein	Subtype	Phenotype in fish	Genetic Association Database	SNP (ZFIN)	Tg insertion (ZFIN)
ptpn1	PTP1b	PTP1B	NT1	-	Diabetes type 1 and 2; obesity	-	-
ptpn2a, ptpn2b	tcPTPa, tcPTPb	TCPTP	NT1	-	Diabetes Type 1; Celiac Disease; Crohn's disease; Lupus	-	
ptpn3	PTPh1	PTPH1	NT5	-	Neuroblastoma; Albumins; Echocardiography	-	+
ptpn4a, ptpn4b	meg1a, meg1b	MEG1	NT5	-	-	+	-
ptpn5	PTP-STEP	PTP-STEP	R7	-	-	-	-
ptpn6	shp1	SHP1	NT2	immune system (Kanwal et al., 2013)			
ptpn7	HePTP	HePTP	R7	-	-	-	-
ptpn9a, ptpn9b	meg2a, meg2b	MEG2	NT3	-	Height; (Embryonic lethality in mouse)	+	+
ptpn11a, ptpn11b	shp2a, shp2b	SHP2	NT2	gastrulation; Noonan and LEOPARD syndrome (Jopling et al., 2007)	Leukemia; Noonan and LEOPARD syndrome;Platelet Count	+	+
ptpn12	PEST	PTPPEST	NT4	-	Insulin	-	-
ptpn13	PTPBAS	PTPBAS	NT7	gastrulation (van Eekelen et al., 2012)	Cardiovascular	+	+++
ptpn14	PTP36	PTP36	NT6	heart, somite (Wyatt et al., 2007)	ADD; blood cells; blood flow velocity	-	-
ptpn18	BDP1	BDP1	NT4	-	-	-	-
ptpn20	PTPTyp	TYP	NT8	gastrulation (van Eekelen et al., 2012)	-	+	+
ptpn21	PTPd1	PTPD1	NT6	-	Schizophrenia	+	-
ptpn22	LyPTP	LyPTP	NT4	-	Diabetes type 1 and 2; Rheumathroid arthritis;	+	-
ptpn23a, ptpn23b	hdPTPa, hdPTPb	HDPTP	NT9	-	Cell invasion	+	-

ptpra	RPTPα	RPTPα	R4	gastrulation (van Eekelen et al., 2010b)	-	++	++
ptprb	RPTPβ	RPTPβ	R3	vascular integrity (Carra et al., 2012; Hayashi et al., 2013)	Calcium	-	+++
ptprc	CD45	CD45	R1/R6	-	Multiple Sclerosis; lupus erythematosus	+	+ (dsRed)
ptprda, ptprdb	RPTPδa, RPTPδb	RPTPδ	R2B	-	Diabetes; Cholesterol; Coronary Disease; Heart Failure	+++++	+
ptprea, ptpreb	RPTPεa, RPTPεb	RPTPε	R4	gastrulation (van Eekelen et al., 2010b)	Coronary Disease; Ewing sarcoma	++	+
ptprfa, ptprfb	LARa, LARb	LAR	R2B	peripheral sensory axons (Wang et al., 2012)	-	+++	++
ptprga, ptprgb	RPTPγa, RPTPγb	RPTPγ	R5	-	Coronary Artery Disease; QT interval; Inflammation	+	+
ptprh	sap1	SAP1	R3	-	-	-	-
ptprja, ptprjb	dep1a, dep1b	DEP1	R3	arterial venous cell fate decision (Rodriguez et al., 2008)	Thyroid cancer; Precursor Cell Lymphoblastic Leukemia	+++	-
ptprk	RPTPκ	RPTPκ	R2A	-	Celiac disease; Albuminuria	-	-
ptprm	RPTPμ	RPTPμ	R2A	-	Prostatic Neoplasms; Fibrinogen	-	-
ptprna, ptprnb	IA2a, IA2b	IA2	R8	-	-	+	+
ptprn2	IA2β	IA2β	R8	-	Mental disorders; Albumins	+++	++
ptpro	GLEPP	GLEPP1	R3	cerebellar formation (Liao et al., 2013)	Mental Processes; Body Mass Index	-	+
ptprq	PTPS31	PTPS31	R3	-	Bipolar Disorder;Erythrocyte Indices; Electrocardiography	-	-
ptprr	pcPTP	PCPTP	R7	-	Parkinson Disease	-	-

ptprsa, ptprsb	RPTPσa, RPTPσb	RPTPσ	R2B	synaptic vesicles (Chen et al., 2011a)	Alcoholism	++	++ (knockin)
ptprt	RPTPρ	RPTPρ	R2A	-	Depressive Disorder; Diabetes Mellitus;	+++	++++
ptprua, ptprub	RPTPλa, RPTPλb	RPTPλ	R2A	gastrulation (Aerne and Ish-Horowicz, 2004)	Heart Failure; Bipolar Disorder; Diabetes Mellitus, Type 2	+	-
ptprza, ptprzb	RPTPζa, RPTPζb	RPTPζ	R5	-	Cholesterol, LDL	++	-
ptena, ptenb	Ptena, Ptenb	PTEN	DSP	early development (Faucherre et al., 2008) , hemangiosarcoma (Choorapoikayil et al., 2012)	Hemangiosarcoma; Prostate cancer	++	++

Table 1. Zebrafish phosphatases. The zebrafish genes, their protein names and the human orthologues are depicted here with phenotypes described in fish, genetic associations and available mutant zebrafish lines. Genetic associations are derived from the Genetic Association Database: http://geneticassociationdb.nih.gov/cgi-bin/index.cgi. Not all genetic associations are mentioned here due to space constrictions. Data describing Single Nucleotide Polymorphisms (SNPs) from mutagenesis screens and transgenic insertions disrupting gene function (Wang et al., 2007) are derived from www.zfin.org. + indicates single SNP or transgenic insertion, ++ indicates two SNPs or transgenic insertions etc. – indicates no SNP or transgenic insertion was identified in this gene. Further details of transgenics and zebrafish phenotypes are described in the text.

4.3 Gene targeting

Specific gene inactivation by directing nuclease activity to target genes has been developed successfully for zebrafish as well. Zinc Finger Nuclease (ZFN) technology has been used [29,30] and more recently, Transcription Activator Like Effector Nuclease (TALEN) technology appears even more successful [31]. Clustered Regularly Interspaced Short Palindromic Repeat (CRISPR)-associated systems (Cas) technology has also been applied to inactivate genes in zebrafish [32] and holds much promise for future inactivation of target genes. All nuclease technologies are based on the generation of double-stranded breaks in the target gene, which are repaired by endogenous DNA repair mechanisms, particularly non-homologous end-joining (NHEJ). NHEJ frequently makes mistakes, leading to short deletions and these actually result in frame shifts and hence inactivation of the target genes. In principle, a template can be provided exogenously for DNA repair by homologous recombination, facilitating the introduction of (disease-associated) mutations or insertions at will. Successful homologous recombination in zebrafish using TALENs to introduce an exogenous restriction site or loxP sites has been reported [31].

5. PTPs in zebrafish gastrulation cell movements.

Several PTPs have an essential role in gastrulation cell movements, in particular convergence and extension (C&E) cell movements. These morphogenetic cell movements shape the developing zebrafish embryo [33]. Cell movements in the developing embryo were determined by *in toto* imaging using light sheet microscopy, which provides a stunning view of gastrulation cell movements and at the same time illustrates the strength of the zebrafish as a model for intravital imaging [34]. Signaling has a crucial role in gastrulation cell movements and we and others found that several PTPs are essential for C&E cell movements. Knockdown of Shp2 results in defective gastrulation cell movements, without affecting cell fate specification [35]. RPTPα and PTPε are also required for normal gastrulation cell movements. Transient morpholino-mediated knockdown of RPTPα and PTPε, but also a genetic mutant of *ptpra* display C&E cell movement defects [36]. Moreover, knockdown of RPTPψ results in defects in C&E cell movements during gastrulation [37]. Finally, knockdown of PTP-BL and Ptpn20 induces gastrulation cell movement defects [14]. Not only knockdowns of PTPs induce gastrulation cell movement defects, but also expression of mutant Shp2 with mutations that were identified in human patients with Noonan Syndrome or LEOPARD syndrome display C&E cell movement defects. These embryos display defects at later stages that are reminiscent of the symptoms observed in human patients, including short stature, hypertelorism and cardiac defects [35]. Interestingly, expression of LEOPARD mutant Shp2 induces defects in neural crest specification and migration [38]. It remains to be determined how an activating mutation (Noonan Syndrome), an inactivating mutation (LEOPARD syndrome) and a knockdown induce similar developmental defects in early embryonic development.

PTP signaling, resulting in gastrulation cell movements, was investigated by analysis of genetic epistasis interactions. Particularly, we studied the role of Src family kinases, because these are activated by PTPs and have a role in C&E cell movements [39,40], and Rho family GTPases, because these are downstream regulators of gastrulation cell movements [41]. Partial knockdown of Shp2, RPTPα or PTPε does not affect development, nor does partial knockdown of the Src family kinases, Fyn and Yes, but combined partial knockdown of these PTPs and Src family kinases induces severe gastrulation cell movement defects [35,36], indicating a genetic interaction. RhoA, but not Rac was identified to act downstream of Src family kinases in gastrulation cell movements

[39]. Constitutively active RhoA rescues Shp2, RPTPα and PTPε knockdowns [35,36], which provides insight into the mechanism underlying PTP signaling in gastrulation cell movements. Intriguingly, the PTP-BL and ptpn20 knockdowns are rescued by dominant negative RhoA, in contrast to the RPTPα and PTPε knockdowns. We suggest a model in which PTPs regulate cell polarization, which is at the basis of normal C&E cell movements during gastrulation [14]. Some PTPs have positive effects on cell polarization and others negatively affect polarization. Both effects result in decreased directed cell migration and hence to defective C&E cell movements. Many PTPs are essential for normal C&E cell movements, which probably reflects the high level of regulation of C&E cell movements. Detailed analysis of the role of each PTP in C&E cell movements will provide insight into the interplay between PTPs – if any – in the regulation of C&E cell movements.

6. Quantitative analysis of gastrulation defects

While analyzing gastrulation cell movement defects in zebrafish embryos we developed assays to quantitatively determine defective cell movements, based on (1) the shape of the embryo, (2) molecular markers and (3) cell migration:

6.1 Detecting oval-shaped embryos

Defective cell movements during epiboly and gastrulation lead to oval-shaped embryos [42,43]. Using Image J, we have developed a semi-automated tool to determine the oval shape of embryos. The circumference of the embryo is detected and subsequently, the long axis and perpendicular to that the short axis is determined (Fig. 2A). The ratio long axis/short axis directly represents the extent of oval shape. Wild type non-injected embryos display a ratio of 1.1, i.e. close to 1.0, the perfect sphere. The ratios of embryos with epiboly defects are usually 1.3 and up, significantly higher than 1.1 in wildtype and control-injected embryos. Interestingly, CI-1040, a specific inhibitor of MEK, which acts downstream in the pathway rescues the oval shape of the embryos, whereas it does not affect the ratio of wildtype embryos [43]. Detecting oval shapes of zebrafish embryos is a straightforward method to quantitatively determine the deviation from the normal shape of control embryos and therefore the severity of gastrulation defects.

6.2 Molecular markers

Embryos with C&E cell movement defects are characterized by a broader body and reduced extension of the body axis. Cell fate is not affected by defects in C&E cell movements and all cell types that are normally observed in the developing embryo are detectable in embryos with defective gastrulation cell movements. We routinely use a panel of markers to assess that cell fate is not affected. These include markers for: the dorsal organizer (*goosecoid, gsc*), ventral cell fate (*bone morphogenetic protein 2b, bmp2b*), dorsalizing factor (*chordin, chd*) and mesendoderm (*notail, ntl*) at shield stage; axial mesendoderm at 70% epiboly (cyclops, cyc) and at budstage forebrain (*six3*) and mid-hindbrain boundary (*pax2*). Several markers have been identified that provide quantifiable traits of C&E cell movements in the developing embryo at early developmental stages. *Dlx3* (currently known as *dlx3b*) marks the edges of the neural plate and *hgg1* (current name *ctsl1b*) marks precursors of the hatching gland. Double labeling with *dlx3* and *hgg1* provides a characteristic pattern (Fig. 2B). The position of the hatching gland, relative to the anterior-most *dlx3* staining provides a direct measure for body axis extension and the angle of the *dlx3*-positive edges of the neural plate are directly representative of convergence [36]. In embryos with defective C&E cell movements, the *hgg1* staining is located more posteriorly and the *dlx3* staining is significantly wider (Fig. 2B).

Krox20/myod double labeling at the 8-10 somite stage and subsequent flat-mounting of the embryos leads to a highly reproducible pattern that can be used for quantification of the width and length of the embryo [44](Fig. 2C). The *krox20* marker stains rhombomeres 3 and 5 and *myod* marks the somites. Embryos with 8-10 somites are used, and staining of the somites provides a good means to determine the age of the embryos, as a new somite is added every 30 min at this stage. The distance from the first to the eighth somite remains identical from the 8-somite to the 10-somite stage. The width of the *krox20*-positive rhombomere 3 and the length of somites 1-8 is directly proportional to the width and length of the embryo, respectively, and the ratio of width and length allows direct quantitative comparison between groups of experimental embryos.

6.3 Cell migration

Identification of differences in the migration of paraxial mesendodermal cells between groups of embryos is definitive evidence for differences in C&E cell movements. Initially, we used a photoactivatable dye, 4,5-dimethoxy-2-nitrobenzyl (DMND)-caged fluorescein dextran (10,000 MW; Molecular Probes, Leiden, the Netherlands) that was uncaged by local illumination with UV light at 6 hpf as described [45]. The fluorescent group of cells was subsequently followed using an Axioplan microscope, equipped with a UV light source, adjustable pinhole and 40X objective. Either a group of cells in the embryo proper was photo-activated, allowing assessment of extension, or a group of mesendodermal cells was labeled, allowing assessment of convergence. Pictures were taken immediately following uncaging (6 hpf), at 80% epiboly (8hpf) and at tailbud stage (10 hpf). As a measure for cell migration, the angles for dorsal convergence and anterior extension were determined using Image J software. Knockdown of Shp2 and expression of Noonan Syndrome mutant Shp2 induced significant defects in C&E cell movements, assessed using a caged fluorophore as described above [35]. We developed an alternative for these photo-activation experiments: time-lapse imaging of mesendodermal cells during gastrulation [36]. Briefly, all nuclei of a developing embryo are labeled by microinjection at the one-cell stage with fluorescently labeled Histone 1 protein (Histone 1 Alexa fluor 488; Molecular Probes). The embryos are dechorionated at 30% epiboly and mounted at shield stage in 1% low melting point agarose with the dorsal side against the coverslip approximately 100 µm anterior to shield position, facilitating visualization of the C&E cell movements of the epiblast. We use a Leica SP2 confocal microscope with a 40x objective and a 488 nm laser line for excitation of the fluorophore. Images are recorded every 2 minutes from shield stage until 1-somite stage. The timelapse images are analyzed using Image J software. The nuclear Histone 1 labeling is used to determine the position of individual nuclei in a single optical slice for each time point. Due to innate changes in intensity, size and shape of the fluorescent signal of the nuclei, additional image processing is needed for efficient tracing of the cells. The images are successively made binary, separated by a watershedding algorithm, eroded to a single pixel and dilated. Projection of the resulting image onto the original shows that the generated objects represent cell positions with a very high accuracy (> 99%) (Fig. 2D). These objects are readily traced over time, which generates a report with the Cartesian coordinates for all traced objects at each time point. These coordinates represent the contribution of cell migration to convergence (X-axis) and extension (Y-axis) and allow for quantification of migration of individual cells and of groups of cells. We have used this cell tracking method to compare C&E cell movements between wild type and *ptpra*-/- mutant embryos that lack functional RPTPα. *Ptpra*-/- embryos display significantly impaired C&E cell movements [36]. The latter cell tracking method does not rely on the use of a caged fluorophore, but instead a general cell identifier can be used. We have used fluorescently labeled Histone 1 for our experiments as well as a transgenic line, expressing nuclear GFP, with similar results (Runtuwene and den Hertog, unpublished results).

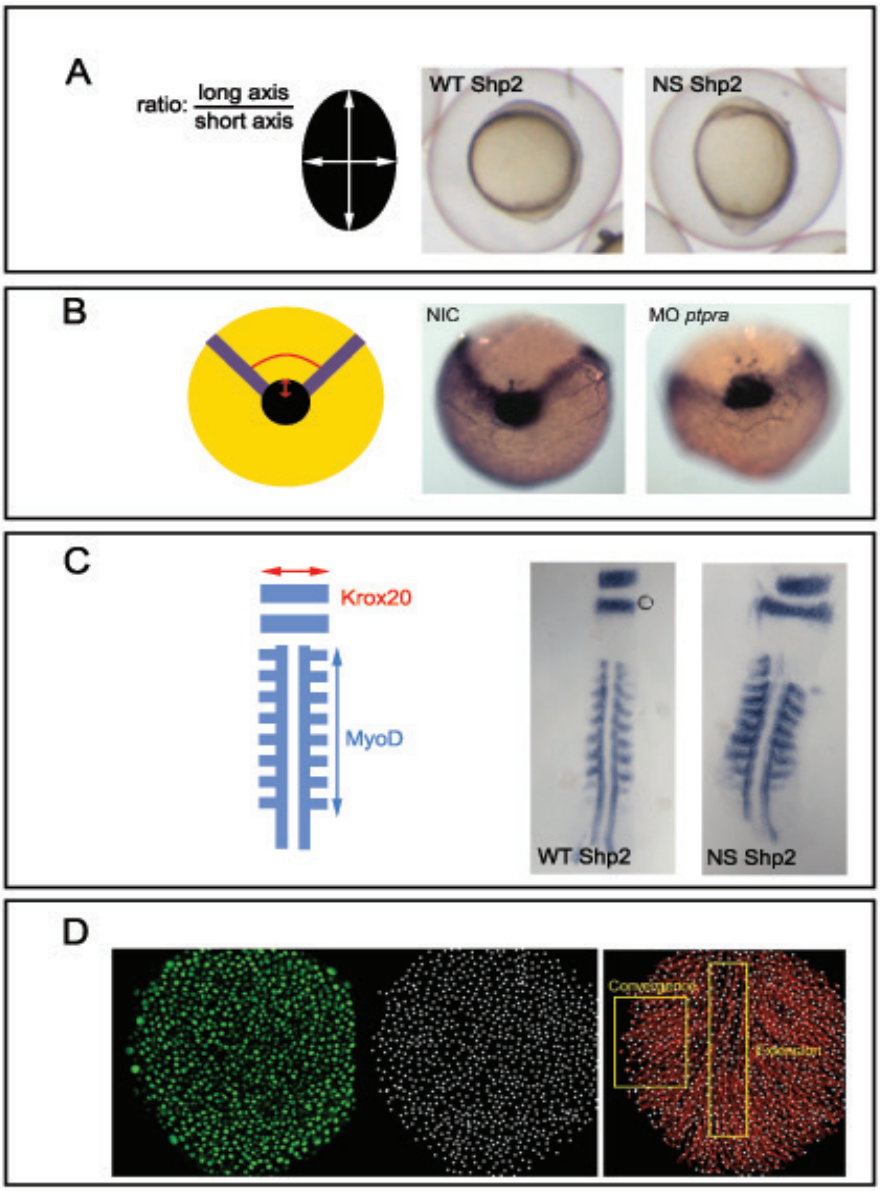

Figure 2. Quantitative analysis of defects in gastrulation cell movements. (A) Assessment of oval shape, (B) the width and relative position of molecular markers, *dlx3* and *hgg1* (currently known as *dlx3b* and *ctsl1b*, respectively), (C), the length and width of the developing embryo using molecular markers, *krox20* and *myod* and (D) migration of mesendodermal cells in the developing embryo can all be used as quantitative traits of C&E cell movements. In A-C a schematic representation is given next to an actual comparison of a control embryo (wildtype Shp2 injected, WT Shp2, or non-injected control, NIC) and an experimental embryo (Noonan Shp2 injected, NS Shp2, or *ptpra* morpholino-injected). In panel D the actual confocal image is compared to the image after processing. The right panel shows the cell tracks. Cell movements in the boxed areas are directly proportional to convergence (Con) and extension (Ext) cell movements, respectively. See text for details.

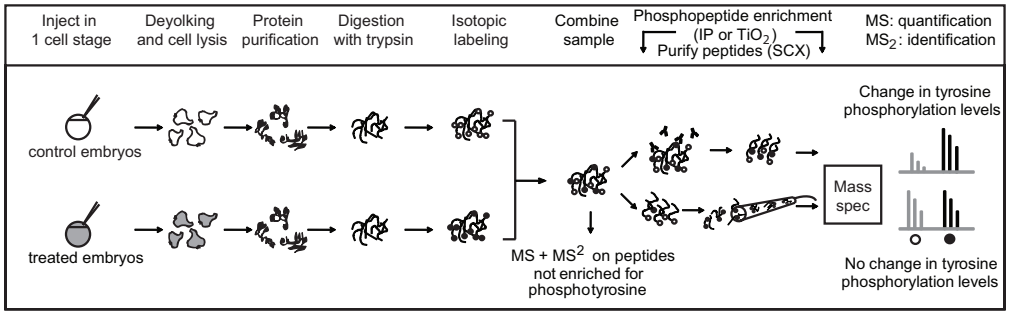

Figure 3. Phosphoproteomics analysis of zebrafish embryos. Zebrafish embryos (control and/or treated) are deyolked to remove excess yolk proteins which would otherwise interfere with mass spectrometric analysis. Embryos are lysed and proteins are purified and digested with trypsin. For quantification, we have used isotopic dimethyl labeling. Samples are then combined for direct analysis (reference pool of all peptides) and the samples are used for further processing. To enrich for phosphopeptides, either anti-pTyr immunoprecipitation or TiO_2 enrichment (for pSer, pThr and pTyr) are being used. Fractionation of peptides is performed using strong cation exchange after (pTyr IP) or prior to (TiO_2) phosphopeptide enrichment. Mass spectrometric analysis is performed to quantify (MS) and identify (MS_2) peptides of interest. See text for further details.

7. Phosphoproteomics in zebrafish

The methods above facilitate the analysis of PTP function at the organismal and cellular level. Biochemical analyses are required to understand the function of PTPs at the molecular level. Whereas the zebrafish is an excellent model system to unravel genetic pathways, biochemical analyses are lagging behind due to ill-understood difficulties in the use of antibodies in zebrafish lysates, even though the epitopes of the antibodies that are being used are highly or even perfectly conserved. Highly abundant yolk proteins are likely to interfere with protein analyses in zebrafish lysates, yet some antibodies work remarkably well in immunoblots and immunoprecipitation. Nevertheless, phosphoproteomic analysis of zebrafish embryos by mass spectrometry has provided some insight into the overall phosphoproteome of zebrafish embryos and may provide means to analyze the function of PTPs *in vivo* at the phosphoprotein level. As a first step to analyze PTP function at the molecular level *in vivo*, we set out to map the pTyr phosphoproteome in zebrafish embryos by anti-pTyr immunoprecipitation and mass spectrometry to identify phosphoproteins and protein phosphorylation sites [46]. In the process, we developed a protocol for quantitative phosphoproteomic analyses of zebrafish embryos: First, embryos are collected and excess yolk proteins are removed by washing with ice-cold deyolking buffer (Figure 3). The deyolked embryos may be snap-frozen until a sufficient amount of sample has been collected. Labeling of zebrafish embryos, similar to tissue culture cells with stable isotope labeling in culture (SILAC) is not feasible. Therefore, in order to compare different samples with eachother, peptides are labeled, either using iTRAQ or using stable isotope containing dimethyl [47]. While iTRAQ allows for a comparison of up to eight different conditions, dimethyl labeling is cost-effective and facilitates a comparison of up to three different samples. Purification of the sample is performed using either TiO2 columns which enrich for all phosphorylated peptides, or by pTyr-specific immunoprecipitation. Note that for pTyr immunoprecipitation collection of more sample (preferably >6 µg, or more than 2000 zebrafish embryos) is necessary than for TiO2. In contrast to pTyr immunoprecipitation, TiO2 can be used to purify all phosphopeptides and to analyze the phosphoproteome in relatively small samples, down to a single zebrafish embryo [48]. Using the TiO2 approach, we successfully analyzed the phosphoproteome of Fyn/Yes knockdown embryos that exhibit gastrulation cell movement defects [47]. Future analysis specifically of the pTyr

phosphoproteome of PTP knockdown or knockout embryos by immunoprecipitation of pTyr-containing peptides after proteolysis and subsequent peptide identification by mass spectrometry may lead to identification of direct substrates and elucidate PTP-proximal signaling.

8. Outlook

Here we describe genetic methods to manipulate gene function in zebrafish with the emphasis on PTPs. We explain how zebrafish can be used to study PTP function using a variety of quantitative methods to study general morphology and cell migration. Furthermore, we provide an overview of PTP studies performed in zebrafish and the genetic mutants available. In Table 1 we show that several PTPs have been studied in zebrafish, however, many are yet to be investigated. Additionally, genetic association studies have shown a role for PTPs in several diseases. Combined with the availability of genetic mutants this holds a big promise for zebrafish as tools to study PTPs. In addition, the advent of TALEN and CRISPR technology has facilitated the generation of targeted genetic mutations in the zebrafish genome and many more zebrafish mutants will be generated in the near future in which genes encoding PTPs are inactivated or contain mutations at specific positions. These genetic mutations will be crossed with transgenic lines in which fluorescent proteins are expressed in specific cells or tissues, allowing analysis of cell behavior *in vivo* by intravital imaging, thus providing insight into the function of PTPs at the cellular/organismal level. Analysis of the pTyr phosphoproteome of zebrafish embryos that lack the function of a specific PTP or that express mutant PTPs may result in identification of specific substrates and signaling pathways, thus providing insight into the function of PTPs at the molecular level *in vivo*. Using these methods, the zebrafish provides great opportunities to study PTP function in development and disease *in vivo*.

References

1. Tonks NK (2013) Protein tyrosine phosphatases--from housekeeping enzymes to master regulators of signal transduction. FEBS J 280: 346-378.
2. Hendriks WJ, Elson A, Harroch S, Pulido R, Stoker A, et al. (2013) Protein tyrosine phosphatases in health and disease. FEBS J 280: 708-730.
3. Hendriks WJ, Elson A, Harroch S, Stoker AW (2008) Protein tyrosine phosphatases: functional inferences from mouse models and human diseases. Febs J 275: 816-830.
4. Choorapoikayil S, Overvoorde J, den Hertog J (2013) Deriving cell lines from zebrafish embryos and tumors. Zebrafish: in press.
5. Driever W, Solnica-Krezel L, Schier AF, Neuhauss SC, Malicki J, et al. (1996) A genetic screen for mutations affecting embryogenesis in zebrafish. Development 123: 37-46.
6. Haffter P, Granato M, Brand M, Mullins MC, Hammerschmidt M, et al. (1996) The identification of genes with unique and essential functions in the development of the zebrafish, Danio rerio. Development 123: 1-36.
7. Lieschke GJ, Currie PD (2007) Animal models of human disease: zebrafish swim into view. Nat Rev Genet 8: 353-367.
8. Peterson RT, Link BA, Dowling JE, Schreiber SL (2000) Small molecule developmental screens reveal the logic and timing of vertebrate development. Proc Natl Acad Sci U S A 97: 12965-12969.
9. den Hertog J (2005) Chemical genetics: Drug screens in Zebrafish. Biosci Rep 25: 289-297.
10. Howe K, Clark MD, Torroja CF, Torrance J, Berthelot C, et al. (2013) The zebrafish reference genome sequence and its relationship to the human genome. Nature 496: 498-503.
11. Jaillon O, Aury JM, Brunet F, Petit JL, Stange-Thomann N, et al. (2004) Genome duplication in the teleost fish Tetraodon nigroviridis reveals the early vertebrate proto-karyotype. Nature 431: 946-957.
12. Vandepoele K, De Vos W, Taylor JS, Meyer A, Van de Peer Y (2004) Major events in the genome evolution of vertebrates: paranome age and size differ considerably between ray-finned fishes and land vertebrates. Proc Natl Acad Sci U S A 101: 1638-1643.
13. van Eekelen M, Overvoorde J, van Rooijen C, den Hertog J (2010) Identification and expression of the family of classical protein-tyrosine phosphatases in zebrafish. PLoS ONE 5: e12573.
14. van Eekelen M, Runtuwene V, Masselink W, den Hertog J (2012) Pair-Wise Regulation of Convergence and Extension Cell Movements by Four Phosphatases via RhoA. PLoS ONE 7: e35913.
15. Thisse C, Thisse B (2008) High-resolution in situ hybridization to whole-mount zebrafish embryos. Nat Protoc 3: 59-69.
16. Lele Z, Bakkers J, Hammerschmidt M (2001) Morpholino phenocopies of the swirl, snailhouse, somitabun, minifin, silberblick, and pipetail mutations. Genesis 30: 190-194.
17. Nasevicius A, Ekker SC (2000) Effective targeted gene 'knockdown' in zebrafish. Nat Genet 26: 216-220.
18. Wyatt L, Wadham C, Crocker LA, Lardelli M, Khew-Goodall Y (2007) The protein tyrosine phosphatase Pez regulates TGFbeta, epithelial-mesenchymal transition, and organ development. J Cell Biol 178: 1223-1235.
19. Chen X, Yoshida T, Sagara H, Mikami Y, Mishina M (2011) Protein tyrosine phosphatase sigma regulates the synapse number of zebrafish olfactory sensory neurons. J Neurochem 119: 532-543.
20. Wang F, Wolfson SN, Gharib A, Sagasti A (2012) LAR receptor tyrosine phosphatases and HSPGs guide peripheral sensory axons to the skin. Curr Biol 22: 373-382.
21. Carra S, Foglia E, Cermenati S, Bresciani E, Giampietro C, et al. (2012) Ve-ptp modulates vascular integrity by promoting adherens junction maturation. PLoS One 7: e51245.
22. Hayashi M, Majumdar A, Li X, Adler J, Sun Z, et al. (2013) VE-PTP regulates VEGFR2 activity in stalk cells to establish endothelial cell polarity and lumen formation. Nat Commun 4: 1672.
23. Liao WH, Cheng CH, Hung KS, Chiu WT, Chen GD, et al. (2013) Protein tyrosine phosphatase receptor type O (Ptpro) regulates cerebellar formation during zebrafish development through modulating Fgf signaling. Cell Mol Life Sci.
24. Kanwal Z, Zakrzewska A, den Hertog J, Spaink HP, Schaaf MJ, et al. (2013) Deficiency in hematopoietic phosphatase ptpn6/Shp1 hyperactivates the innate immune system and impairs control of bacterial infections in zebrafish embryos. J Immunol 190: 1631-1645.
25. Wienholds E, Schulte-Merker S, Walderich B, Plasterk RH (2002) Target-selected inactivation of the zebrafish rag1 gene. Science 297: 99-102.
26. Kettleborough RN, Busch-Nentwich EM, Harvey SA, Dooley CM, de Bruijn E, et al. (2013) A systematic genome-wide analysis of zebrafish protein-coding gene function. Nature 496: 494-497.
27. Faucherre A, Taylor GS, Overvoorde J, Dixon JE, den Hertog J (2008) Zebrafish pten genes have overlapping and non-redundant functions in tumorigenesis and embryonic development. Oncogene 27: 1079-1086.
28. Choorapoikayil S, Kuiper RV, de Bruin A, den Hertog J (2012) Haploinsufficiency of the genes encoding the tumor suppressor Pten predisposes zebrafish to hemangiosarcoma. Dis Model Mech 5: 241-247.
29. Doyon Y, McCammon JM, Miller JC, Faraji F, Ngo C, et al. (2008) Heritable targeted gene disruption in zebrafish using designed zinc-finger nucleases. Nat Biotechnol 26: 702-708.
30. Meng X, Noyes MB, Zhu LJ, Lawson ND, Wolfe SA (2008) Targeted gene inactivation in zebrafish using engineered zinc-finger nucleases. Nat Biotechnol 26: 695-701.

31. Bedell VM, Wang Y, Campbell JM, Poshusta TL, Starker CG, et al. (2012) In vivo genome editing using a high-efficiency TALEN system. Nature 491: 114-118.
32. Hwang WY, Fu Y, Reyon D, Maeder ML, Tsai SQ, et al. (2013) Efficient genome editing in zebrafish using a CRISPR-Cas system. Nat Biotechnol 31: 227-229.
33. Solnica-Krezel L (2006) Gastrulation in zebrafish -- all just about adhesion? CurrOpinGenetDev 16: 433-441.
34. Keller PJ, Schmidt AD, Wittbrodt J, Stelzer EH (2008) Reconstruction of zebrafish early embryonic development by scanned light sheet microscopy. Science 322: 1065-1069.
35. Jopling C, van Geemen D, den Hertog J (2007) Shp2 knockdown and Noonan/LEOPARD mutant Shp2-induced gastrulation defects. PLoS Genet 3: e225.
36. van Eekelen M, Runtuwene V, Overvoorde J, den Hertog J (2010) RPTPalpha and PTPepsilon signaling via Fyn/Yes and RhoA is essential for zebrafish convergence and extension cell movements during gastrulation. Dev Biol 340: 626-639.
37. Aerne B, Ish-Horowicz D (2004) Receptor tyrosine phosphatase psi is required for Delta/Notch signalling and cyclic gene expression in the presomitic mesoderm. Development 131: 3391-3399.
38. Stewart RA, Sanda T, Widlund HR, Zhu S, Swanson KD, et al. (2010) Phosphatase-dependent and -independent functions of Shp2 in neural crest cells underlie LEOPARD syndrome pathogenesis. Dev Cell 18: 750-762.
39. Jopling C, den Hertog J (2005) Fyn/Yes and non-canonical Wnt signalling converge on RhoA in vertebrate gastrulation cell movements. EMBO Rep 6: 426-431.
40. Jopling C, den Hertog J (2007) Essential role for Csk upstream of Fyn and Yes in zebrafish gastrulation. Mech Dev 124: 129-136.
41. Habas R, Dawid IB, He X (2003) Coactivation of Rac and Rho by Wnt/Frizzled signaling is required for vertebrate gastrulation. Genes Dev 17: 295-309.
42. Anastasaki C, Estep AL, Marais R, Rauen KA, Patton EE (2009) Kinase-activating and kinase impaired cardio-facio-cutaneous syndrome alleles have activity during zebrafish development and are sensitive to small molecule inhibitors. Hum Mol Genet 18: 2543-2554.
43. Runtuwene V, van Eekelen M, Overvoorde J, Rehmann H, Yntema HG, et al. (2011) Noonan syndrome gain-of-function mutations in NRAS cause zebrafish gastrulation defects. Dis Model Mech 4: 393-399.
44. Li C, Inglis PN, Leitch CC, Efimenko E, Zaghloul NA, et al. (2008) An essential role for DYF-11/MIP-T3 in assembling functional intraflagellar transport complexes. PLoS Genet 4: e1000044.
45. Bakkers J, Kramer C, Pothof J, Quaedvlieg NE, Spaink HP, et al. (2004) Has2 is required upstream of Rac1 to govern dorsal migration of lateral cells during zebrafish gastrulation. Development 131: 525-537.
46. Lemeer S, Ruijtenbeek R, Pinkse MW, Jopling C, Heck AJ, et al. (2007) Endogenous phosphotyrosine signaling in zebrafish embryos. Mol Cell Proteomics 6: 2088-2099.
47. Lemeer S, Jopling C, Gouw J, Mohammed S, Heck AJ, et al. (2008) Comparative phosphoproteomics of zebrafish Fyn/Yes morpholino knockdown embryos. Mol Cell Proteomics 7: 2176-2187.
48. Lemeer S, Pinkse MW, Mohammed S, van Breukelen B, den Hertog J, et al. (2008) Online automated in vivo zebrafish phosphoproteomics: from large-scale analysis down to a single embryo. J Proteome Res 7: 1555-1564.

Noonan and LEOPARD syndrome: an overview

Monica Bonetti[1] and Jeroen den Hertog[1,2]

1.Hubrecht Institute-KNAW and University Medical Centre Utrecht, the Netherlands
2. Institute of Biology Leiden, Leiden University, the Netherlands

Noonan syndrome (NS) (OMIM:163950) is a common (1:2000) heterogeneous syndrome that is related to other clinical syndromes associated with the RAS-MAPK pathway, including LEOPARD syndrome (LS) (OMIM:151100), cardio-facio-cutaneous (CFC) syndrome (OMIM:115150), neurofibromatosis type 1 (NF1) (OMIM:162200) and Costello syndrome (CS) (OMIM:218040). Collectively, these syndromes are termed RASopathies.

1. Symptoms

Noonan syndrome is characterized by short stature, congenital heart defects, including pulmonary stenosis, low set ears, webbed neck, hypertelorism, low set eyelids and chest deformities [1] (Figure 1). Whereas these features are prominent in a large group of NS patients, some patients may either be of normal height, or have less prominent craniofacial features. Other features include scoliosis, deafness and an increased propensity to develop leukemia. Whereas some patients exhibit cognitive defects as well, many NS patients have normal intelligence [2]. Noonan patients have a higher chance of developing juvenile myelomonocytic leukaemia (JMML), and mice carrying the D61G NS mutation develop myeloproliferative disease [3]. Moreover, Gab2, a downstream effector of Shp2, is essential for the aetiology of the myeloproliferative disorder, since double-mutant mice lacking Gab2 are less likely to develop myeloproliferative disease than Shp2 D61G knock-in mice [3]. A paternal origin for *de novo* mutations has been observed in NS, with a possible link to the age of the father as well [4]. Additionally, transmission of NS is skewed maternally, that may be attributed to the reduced fertility in male NS patients [4].

LEOPARD syndrome, an acronym of Lentigines, Electrocardiographic conduction anomalies, Ocular hypertelorism, Pulmonary stenosis, Abnormal genitalia, Retarded growth and sensorineural Deafness is clinically very similar to NS. Patients exhibiting LS are often initially diagnosed with NS. Only when certain 'café au lait' spots or lentigines appear during early adolescence a clinical distinction is often made between NS and LS. Whereas NS and LS share many common characteristics, several clinical features are unevenly distributed among NS and LS patients. For instance, pulmonary stenosis (PS) is more common in NS, whereas hypertrophic cardiomyopathy (HCM) is more prevalent in LS [5]. Additionally, craniofacial defects are more prominent in NS than in LS patients and LS patients exhibit less height deficits than NS. Postnatal growth retardation is a clinical manifestation of NS and LS patients. Approximately 70% of adults with NS are below the 10th percentile for height [6] and 85% of adults with LS are below the 25th percentile [7]. The short stature in NS patients is generally due to a decrease in responsiveness to growth hormone (GH), as evidenced by reduced levels of insulin-like growth factor 1 (IGF-1) [8-11]. A Ptpn11 Noonan syndrome mouse model displays increased ERK activation in response to growth hormone; blocking MAPK signaling restores IGF-1 levels, thus reducing the postnatal growth retardation in these mice [8]. The molecular basis of growth defects in LS is less well understood.

2. Genetics

Roughly 50% of all cases of NS are caused by mutations in *PTPN11* while heterozygous missense mutations in *PTPN11* are observed in up to 90% of LS cases. Other mutations have been identified in genes encoding for proteins along the RAS-MAPK pathway. Mutations were identified in *MEK1*, *MEK2*, *KRAS*, *NRAS* and in *SHOC2* [12-16]. Also *RAF1* and *BRAF* gain of function mutations were identified in patients with NS and LS [17,18] (Figure. 2). Mutations in *CBL*, an E3 ubiquitin ligase with tumour suppressing activity, are causative of Noonan-like syndrome [19]. Moreover, Noonan-

like symptoms are associated with mutations in the histone methyltransferase, *MYST4*, resulting in enhanced MAPK signalling [20]. The genetic cause of some 25% of all Noonan cases still remains to be determined. It is evident that these patients do not have mutations in any of the known Noonan syndrome-associated genes.

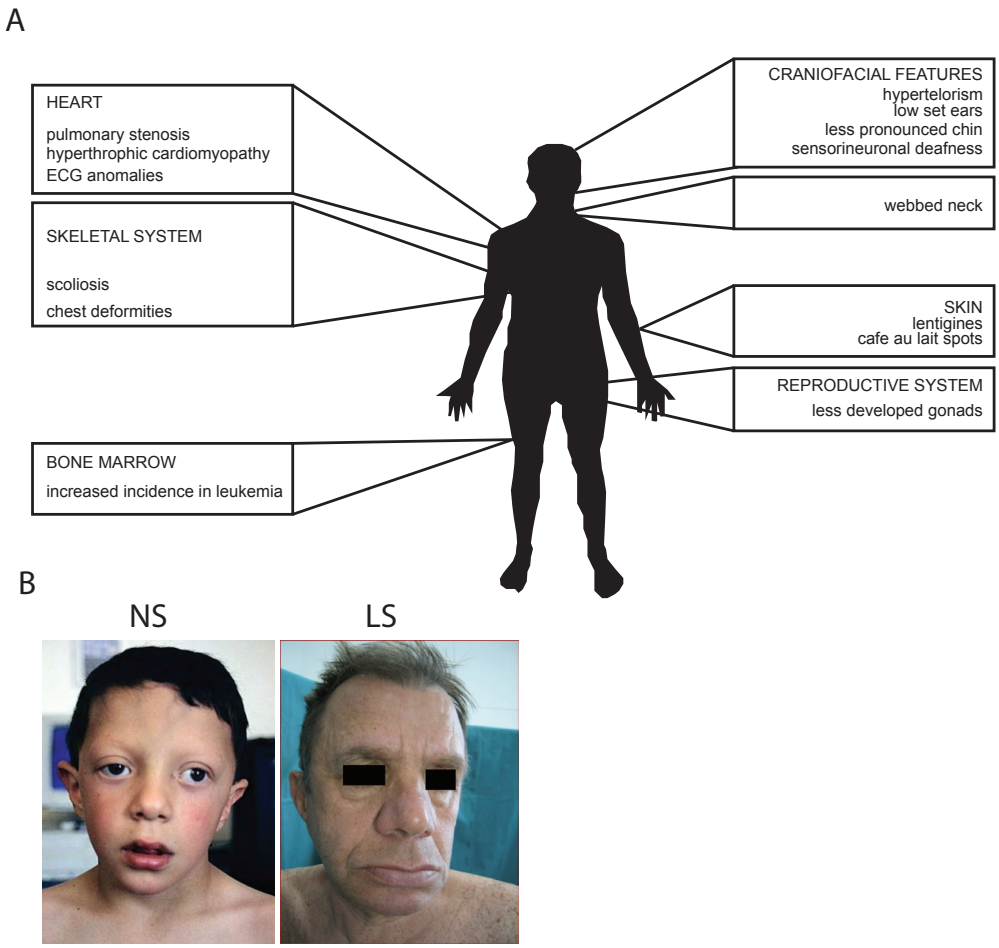

Figure 1. Clinical characteristics and facies of Noonan and LEOPARD syndrome patients. A) Diagnosis of Noonan and LEOPARD syndrome is primarily dependent on clinical features, including short stature, typical face dysmorphology, and congenital heart defects. Diagnosis can be difficult due to the wide spectrum of clinical features, not all of which need to be present for diagnosis. Cardinal features of Noonan and LEOPARD syndrome include hypertelorism, ptosis, and low-set, posteriorly rotated ears with a thickened helix. Cardiac abnormalities most commonly associated with the two syndromes include pulmonary stenosis (NS) and hypertrophic cardiomyopathy (LS). Other associated features include the presence of a webbed neck, chest deformity, mild intellectual deficit, cryptorchidism, poor feeding in infancy, bleeding tendencies, and lymphatic issues. B) Photographs of families diagnosed with Noonan [81] and LEOPARD [82] syndrome with mutations in *PTPN11*.

3. Mechanism

Whereas mutations that cause NS all result in a phosphatase hyperactive form of Shp2, LS causing mutations in Shp2 all display strongly reduced phosphatase activity [21,22]. How is it possible that two seemingly opposite mutations cause similar clinical features? Examination of the structural mechanism of Shp2 revealed a gain-of-function in NS forms of Shp2, giving rise to a hyperactive form [23]. NS mutations predominantly reside in the interface between the N-SH2 domain and the PTP domain, resulting in the impairment of the closed conformation and enhanced catalytic activity of NS-Shp2 [24,25]. By contrast, most LS mutations reside close to the active site and result in strongly reduced, yet detectable, catalytic activity [24,26,27] (Chapter 1). Phosphatase assays have shown a catalytic defect in LS Shp2 [24,26,28]. LS-Shp2 mutations are mostly located in the protein-tyrosine phosphatase (PTP) domain, and the local conformational changes induced by LS-Shp2 mutations impair the catalytic properties of Shp2 [29]. However, in vivo, LS Shp2 may act as a gain-of-function as well [30]. In flies, LS mutations give rise to gain-of-function defects that cause upregulation of MAPK and require residual PTP activity of Shp2 [30]. LS-Shp2 displays residual phosphatase activity [26,27]. LS mutations cause loss of phosphatase activity and at the same time result in enhanced binding to Gab1 and PI3K [26]. Further investigation showed that LS, unlike NS causes activation of the PI3K-AKT pathways upon growth factor stimulation [31]. This is due to enhanced phosphorylation of Gab1 due to the loss of phosphatase activity of LS Shp2 [31]. Enhanced PI3K activation likely contributes to the discrepancies between NS and LS. PI3K/AKT signaling is upregulated in hearts of LS/+ knock-in mice [22] as well as in fibroblasts isolated from LS patients [31]. Despite these explanations it remains unclear how activating and inactivating mutants of Shp2 can generate overlapping syndromes. Most probably, NS and LS share some of their targets in order for them to generate the overlapping clinical features.

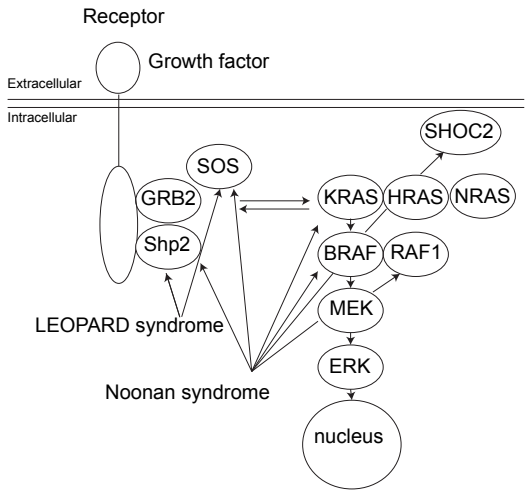

Figure 2. Overview of the RAS-MAPK pathway associated with NS/LS disorders. Syndromes caused by mutations in genes of RAS-MAPK signalling proteins are indicated.

4. Spatiotemporal control

Cardio-facio-cutaneous (CFC) syndrome is one of the RASopathies, and is caused by mutations in *BRAF*, *MEK1* or *MEK2*. Like NS, activating mutations give rise to short stature, heart defects and craniofacial defects arising from hyperactivation of the MAPK pathway. In zebrafish, NS and CFC induced gastrulation defects can be rescued by treatment with the MEK inhibitor CI-1040 [14,32]. Importantly, inhibitor treatment is only required during a small temporal window prior to shield formation [14,32]. Not only temporal control but also spatial control (membrane-bound versus cytoplasmic, or lipid-raft versus non-lipid raft localization) of protein signalling is likely a vital aspect in the aetiology of RASopathies. SHOC2 is a scaffolding protein that binds RAS and RAF. Under normal stimulation, SHOC2 is

targeted to late endosomes and activates ERK1/2 [33]. An interesting finding was that a mutation in SHOC2 that causes Noonan-like syndrome with loose anagen hair results in N-myristoylation of SHOC2. This causes aberrant translocation of SHOC2 to the cell membrane instead of late endosomes, which results in enhanced MAPK activation in a cell-type specific manner [13,33]. Interestingly, whereas NS mutations in Shp2 and SHOC2 are additive [34], NS and LS mutations in Shp2 are not [28]. Moreover, NS associated mutations in *RAF1* cause enhanced heterodimerization with BRAF which also results in enhanced ERK activation [35]. More importantly, not only kinase-impaired D486N RAF1 but also kinase-activating NS forms of RAF1 required heterodimerization with BRAF to enhance MEK/ERK activation [35]. Interestingly, RAF1 mutations have been found in NS and LS patients, suggesting a common mechanism for NS and LS [17].

Targeting of Shp2 to lipid rafts results in integrin clustering, Focal Adhesion Kinase phosphorylation, Rho and ERK activation, all of which are hallmarks of fibronectin attachment [36]. Shp2 is targeted to lipid rafts upon adhesion, and dominant negative RhoA blocks Shp2 induced signalling. In addition, Shp2 phosphatase activity is essential for negative feedback to Rho [36]. The downstream target of Shp2, RhoA, also prevents apoptosis by activating the MAPK pathway and expression of *bcl-2*, in zebrafish [37]. A phosphatase independent, but SH2 domain dependent role for LS Shp2 was described in preventing p53 mediated apoptosis in the brain and neural crest, suggesting that the SH2 domain of Shp2 may be essential for RhoA activation [37,38]. An emerging model is that under basal conditions, Shp2 binds Abl, which activates p190 RhoGAP, which in turn inactivates Rho. In its active state, Shp2 inactivates p190 RhoGAP by dephosphorylation. In addition, Shp2 dephosphorylates an inhibiting tyrosine phosphorylation site on ROCKII, causing activation of the pathway [39]. It is noteworthy that NS Shp2-mediated activation of ROCKII causes heart defects in Xenopus [40].

Recently, a role for Ephrin signalling has been implicated in Shp2 mediated ERK activation [41]. Hepatic growth factor (HGF) induced ERK activation is dependent on EphA2 phosphorylating the C-terminal tyrosines, Y542 and Y580 of Shp2, thereby mediating prolonged Grb2 binding and ERK activation. Interestingly, ERK activation is independent of Shp2 phosphatase activity, since expression of T468M (LS) or a N308D (NS) variant enhanced ERK activation. Mutation of the C-terminal tyrosines in the LS background suppress ERK activation as well, suggesting an essential role for these tyrosines in mediating ERK activation. Comparison of Shp2 knockdown embryos and zebrafish embryos expressing LS-Shp2 allowed assessment of a phosphatase and ERK dependent role for Shp2 in zebrafish neural crest specification and cell migration [38].

Shp2 phosphatase activity plays a role in cell migration. IGF1, which cooperates with integrins to promote cellular migration and invasion [42,43] , mediates IRS1 binding to a complex containing FAK, paxilin and Shp2. This results in the dephosphorylation of FAK and paxilin. Interestingly, Shp2 phosphatase activity is essential for integrin deactivation since Shp2 C460S expressing cells show higher numbers of focal adhesion contacts [44]. This is likely independent of ERK activation since treatment with a MEK inhibitor did not attenuate this effect [44]. Shp2 also mediates activation of Fyn kinase at focal adhesion sites in a catalytic activity independent manner, where Shp2 binds to a6b4 integrin via its N-SH2 domain and to Fyn with its C terminal tyrosine Y580, thereby acting as a docking protein [45]. Additionally, Fyn phosphorylates Shp2 Y542, thereby providing a positive feedback loop [45]. Also Src kinase is known to be activated by, and bound to Shp2 in a catalytically independent manner [46]. Whereas the SH3 domain of Src was essential for this binding, a specific Src binding site has not yet been identified in Shp2 [46]. Other kinases also influence Shp2 function, as Abl phosphorylates Shp2, at Y580. Interestingly, Abl indirectly causes

phosphorylation of target sites in Shp2 that are located at or near residues often mutated in NS and LS respectively, namely Y63 and Y279 [47]. Phosphorylation of Y279 caused a decrease in growth factor mediated ERK activation [47]. Other pathways than the Rho, MAPK and Src pathways are also controlled by Shp2, like the JAK/STAT pathway. In contrast to these other pathways, Shp2 plays an inhibiting role [48]. Interestingly, down regulation of Stat3 by activating variants of Shp2 may contribute to pulmonary stenosis in NS and myeloproliferative disorder in JMML [49]. Indeed, phosphorylated Stat3 is inhibited by active Shp2, and expression of active Stat3 rescues the activating Shp2 defects in bone marrow cells [49].

Several attempts have been made to find an inhibitor for Shp2 for treatment and use in biochemical assays [50]. One of these, NSC-87877 binds to the catalytic site of the PTP domain and is able to inhibit Shp2 mediated, growth factor induced ERK activation [50]. In addition, phenylhydrazonopyrazolone sulfonate (PHPS1) was identified by an *in silico* screen, and further tested *in vitro* for its phosphatase inhibitory capacity [51]. PHPS1 was able to inhibit HGF induced cell scattering that is mediated by Shp2 phosphatase activity [51]. However, these compounds only target the phosphatase dependent function of Shp2, while Shp2 also exhibits phosphatase independent mechanisms.

Thus, Shp2 is involved in a plethora of signalling mechanisms and one can imagine that biochemical changes in the enzyme may result in widespread defects. In LS patient derived induced pluripotent stem (iPS) cells, several downstream proteins are hyper- or hypo-tyrosyl phosphorylated [52]. Interestingly, although LS Shp2 is thought to result in a decreased ability to activate the ERK pathway following growth factor stimulation due to its loss of phosphatase activity, basal levels of MEK are upregulated in these cells [52]. Gene expression profiling of NS and Noonan-like syndrome patients show that many alterations are present on the transcriptional level and that NS-specific gene expression signatures are distinguished [53]. NS Shp2 expressing cells show enhanced expression of Src family kinase substrates, indicating that these proteins may play an essential role in the aetiology of Shp2 induced NS [53].

5. Cardiac defects associated with NS and LS

Noonan and LEOPARD patients share several clinical manifestations, including scoliosis, facial dysmorphic features, short stature and congenital heart defects. Despite those clinical similarities, the heart defects are quite distinct between Noonan and LEOPARD patients. The most common cardiac defect in NS is pulmonary stenosis (PS) resulting from dysplastic valve leaflets, but stenosis of mitral valve, atrial, ventricular, and atrio-ventricular septal defects, or, rarely, double-outlet right ventricle are also seen [54,55]. Moreover, hypertrophic cardiomyopathy (HCM) has been found in few NS patients without Shp2 mutations [56] and genotype-phenotype correlation studies show that only 8% of Shp2-associated NS patients present with HCM [57]. HCM is most commonly present in NS patients with mutations in *RAF1* [58]. Electrocardiogram (ECG) of NS patients often shows a characteristic pattern, with a left axis deviation, abnormal R/S ratio over the left precordium, and an abnormal Q wave. These ECG features are characteristic for NS and they are not related to a specific cardiac defect (PS or HCM) [59]. In contrast, the most common cardiac defect in LS is HCM, but similar valve anomalies to NS are also observed [60].

Although Shp2 is a major player in cardiac disease, its function in heart development in NS and LS remains poorly addressed. Several animal models have been used to investigate the role of Shp2 in NS and LS. The injection of the most prevalent human NS Shp2 mutations into *Xenopus* results

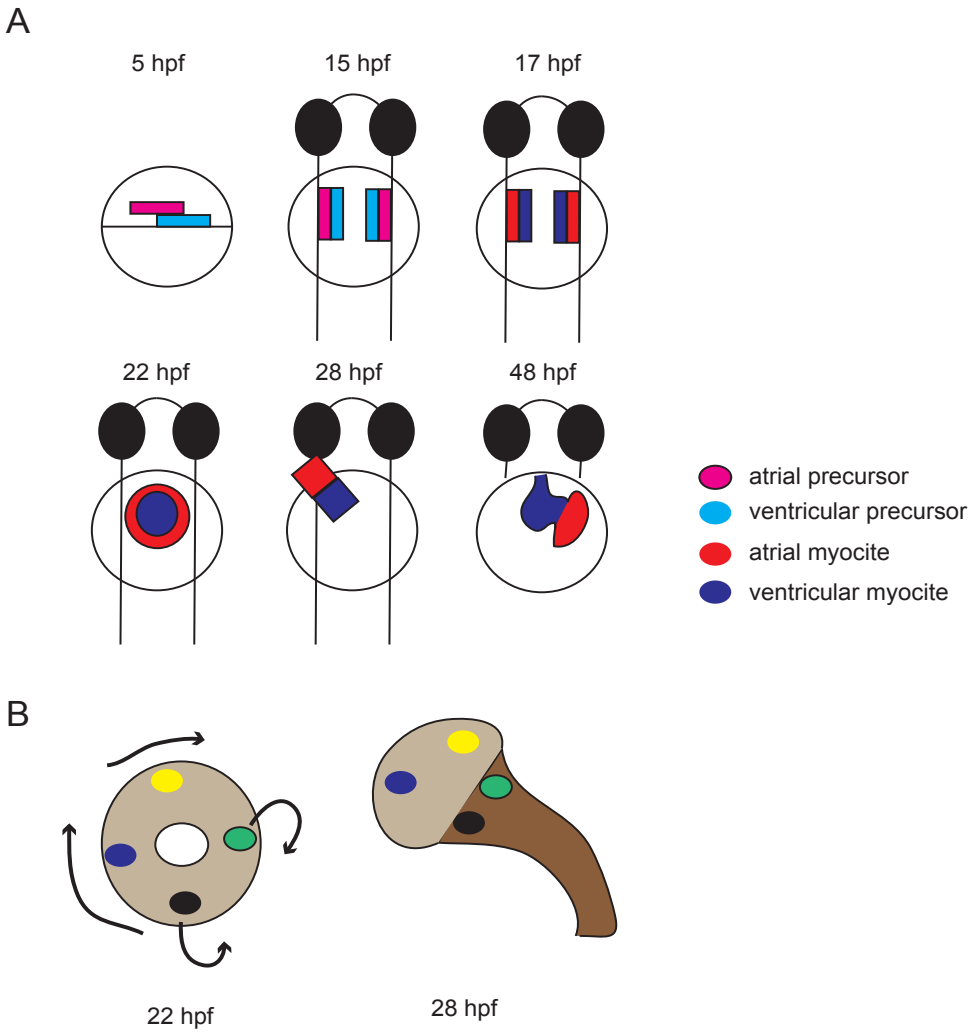

Figure 3. Stages of cardiac development.
A) At 5 h post fertilization (hpf) cardiac progenitor cells are positioned bilaterally in the lateral marginal zone of the blastula. Atrial progenitor cells (pink) are located more ventrally than the ventricle progenitor cells (light blue). During gastrulation, the cardiac progenitor cells move dorsally towards the mid-line to end up in the anterior later plate mesoderm (ALPM). At 17 hpf, the future ventricle and atrial myocardial cells differentiate because of the expression of cardiac myosins (blue/red). The bilateral heart fields fuse at the mid-line (22hpf), forming a cardiac disc structure with the ventricular myocytes internally and atrial myocytes externally of the disc. Cardiac morphogenesis transforms the cardiac disc into a cardiac tube. At 28 hpf, the linear heart tube has formed. At 36 hpf, cardiac looping has started, with a displacement of the ventricle towards the mid-line. The heart tube continues to loop and forms an S-shaped loop (48 hpf).
B) Cartoon in which the migration, rotation and involution of the cardiac tissue during heart tube formation is indicated. The color-coding of the 4 cells indicates the original and the final position of the cardiomyocytes [63, 69].

in hearts that failed to complete looping or undergo chamber formation coupled with a delay or arrest of the cardiac cell cycle in M-phase [40]. Similarly, the overexpression of NS and LS Shp2 mRNA in zebrafish embryos at the 1-cell stage result in heart displacement defects at 24 hpf [28]. Moreover, NS and LS Shp2 induce convergence and extension cell movement defects at the end of gastrulation, followed by the development of craniofacial defects and reduced body axis length at 4dpf [28].

The mouse model expressing the NS-associated mutant D61G develops short stature, craniofacial abnormalities and multiple cardiac defects, including pulmonary stenosis and double outlet of the right ventricle (DORV). Their endocardial cushions show an increased Erk activation. When homozygous, the D61G mutant is embryonic lethal [61]. Similarly the knockin mice harboring the LS *Ptpn11* mutation Y279C recapitulates the human disorder, showing short stature, craniofacial dysmorphia, and HCM. LS/+ mice also exhibit increased Akt/mTOR activity and the inhibition of mTOR signaling with rapamycin completely normalized and reversed the LS cardiac defects [62]. Conclusively, LS models support the conclusion that excessive AKT/mTOR activity, not MAPK, is essential for the development and maintenance of HCM.

6. Zebrafish as a model to study heart development.

The role of NS and LS Shp2 variants in the development of cardiac defects is still unclear. Zebrafish has become a powerful model to study cardiac development in recent years [63,64]. Moreover, the transparency of zebrafish embryos facilitates time-lapse analysis of the onset and nature of the cardiac defects *in vivo*. The heart is the first organ to form and function during zebrafish embryo development. Heart development begins with the specification of myocardial and endocardial progenitor cells. Before gastrulation, 5 h post fertilization (hpf), the heart progenitor cells are formed and placed in the ventral and lateral regions of the embryo. Atrial progenitor cells are located more ventrally in the lateral marginal zone when compared with ventricular progenitor cells [65]. By 14 somites (17hpf), the cardiac progenitors cells appear as two bilateral pools on the lateral plate mesoderm (LPM) [66]. Next, by 22 somites (22 hpf), these pools combine at the LPM to form the heart disk. This disk moves anteriorly and to the left and forms the heart tube (24-28 hpf). Afterwords, by 30 hpf, ventricular and atrial chambers form. By 36 hpf, the heart undergoes looping morphogenesis and, by 48 hpf, functional valves are formed (Figure 3A)[66]. Up to 22 somites, the heart morphogenesis is a symmetrical process because there are no morphological differences between the left and right cardiac fields. However, after the cardiac disc formation, the myocardial tissue originating from the right cardiac field involutes ventrally and moves towards the anterior/left (Figure 3B). In this way, the left–right organization of the cardiac disc change into a dorsal–ventral organization of the cardiac tube. Four-dimensional confocal miscroscopy and the automated cell tracking showed that co-occurring with right-field involution, the myocardial disc rotates in a clockwise direction [67-69]. As a consequence of these moviments, the cardiac tube is created, with its venous pole located at the left side and its arterial pole located at the mid-line. Breaking of the heart symmetry is initiated by a transient ciliated organ called Kupffer's vesicle that is derived from the dorsal forerunner cells (DFCs) [70,71]. Cilia within the KV rotate in a counter-clockwise direction, thus generating a fluid flow in the same direction [72,73]. The directional fluid flow in the KV induces asymmetric expression of two conserved L/R signaling genes *pitx2* (a *bicoid*-related transcription factor) and *southpaw* (*spaw*, a Nodal-related gene) in the LPM. The bilateral expression of *spaw*/*nodal* starts around the KV at the 4 somite stage and its expression resides in the perinodal area [74]. At around the 10–12 somite stage, *spaw*/*nodal* expression starts in the LPM. The left-sided *spaw*/*nodal* expression moves to the

anterior part of the embryo [74]. At late somite stages, the leftward expression of *southpaw* overlaps with the left-sided expression of other genes, such as *lefty2*. *Spaw*/*nodal* is proposed to be a significant player in the diffusion of the asymmetric expression in the left LPM, together with the activation of its own antagonists, Lefty1 and Lefty2 [75]. In particular, Lefty1 has the function to block the nodal expression on the right-side of the LPM. *Lefty1* expression acts in the midline as physical barrier to avoid the diffusion of asymmetric signal in the LPM to the right side, preventing the right LPM to acquire a left-sided identity [76]. Impairment of the L/R patterning determination can cause either a randomized positioning of organs (*situs ambiguus*) or a mirror-image duplication of organs (*situs inversus*). In humans, clinically significant laterality defects occur in 1 in 10,000 births [77]. The mortality associated with laterality defects is always ascribed to complex congenital heart defects. In fact the heart morphogenesis is very susceptible to impairments in the left-right (LR) body plan. The heart tube undergoes looping morphogenesis quite early in vertebrate development and before the heart tube has completed its formation. Because cardiac looping is a highly conserved process, the directionality of the heart loop can predict the body *situs* [78]. As the heart tube proceeds in the elongation, it develops a dextral loop ("d" loop). The process of looping and the directionality of the loop are important for normal heart development. Because most cardiac structures originate from cells derived from more than one area of the heart tube, the significant function of looping is to rearrange regions of the heart tube so they are appropriately positioned for proper formation and alignment of chambers, valves, and septa. Thus, the directionality of looping establishes once the left ventricle underlies the left atrium, and the right ventricle beneath the right atrium [79]. The heart shows an atrio-ventricular (A-V) concordance only when the position of the ventricles is correct. Moreover, L/R chambers division is fundamental for the functions of the heart and if L/R asymmetry is abnormal, one or more congenital defects may arise. These defects range from atrial septal defects (ASD) or ventral septal defects (VSD) to the double outlet of the right ventricle (DORV) and transposition of the great arteries (TGA). It is noteworthy that laterality disease is frequently associated with congenital heart defects (CHD) [80]. However, cardiac defects associated with laterality diseases are also reported in Shp2-D61G knock-in mice. A proportion of the heterozygous Shp2-D61G mice displays septal defects and DORV [61]. However, laterality defects are not the only cause of septation defects or DORV. Hence, it remains to be determined whether laterality defects have a role in human NS and LS. Overall the zebrafish model is becoming a very powerful model to study cardiac development. By evolving new and more specific assays, the zebrafish model can be used to study mechanisms leading to human cardiac diseases and to model human congenital cardiac diseases.

References

1. Tartaglia M, Gelb BD (2005) Noonan syndrome and related disorders: genetics and pathogenesis. Annu Rev Genomics Hum Genet 6: 45-68.
2. van der Burgt I (2007) Noonan syndrome. Orphanet J Rare Dis 2: 4.
3. Xu D, Wang S, Yu WM, Chan G, Araki T, et al. (2010) A germline gain-of-function mutation in Ptpn11 (Shp-2) phosphatase induces myeloproliferative disease by aberrant activation of hematopoietic stem cells. Blood 116: 3611-3621.
4. Tartaglia M, Cordeddu V, Chang H, Shaw A, Kalidas K, et al. (2004) Paternal germline origin and sex-ratio distortion in transmission of PTPN11 mutations in Noonan syndrome. Am J Hum Genet 75: 492-497.
5. Sarkozy A, Conti E, Seripa D, Digilio MC, Grifone N, et al. (2003) Correlation between PTPN11 gene mutations and congenital heart defects in Noonan and LEOPARD syndromes. J Med Genet 40: 704-708.
6. Noonan JA, Raaijmakers R, Hall BD (2003) Adult height in Noonan syndrome. Am J Med Genet A 123A: 68-71.
7. Gorlin RJ, Anderson RC, Blaw M (1969) Multiple lentigenes syndrome. Am J Dis Child 117: 652-662.
8. De Rocca Serra-Nedelec A, Edouard T, Treguer K, Tajan M, Araki T, et al. (2012) Noonan syndrome-causing SHP2 mutants inhibit insulin-like growth factor 1 release via growth hormone-induced ERK hyperactivation, which contributes to short stature. Proc Natl Acad Sci U S A 109: 4257-4262.
9. Binder G, Neuer K, Ranke MB, Wittekindt NE (2005) PTPN11 mutations are associated with mild growth hormone resistance in individuals with Noonan syndrome. J Clin Endocrinol Metab 90: 5377-5381.
10. Limal JM, Parfait B, Cabrol S, Bonnet D, Leheup B, et al. (2006) Noonan syndrome: relationships between genotype, growth, and growth factors. J Clin Endocrinol Metab 91: 300-306.
11. Noordam C, Peer PG, Francois I, De Schepper J, van den Burgt I, et al. (2008) Long-term GH treatment improves adult height in children with Noonan syndrome with and without mutations in protein tyrosine phosphatase, non-receptor-type 11. Eur J Endocrinol 159: 203-208.
12. Schubbert S, Zenker M, Rowe SL, Boll S, Klein C, et al. (2006) Germline KRAS mutations cause Noonan syndrome. Nat Genet 38: 331-336.
13. Cordeddu V, Di Schiavi E, Pennacchio LA, Ma'ayan A, Sarkozy A, et al. (2009) Mutation of SHOC2 promotes aberrant protein N-myristoylation and causes Noonan-like syndrome with loose anagen hair. Nat Genet 41: 1022-1026.
14. Runtuwene V, van Eekelen M, Overvoorde J, Rehmann H, Yntema HG, et al. (2011) Noonan syndrome gain-of-function mutations in NRAS cause zebrafish gastrulation defects. Dis Model Mech 4: 393-399.
15. Carta C, Pantaleoni F, Bocchinfuso G, Stella L, Vasta I, et al. (2006) Germline missense mutations affecting KRAS Isoform B are associated with a severe Noonan syndrome phenotype. Am J Hum Genet 79: 129-135.
16. Dentici ML, Sarkozy A, Pantaleoni F, Carta C, Lepri F, et al. (2009) Spectrum of MEK1 and MEK2 gene mutations in cardio-facio-cutaneous syndrome and genotype-phenotype correlations. Eur J Hum Genet 17: 733-740.
17. Pandit B, Sarkozy A, Pennacchio LA, Carta C, Oishi K, et al. (2007) Gain-of-function RAF1 mutations cause Noonan and LEOPARD syndromes with hypertrophic cardiomyopathy. Nat Genet 39: 1007-1012.
18. Sarkozy A, Carta C, Moretti S, Zampino G, Digilio MC, et al. (2009) Germline BRAF mutations in Noonan, LEOPARD, and cardiofaciocutaneous syndromes: molecular diversity and associated phenotypic spectrum. Hum Mutat 30: 695-702.
19. Martinelli S, De Luca A, Stellacci E, Rossi C, Checquolo S, et al. (2010) Heterozygous germline mutations in the CBL tumor-suppressor gene cause a Noonan syndrome-like phenotype. Am J Hum Genet 87: 250-257.
20. Kraft M, Cirstea IC, Voss AK, Thomas T, Goehring I, et al. (2011) Disruption of the histone acetyltransferase MYST4 leads to a Noonan syndrome-like phenotype and hyperactivated MAPK signaling in humans and mice. J Clin Invest 121: 3479-3491.
21. Tartaglia M, Martinelli S, Stella L, Bocchinfuso G, Flex E, et al. (2006) Diversity and functional consequences of germline and somatic PTPN11 mutations in human disease. Am J Hum Genet 78: 279-290.
22. Kontaridis MI, Swanson KD, David FS, Barford D, Neel BG (2006) PTPN11 (Shp2) mutations in LEOPARD syndrome have dominant negative, not activating, effects. J Biol Chem 281: 6785-6792.
23. Darian E, Guvench O, Yu B, Qu CK, MacKerell AD, Jr. (2011) Structural mechanism associated with domain opening in gain-of-function mutations in SHP2 phosphatase. Proteins 79: 1573-1588.
24. Keilhack H, David FS, McGregor M, Cantley LC, Neel BG (2005) Diverse biochemical properties of Shp2 mutants. Implications for disease phenotypes. J Biol Chem 280: 30984-30993.
25. Nakamura T, Gulick J, Pratt R, Robbins J (2009) Noonan syndrome is associated with enhanced pERK activity, the repression of which can prevent craniofacial malformations. Proc Natl Acad Sci U S A 106: 15436-15441.
26. Hanna N, Montagner A, Lee WH, Miteva M, Vidal M, et al. (2006) Reduced phosphatase activity of SHP-2 in LEOPARD syndrome: consequences for PI3K binding on Gab1. FEBS Lett 580: 2477-2482.
27. Yu ZH, Xu J, Walls CD, Chen L, Zhang S, et al. (2013) Structural and mechanistic insights into LEOPARD syndrome-associated SHP2 mutations. J Biol Chem 288: 10472-10482.
28. Jopling C, van Geemen D, den Hertog J (2007) Shp2 knockdown and Noonan/LEOPARD mutant Shp2-induced gastrulation defects. PLoS Genet 3: e225.
29. Qiu W, Wang X, Romanov V, Hutchinson A, Lin A, et al. (2014) Structural insights into Noonan/LEOPARD syndrome-related mutants of protein-tyrosine phosphatase SHP2 (PTPN11). BMC Struct Biol 14: 10.

30. Oishi K, Zhang H, Gault WJ, Wang CJ, Tan CC, et al. (2009) Phosphatase-defective LEOPARD syndrome mutations in PTPN11 gene have gain-of-function effects during Drosophila development. Hum Mol Genet 18: 193-201.
31. Edouard T, Combier JP, Nedelec A, Bel-Vialar S, Metrich M, et al. (2010) Functional effects of PTPN11 (SHP2) mutations causing LEOPARD syndrome on epidermal growth factor-induced phosphoinositide 3-kinase/AKT/glycogen synthase kinase 3beta signaling. Mol Cell Biol 30: 2498-2507.
32. Anastasaki C, Estep AL, Marais R, Rauen KA, Patton EE (2009) Kinase-activating and kinase-impaired cardio-facio-cutaneous syndrome alleles have activity during zebrafish development and are sensitive to small molecule inhibitors. Hum Mol Genet 18: 2543-2554.
33. Galperin E, Abdelmoti L, Sorkin A (2012) Shoc2 is targeted to late endosomes and required for Erk1/2 activation in EGF-stimulated cells. PLoS One 7: e36469.
34. Ekvall S, Hagenas L, Allanson J, Anneren G, Bondeson ML (2011) Co-occurring SHOC2 and PTPN11 mutations in a patient with severe/complex Noonan syndrome-like phenotype. Am J Med Genet A 155A: 1217-1224.
35. Wu X, Yin J, Simpson J, Kim KH, Gu S, et al. (2012) Increased BRAF heterodimerization is the common pathogenic mechanism for noonan syndrome-associated RAF1 mutants. Mol Cell Biol 32: 3872-3890.
36. Lacalle RA, Mira E, Gomez-Mouton C, Jimenez-Baranda S, Martinez AC, et al. (2002) Specific SHP-2 partitioning in raft domains triggers integrin-mediated signaling via Rho activation. J Cell Biol 157: 277-289.
37. Zhu S, Korzh V, Gong Z, Low BC (2008) RhoA prevents apoptosis during zebrafish embryogenesis through activation of Mek/Erk pathway. Oncogene 27: 1580-1589.
38. Stewart RA, Sanda T, Widlund HR, Zhu S, Swanson KD, et al. (2010) Phosphatase-dependent and -independent functions of Shp2 in neural crest cells underlie LEOPARD syndrome pathogenesis. Dev Cell 18: 750-762.
39. Tandon P, Conlon FL, Taylor JM (2012) ROCKs cause SHP-wrecks and broken hearts. Small GTPases 3: 209-212.
40. Langdon Y, Tandon P, Paden E, Duddy J, Taylor JM, et al. (2012) SHP-2 acts via ROCK to regulate the cardiac actin cytoskeleton. Development 139: 948-957.
41. Miura K, Wakayama Y, Tanino M, Orba Y, Sawa H, et al. (2013) Involvement of EphA2-mediated tyrosine phosphorylation of Shp2 in Shp2-regulated activation of extracellular signal-regulated kinase. Oncogene.
42. Akiyama SK, Olden K, Yamada KM (1995) Fibronectin and integrins in invasion and metastasis. Cancer Metastasis Rev 14: 173-189.
43. Felding-Habermann B, Mueller BM, Romerdahl CA, Cheresh DA (1992) Involvement of integrin alpha V gene expression in human melanoma tumorigenicity. J Clin Invest 89: 2018-2022.
44. Manes S, Mira E, Gomez-Mouton C, Zhao ZJ, Lacalle RA, et al. (1999) Concerted activity of tyrosine phosphatase SHP-2 and focal adhesion kinase in regulation of cell motility. Mol Cell Biol 19: 3125-3135.
45. Yang X, Dutta U, Shaw LM (2010) SHP2 mediates the localized activation of Fyn downstream of the alpha6beta4 integrin to promote carcinoma invasion. Mol Cell Biol 30: 5306-5317.
46. Walter AO, Peng ZY, Cartwright CA (1999) The Shp-2 tyrosine phosphatase activates the Src tyrosine kinase by a non-enzymatic mechanism. Oncogene 18: 1911-1920.
47. Mitra S, Beach C, Feng GS, Plattner R (2008) SHP-2 is a novel target of Abl kinases during cell proliferation. J Cell Sci 121: 3335-3346.
48. You M, Yu DH, Feng GS (1999) Shp-2 tyrosine phosphatase functions as a negative regulator of the interferon-stimulated Jak/STAT pathway. Mol Cell Biol 19: 2416-2424.
49. Zhang W, Chan RJ, Chen H, Yang Z, He Y, et al. (2009) Negative regulation of Stat3 by activating PTPN11 mutants contributes to the pathogenesis of Noonan syndrome and juvenile myelomonocytic leukemia. J Biol Chem 284: 22353-22363.
50. Chen L, Sung SS, Yip ML, Lawrence HR, Ren Y, et al. (2006) Discovery of a novel shp2 protein tyrosine phosphatase inhibitor. Mol Pharmacol 70: 562-570.
51. Hellmuth K, Grosskopf S, Lum CT, Wurtele M, Roder N, et al. (2008) Specific inhibitors of the protein tyrosine phosphatase Shp2 identified by high-throughput docking. Proc Natl Acad Sci U S A 105: 7275-7280.
52. Carvajal-Vergara X, Sevilla A, D'Souza SL, Ang YS, Schaniel C, et al. (2010) Patient-specific induced pluripotent stem-cell-derived models of LEOPARD syndrome. Nature 465: 808-812.
53. Ferrero GB, Picco G, Baldassarre G, Flex E, Isella C, et al. (2012) Transcriptional hallmarks of Noonan syndrome and Noonan-like syndrome with loose anagen hair. Hum Mutat 33: 703-709.
54. Marino B, Digilio MC, Toscano A, Giannotti A, Dallapiccola B (1999) Congenital heart diseases in children with Noonan syndrome: An expanded cardiac spectrum with high prevalence of atrioventricular canal. J Pediatr 135: 703-706.
55. Yoshida R, Hasegawa T, Hasegawa Y, Nagai T, Kinoshita E, et al. (2004) Protein-tyrosine phosphatase, nonreceptor type 11 mutation analysis and clinical assessment in 45 patients with Noonan syndrome. J Clin Endocrinol Metab 89: 3359-3364.
56. Tartaglia M, Kalidas K, Shaw A, Song X, Musat DL, et al. (2002) PTPN11 mutations in Noonan syndrome: molecular spectrum, genotype-phenotype correlation, and phenotypic heterogeneity. Am J Hum Genet 70: 1555-1563.
57. Sznajer Y, Keren B, Baumann C, Pereira S, Alberti C, et al. (2007) The spectrum of cardiac anomalies in Noonan syndrome as a result of mutations in the PTPN11 gene. Pediatrics 119: e1325-1331.
58. Roberts AE, Allanson JE, Tartaglia M, Gelb BD (2013) Noonan syndrome. Lancet 381: 333-342.

59. Raaijmakers R, Noordam C, Noonan JA, Croonen EA, van der Burgt CJ, et al. (2008) Are ECG abnormalities in Noonan syndrome characteristic for the syndrome? Eur J Pediatr 167: 1363-1367.
60. Limongelli G, Pacileo G, Marino B, Digilio MC, Sarkozy A, et al. (2007) Prevalence and clinical significance of cardiovascular abnormalities in patients with the LEOPARD syndrome. Am J Cardiol 100: 736-741.
61. Araki T, Mohi MG, Ismat FA, Bronson RT, Williams IR, et al. (2004) Mouse model of Noonan syndrome reveals cell type- and gene dosage-dependent effects of Ptpn11 mutation. Nat Med 10: 849-857.
62. Marin TM, Keith K, Davies B, Conner DA, Guha P, et al. (2011) Rapamycin reverses hypertrophic cardiomyopathy in a mouse model of LEOPARD syndrome-associated PTPN11 mutation. J Clin Invest 121: 1026-1043.
63. Bakkers J (2011) Zebrafish as a model to study cardiac development and human cardiac disease. Cardiovasc Res 91: 279-288.
64. Lien CL, Harrison MR, Tuan TL, Starnes VA (2012) Heart repair and regeneration: recent insights from zebrafish studies. Wound Repair Regen 20: 638-646.
65. Keegan BR, Meyer D, Yelon D (2004) Organization of cardiac chamber progenitors in the zebrafish blastula. Development 131: 3081-3091.
66. Yelon D, Horne SA, Stainier DY (1999) Restricted expression of cardiac myosin genes reveals regulated aspects of heart tube assembly in zebrafish. Dev Biol 214: 23-37.
67. Baker K, Holtzman NG, Burdine RD (2008) Direct and indirect roles for Nodal signaling in two axis conversions during asymmetric morphogenesis of the zebrafish heart. Proc Natl Acad Sci U S A 105: 13924-13929.
68. de Campos-Baptista MI, Holtzman NG, Yelon D, Schier AF (2008) Nodal signaling promotes the speed and directional movement of cardiomyocytes in zebrafish. Dev Dyn 237: 3624-3633.
69. Smith KA, Chocron S, von der Hardt S, de Pater E, Soufan A, et al. (2008) Rotation and asymmetric development of the zebrafish heart requires directed migration of cardiac progenitor cells. Dev Cell 14: 287-297.
70. Cooper MS, D'Amico LA (1996) A cluster of noninvoluting endocytic cells at the margin of the zebrafish blastoderm marks the site of embryonic shield formation. Dev Biol 180: 184-198.
71. Melby AE, Warga RM, Kimmel CB (1996) Specification of cell fates at the dorsal margin of the zebrafish gastrula. Development 122: 2225-2237.
72. Essner JJ, Amack JD, Nyholm MK, Harris EB, Yost HJ (2005) Kupffer's vesicle is a ciliated organ of asymmetry in the zebrafish embryo that initiates left-right development of the brain, heart and gut. Development 132: 1247-1260.
73. Kramer-Zucker AG, Olale F, Haycraft CJ, Yoder BK, Schier AF, et al. (2005) Cilia-driven fluid flow in the zebrafish pronephros, brain and Kupffer's vesicle is required for normal organogenesis. Development 132: 1907-1921.
74. Long S, Ahmad N, Rebagliati M (2003) The zebrafish nodal-related gene southpaw is required for visceral and diencephalic left-right asymmetry. Development 130: 2303-2316.
75. Branford WW, Yost HJ (2002) Lefty-dependent inhibition of Nodal- and Wnt-responsive organizer gene expression is essential for normal gastrulation. Curr Biol 12: 2136-2141.
76. Lohr JL, Danos MC, Groth TW, Yost HJ (1998) Maintenance of asymmetric nodal expression in Xenopus laevis. Dev Genet 23: 194-202.
77. Peeters H, Devriendt K (2006) Human laterality disorders. Eur J Med Genet 49: 349-362.
78. Manner J (2000) Cardiac looping in the chick embryo: a morphological review with special reference to terminological and biomechanical aspects of the looping process. Anat Rec 259: 248-262.
79. Franco D, Kelly R, Moorman AF, Lamers WH, Buckingham M, et al. (2001) MLC3F transgene expression in iv mutant mice reveals the importance of left-right signalling pathways for the acquisition of left and right atrial but not ventricular compartment identity. Dev Dyn 221: 206-215.
80. Ramsdell AF (2005) Left-right asymmetry and congenital cardiac defects: getting to the heart of the matter in vertebrate left-right axis determination. Dev Biol 288: 1-20.
81. Digilio M, Marino B (2001) Clinical manifestations of Noonan syndrome. Images Paediatr Cardiol 3: 19-30.
82. Porciello R, Divona L, Strano S, Carbone A, Calvieri C, et al. (2008) Leopard syndrome. Dermatol Online J 14: 7.

Distinct and overlapping functions of *ptpn11* genes in zebrafish development

Monica Bonetti[1], Virginia Rodriguez-Martinez[1], Jeroen Paardekooper Overman[1], John Overvoorde[1], Mark van Eekelen[1], Chris Jopling[1] and Jeroen den Hertog[1,2]

1 Hubrecht Institute-KNAW and University Medical Center Utrecht, 3584 CT Utrecht, The Netherlands
2 Institute of Biology 2333 CC, Leiden, The Netherlands; Corresponding author (j.denhertog@hubrecht.eu).

PLoS One, 2014, April 15; 9(4): e94884

Abstract

The *PTPN11* (protein-tyrosine phosphatase, non-receptor type 11) gene encodes SHP2, a cytoplasmic PTP that is essential for vertebrate development. Mutations in *PTPN11* are associated with Noonan and LEOPARD syndrome. Human patients with these autosomal dominant disorders display various symptoms, including short stature, craniofacial defects and heart abnormalities. We have used the zebrafish as a model to investigate the role of Shp2 in embryonic development. The zebrafish genome encodes two *ptpn11* genes, *ptpn11a* and *ptpn11b*. Here, we report that *ptpn11a* is expressed constitutively and *ptpn11b* expression is strongly upregulated during development. In addition, the products of both *ptpn11* genes, Shp2a and Shp2b, are functional. Target-selected inactivation of *ptpn11a* and *ptpn11b* revealed that double homozygous mutants are embryonic lethal at 5-6 days post fertilization (dpf). *Ptpn11a*$^{-/-}$*ptpn11b*$^{-/-}$ embryos showed pleiotropic defects from 4 dpf onwards, including reduced body axis extension and craniofacial defects, which was accompanied by low levels of phosphorylated Erk at 5 dpf. Interestingly, defects in homozygous *ptpn11a*$^{-/-}$ mutants overlapped with defects in the double mutants albeit they were milder, whereas *ptpn11b*$^{-/-}$ single mutants did not show detectable developmental defects and were viable and fertile. *Ptpn11a*$^{-/-}$*ptpn11b*$^{-/-}$ mutants were rescued by expression of exogenous *ptpn11a* and *ptpn11b* alike, indicating functional redundance of Shp2a and Shp2b. The *ptpn11* mutants provide a good basis for further unravelling of the function of Shp2 in vertebrate development.

Introduction

The *PTPN11* (protein-tyrosine phosphatase, non-receptor type 11) gene encodes SHP2, a ubiquitously expressed cytoplasmic protein-tyrosine phosphatase (PTP) with two Src homology 2 (SH2) domains that is essential for normal development [1-3]. SHP2 is a positive effector of extracellular regulated kinase (ERK)/MAPK signal transduction, downstream of most receptor tyrosine kinases (RTKs) [2] [3]. Moreover, Shp2 is involved in other signal transduction processes as well, including Jak-STAT signaling [3] and PI3K-AKT (also known as PI3K-PKB) signaling [2].
Missense mutations in the *PTPN11* gene are associated with the dominantly inherited genetic disorders, Noonan syndrome (NS) (OMIM 163950) and LEOPARD syndrome (LS) (OMIM 151100) [4-9]. These syndromes share several overlapping features, including facial dysmorphism, cardiovascular defects, hearing loss, growth retardation and scoliosis [7,10]. NS variants of SHP2 have increased PTP activity [2]. By contrast, most LS variants of SHP2 display reduced catalytic activity [11-14]. NS-associated mutations in Shp2 promote Erk/MAPK signaling [2]. Yet, the role of LS Shp2-variants in Erk/MAPK signaling is less clear, in that both activation and inhibition of Erk/MAPK signaling have been observed in LS [11,14-18]. Nevertheless, signaling by NS- and LS-variants of SHP2 is distinct, because LS-SHP2, but not NS-SHP2, affects AKT (PKB) signaling [12,19]. The mechanism underlying how NS- and LS-variants of SHP2 induce similar defects in development remains to be determined.

Shp2 has an essential role in early development in the mouse [20]. Homozygous *Ptpn11*$^{-/-}$ embryos die pre-implantation due to defective Erk activation and trophoblast stem cell death [20], precluding the possibility to study Shp2 function in differentiated cell types in adult animals. This problem was partially overcome with the use of conditional Shp2 knockout mice [21-23]. For example, mice with a *Ptpn11* deletion in the cardiomyocytes show that Shp2 is required for the suppression of dilated cardiomyopathy [22]. Conditional deletion of Shp2 in neural progenitor cells results in early postnatal lethality, impaired corticogenesis, and reduced proliferation of progenitor cells in the ventricular zone [21]. In an aged mouse model, hepatocyte-specific deletion of *Ptpn11* promotes inflammatory signalling and hepatic inflammation/necrosis, resulting in regenerative hyperplasia and spontaneous development of tumors [24]. Furthermore, a study in *Xenopus* shows that dominant-negative Shp2 mutants failed to complete gastrulation, resulting in severe posterior truncations [25]. In zebrafish, Shp2 knockdown embryos show a reduction of the body axis extension at 10 hours post fertilization (hpf) that is consistent with gastrulation defects. In addition, at later stages, the embryos are shorter and develop a hammerhead phenotype [26,27]. These data show that Shp2 is a crucial player in the development of many different organisms.

In our study we used zebrafish as a model to further investigate the role of Shp2. The zebrafish has proven to be an excellent experimental model to study gene function *in vivo* and to analyze vertebrate embryogenesis as development occurs externally and the embryos are transparent [28]. We identified two zebrafish *ptpn11* genes (*ptpn11a* and *ptpn11b*), encoding Shp2a and Shp2b, respectively. We demonstrate that *ptpn11a* was constitutively expressed and *ptpn11b* expression increased during early embryogenesis. *Ptpn11a* and *ptpn11b* both encoded functional proteins with similar catalytic activity. We used target selected gene inactivation (TSGI) to identify stop mutations in the N-terminal SH2 domain of each of the two *ptpn11* genes. Our study showed that *ptpn11b*$^{-/-}$ zebrafish were viable and fertile and showed no abnormal phenotype during development. However, single homozygous mutants for *ptpn11a* and double homozygous mutant embryos exhibited abnormalities such as craniofacial defects and reduced length, and these

mutants died at 5 days post fertilization (dpf). Moreover, we found that Shp2 deletion suppressed Erk activation in double mutant embryos, but not in embryos lacking only Shp2a or Shp2b. Together, our observations demonstrate that Shp2 is essential for zebrafish development, and that *ptpn11a* has a more pronounced role as the result of its higher expression level at early stages.

Results

Characterization of zebrafish ptpn11 *genes*

The zebrafish genome encodes two *ptpn11* genes: *ptpn11a* and *ptpn11b* [33]. The homology between human Shp2 and zebrafish Shp2a and Shp2b, encoded by *ptpn11a* and *ptpn11b* genes, is 91% and 64% respectively (Figure S1). Due to the genome duplication that occurred in teleosts it is not uncommon for zebrafish to have two homologous copies of a gene that is present as a single copy in other vertebrates [34,35]. To analyze stage-specific expression of *ptpn11a* and *ptpn11b* mRNA in wild-type (WT) embryos, we used a reverse transcription PCR (RT-PCR) approach. Expression levels were analysed at 4 hpf, 10 hpf, 1 dpf, 2 dpf, 3 dpf and 5 dpf. *Ptpn11a* and *ptpn11b* mRNA are both expressed from 4 hpf to 5 dpf (Figure 1A). *Ptpn11a* mRNA was expressed at similar levels at all stages. By contrast, *ptpn11b* mRNA was hardly detectable at early stages and *ptpn11b* expression increased during development. To confirm this result, *ptpn11a* and *ptpn11b* expression levels were examined at 10 hpf, 1dpf, 2dpf, 3dpf and 5 dpf by quantitative PCR. *Ptpn11a* expression was constantly maintained in all the stages whereas *ptpn11b* gene was expressed at low levels at early stages and became strongly upregulated over time (Figure 1B). *In situ* hybridization experiments showed that the two zebrafish *ptpn11* genes were broadly expressed throughout embryonic development (Figure 1C). Both *ptpn11* genes were maternally expressed and later in development the expression was restricted to the more anterior region of the developing embryo. Overall, these results show that both *ptpn11* genes were expressed throughout developing zebrafish embryos. *Ptpn11a* appears to be expressed at a constant level, whereas *ptpn11b* expression is low initially and is strongly upregulated over time.

Zebrafish Shp2a and Shp2b displayed phosphatase activity

Previously, we assessed that Shp2a is an active phosphatase and that mutant Shp2a-D61G with a mutation that was identified in human NS patients shows an increased phosphatase activity compared to wild type Shp2a [26]. To investigate if the *ptpn11b* gene product was functional, we expressed Shp2b in bacteria in parallel with Shp2a and investigated phosphatase activity. Both Shp2a and Shp2b displayed phosphatase activity and dephosphorylated *p*-nitrophenylphosphate (*p*NPP) to a similar extent. Moreover, Shp2b-D61G showed an increase in activity compared to WT-Shp2b, resembling the Shp2a-D61G mutant (Figure 2). These results demonstrate that both Shp2 proteins encoded by the zebrafish genome were functional PTPs *in vitro*.

Generation of ptpn11 *knock-out zebrafish*

We identified germline mutations in the zebrafish *ptpn11* genes, using the target-selected gene inactivation (TSGI) strategy, developed at the Hubrecht Institute [30]. Mutant alleles *ptpn11a* hu3459 and *ptpn11b* hu5920 contained nonsense mutations in exon 3 of *ptpn11a* and *ptpn11b*, respectively (Figure 3). We denoted the homozygous mutants as *ptpn11a*$^{-/-}$ and *ptpn11b*$^{-/-}$ because the premature stops are well upstream of the phosphatase catalytic site and hence, no functional protein is produced. *Ptpn11a*$^{+/-}$ and *ptpn11b*$^{+/-}$ fish were viable and fertile and these fish were incrossed to generate homozygous fish. Genotypes were obtained at mendelian ratios until 5 dpf. *Ptpn11a*$^{-/-}$ fish did not reach adulthood. By contrast, homozygous *ptpn11b*$^{-/-}$ fish were viable and

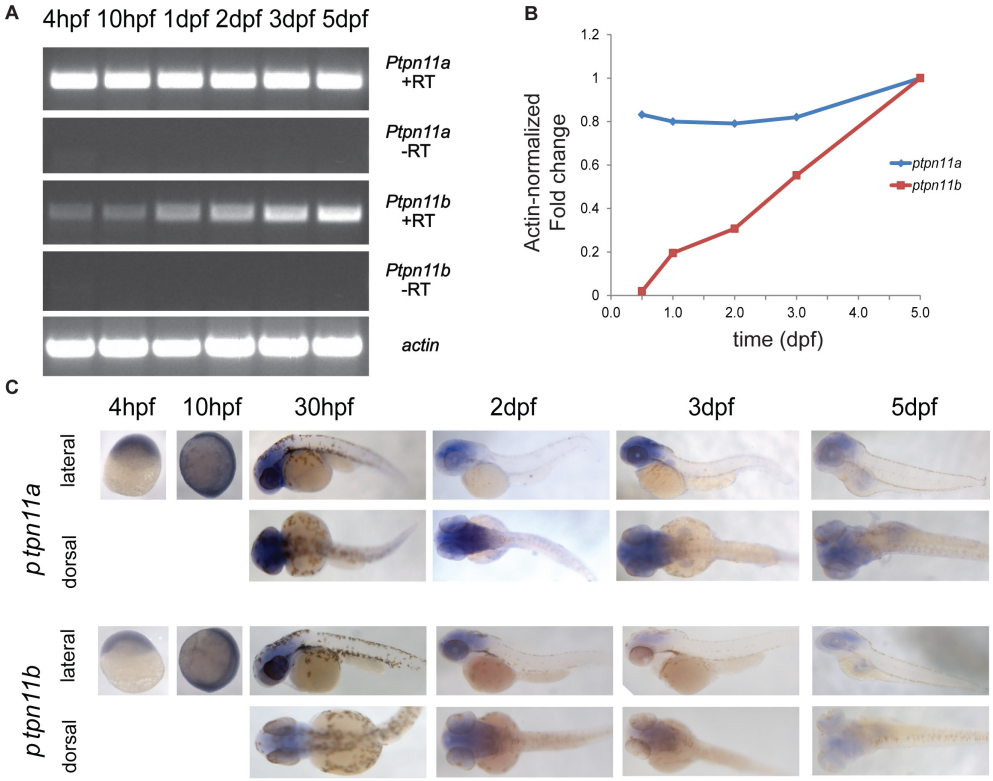

Figure 1. Expression of zebrafish *ptpn11a* and *ptpn11b* mRNA during embryogenesis. (a) RNA was isolated from zebrafish embryos at 4hpf, 10 hpf, 1 dpf, 2 dpf, 3dpf and 5dpf. Reverse transcription PCR was performed to detect the indicated genes; reverse transcriptase was omitted from the reaction as a control (-RT). (b) Quantitative PCR for *ptpn11a* and *ptpn11b* gene expression was performed from a pool of wild-type embryos (n=30) collected at 10 hpf, 1 dpf, 2 dpf, 3 dpf and 5dpf. The values were normalized using Actin as a control and relative expression is depicted here (value at 5 dpf set to 1.0). Error bars indicate standard error of the mean. (c) Whole-mount *in situ* hybridization using *ptpn11a* and *ptpn11b* specific probes of 4 hpf, 10 hpf, 30 hpf, 2 dpf, 3 dpf and 5 dpf embryos. Lateral and dorsal views are given as indicated.

Characteristics	***ptpn11a*$^{-/-}$**	***ptpn11b*$^{-/-}$**	***ptpn11a*$^{-/-}$ *ptpn11b*$^{-/-}$**
Head	Reduced in some cases	Normal	Enlarged by edema. Prominent jaw
Heart	Normal	Normal	Severe edema
Swim bladder	Absent	Normal	Absent
Length	Shorter	Normal	Shorter
Ventral region	Reduced, skinny appearance	Normal	Grossly edematous. Reduced organs.

Table1. Characteristic features of *ptpn11a*$^{-/-}$, *ptpn11b* $^{-/-}$ and double mutant embryos.

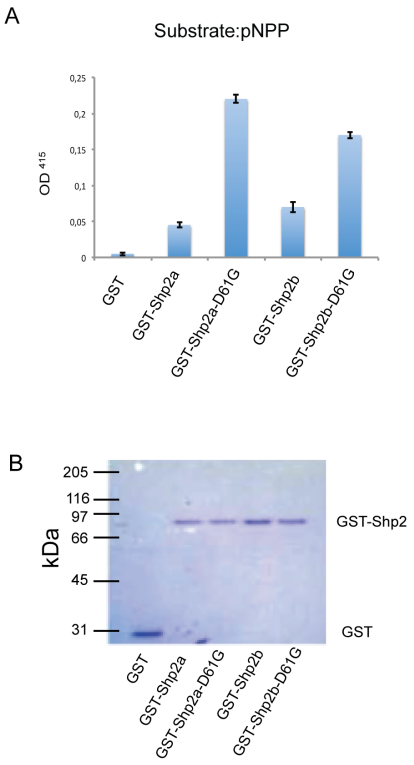

Figure 2. Shp2a and Shp2b proteins displayed phosphatase activity.
(a) PTP activity of pGEX, WT-Shp2a, Shp2a-D61G, WT-Shp2b and Shp2b-D61G was assayed using *p*-nitrophenylphosphate (*p*NPP) and quantified spectrophotometrically. Approximately 1 µg purified fusion protein was used in the assay. Experiments were done in quadruplicate; averages are depicted and error bars indicate standard error of the mean. (b) Equivalent amounts of fusion protein that were used in the activity assays in (a) were run on an SDS-PAGE gel and stained with Coomassie blue.

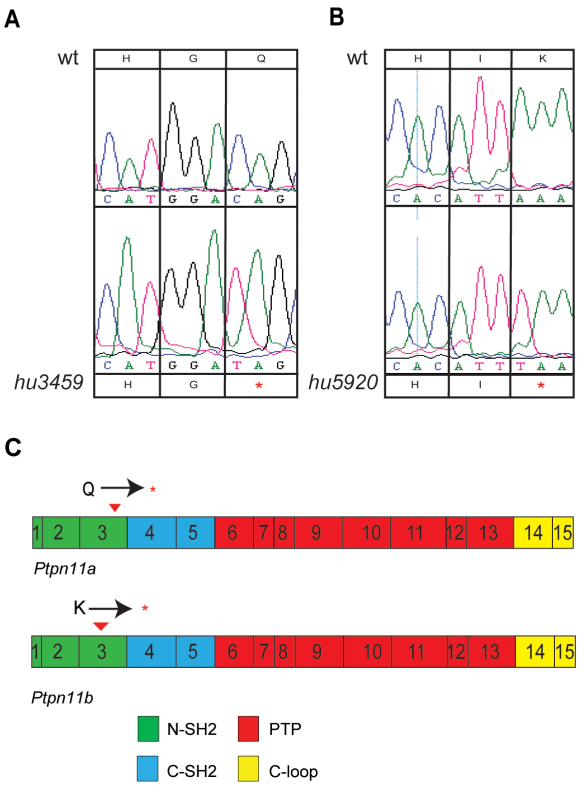

Figure 3. Nonsense mutations in zebrafish *ptpn11a* and *ptpn11b*.
Sequence analysis of homozygous *ptpn11a* and *ptpn11b* mutants. (a) A C–>T mutation in *ptpn11ahu3459* resulted in a glutamine to a STOP mutation. (b) A T–>A mutation in *ptpn11bhu5920* changed lysine to a STOP mutation. (c) Schematic representation of the exon organization and structural domains of *ptpn11a* and *ptpn11b*. Nonsense mutations upstream of the catalytic domain are represented by red arrows.

incross	injection (mRNA)	phenotype	*ptpn11a*$^{-/-}$/total
ptpn11a$^{+/-}$*ptpn11b*$^{-/-}$	-	40/199	40/199
ptpn11a$^{+/-}$*ptpn11b*$^{-/-}$	*ptpn11a*	1/98	23/98
ptpn11a$^{+/-}$*ptpn11b*$^{-/-}$	*ptpn11b*	5/65	12/65
ptpn11a$^{+/-}$*ptpn11b*$^{+/+}$	-	25/102	25/102
ptpn11a$^{+/-}$*ptpn11b*$^{+/+}$	*ptpn11b*	15/360	75/360

fertile. Next, fifth generation *ptpn11a*$^{+/-}$ and *ptpn11b*$^{+/-}$ fish were incrossed and double heterozygous *ptpn11a*$^{+/-}$*ptpn11b*$^{+/-}$ fish were selected. Incrosses were used to investigate zebrafish development in double homozygous *ptpn11a*$^{-/-}$*ptpn11b*$^{-/-}$ embryos. Phenotypically, all genotypes were indistinguishable from wild type embryos up to 3 dpf (data not shown). However, at 5dpf, *ptpn11a*$^{-/-}$ and double mutant embryos displayed significant phenotypic changes such as reduced body length, malformed head, absence of swim bladder, heart edema and eye edema (Figure 4A-D). Furthermore, these embryos were unable to move, even after stimulation. *Ptpn11b*$^{-/-}$ embryos were indistinguishable from wild type embryos at 5 dpf and did not display morphological defects (Figure 4A,C; Table 1). *Ptpn11a*$^{-/-}$ embryos and *ptpn11a*$^{-/-}$*ptpn11b*$^{-/-}$ embryos were embryonic lethal. Whereas the developmental defects of *ptpn11a*$^{-/-}$ and *ptpn11a*$^{-/-}$*ptpn11b*$^{-/-}$ embryos were overlapping (Figure 4 B,D), the phenotype of double mutant embryos was more severe than that of ptpn11a$^{-/-}$ embryos.

Ptpn11a$^{-/-}$ and double mutants appeared shorter than wild type embryos and we measured the body length of wildtype and mutant embryos at 5 dpf. *Ptpn11a*$^{-/-}$ (3.33 mm ± 0.03, n = 20) and *ptpn11a*$^{-/-}$*ptpn11b*$^{-/-}$ (3.28 mm ± 0.05, n = 10) embryos were significantly shorter ($p < 0,001$, Student's t-test) than wild type embryos (3.59 mm ± 0.02, n = 21) (Figure 4E). The length of wildtype embryos and *ptpn11b*$^{-/-}$ embryos (3.55 mm ± 0.02, n = 15) did not differ significantly. Collectively, our results show that *ptpn11a*, but not *ptpn11b*, is essential for normal development. Yet, *ptpn11b* appears to be functional, because the double mutant *ptpn11a*$^{-/-}$*ptpn11b*$^{-/-}$ displayed more severe defects than *ptpn11a*$^{-/-}$ by itself.

Craniofacial defects in Ptpn11a$^{-/-}$ *and double mutant Shp2 embryos*

Patients affected by NS and LS often suffer from craniofacial defects, including positional anomalies of the eyes and ears and a short, webbed neck. Craniofacial defects were apparent in double mutant *ptpn11a*$^{-/-}$*ptpn11b*$^{-/-}$ embryos at 5 dpf. Alcian blue staining of the cartilage revealed craniofacial defects that were quantified by assessment of the angle of the ceratohyal, a direct measure for the width of the head (Figure 5A). There was a significant difference between wildtype (60.72° ± 1.51, n=24) and double mutant embryos (95.14° ± 6.12, n=10) ($p< 0.001$, Student's t-test). Moreover, also *ptpn11a*$^{-/-}$ embryos (79.56° ± 5.29, n=15 $p< 0.01$) had a significantly wider ceratohyal compared to wildtype embryos, although the defect was milder. *Ptpn11b*$^{-/-}$ embryos (62.84° ± 5.73, n = 11) did not show a significant difference compared to wildtype embryos (Figure 5I). Taken together, these results show that particularly *ptpn11a* is indispensable for craniofacial development.

Double mutant Shp2 phenotype was rescued upon ptpn11a *and* ptpn11b *mRNA injections.*

To investigate if the double mutant phenotype could be suppressed by introduction of the full-length *ptpn11a* and *ptpn11b* mRNA, we performed rescue experiments. Clutches of embryos from *ptpn11a*$^{+/-}$*ptpn11b*$^{-/-}$ zebrafish were split and injected with *ptpn11a* or *ptpn11b* mRNA, or were not injected. The embryos were sorted based on their morphology at 5 dpf and genotyped by sequencing. The overall morphology of double mutant embryos is nicely distinguishable from

Table 2. Rescue of *ptpn11a* mutant phenotype by injection of *ptpn11a* and *ptpn11b*. Clutches of embryos from *ptpn11a*$^{+/-}$*ptpn11b*$^{-/-}$ or *ptpn11a*$^{+/-}$*ptpn11b*$^{+/+}$ zebrafish were split and injected with *ptpn11a* mRNA or *ptpn11b* mRNA. The embryos were scored based on their morphology at 5 dpf. Phenotype represents the number of embryos with mutant morphology/ total number of embryos. Subsequently, the genotype was determined by sequencing and is depicted as number of *ptpn11a*$^{-/-}$ embryos/ total number of embryos analyzed. *Ptpn11b* was homozygous (*ptpn11b*$^{-/-}$ or *ptpn11b*$^{+/+}$) and was not determined in these embryos.

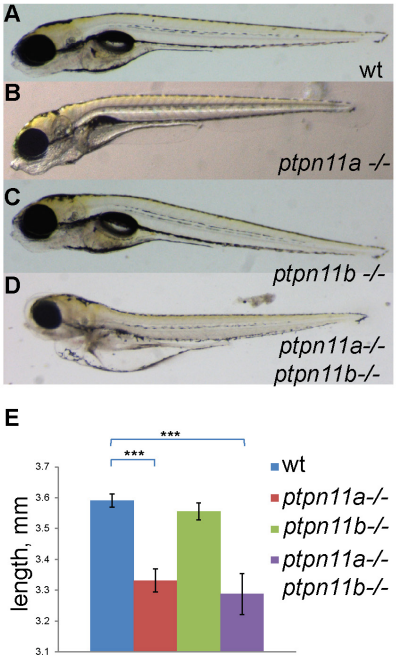

Figure 4. Loss of Shp2 causes severe morphological defects at 5 dpf. Morphology of 5 dpf zebrafish embryos. (a) Representative wild-type, (b) *ptpn11a*$^{-/-}$, (c) *ptpn11b*$^{-/-}$ and (d) double homozygous mutant are depicted. (e) The length was measured from nose to tip of tail at the same magnification. Bars show average length of the studied genotypes (n = 10-20). Statistics were determined using a student's t-test; * indicates a p value < 0.05.

wildtype embryos and 40/199 - close to the expected 25% - of the embryos are shorter and particularly the trunk and tail region is wider (Figure 6A). Microinjection of *ptpn11a* mRNA in offspring of *ptpn11a*$^{+/-}$*ptpn11b*$^{-/-}$ mutants at the one-cell stage largely suppressed the morphological phenotype in double mutant embryos at 5 dpf (Figure6B, Table 2). Interestingly, injection of *ptpn11b* mRNA also led to rescue of the morphological defects (Figure 6C, Table 2), indicating that *ptpn11a* and *ptpn11b* have redundant biochemical functions. The difference in the function of *ptpn11a* and *ptpn11b* in development may be caused by the observed difference in expression level at early stages of development. To test this hypothesis directly, we investigated whether *ptpn11b* RNA was able to rescue the *ptpn11a*$^{-/-}$*ptpn11b*+/+ phenotype. *Ptpn11b* mRNA injections at 1 cell stage indeed largely suppressed the *ptpn11a*$^{-/-}$ embryo phenotype (Figure6D,E, Table 2). These results show that *ptpn11a* and *ptpn11b* mRNA injections largely rescued the developmental defects in the double mutant embryos at 5 dpf and that injections of*ptpn11b* alone suppressed the *ptpn11a*$^{-/-}$ phenotype.

Impaired Erk/MAPK, but not Akt/PKB signalling in Shp2 double mutant embryos

Shp2 is required to promote the activation of the MAPK cascade in response to growth factors, cytokine receptors and integrins [3,36]. Thus, we examined the functional consequences of loss of

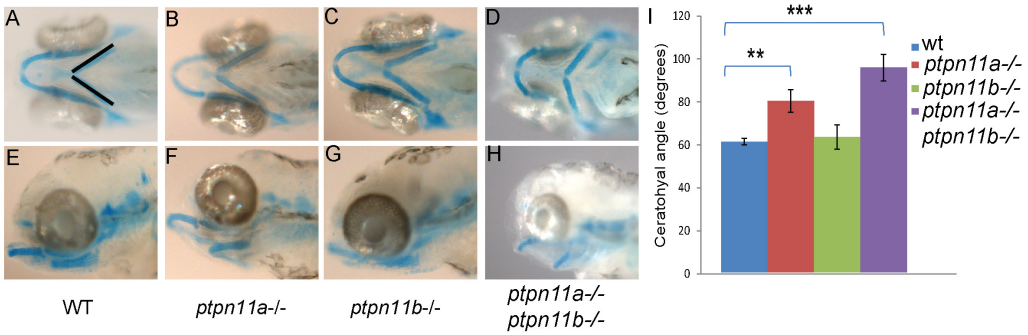

Figure 5. *Ptpn11a*-/- and double mutant embryos exhibit craniofacial defects at 5 dpf. Alcian blue staining was done to visualize the cartilage. (a,e) wild-type, (b,f) *ptpn11a*$^{-/-}$, (c,g) *ptpn11b*$^{-/-}$ and (d,h) double homozygous mutant. (i) Average width of the ceratohyal angle (indicated in panel a) was determined for each genotype (n = 10-24). Statistics were determined using a student's t-test; ** indicates a p value of < 0.01, *** indicates a p value < 0.001

Shp2 on downstream signaling by investigating Erk phosphorylation in wildtype, *ptpn11a*$^{-/-}$, *ptpn11b*$^{-/-}$ and double mutant embryos at 5 dpf. Immunoblotting showed that Erk activation was decreased in double mutant embryos compared to wild type, whereas Erk levels were not impaired in the single homozygous mutants (Figure 7A). Shp2 has been reported to act upstream of Akt/PKB signalling [12,18]. We investigated Akt signaling by immunoblotting for phosphorylated Akt in wild-type, *ptpn11a*$^{-/-}$, *ptpn11b*$^{-/-}$ and double mutant embryos at 5 dpf. We found that Akt activation was not affected in both single *ptpn11* homozygous mutants, nor in the double mutants (Figure 7B). Together, these data indicate that Erk/MAPK signaling, but not Akt (PKB) signaling is affected in mutants lacking functional Shp2.

Discussion

In this paper we characterized the two *ptpn11* genes in zebrafish, *ptpn11a* and *ptpn11b*. The products of these genes, Shp2a and Shp2b, respectively, are both active and exhibit comparable phosphatase activities. Using a TSGI approach, we identified nonsense mutations in *ptpn11a* and *ptpn11b*, well upstream of the catalytic site that abolished Shp2 function. In agreement with previous studies in mice with targeted *ptpn11* [20,37], double mutant zebrafish embryos lacking all functional Shp2 were found to be embryonic lethal. Mouse embryos lacking functional Shp2 die around implantation [20,37], whereas zebrafish embryos lacking functional Shp2 survive until 5-6 dpf. The difference in the developmental stage at which the lack of Shp2 is embryonic lethal between mice and zebrafish might be explained by the difference in maternal contribution of Shp2 in zebrafish eggs compared to mouse embryos.Whereas double mutant zebrafish embryos are embryonic lethal, lack of *ptpn11b* in homozygous single mutant fish resulted in viable and fertile fish without developmental defects. Yet, *ptpn11a*$^{-/-}$ single mutant embryos did not survive, suggesting a distinct role of the two *ptpn11* genes in zebrafish development. Biochemically, Shp2a and Shp2b have similar catalytic activities. However, expression analyses showed that *ptpn11a* was abundant in all developmental stages whereas *ptpn11b* was hardly detectable at early stages. *Ptpn11b* expression increased strongly over time. This may explain why the lack of *ptpn11a* affected development and lack of *ptpn11b* did not. Low levels of *ptpn11b* in *ptpn11a*$^{-/-}$ embryos at early stages cannot compensate for the lack of *ptpn11a*. Conversely, high levels of *ptpn11a* in *ptpn11b*$^{-/-}$ embryos can compensate for the lack of *ptpn11b*. *Ptpn11a* as well as *ptpn11b* rescued developmental defects in double mutant embryos, indicating that Shp2a and Shp2b have redundant functions. It is noteworthy that expression of exogenous *ptpn11b* rescued *ptpn11a*$^{-/-}$ embryos, demonstrating that the difference in developmental function of *ptpn11a* and *ptpn11b* is mainly caused by differences in expression levels during early development.

The developmental defects we observed in *ptpn11a*$^{-/-}$*ptpn11b*$^{-/-}$ embryos became apparent relatively late during development. Only at 4-5 dpf the first morphological defects were visible. This is in contrast with earlier reports of morpholino (MO)-mediated knockdown of Shp2, where we and others observed developmental defects as early as gastrulation [26,27]. The lack of gastrulation defects in *ptpn11a*$^{-/-}$*ptpn11b*$^{-/-}$ embryos may be due to maternal contribution of *ptpn11a* in the double mutants. The reduced body axis and craniofacial defects we observed in double mutants are comparable to the phenotypes of Shp2 knockdown embryos and of embryos expressing NS or LS variants of Shp2, that we and others reported earlier [26,27]. It is evident that Shp2 has an important role in body axis extension and craniofacial development: short stature is one of the most recognized symptoms in individuals with NS and LS. During the first years of life the body length drops below the 10th percentile for height in NS [38] and below the 25th percentile in LS [39]. Knock-in mice expressing Shp2 variants of NS or LS show postnatal growth retardation

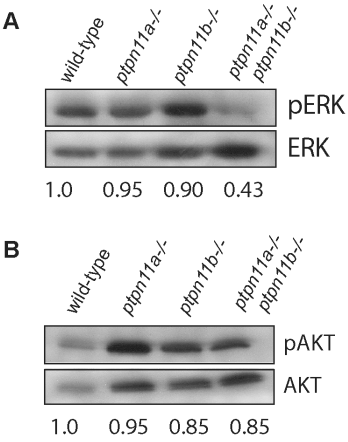

Figure 7. Impaired Erk/MAPK, but not Akt/PKB signalling in Shp2 double mutant embryos. WT, *ptpn11a*$^{-/-}$, *ptpn11b*$^{-/-}$ and *ptpn11a*$^{-/-}$ *ptpn11b*$^{-/-}$ embryos were lyzed and immunoblotted with phosho-specific antibody for ERK and AKT; membranes were then reprobed for total Erk and Akt expression to control for loading. The blots were quantified and the ratio of phosphorylated protein/ total protein from three independent experiments is indicated below each lane.

[40,41]. Moreover, human patients with NS or LS show visible craniofacial symptoms, including high forehead, hypertelorism, downslanting palpebral fissures, epicantal folds, ptosis, low-set and/or posteriorly rotated ears [5,42,43]. The ablation of Shp2 in neural crest cell leads to severe craniofacial anomalies in mice [44,45]. Similarly, expression of morpholino Shp2 and Noonan or LEOPARD Shp2 embryos, induced craniofacial defects in zebrafish at 4dpf [26,27]. Collectively, our results showed craniofacial defects and body axis extension defects in mutant zebrafish embryos, lacking functional Shp2, that are consistent with defects observed in mouse models lacking functional Shp2 in relevant cell types as well as with developmental defects in mouse models for NS or LS and symptoms in human individuals with NS or LS.

SHP2 positively regulates (ERK)/MAPK signal transduction [2] and downregulation of the (ERK)/MAPK pathway, due to the disruption of Shp2, leads to the formation of skeletal abnormalities and skull defects in mice [46,47] .We show that at 5dpf, pERK levels are downregulated in *ptpn11a*$^{-/-}$ *ptpn11b*$^{-/-}$ embryos, which is consistent with an essential role for Shp2 in Erk/MAPK signaling upstream of craniofacial development. However, even though in the *ptpn11a*$^{-/-}$ embryos pERK levels are comparable to wildtype, these embryos still showed craniofacial defects and reduced body length at 5dpf, albeit to a lesser extent than *ptpn11a*$^{-/-}$*ptpn11b*$^{-/-}$ double mutant embryos. We cannot exclude the possibility that craniofacial development is independent of Erk/MAPK signaling. However, the *ptpn11a*$^{-/-}$ phenotype may be the consequence of reduced Erk/MAPK signaling at earlier stages, i.e. prior to 5 dpf. *Ptpn11b* is only expressed at low levels at these early developmental stages, which may not compensate for the loss of *ptpn11a* to sustain physiological levels of Shp2-dependent Erk/MAPK signaling at stages that are crucial for craniofacial development. At 5 dpf, *ptpn11b* expression is high and may compensate for the lack of Shp2a in *ptpn11a*$^{-/-}$ mutants with respect to Erk/MAPK signaling. To prove temporal dependence on Erk/MAPK signaling in *ptpn11a*$^{-/-}$ mutant embryos is not trivial as it requires assessment of Erk phosphorylation at early developmental stages, i.e. in embryos that do not yet display developmental defects. Collectively, our data show that functional Shp2 is required for Erk/MAPK signaling at 5 dpf and whether Erk/MAPK signaling is involved in the developmental defects remains to be determined definitively.

In conclusion, we characterized the two *ptpn11* genes in zebrafish and found that the function of the two genes in development is distinct which is due to differences in their temporal expression patterns. The developmental defects that were observed in double mutant zebrafish embryos lacking functional Shp2 are consistent with developmental defects in mouse models lacking Shp2. The observed body axis extension and craniofacial defects are reminiscent of defects observed in mouse models for NS and LS, as well as the symptoms observed in human patients with NS and LS, underlining the importance of Shp2 for craniofacial development and body axis extension. The

ptpn11 mutants that we have identified constitute a useful system to further unravel the function of Shp2 in development. Moreover, these mutants provide a good starting point for the development of genetic models for NS and LS in zebrafish that will complement other animal models for these syndromes.

Materials and Methods

Ethics statement

All procedures involving experimental animals described here were approved by the local animal experiments committee (KNAW-DEC protocol HL05.1501) and performed according to local guidelines and policies in compliance with national and European law.

Zebrafish care and generation of ptpn11 *mutant lines*

Zebrafish maintenance, breeding and staging were performed following published protocols [29]. ENU mutagenesis was performed on TL males [30] and exons 1–4 of the zebrafish *ptpn11a* and *ptpn11b* genes were sequenced using DNA from F1 generation zebrafish. Each mutation was confirmed by resequencing. Genomic DNA was extracted from adult fish fin clip or fixed embryos. The genotyping assay for the *ptpn11* mutations was performed by nested PCR with primer sets: *ptpn11a*, 5'-GCGCTGTCACACACATTAAGA, 5'-TCACAGCCAATAAAGAGAAGC; nested *ptpn11a* 5'-CGACCTGTATGGTGGAGAGAA, 5'-TCCCAAATTGTCATGTAAGG; *ptpn11b*, 5'-TTCAACAACATCCTCCTAACTG, 5'-AAACAAACCACAGCTCTTCC and nested *ptpn11b* 5'-GTCTGTCATCCCTCATTTCC, 5'-GCAGGATTTATTCTGTCCAC, followed by sequencing to detect the mutations.

RNA isolation, cDNA synthesis and quantitative PCR

For the reverse transcription PCR (RT-PCR) experiment, thirty zebrafish embryos at various stages of development (4 hpf, 10hpf, 1 dpf, 2 dpf, 3 dpf and 5 dpf) were collected and homogenized in TRIzol Reagent (Invitrogen; Carlsbad, CA). The homogenate was centrifuged (12000g, 4ºC, 10 min.). 0.2 ml of Chloroform were added to the supernatant, vortexed for 15 sec., incubated for 3 min. at room temperature (RT) and then centrifuged (12000g, 4ºC, 15 min.). 0.5 ml isopropanol were added to the upper phase, incubated for 10 min. at RT and centrifuged (12000g, 4ºC, 15 min.). The pellet was washed with 75% EtOH and after vortexing, centrifuged (10000g, 4ºC, 5 min.). The pellet was then dried for 5 min. and dissolved in 100 µl MQ. After, the solution was incubated for 10 min. at 37 ºC, precipitated in 250 µl 100% EtOH and 10 µl 3M NaAc and stored at -80 ºC.

For RT-PCR with M-MLV-RT (Promega) 1 µg of total RNA was used. PCR of cDNA was performed using the standard protocol of GoTaq (Promega) using oligonucleotides listed as follow; *ptpn11a* forward: 5'- ATGTGCCCAAGACTATCCAGATG,
ptpn11a reverse: 5'- CCCACGTTCTCATAGACTCGAGA,
ptpn11b forward: 5'- ACTGTGACATTGACATCCCAAAAA,
ptpn11b reverse: TACTGCTGGTGGAGCCCTTTGGAT. The same primers were used for sequencing of the DNA fragments.

Real-time RT-PCR was performed using the IQ SYBR® Green Supermix (Biorad). Real time PCR MyIQ software (Bio-rad) was used to determine the amplification cycle in which product accumulation was above the threshold cycle values (Ct). PCR was carried out after incubation at

50°C for 2 min and pre-denaturing at 95°C for 3 min, followed by 40 cycles at 95°C for 30 sec and 62°C for 1 min. The relative quantification was given by the CT values, determined by triplicate reactions for all of the samples for *ptpn11a*, *ptpn11b* and *β-actin*. Real time PCR Ct values were analyzed using the 2–ΔCT method [31].

For the quantification of *ptpn11a* and *ptpn11b* mRNA levels, the housekeeping gene *actin* was used as internal standard. ΔCT-values were calculated as follows: CT(*β-actin*)-CT(*ptpn11*) and were normalized to the starting point T0 (4hpf) .

In situ *hybridization*

In situ hybridizations were done essentially as described [32]. .Digoxigenin-UTP-labeled riboprobes for *ptpn11a* and *ptpn11b* were synthesized from PCR products. The PCR products were amplified with primers containing the T7 promoter and then sequenced. Primers were designed as follows: *ptpn11a* forward, 5'- ATTTAGGTGACACTATAGGGAGCTACATTGCCACACAA, *ptpn11a* reverse: 5'- TAATACGACTCACTATAGGGTTTTTCATCTCTCGGTTTAGTCA . For *ptpn11b*, primers that attached to the 3'UTR region of the gene were designed: *ptpn11b* forward: 5'-ATTTAGGTGACACTATAGGGAACAAAACGAAGGAGAGG, *ptpn11b* reverse: 5'-TAATACGACTCACTATAGGGGCCTGCCTCATTTTTAGCTG. Embryos were cleared in methanol and mounted in Benzyl Benzoate/Benzyl Alcohol (2:1) before pictures were taken.

Alcian blue staining

Morphological phenotypes were assessed at 5 dpf. Embryos were anesthesized at 5 dpf with MS-222 (Sigma), fixed in 4% paraformaldehyde (PFA) and the cartilage was stained with alcian blue. Briefly, fixed embryos were washed for 10 min in 50 % ETOH in water. Next, the embryos were stained overnight at 4C in staining solution (0.04% alcian blue, 50mM MgCl2, 70 % EtOH). Embryos were washed in 0.2% of Triton X-100 in water. Pictures of lateral and ventral views were taken. The width of the ceratohyal angle was determined using Image J software and the ratio was determined as a direct measure for craniofacial defects. Averages were determined and a student t-test was done to determine whether the differences between the diverse conditions were statistically significant.

Immunoblotting

Zebrafish embryos were raised in standard conditions. At 5dpf, 5 embryos were pooled and lysed in buffer containing 50 mM Tris, pH 7.5, 150 mM NaCl, 1 mM EDTA, 1 mM sodium orthovanadate, 1% Nonidet P-40, 0.1% sodium deoxycholate, protease inhibitor mixture (Complete Mini, Roche Diagnostics) and vanadate, and 40 µl lysisbuffer. Lysates were spun down and 4× sample buffer was added to supernatant; Samples were run on SDS-PAGE gel (10%) and transferred to PVDF membrane. After transfer the membrane was stained with Coomassie Blue stain to verify equal loading of the lysates. Subsequently the PVDF membrane was blocked with 5% BSA and then incubated with the corresponding antibodies targeting mouse monoclonal antibody anti-pERK, rabbit monoclonal antibody anti-ERK, rabbit monoclonal antibody pAKT and rabbit monoclonal antibody anti-AKT. All the primary antibodies were diluted 1:1000 in blocking solution and they were purchased from Cell-Signaling. The secondary antibodies (mouse and rabbit) conjugated to horseradish peroxidase (HRP), were purchased from BD bioscience Pharmaceutical and they were diluted 1:10,000 in TBST. The membranes were subjected to detection by enhanced chemiluminescence (Thermo Scientific kit).

Phosphatase assay

We generated zebrafish *ptpn11a* and *ptpn11b* cDNA constructs and cloned them in a pGEX-4t vector, allowing production and purification of recombinant Shp2 proteins, fused to six histidine residues in their C-termini. Purified GST-fusion proteins were directly incubated in PTP assay buffer (20 mM MES buffer pH 6.0, 1 mM EDTA, 150 mM NaCl, 1 mM dithiotreitol, and 10 mM p-nitrophenylphosphate) for 45 min. at 30 °C. The reactions were quenched with 0.4 M NaOH, and optical density was measured with a spectrophotometer at 415 nm (wavelength).

Statistical analysis

Statistical significance was assessed by two-tailed Student's t-test in all experiments. Significance is represented in the graphs. Results are considered significant when $p < 0.05$ and are expressed as mean ± standard error of the mean. * indicates a p value of < 0.05, ** indicates a p value of < 0.01 and *** indicates a p value of < 0.001.

References

1. Dance M, Montagner A, Salles JP, Yart A, Raynal P (2008) The molecular functions of Shp2 in the Ras/Mitogen-activated protein kinase (ERK1/2) pathway. Cell Signal 20: 453-459.
2. Feng GS (1999) Shp-2 tyrosine phosphatase: signaling one cell or many. Exp Cell Res 253: 47-54.
3. Neel BG, Gu H, Pao L (2003) The 'Shp'ing news: SH2 domain-containing tyrosine phosphatases in cell signaling. Trends Biochem Sci 28: 284-293.
4. Tartaglia M, Mehler EL, Goldberg R, Zampino G, Brunner HG, et al. (2001) Mutations in PTPN11, encoding the protein tyrosine phosphatase SHP-2, cause Noonan syndrome. Nat Genet 29: 465-468.
5. Legius E, Schrander-Stumpel C, Schollen E, Pulles-Heintzberger C, Gewillig M, et al. (2002) PTPN11 mutations in LEOPARD syndrome. J Med Genet 39: 571-574.
6. Digilio MC, Conti E, Sarkozy A, Mingarelli R, Dottorini T, et al. (2002) Grouping of multiple-lentigines/LEOPARD and Noonan syndromes on the PTPN11 gene. Am J Hum Genet 71: 389-394.
7. Martinez-Quintana E, Rodriguez-Gonzalez F (2013) RASopathies: From Noonan to LEOPARD Syndrome. Rev Esp Cardiol.
8. Rodriguez-Viciana P, Tetsu O, Tidyman WE, Estep AL, Conger BA, et al. (2006) Germline mutations in genes within the MAPK pathway cause cardio-facio-cutaneous syndrome. Science 311: 1287-1290.
9. Zenker M (2009) Noonan Syndrome and Related Disorders. A matter of Deregulated Ras Signaling.; Schmid M, editor. Basel, Switzerland: Karger. 24 p.
10. Tartaglia M, Zampino G, Gelb BD (2010) Noonan syndrome: clinical aspects and molecular pathogenesis. Mol Syndromol 1: 2-26.
11. Hanna N, Montagner A, Lee WH, Miteva M, Vidal M, et al. (2006) Reduced phosphatase activity of SHP-2 in LEOPARD syndrome: consequences for PI3K binding on Gab1. FEBS Lett 580: 2477-2482.
12. Kontaridis MI, Swanson KD, David FS, Barford D, Neel BG (2006) PTPN11 (Shp2) mutations in LEOPARD syndrome have dominant negative, not activating, effects. J Biol Chem 281: 6785-6792.
13. Tartaglia M, Martinelli S, Stella L, Bocchinfuso G, Flex E, et al. (2006) Diversity and functional consequences of germline and somatic PTPN11 mutations in human disease. Am J Hum Genet 78: 279-290.
14. Yu ZH, Xu J, Walls CD, Chen L, Zhang S, et al. (2013) Structural and mechanistic insights into LEOPARD syndrome-associated SHP2 mutations. J Biol Chem 288: 10472-10482.
15. Keilhack H, David FS, McGregor M, Cantley LC, Neel BG (2005) Diverse biochemical properties of Shp2 mutants. Implications for disease phenotypes. J Biol Chem 280: 30984-30993.
16. Oishi K, Gaengel K, Krishnamoorthy S, Kamiya K, Kim IK, et al. (2006) Transgenic Drosophila models of Noonan syndrome causing PTPN11 gain-of-function mutations. Hum Mol Genet 15: 543-553.
17. Oishi K, Zhang H, Gault WJ, Wang CJ, Tan CC, et al. (2009) Phosphatase-defective LEOPARD syndrome mutations in PTPN11 gene have gain-of-function effects during Drosophila development. Hum Mol Genet 18: 193-201.
18. Edouard T, Combier JP, Nedelec A, Bel-Vialar S, Metrich M, et al. (2010) Functional effects of PTPN11 (SHP2) mutations causing LEOPARD syndrome on epidermal growth factor-induced phosphoinositide 3-kinase/AKT/glycogen synthase kinase 3beta signaling. Mol Cell Biol 30: 2498-2507.
19. De Rocca Serra-Nedelec A, Edouard T, Treguer K, Tajan M, Araki T, et al. (2012) Noonan syndrome-causing SHP2 mutants inhibit insulin-like growth factor 1 release via growth hormone-induced ERK hyperactivation, which contributes to short stature. Proc Natl Acad Sci U S A 109: 4257-4262.
20. Yang W, Klaman LD, Chen B, Araki T, Harada H, et al. (2006) An Shp2/SFK/Ras/Erk signaling pathway controls trophoblast stem cell survival. Dev Cell 10: 317-327.
21. Ke Y, Zhang EE, Hagihara K, Wu D, Pang Y, et al. (2007) Deletion of Shp2 in the brain leads to defective proliferation and differentiation in neural stem cells and early postnatal lethality. Mol Cell Biol 27: 6706-6717.
22. Kontaridis MI, Yang W, Bence KK, Cullen D, Wang B, et al. (2008) Deletion of Ptpn11 (Shp2) in cardiomyocytes causes dilated cardiomyopathy via effects on the extracellular signal-regulated kinase/mitogen-activated protein kinase and RhoA signaling pathways. Circulation 117: 1423-1435.
23. Bard-Chapeau EA, Yuan J, Droin N, Long S, Zhang EE, et al. (2006) Concerted functions of Gab1 and Shp2 in liver regeneration and hepatoprotection. Mol Cell Biol 26: 4664-4674.
24. Bard-Chapeau EA, Li S, Ding J, Zhang SS, Zhu HH, et al. (2011) Ptpn11/Shp2 acts as a tumor suppressor in hepatocellular carcinogenesis. Cancer Cell 19: 629-639.
25. Tang TL, Freeman RM, Jr., O'Reilly AM, Neel BG, Sokol SY (1995) The SH2-containing protein-tyrosine phosphatase SH-PTP2 is required upstream of MAP kinase for early Xenopus development. Cell 80: 473-483.
26. Jopling C, van Geemen D, den Hertog J (2007) Shp2 knockdown and Noonan/LEOPARD mutant Shp2-induced gastrulation defects. PLoS Genet 3: e225.
27. Stewart RA, Sanda T, Widlund HR, Zhu S, Swanson KD, et al. (2010) Phosphatase-dependent and -independent functions of Shp2 in neural crest cells underlie LEOPARD syndrome pathogenesis. Dev Cell 18: 750-762.
28. Lieschke GJ, Currie PD (2007) Animal models of human disease: zebrafish swim into view. Nat Rev Genet 8: 353-367.
29. Kimmel CB, Ballard WW, Kimmel SR, Ullmann B, Schilling TF (1995) Stages of embryonic development of the zebrafish. Dev Dyn 203: 253-310.

30. Wienholds E, van Eeden F, Kosters M, Mudde J, Plasterk RH, et al. (2003) Efficient target-selected mutagenesis in zebrafish. Genome Res 13: 2700-2707.
31. Livak KJ, Schmittgen TD (2001) Analysis of relative gene expression data using real-time quantitative PCR and the 2(-Delta Delta C(T)) Method. Methods 25: 402-408.
32. Thisse C, Thisse B, Schilling TF, Postlethwait JH (1993) Structure of the zebrafish snail1 gene and its expression in wild-type, spadetail and no tail mutant embryos. Development 119: 1203-1215.
33. van Eekelen M, Overvoorde J, van Rooijen C, den Hertog J (2010) Identification and expression of the family of classical protein-tyrosine phosphatases in zebrafish. PLoS One 5: e12573.
34. Vandepoele K, De Vos W, Taylor JS, Meyer A, Van de Peer Y (2004) Major events in the genome evolution of vertebrates: paranome age and size differ considerably between ray-finned fishes and land vertebrates. Proc Natl Acad Sci U S A 101: 1638-1643.
35. Jaillon O, Aury JM, Brunet F, Petit JL, Stange-Thomann N, et al. (2004) Genome duplication in the teleost fish Tetraodon nigroviridis reveals the early vertebrate proto-karyotype. Nature 431: 946-957.
36. Nadler MJ, Chen B, Anderson JS, Wortis HH, Neel BG (1997) Protein-tyrosine phosphatase SHP-1 is dispensable for FcgammaRIIB-mediated inhibition of B cell antigen receptor activation. J Biol Chem 272: 20038-20043.
37. Saxton TM, Henkemeyer M, Gasca S, Shen R, Rossi DJ, et al. (1997) Abnormal mesoderm patterning in mouse embryos mutant for the SH2 tyrosine phosphatase Shp-2. EMBO J 16: 2352-2364.
38. Noonan JA, Raaijmakers R, Hall BD (2003) Adult height in Noonan syndrome. Am J Med Genet A 123A: 68-71.
39. Gorlin RJ, Anderson RC, Blaw M (1969) Multiple lentigenes syndrome. Am J Dis Child 117: 652-662.
40. Araki T, Mohi MG, Ismat FA, Bronson RT, Williams IR, et al. (2004) Mouse model of Noonan syndrome reveals cell type- and gene dosage-dependent effects of Ptpn11 mutation. Nat Med 10: 849-857.
41. Marin TM, Keith K, Davies B, Conner DA, Guha P, et al. (2011) Rapamycin reverses hypertrophic cardiomyopathy in a mouse model of LEOPARD syndrome-associated PTPN11 mutation. J Clin Invest 121: 1026-1043.
42. Noonan JA (1968) Hypertelorism with Turner phenotype. A new syndrome with associated congenital heart disease. Am J Dis Child 116: 373-380.
43. Tartaglia M, Kalidas K, Shaw A, Song X, Musat DL, et al. (2002) PTPN11 mutations in Noonan syndrome: molecular spectrum, genotype-phenotype correlation, and phenotypic heterogeneity. Am J Hum Genet 70: 1555-1563.
44. Nakamura T, Gulick J, Colbert MC, Robbins J (2009) Protein tyrosine phosphatase activity in the neural crest is essential for normal heart and skull development. Proc Natl Acad Sci U S A 106: 11270-11275.
45. Nakamura T, Gulick J, Pratt R, Robbins J (2009) Noonan syndrome is associated with enhanced pERK activity, the repression of which can prevent craniofacial malformations. Proc Natl Acad Sci U S A 106: 15436-15441.
46. Lapinski PE, Meyer MF, Feng GS, Kamiya N, King PD (2013) Deletion of SHP-2 in mesenchymal stem cells causes growth retardation, limb and chest deformity, and calvarial defects in mice. Dis Model Mech 6: 1448-1458.
47. Bauler TJ, Kamiya N, Lapinski PE, Langewisch E, Mishina Y, et al. (2011) Development of severe skeletal defects in induced SHP-2-deficient adult mice: a model of skeletal malformation in humans with SHP-2 mutations. Dis Model Mech 4: 228-239.

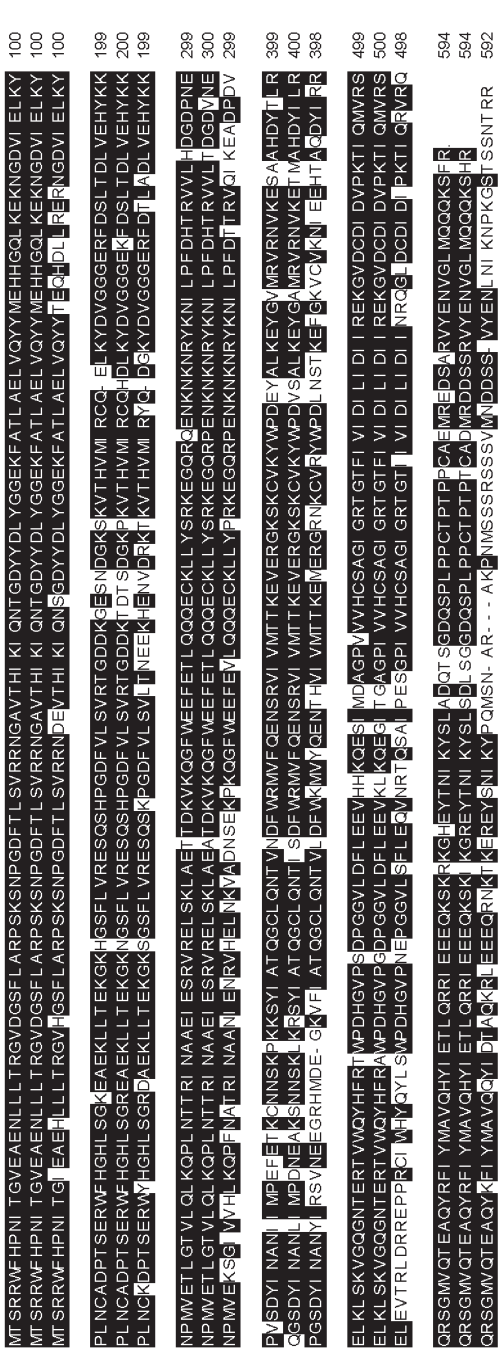

Additional information

Figure S1. Comparison of human SHP2 and zebrafish Shp2a and Shp2b polypeptides. The alignment was done using ClustalW. Identical amino acids are highlighted in black. The consensus sequence is shown underlined, on top of the rows. Amino acids are numbered to the right of each row.

Phosphoproteomics-mediated identification of Fer kinase as a target of mutant Shp2 in Noonan and LEOPARD syndrome

Jeroen Paardekooper Overman[1], Christian Preisinger[2,3,4], Karin Prummel[1], Monica Bonetti[1], Piero Giansanti[2,3], Albert Heck[2,3,5] and Jeroen den Hertog[1,6].

1. Hubrecht Institute-KNAW and University Medical Center Utrecht, 3584 CT Utrecht, Netherlands 2. Biomolecular Mass Spectrometry and Proteomics, Bijvoet Center for Biomolecular Research and Utrecht Institute for Pharmaceutical Research, Utrecht University, 3584 CH Utrecht, The Netherlands 3. Netherlands Proteomics Centre, 3584 CH Utrecht, The Netherlands 4. Proteomics Facility, Interdisciplinary Centre for Clinical Research (IZKF) Aachen, RWTH Aachen University, Aachen Germany 52074 5. Centre for Biomedical Genetics, 3584 CH Utrecht, The Netherlands 6. Institute Biology Leiden, 2333 CC Leiden, Netherlands Corresponding author (j.denhertog@hubrecht.eu).

Accepted, PLoS One

Abstract

Noonan syndrome (NS) and LEOPARD syndrome (LS) cause congenital afflictions such as short stature, hypertelorism and heart defects. More than 50% of NS and almost all of LS cases are caused by activating and inactivating mutations of the phosphatase Shp2, respectively. How these biochemically opposing mutations lead to similar clinical outcomes is not clear. Using zebrafish models of NS and LS and mass spectrometry-based phosphotyrosine proteomics, we identified a down-regulated peptide of Fer kinase in both NS and LS. Further investigation showed a role for Fer during development, where morpholino-based knockdown caused craniofacial defects, heart edema and short stature. During gastrulation, loss of Fer caused convergence and extension defects without affecting cell fate. Moreover, Fer knockdown cooperated with NS and LS, but not wild type Shp2 to induce developmental defects, suggesting a role for Fer in the pathogenesis of both NS and LS.

Introduction

Noonan syndrome (NS) (OMIM 163950) is a congenital disorder that manifests itself in heart defects, short stature, webbed neck, hypertelorism and an increase in the occurrence of juvenile myelomonocytic leukemia (JMML) and other malignancies. The most common causes for NS are mutations in *PTPN11* encoding for Src-homology domain 2 (SH2) containing phosphatase 2 (Shp2) [1] A similar syndrome is also caused by mutations in *PTPN11* and patients display similar symptoms as NS. An acronym of the symptoms, Lentigines, Electrocardiographic conduction anomalies, Ocular hypertelorism, Pulmonary stenosis, Abnormal genitalia, Retarded growth and Deafness gave this syndrome its name, LEOPARD syndrome (LS)(OMIM 151100) [1]. Both NS and LS are part of a group of congenital syndromes caused by mutations in the RAS mitogen activated protein kinase (MAPK) pathway called RASopathies. Despite the similarities in the clinical manifestations of NS and LS, NS mutations lead to an 'active' form of the Shp2 phosphatase, while LS is thought to result from 'inactivating' mutations [2,3]. However, a gain-of-function for LS has also been described in *Drosophila* [4].

The phosphatase Shp2 consists of two N-terminal SH2 domains that are able to bind to tyrosine phosphorylated targets of Shp2, a protein tyrosine phosphatase (PTP) domain, and a C-terminal tail with a proline rich domain and two tyrosines that are able to bind Grb2 when phosphorylated. Under basal conditions, the N-SH2 domain blocks access of the PTP domain to its substrates, resulting in an inactive conformation of Shp2 [5]. In NS, mutations cause a disruption of the interaction between the N-SH2 domain and the PTP domain, resulting in a hyperactive form of Shp2 [1,2]. In LS however, mutations are mostly present in the PTP domain at the interface of the PTP and SH2 domain, resulting in a loss of catalytic activity. How both activating and inactivating mutations of Shp2 lead to similar developmental defects is largely unknown.

Homozygous mice defective for Shp2 die *in utero* and have gastrulation defects, showing malformations of the notochord and posterior truncations [6]. Embryos lacking Shp2 also develop failure of neural tube closure resulting in spina bifida and secondary neural tubes resulting from gastrulation defects [7]. Shp2 is essential for limb formation since chimeric mice with defective Shp2 expressed in the mesenchyme of the progress zone showed limb bud defects [8]. More recent results have shown cell migration defects during gastrulation in NS and LS Shp2 expressing zebrafish embryos as well [9]. These convergence and extension (C&E) cell movements mediate the anterior-posterior lengthening and lateral narrowing of the developing embryo. C&E cell movements are under strict spatiotemporal control of various signaling pathways [10]. Being a protein proximal to many RTKs, Shp2 acts upstream of multiple signaling pathways [2].

As NS and LS Shp2 are thought to act biochemically opposite, yet give rise to similar clinical symptoms, we sought to identify potential common targets of NS and LS Shp2 in a zebrafish model. Pinpointing disease associated Shp2 signaling shared by NS and LS, may contribute to the understanding of the underlying mechanisms of NS and LS pathogenesis and the development of therapeutic strategies for both NS and LS. Using a comparative phosphoproteomics approach, phosphotyrosine (pTyr)-containing peptides of NS- and LS-Shp2 expressing zebrafish embryos were isolated, identified and compared to peptides of WT embryos. A peptide corresponding to the autophosphorylation site of Fer kinase was identified as one of the most down-regulated peptides in developing NS and LS zebrafish. Further investigation revealed a role for Fer in C&E cell movements during gastrulation. Downregulation of Fer cooperated with NS and LS to induce developmental defects, suggesting a genetic interaction between Fer and the NS and LS variants of Shp2.

Results

Mass spectrometric analysis identifies Fer kinase as a hypotyrosyl-phosphorylated protein in NS and LS zebrafish embryos.

To identify novel downstream targets of disease associated Shp2 that are affected similarly in NS and LS, we performed a mass spectrometric analysis on zebrafish embryos as outlined in Figure 1A. In short, zebrafish embryos were injected with synthetic mRNA encoding wild type Shp2, NS-Shp2 (D61G) or LS-Shp2 (A462T) which induced developmental defects at 24 hpf [9] (Figure 1B). Embryos were co-injected with mRNA encoding GFP, which facilitated selection of embryos that were injected properly. Approximately 2000 embryos per condition were lysed and combined prior to digestion with LysC and Trypsin. Zebrafish lysates were isotopically labeled with normal formaldehyle (CH_2O, light) for the WT embryos, deuteroformaldehyde (CD_2O, medium) for the NS embryos and ^{13}C deuteroformaldehyde ($^{13}CD_2O$, heavy), for LS embryos. Labeled peptides were then combined and the mixture was processed further. The labeled peptide mixtures were enriched for pTyr by immunoprecipitation, using PY99 agarose beads [17,18] (Figure 1A).

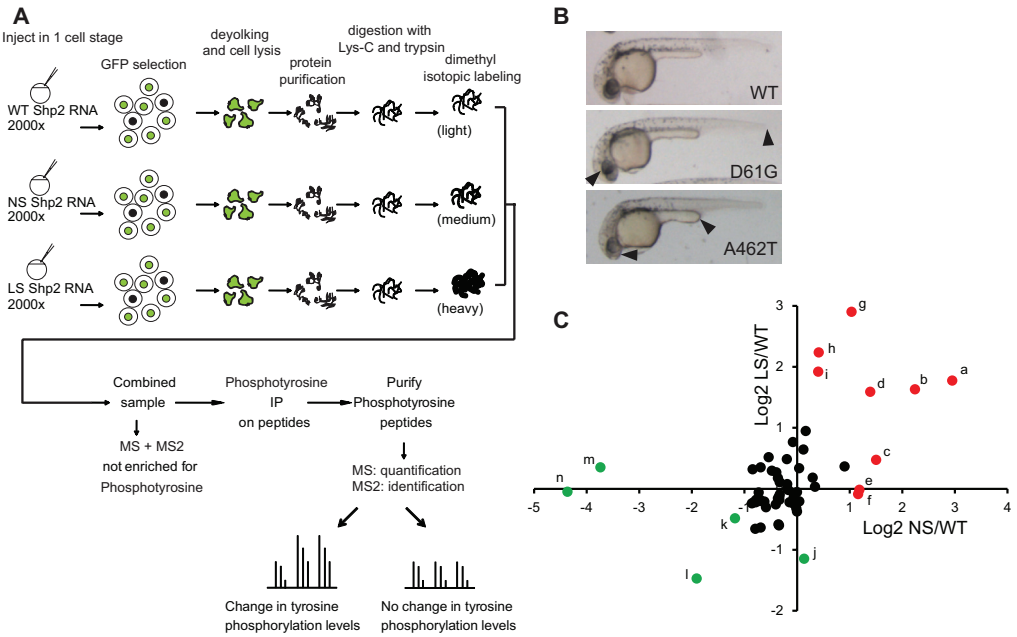

Figure 1. Comparative pTyr mass spectrometry on 1 day old zebrafish embryos expressing wild type, NS (D61G) or LS (A462T) Shp2.
A. Work flow depicting the mass spectrometry approach. Approximately 2000 zebrafish embryos per condition were injected at the 1-cell stage and sorted for GFP expression. Embryos were lysed, trypsinised and labeled using the dimethyl labeling method. WT, NS and LS samples were combined and immunoprecipitated using pTyr specific antibodies. Immunoprecipitate was subjected to MS and peptides were identified and quantified based on MS2 and MS1 spectra, respectively. B. 1dpf zebrafish embryos expressing WT, D61G and A462T Shp2. Body axis length, craniofacial defects and heart edema in D61G and A462T Shp2 expressing zebrafish are indicated with arrowheads. C. Normalized plot of quantified phosphopeptides Log_2 ratios. Peptide ratios with Log_2 ratios >-1 and <1 are indicated in black. Peptides with more that 1x Log_2 difference are annotated with a-n (see Table 1 for reference). Peptides changed with Log_2 ratios <-1 in either NS or LS are indicated in green and Log_2 ratios >1 in either NS or LS are indicated in red. See text for further details.

LC-MS was performed and MS1 and MS2 spectra were obtained. Ratios of light/medium and light/heavy peptides were determined with Proteome Discoverer 1.3.0.399 using the MS1 spectra and normalized to the total ratio of all (non-phosphorylated) peptides as input. The input corresponding to the LEOPARD Shp2 expressing embryos (heavy labeled) was 2.35 fold higher than wild type (light labeled), whereas Noonan (medium labeled), was 1.38 fold higher than wild type. Whereas many peptides were identified, only a small number of phosphopeptides were identified and of suitable quality for quantification (see Table S1). In total, we identified and quantified 69 phosphorylation sites, of which 44 were pTyr sites with a pRS score of >75%. The other phosphorylation sites were predicted to be on serine or threonine, or the pTyr site could not be localized. The low abundance of tyrosine phosphorylation is likely the cause of the low number of identified and quantified pTyr peptides. In addition, many peptides that were identified corresponded to highly abundant proteins like actin, keratin and vitellogenin, a zebrafish yolk protein. These abundant proteins may have interfered with binding of the antibody to peptides of interest, leading to reduced specificity/efficiency for the enrichment of pTyr containing peptides. The normalized Log_2 ratios of the quantified phosphopeptides indicate that the majority of phosphopeptides was unaltered upon expression of NS or LS Shp2 compared to WT Shp2 (Table 1, Figure 1C). For clarity, the human phosphorylation sites are used in the text. A minor fraction of phosphopeptides was up- or down-regulated in NS and LS Shp2 expressing zebrafish embryos, compared to WT Shp2 expressing embryos. This fraction of peptides may represent downstream factors that contribute to the etiology of both NS and LS. As an internal control for the expression of NS and LS Shp2 compared to wild type, we confirmed similar levels of Shp2 Y63 phosphopeptide in the WT compared to LS. Indeed, the 'WT' Shp2 pY63 peptide was not observed in the medium labeled (NS) sample, as this peptide has a D61G substitution and was thus not identified (See Table 1, Figure 1B, peptides "m" and "n").

Direct targets of Shp2 PTP activity were expected to have decreased pTyr in NS and an increase in LS. Surprisingly, these peptides were not abundant in our results (see Figure 1C upper-left quadrant). However, we identified pTyr peptide Y612 of IRS1B (peptide "k"), a known Shp2 substrate, which was decreased (Log_2: -1.18 fold) in NS but unaltered in LS compared to WT. Peptides that were increased in LS included a putative phoshorylation site of cell division kinase 15 and/or 16 (CDK15/CDK16)(peptide "i")(Log_2: 1.92 fold). However, these sites could not be localized with a precision score of >75%. In addition, S39 of eukaryotic translation initiation factor 3 subunit C (EIF3C) (peptide "h") was increased (Log_2: 2.24 fold) in LS.
Alternatively, proteins that are phosphorylated downstream of Shp2 in a phosphatase-dependent manner would be expected in the lower right quadrant with increased phosphorylation in response to NS Shp2 and decreased phosphorylation in response to LS Shp2. We identified phosphopeptides that were increased in NS, including Y43 of Histone 2B (H2B) (peptide "c") (Log_2: 1.50 fold), Y185 (Log_2: 1.16 fold) (peptide "f") and T183 (Log_2: 1.18 fold) (peptide "e") of a MAPK12/MAPK14 protein (zgc:171775). Additionally, we identified a phosphopeptide that was decreased in LS including Y666 of receptor tyrosine kinase-like orphan receptor 2 (ROR2) (peptide "j") (Log_2: -1.15 fold).

Multiple peptides that were affected in a similar way (upregulation or downregulation in both NS and LS) were identified (lower-left and upper-right quadrant). To gain further understanding in how activating and inactivating mutations in NS and LS, respectively lead to similar outcomes, we chose to focus on this group of peptides. Two of the main hyperphosphorylated peptides in both NS and LS corresponded to PZR, an earlier identified target of Shp2 [19,20]. Peptides corresponding to Y241 (peptide "a") and Y263 (peptide "b") were increased (Log_2: 2.95 fold and Log_2: 2.24 fold,

Protein name	accession number	Identified peptide sequence	Site in zebrafish	Site in human	NS/ WT Log_2	LS/ WT Log_2	
Mpzl1	E7F7T2	CSSPSAPVQGPVI(pY)AQLDHSGSK	Y236	Y241	2,95	1,77	*a*
Mpzl1	E7F7T2	MEPVV(pY)ADIR	Y258	Y263	2,24	1,63	*b*
Histone 2B 1/2	Q5BJA5	ESYAIYV(pY)K	Y43	Y43	1,50	0,47	*c*
Irs1b*	XP_001920152.3*	TGSD(pY)MNMSPISAR	Y689	Y989	1,39	1,59	*d*
zgc:171775	F1QHF2	HTETEM(pT)GYVVTR	T181	T183	1,18	-0,02	*e*
zgc:171775	F1QHF2	HTETEMTG(pY)VVTR	Y183	Y185	1,16	-0,09	*f*
Ephb3*	XP_005174117.1*	FLEDDPTDPTYTSSLGGK	Y737**	Y792**	1,04	2,90	*g*
wu:fc15a01	E7F486	GPLDGSL(pY)AQVK	Y478	Y483	0,90	0,37	
Eif3c	NP_998628.1*	QQALLL(pS)DDEEDTK	S39	S39	0,41	2,24	*h*
Cdk15; Cdk16*	NP_001035398.1; XP_003199208.1*	LGEGTYATVYK	Y99; Y148**	Y114;Y176**	0,40	1,92	*i*
Prpf4ba	B0V1K6	LCDFGSASHVADNDITPYLV(pS)R	S855	S852	0,34	0,03	
Prpf4ba	B0V1K6	LCDFGSASHVADNDITP(pY)LVSR	Y852	Y849	0,30	0,18	
Rplp; Rplp2l	Q6P5K5	KEESEE(pS)DDDMGFGLFD	S80	S104	0,17	0,95	
Ror2	E7FCE4	WMSPEAIL(pY)GK	Y668	Y666	0,13	-1,15	*j*
Fynrk	E7F1M5	LDNGGY(pY)LSTAR	Y181	Y214	0,12	0,64	
Histone 2B 1/2	Q5BJA5	ESYAI(pY)VYK	Y39, Y41	Y41	0,04	-0,21	
Pard3	A2BEM7	TLSP(pS)PDDHER	S705	S695	0,04	0,34	
Mapk14a	Q9DGE2	HTDDEMTG(pY)VATR	Y183	Y182	0,00	-0,06	
Flo11*	XP_005172506.1*	TEEDHV(pY)SFPNK	Y139	Y118	0,00	-0,37	
Hmga1*	NP_998333.1*	KHPQQEASG(pS)PTPK	S36	S49	-0,01	-0,32	
Mapk14a	Q9DGE2	HTDDEM(pT)GYVATR	T181	T180	-0,03	-0,07	
Fynrk	E7F1M5	ELVEHY(pS)K	S199	Y193	-0,06	-0,13	
Dyrk2	Q5RHV3	VYT(pY)IQSR	Y379	Y382	-0,07	-0,24	
Krt8	Q6NWF6	NFSSLSYSGPSMSR	Y29**	Y25**	-0,08	0,77	
Mapk12b	Q5RHW0	QADSEMTG(pY)VVTR	Y183	Y185	-0,14	-0,22	
Peak1	E7F7V3	AT(pY)TNLGQSR	Y1096	Y1107	-0,17	-0,02	
Dyrk1b; Dyrk1ab	D1L3Y5;A9QVW5	IYQ(pY)IQSR	Y326; Y273	Y321	-0,19	0,00	
Fynrk	E7F1M5	LDNGG(pY)YLSTAR	Y180	Y213	-0,19	0,08	
Ybx1	A1A605	REGAE(pS)APEGEMQQQQR	S159	S176	-0,20	0,48	
Hipk2	Q1MTA8	AVCST(pY)LQSR	Y375	Y352	-0,33	-0,09	
Prkcda	Q7ZUC5	RPDNNTQDVGV(pY)QDFNK	Y314	Y313	-0,33	0,11	
Mapk14b	Q9DGE1	LTDDEM(pT)GYVATR	T181	T180	-0,34	-0,18	
Mapk11	Q6IQ84	QTDDEMTG(pY)VATR	Y181	Y182	-0,34	-0,13	
Hipk2; Hipk3	Q1LUZ7;Q1MTA8	AVCSTYLQ(pS)R	S366	S355	-0,34	-0,14	
Mapk12	O42376	QTDSEMTG(pY)VVTR	Y183	Y185	-0,34	-0,60	
Mapk12	O42376	QTDSEM(pT)GYVVTR	T181	T183	-0,35	-0,58	
Afap1l2	E7FH23	SSNAGGDEE(pY)I(pY)MNK	Y55, Y57	Y54, Y56	-0,36	0,18	
Mapk14b	Q9DGE1	L(pT)DDEMTGYVATR	T176	T175	-0,36	-0,16	
Eppk1	I3ISA6	AVTGYTDP(pY)TGK	Y1642	Y1656	-0,39	0,27	
Mapk14b	Q9DGE1	LTDDEMTG(pY)VATR	Y183	Y182	-0,40	-0,26	
Cdk1; Cdk2	Q7T3L7;Q7ZWB1	IGEGTYGVV(pY)K	Y19; Y19	Y19; Y19	-0,48	0,29	

Ctnnd	XP_005160310.1*	YRPVDG(pY)R	Y215	Y248	-0,54	0,52	
Hck	E7F0I7	IIEDNE(pY)TAR	Y384	Y419	-0,59	-0,30	
Cdk1; Cdk2	Q7T3L7;Q7ZWB1	IGEGT(pY)GVVYK	Y15	Y15	-0,62	-0,21	
Ptk2.1	F1QT14	YMEDS(pS)(pY)YK	S579, Y580	S576, Y577	-0,69	-0,64	
Keratin 4	F1QK60	GYTSQ(pS)AYAVPAGSTR	S22	S51	-0,69	0,35	
Chrnb1*	NP_001240739.1*	VADE(pY)FIR	Y380	Y390	-0,70	-0,18	
Abl1; Abl2	E7FDC6;B0UXN7	LMTGDT(pY)TAHAGAK	Y412; Y407	Y393; Y439	-0,70	-0,20	
Ptk6a	F1Q7D7	ASACEPGSEL(pY)K	Y111	Y13	-0,73	-0,06	
Gsk2aa; Gsk3b	Q9YH61;Q9YH60	GEPNVS(pY)ICSR	Y216	Y216	-0,78	-0,18	
Ptk2.1	F1QT14	YMED(pS)SYYk	S578	S575	-0,78	-0,22	
Ptk6a	F1Q7D7	ESV(pY)SSEDAQIPYK	Y446	Y432	-0,79	-0,66	
Ptk2.1	F1QT14	YMEDSS(pY)YK	Y580	Y577	-0,82	-0,22	
Pfn2	Q802D5	SQGGEPT(pY)NIAVGK	Y99	Y99	-0,85	0,32	
Abl1; Abl2	E7FDC6;B0UXN7	LMTGDTY(pT)AHAGAk	T413, T408	T394; T440	-0,86	-0,24	
Irs1b*	XP_005157831.1*	SSD(pY)MPMSPK	Y584	Y612	-1,18	-0,48	*k*
Fer	F1QBS0	QEDDGIYSSSGLK	Y716**	Y714**	-1,91	-1,47	*l*
Ptpn11a	F1QZU5	IQNTGD(pY)YDLYGGEK	Y60	Y62	-3,74	0,35	*m*
Ptpn11a	F1QZU6	IQNTGDY(pY)DLYGGEK	Y61	Y63	-4,36	-0,05	*n*

Table 1: Comparative mass-spectrometry of pTyr immunoprecipitated zebrafish lysates
Zebrafish embryos were injected at the 1-cell stage with synthetic mRNA constructs encoding WT Shp2, NS (D61G) Shp2 or LS (A462T) Shp2 and co-injected with mRNA encoding eGFP. Lysates were subjected to mass spectrometry as described in Materials and Methods. Normalized ratios (Log2 scale) based on total levels of non-phosphorylated peptides are given. * Protein name based on BLAST sequence of peptide. Accession numbers from BLAST hits are used for non-annotated peptides. ** pRS score <75, phosphorylation site could not be determined but the most commonly identified site from Phsophosite.org is used. a-n: indicators for Figure 1C.

respectively in NS and Log_2: 1.77 and Log_2: 1.63 fold, respectively in LS). A further analysis of the role of PZR in NS and LS is described elsewhere [21]. In addition, we identified a pTyr peptide corresponding to Y989 in human Insulin receptor substrate 1B (IRS1B) to be highly abundant in NS (Log_2: 1.39 fold) and LS (1.59 fold) (peptide "d"). A phosphopeptide corresponding to Y792 of EphB3 (peptide "g") was also upregulated in NS and LS (Log_2: 1.04 fold in NS and Log_2: 2.90 in LS).

At the other end of the spectrum, the most decreased phosphopeptide in NS and LS corresponded to Fer kinase (peptide "l", NS: Log_2 -1.91 fold, LS: Log_2 -1.47 fold). The MS2 spectrum of the Fer phosphopeptide is given in Figure S1. Unfortunately, a reference peptide for total Fer levels was not identified. Thus, the reduced levels of Fer phosphopeptide may represent reduced Fer phosphorylation, reduced total Fer levels or a combination of both. While phosphorylation of serine instead of tyrosine in this peptide could not be excluded, the tyrosine in this peptide is found frequently in other mass spectrometry based experiments (http://www.phosphosite.org). In addition, the peptide was immunoprecipitated with anti-pTyr antibodies, which indicates that this tyrosine is likely phosphorylated. Interestingly, this tyrosine is the autophosphorylation site of Fer [21]. Since Fer had not been studied in zebrafish nor had Fer been implicated in NS and LS, we further investigated the role of Fer in these syndromes,

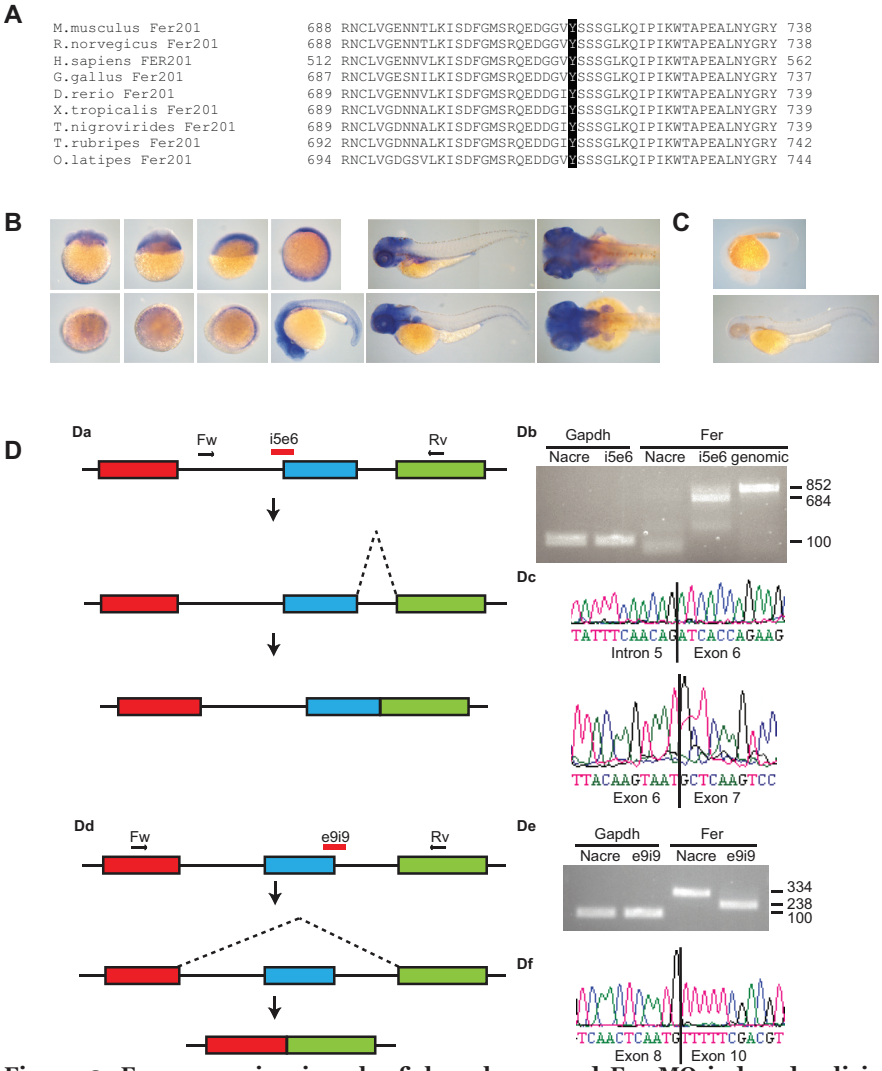

Figure 2. Fer expression in zebrafish embryos and Fer MO induced splicing defects. A. Alignment of zebrafish Fer kinase sequence encompassing the autophosphorylation site (black) that was identified by phosphoproteomics with the mammals *M. musculus*, *R. norvegicus*, *H. sapiens*, the avian *G. gallus*, the amphibian *Xenopus tropicalis*, and the fish *Tetraodon nigrovirides*, *Takifugu rupripes* and *Oryzias latipes*. B. *fer* expression during the first 24 hpf and at 3dpf and 4dpf was observed using *in situ* hybridization with an antisense fer probe. C. ISH with negative control sense fer probe. D. RT-PCR showing altered splicing of *fer* in MO injected embryos. Da. Model of altered splicing by Fer MO i5e6. Exons 5, 6 and 7 are indicated in red, blue and green, respectively. Primers used for RT-PCR are indicated as arrows. MO is indicated in red. Due to splice blocking, intron 5 is not spliced out of the processed mRNA. Db. RT-PCR showing *gapdh* control in Nacre (control) MO and Fer MO injected embryos. RT-PCR showing *fer* product in Nacre control MO and Fer i5e6 MO injected embryos, and genomic DNA as a positive control. Dc. Sanger sequencing showing the inclusion of intron 5 and the normal splicing of exon 6 in the RT-PCR product. Dd. Model of altered splicing by Fer MO e9i9. Exons 8, 9 and 10 are indicated in red, blue and green, respectively. Primers used for RT-PCR are indicated as arrows. MO is indicated in red. Due to defective splicing, exon 9 is spliced out of the processed mRNA. De. RT-PCR showing *gapdh* control in Nacre (control) MO and Fer e9i9 MO injected embryos. RT-PCR showing Fer product in Nacre control MO and Fer e9i9 MO injected embryos with a decrease in size of the product in e9i9 MO injected embryos. Df. Sanger sequencing showing the exclusion of exon 9.

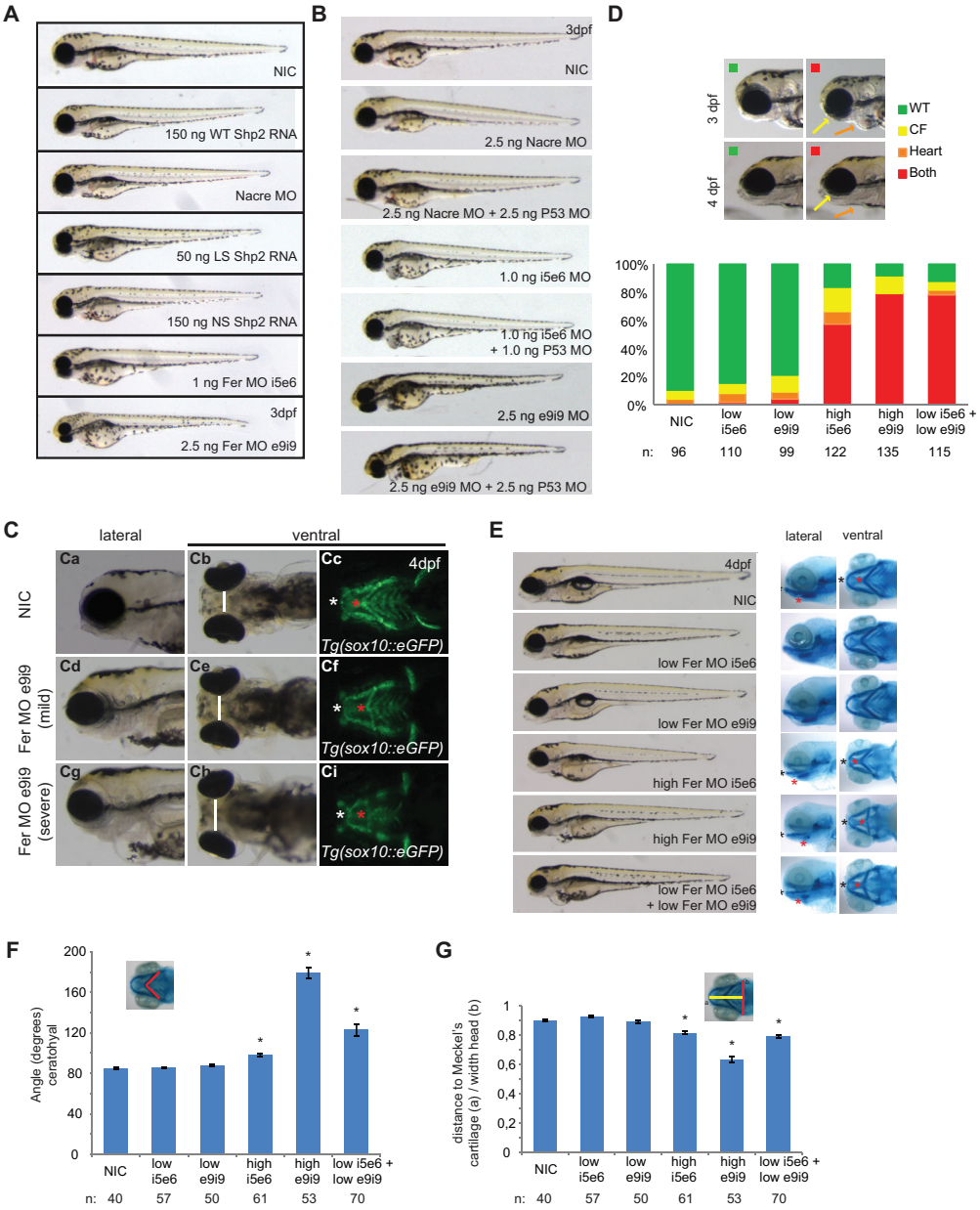

Figure 3. Fer knockdown induced craniofacial defects in zebrafish embryos.
A. Embryos were injected at the 1-cell stage with 1 ng Fer i5e6 MO, 2.5 ng e9i9 MO or 2.5 ng Nacre MO as a negative control. Additionally, embryos were injected with 150 ng WT Shp2 RNA, 150 ng NS Shp2 RNA or 50 ng LS Shp2 RNA. B. Embryos were injected at the 1-cell stage with 2.5 ng Nacre control MO, 1.0 ng Fer i5e6 MO, 2.5ng Fer e9i9 MO or in combination with 2.5 ng P53 MO. C. Craniofacial structures were imaged using *Tg(-4.9sox10:EGFP)ba2* embryos expressing eGFP in neural crest cells that also form the cartilage. Embryos were injected with Fer MO e9i9 at the 1 cell stage and imaged at 4dpf. Ceratohyal is indicated with a red asterisk and Meckel's cartilage with a white asterisk. Both moderate and severe phenotypes are depicted together with non-injected controls (NIC). D. Embryos were injected at the 1-cell stage with

Fer kinase expression in zebrafish embryos and Fer MO induced splicing defects.

The Fujinami poultry sarcoma (fps)/Feline sarcoma (*fes*) related kinase (Fer) is a widely expressed, 94 kDa non-transmembrane protein tyrosine kinase (PTK) that is associated with cell migration, tumor growth and was first described in 1986 [22-24]. Fer is involved in focal adhesion and cadherin signaling, as well as ERK, Akt and Stat3 signaling [22]. Fer and Shp2 share many signaling pathways and a requirement for both proteins has been described in synapse formation [25]. It is thus likely that signaling between Fer and Shp2 plays an important role in cell-cell adhesion, migration and morphogenesis.

The identified peptide corresponded to tyrosine 714 (Y716 in zebrafish) which is the Fer autophosphorylation site, phosphorylation of which results in activation of Fer kinase activity [26]. Sequence alignment of the Fer kinase primary amino acid structure showed conservation of FER protein among vertebrates, from *Homo sapiens* to *Danio rerio* (Figure 2A), all coding for the conserved autophosphorylation site tyrosine. We cloned zebrafish fer from cDNA obtained from 1dpf embryos. Sequence analysis confirmed that the *fer* transcript that was cloned was identical to *ENSDART00000050957* or zebrafish *fer-201* encoding full-length Fer protein. Thus, Fer and its autophosphorylation site are evolutionarily conserved in vertebrates, including zebrafish.

As a first step to investigate the role of Fer kinase during development, *in situ* hybridization (ISH) was performed on zebrafish embryos, using a *fer*-specific probe (Figure 2B). As a negative control sense fer probe was used (Figure 2C). Ubiquitous expression of Fer is already apparent at the 8-cell stage, prior to zygotic transcription, indicating maternal contribution of *fer* mRNA. *Fer* remained ubiquitously expressed until 10 somite stage. At later stages, *fer* expression was enriched anteriorly and in the pectoral fins. In conclusion, *fer* expression was ubiquitous during gastrulation and more restricted during later stages of development.

To investigate the role of Fer *in vivo*, morpholinos against Fer were injected into zebrafish embryos at the 1-cell stage. As a negative control, non-related Nacre MO was injected that does not induce developmental defects, as we have observed before [27]. We assessed Fer protein knockdown by immunoblotting using commercially available Fer antibodies, but unfortunately, these reagents did not allow detection of endogenous Fer in zebrafish embryos. Instead, knockdown of *fer* was verified by RT-PCR of knockdown embryos (Figure 2D). Injection of Fer e5i6 MO blocked splicing of *fer* intron 5, resulting in the incorporation of intron 5 and introducing multiple stop codons in the aberrantly spliced *fer* mRNA (Figure 2Da and Db). Injection of Fer e9i9 MO caused aberrant splicing, thereby excluding exon 9 of fer (Figure 2Dd and De). These effects of MO injections were verified by sequencing (Figure 2Dc and Df, respectively).

(Figure 3 continued) suboptimal concentrations of MO (0.5 ng i5e6 MO; n=110 and 1.0 ng e9i9 MO; n=99). High levels of both MO's (1.0 ng i5e6 MO; n=122 and 2.5 e9i9 MO; n=135) or low levels of both MO's were co-injected (n=115). Embryos were imaged at 3dpf and 4dpf and grouped by having a WT appearance (green), a craniofacial defect alone (yellow) a heart defect alone (orange) or both (red) at 4dpf. Relative levels of phenotypes are depicted. E. Embryos were injected at the 1-cell stage with normal dose of MO (1.0 ng i5e6 MO; n=61 and 2.5 e9i9 MO; n=53), low doses of MO (0.5 ng i5e6 MO; n=57 and 1.0 ng e9i9 MO; n=50) or a co-injected with low doses of MO (n=70). Morphology at 4 dpf is depicted. Embryos were fixed and stained with Alcian blue at 4dpf and imaged laterally and ventrally. For quantification, the angle of the ceratohyal (F) and the ratio of the distance from the back of the head to Meckel's cartilage and the width of the head was determined (G) (* indicates significance, Student's t-test $p<0.005$).

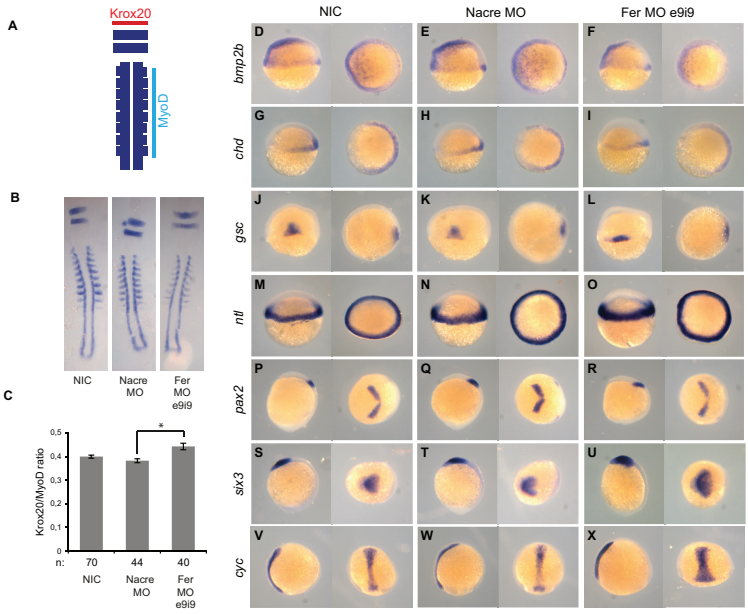

Figure 4. Fer knockdown resulted in C&E defects but not in changes in cell fate. A. *Krox20/myoD in situ* hybridization as a method to quantify C&E defects. Krox20 (red) staining for rhombomeres 3 and 5 was used to measure the width, which correlates with convergence cell movements in the embryo. *myoD* (light blue) staining for the somites was used to measure the length, i.e. extension of the embryo. The ratio of *krox20/myoD* correlates directly with convergence & extension cell movements during gastrulation. B. Flatmounts of *krox20/myoD* stained NIC (n=70), control MO (n=44) and Fer MO (n=40) embryos. C. The ratio of the width of a *krox20*-positive rhombomere and the length of 8 somites was determined (* indicates significance, Student's t-test p<0.005). D-X. Embryos were injected at the 1-cell stage with control MO or Fer e9i9 MO and subjected to ISH for various markers of cell fate determination. Note that the staining of the *gsc*, *pax2*, *six3* and *cyc* probes show broader and shorter expression in Fer knockdown embryos than in controls.

Fer knockdown phenocopies Shp2 knockdown, NS and LS Shp2 expression in zebrafish.

Injection of both Fer morpholinos (i5e6 and i9e9) induced developmental defects including reduced body axis length, heart edema and craniofacial defects at 3dpf (Figure 3A). These defects were similar to the phenotypes observed in zebrafish expressing NS and LS Shp2 that were analyzed in parallel (Figure 3A). MOs are known to induce non-specific p53 activation and apoptosis [12]. To rule out that the observed phenotype is the mere result of p53 activation, co-injection of p53 MO was performed, which is an accepted control to assess specificity of MOs. Knockdown of p53 did not affect the Fer knockdown phenotype, indicating that the phenotype was independent of p53 (Figure 3B). Taken together, two independent Fer MOs were used that blocked normal splicing of fer and induced developmental defects.

The craniofacial defects we observed in Fer knockdown embryos were reminiscent of the defects observed in Shp2 knockdown embryos as well as embryos expressing NS or LS Shp2 [9,28]. To verify these craniofacial defects, we first used the *Tg(-4.9sox10:EGFP)ba2* transgenic line, which expresses GFP in neural crest-derived cartilage in the head [29]. We observed heart edema (Figure 3Ca, Cd and Cg) an increased distance between the eyes (Figure 3Cb, Ce and Ch), an increased angle of the ceratohyal (Figure 3Cc, Cf and Ci, red asterisk), a less protruded Meckel's cartilage (white asterisk), confirming the craniofacial defects. To verify the specificity of the Fer MOs again, we co-injected low doses of the two Fer-MOs that did not induce developmental defects

on their own (Figure 3D). Co-injection of suboptimal doses of both Fer MOs together induced a drastic increase in the Fer knockdown phenotype with reduced body axis extension, heart edema (orange) and craniofacial defects (yellow) as prominent features (see Figure 3D lower panel). This was further verified by alcian blue stainings on Fer knockdown embryos at 4dpf (Figure 3E). The angle of Meckel's cartilage (Figure 3F) and the ratio of the distance between the eyes and the back of the head to the ceratohyal (Figure 3G) were used to quantify these defects. Whereas NIC embryos showed an angle of 85±1 degrees (n=40), injection of high levels of Fer MO e5i6 induced an increased angle of the ceratohyal (98±1 degrees, n=61), as did injection of high levels of Fer MO e9i9 (angle=179±5 degrees, n=53) which were both significant ($p<0.005$ Student's t-test) (Figure 3F). The ratio of the distance from the back of the head to Meckel's cartilage and the width of the head at 4dpf showed a similar significant increase (e5i6 MO: ratio=0.82±0.01; e9i9 MO: ratio=0.63±0.02, compared to NIC: ratio=0.90±0.01; $p<0.001$, Student's t-test) (Figure 3G). Embryos injected with low doses of Fer MO e5i6 alone showed an angle of the ceratohyal of 85±1 degrees, n=57 (n.s.) and a ratio of 0.93±0.01 ($p<0.001$). Low dose Fer MO e9i9 injected embryos showed an angle of 88±1, n=50 (n.s.) and a ratio of 0.89±0.01 (n.s.). Co-injection of both MO's at low doses together resulted in a drastic increase of craniofacial defects. Quantification of the craniofacial defects of these embryos showed an angle of 123±6, n=70 ($p<0.001$) and a ratio of 0.79±0.01 ($p<0.001$) (Figure 3E-G).

We tried to rescue the Fer MO-induced developmental defects by expression of mRNA encoding full length Fer. Unfortunately, despite many attempts, we failed to rescue the Fer MO induced developmental defects (Figure S2A). Expression of Fer by itself induced reduced body axis extension, cardiac edema and craniofacial defects (Figure S2B), which impaired assessment of the rescues. It is not uncommon that up- and down-regulation of signalling proteins, including Shp2 and RhoA, induce similar developmental defects [9]. In conclusion, knockdown of Fer was specific and resulted in craniofacial defects, heart edema and reduced body axis extension, which is reminiscent of the developmental defects in Shp2 knockdown embryos as well as NS and LS Shp2 expressing embryos.

Fer knockdown induced convergence and extension defects

Fer knockdown phenocopied Shp2 knockdown and NS and LS expression at later developmental stages. Loss of Shp2 and expression of NS and LS variants of Shp2 induce C&E defects in developing zebrafish embryos [9]. We investigated whether Fer knockdown caused developmental defects during gastrulation as well. To investigate C&E defects upon Fer knockdown, embryos were subjected to *in situ* hybridization (ISH) using probes for *myoD*, staining the somites and *krox20* staining rhombomeres 3 and 5, a verified method to quantify C&E defects in developing zebrafish embryos (Figure 4A) [30,31]. Indeed, Fer morphant embryos showed C&E defects compared to control morphants (Student's t-test, $p<0.005$) (Figure 4B and 4C). In addition to C&E defects, cell specification may be affected by the loss of Fer function. To investigate this, we subjected developing embryos to ISH using panel of cell fate markers, including *bmp2b*, *cyc*, *chd*, *ntl*, *six3*, *gsc* and *pax2* (Figure 4D-X). Expression levels of these markers were unchanged in Fer MO and control MO injected embryos compared to non-injected controls (NIC). However, expression of *gsc*, *pax2*, *six3* and *cyc* showed broader and shorter signal in Fer knockdown embryos, compared to NIC and control MO injected embryos, likely resulting from C&E defects (Figure 4 J-L, P-R, S-U and V-X, respectively). Thus, loss of Fer leads to C&E defects similar to Shp2 knockdown in developing zebrafish, and does not cause alterations in early cell fate determination.

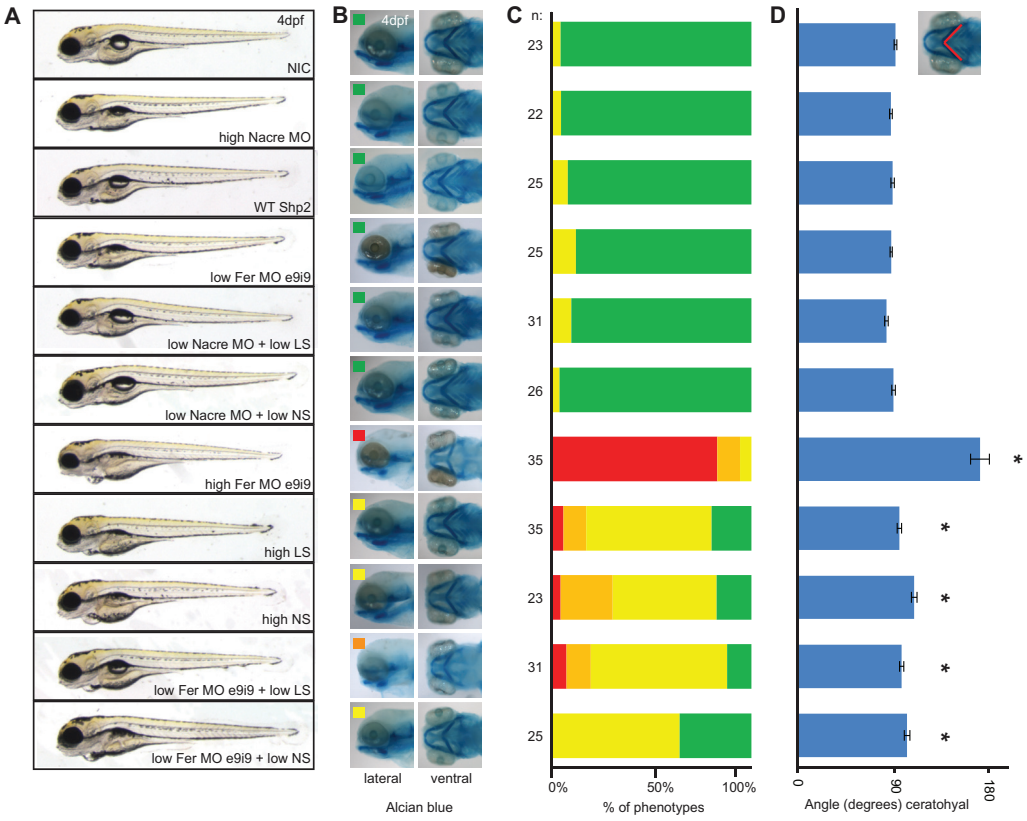

Figure 5. Partial knockdown of Fer cooperated with suboptimal expression of NS- and LS- but not WT Shp2 to induce developmental defects.
A. Embryos were injected with control MO, Fer e9i9 MO and NS, LS or WT Shp2 mRNA as indicated, and imaged at 4dpf. B. Alcian blue staining showing craniofacial defects scored on severity (green: wild type, yellow: mild phenotype, orange: moderate phenotype, red: severe phenotype). C. Embryos were scored based on craniofacial defect upon alcian blue staining. The number of embryos per condition is indicated. D. The angle of the ceratohyal was quantified as a measure of craniofacial defects (* p< 0.005, Student's t-test).

Fer knockdown cooperates with NS and LS, but not WT Shp2 expression.

Mass spectrometric analysis showed reduced Fer Y714 phosphopeptide. In developing zebrafish, we found that loss of Fer phenocopies Shp2 knockdown and expression of NS and LS Shp2, and leads to C&E defects. To investigate if downregulation of Fer contributes to the pathogenesis of NS and LS, we performed a genetic epistasis experiment, where we induced suboptimal knockdown of Fer in combination with injection of low amounts of NS and LS Shp2 mRNA that do not induce defects by themselves. Control injections only marginally affected craniofacial development. The ceratohyal angle in control injected embryos was 93±1 degrees, which was a slight increase compared to the ceratohyal angle of control injected embryos, 88±1 degrees ($p<0.05$). Whereas Fer knockdown caused developmental defects (Figure 5A, B), partial knockdown of Fer using a low dose of Fer MO e9i9 did not induce developmental defects (ceratohyal angle: 89±1 degrees, n.s). Likewise, injection of NS and LS, but not WT Shp2 mRNA at normal doses induced heart

edema, reduced body axis extension and craniofacial defects (NS: ceratohyal angle: 110±3 degrees, $p<0.005$ and LS: angle: 96±2 degrees, $p<0.001$). At lower doses, NS and LS Shp2 also did not cause major developmental defects or an increase in the angle of the ceratohyal compared to control injections (Low NS: 91±2 degrees, n.s and low LS: 84±2 degrees, $p<0.05$). When combined with low doses of Fer MO however, NS and LS showed heart edema and major increases in craniofacial defects (Low NS + low Fer MO: 103±3 degrees, $p<0.001$ and Low LS + low Fer MO: 98±2 degrees, $p<0.001$) (Figure 5A , 5C and 5D). This indicates that a decrease in Fer cooperates with NS and LS to induce developmental defects seen in NS and LS.

Discussion

Using a comparative phosphoproteomics approach focused on pTyr-containing proteins, we identified a phosphopeptide corresponding to Fer kinase as the main decreased phosphopeptide in zebrafish embryos expressing NS or LS mutant Shp2 compared to WT. Fer knockdown induced developmental defects in zebrafish embryos that are reminiscent of defects induced by NS and LS Shp2. Epistatic interaction analyses suggested a genetic interaction between Fer kinase and mutant Shp2.

Previously, we used comparative phosphoproteomics in zebrafish to identify differences between wild type and Fyn/Yes knockdown embryos [18]. At that time, TiO_2 columns were used to enrich for phosphopeptides, and only highly abundant phosphoserine- and phosphothreonine-containing phosphopeptides were identified, excluding low abundant pTyr-containing peptides [18]. Improved methods using immunoprecipitation of pTyr peptides allow for the identification of endogenous tyrosine phosphorylated peptides [27]. Stable isotope dimethyl labelling allows for the quantitative comparison of three different samples in an economical fashion, compared to other peptide labelling methods [17]. Other groups have successfully analysed the proteome of zebrafish under different conditions [32-34], however these experiments often focussed on the whole proteome in a specific organ. Given the crucial role of tyrosine phosphorylation in signalling during development, we hypothesized that specific analysis of the tyrosyl phosphoproteome would provide insights into development and disease. Particularly in case of NS and LS, two syndromes that are associated with expression of mutant Shp2, a protein-tyrosine phosphatase. Recently, a MS based approach was used to identify proteins that were affected by the altered binding properties of NS and leukemia associated Shp2 [35]. Although highly informative, these experiments were performed using the tandem SH2 of Shp2 expressed in cells. As full length NS and LS Shp2 exhibit different dynamic properties than WT [36,37], using the full length protein under physiological conditions in vivo gives more relevant insights into the etiology of the disease. Therefore, we performed for the first time a comparative phosphoproteomics experiment in zebrafish using pTyr immunoprecipitation and stable isotope dimethyl labelling.

Using this technique, we identified several phosphopeptides that were increased or decreased in NS and LS Shp2 embryos. One of these peptides corresponded to the Fer autophosphorylation site and was the most strongly decreased phosphopeptide in the zebrafish disease model for NS and LS. Follow-up experiments showed that *fer* mRNA is maternally contributed and is expressed ubiquitously during gastrulation. Later, *fer* expression is restricted anteriorly and in the pectoral fins of developing zebrafish embryos (Figure 2B). Fer is conserved and *fps/fes/fer* homologues exist in sponges (Fes/FER_SR), *D. melanogaster* (*dfps85D*) and *C. elegans* (FRK-1) [38,39]. In chick, Fer expression is ubiquitous, with higher expression levels during development than at later stages [24]. Also in mammalian cells, Fer expression is widely distributed [23]. Fer expression is

vital for dorsal closure of *C.elegans*, yet its kinase activity seems to be redundant in development [39-41]. We demonstrate that in fish, a decrease in total Fer levels by MO-induced knockdown resulted in developmental defects that were reminiscent of Shp2 knockdown, and NS and LS expression in zebrafish (Figure 3A) [9]. Moreover, loss of Fer resulted in C&E defects during gastrulation, which were also observed in NS and LS zebrafish (Figure 4)[9,31]. Indeed, also at later stages craniofacial malformations and heart edema were observed in Fer knockdown embryos, similar to NS and LS Shp2 expressing embryos (Figure 3) [9,28,31,42]. We show a genetic interaction between *fer* and *ptpn11*, since loss of Fer contributes to the NS and LS phenotype (Figure 5).

The mechanism underlying the role of Fer kinase in development remains to be determined definitively. Fer has been reported to be involved in various signaling pathways. Expression of full length fer is essential for *Drosophila* gastrulation via Src42A, a *Drosophila* Src homologue [40] However, it is unclear if kinase activity is essential for this function of Fer. In C.elegans, FRK-1 is essential for embryonic closure and morphogenesis but this is not dependent on FRK-1 kinase activity [39]. Depletion of Fer kinase activity leads to a reduction in p38 MAPK but not ERK activity in activated mast cells [43] Fer is able to sustain ERK activation under hypoxic conditions but kinase activity is not essential [44]. Interestingly, Fer kinase activity is essential for β-catenin-cadherin complex formation. Expression of kinase dead Fer attenuates formation of this complex. EGF treatment rescues this defect, indicating a compensatory mechanism for the loss of Fer kinase activity. Interestingly, PTP1B, another member of the PTP family, associates with Cadherin in a Fer kinase-dependent manner, but whether PTP1B dephosphorylates Fer remains to be determined [45]. How NS and LS Shp2 cause a downregulation of Fer protein tyrosine phosphorylation remains to be determined. Since both activated NS Shp2 and catalytically impaired LS Shp2 have similar effects on Fer, it is unlikely that Fer is a direct substrate of Shp2. Disease associated Shp2 was found to bind to hyperphosphorylated substrates, both in NS and LS and in experimental conditions [20,46]. Fer and Shp2 share many interacting partners, including PDGFR, integrins, PECAM-1 and others [25,46-48]. In addition, Fer and Src (an important Shp2 interacting protein) share many substrates, including cortactin [41,49]. Disease associated Shp2 exhibits altered dynamics and binding properties [35-37]. Mutant Shp2 may quench binding proteins that are normally required for full activation of Fer kinase, resulting in reduced tyrosine phosphorylation of Fer upon expression of NS and LS Shp2.

Alternatively, Fer activity might be downregulated through enhanced growth factor signaling that occurs in NS and LS [36,45]. While many studies have shown a loss of phosphatase activity in LS Shp2, the ability of LS Shp2 to enhance ERK activation remains subject of debate [4,36]. In zebrafish, we observe enhanced ERK activation in both NS and LS [50] and hence, reduced Fer phosphorylation may result from a negative feedback mechanism, resulting from enhanced growth factor signaling. In conclusion, we identify Fer kinase as a likely downstream target of NS and LS Shp2 and we provide evidence that deregulation of Fer enhanced the NS and LS phenotype in vivo.

Materials and Methods

Ethics statement

Only embryos up to 4 days post fertilization (dpf) were used for these experiments, which do not require approval of the animal experiments committee according to national and European law. Zebrafish maintenance and *in situ* hybridization. Wild type and *Tg(-4.9sox10:EGFP)ba2* zebrafish were kept under standard conditions. Embryos were staged as described by Westerfield [11]. In situ hybridizations were done as described before [9], using probes specific for *bmp2b*, *chd*, *cyc, gsc*, *krox20*, *myod*, *ntl*, *pax2* and six3. For the *fer* probe, Fer-pBSK- was digested with NotI for the antisense probe and with ApaI for the sense probe, respectively. T7 and T3 RNA polymerase were used to generate digoxigenin labeled RNA (Roche). Embryos were fixed at the indicated stages with 4% paraformaldehyde (PFA). Embryos were treated from 24 hpf onwards with 0.2 mM 1-phenyl 2-thiourea (Sigma) in E3-medium to block pigmentation.

Constructs

fer was amplified from cDNA of 1 dpf WT embryos and cloned into EcoRI/XhoI sites of pCS2+ and pBSK- and verified by sequencing using: Fer_out_Fw: 5'-GAGAGAGACTGCGTGCCTTG-3', Fer_out_Rv: 5'-ATGAGATTCTGAGGGCGAAA-3' and Fer_EcoRI_Fw: 5'-GGCGAATTCATGGGGTTCGGCCGGGAC-3', Fer_XhoI_Rv: 5'-CGGCTCGAGTTAGGGATCACCTGGATG-3'. The mutation Y716F was introduced into fer by site-directed mutagenesis using Fer_Y716F_Fw: 5'-TCCTGATGAGGAGAAGATGCCGTCGTC-3' and Fer_Y716F_Rv: 5'-GACGACGGCATCTTCTCCTCATCAGGA-3'.

Morpholinos, RNAs and injections

Fer splicing morpholinos (MOs) were designed for several intron-exon boundaries and ordered from GeneTools (Philomath, OR, USA). The p53 MO (5'-GCGCCATTGCTTTGCAAGAATTG-3') was described before and was used as recommended by the manufacturer [12]. Synthetic mRNA was synthesized using mMessage mMachine kit (Ambion). pCS2+ plasmid was digested with NotI and RNA was synthesized with SP6 RNA polymerase. The NS and LS constructs were previously described [9]. MOs and mRNA was injected at one cell stage and the working concentration was titrated for each MO and mRNA. Fer MO i5e6 (5'-GGCTTCTGGTGATCTGTTGAAATA-3') was used at 1.0 ng/µl (high concentration) or 0.5 ng/µl (low concentration). Fer MO e9i9 (5'-GGGATTACACTTACTGACGAAGAGC-3') was used at 2.5 ng/µl (high concentration) or 1.0 ng/µl (low concentration). For co-injection, suboptimal concentrations of both MOs were combined.

Alcian blue staining

Embryos were anesthetized with tricaine methane sulfonate (Sigma) and fixed in 4% PFA at 4 dpf. After several hours of fixing, embryos were washed for 10 min in 50% ethanol. Embryos were stained overnight at 4 degrees in staining solution (0.04% Alcian blue (Sigma), 70% ethanol and 50 mM magnesiumchloride) and washed in 0.2% Triton X-100 (Sigma). Afterwards, embryos were bleached to remove pigmentation (8.5% hydrogen peroxide, 5% formamide, 0.5x SSC) and washed with 0.2% Triton X-100. Images were quantified by using ImageJ software.

RNA isolation

Total RNA of 3 dpf Nacre MO and Fer MO injected embryos was isolated. Approximately 30 embryos were dissolved in 1.0 ml TriZol (Invitrogen). The homogenate was centrifuged (12.000g, 4 degrees, 10 min). 0.2 ml Chloroform was added to the supernatant, vortexed for 15 sec,

incubated for 3 min at room temperature (RT) and afterwards centrifuged (12.000g, 4 degrees, 15 min). 0.5 ml isopropanol was added to the upper phase, incubated for 10 min at RT and centrifuged (12.000g, 4 degrees, 15 min). The pellet was washed with 75% ethanol and after vortexing centrifuged (10.000g, 4 degrees, 5 min). The pellet was dried for 5 min and dissolved in 100 µl deionized water. Subsequently, the solution was incubated for 10 min at 37 oC, precipitated in 250 µl 100% ethanol and 10 µl 3M sodium acetate and stored at -80oC.

RT-PCR

For the reverse transcription reaction (RT-PCR) with M-MLV-RT (Promega) 1 µg of total RNA was used. PCR of cDNA was performed using standard protocol of GoTaq (Promega) using Fer_Fw_intron_5: 5'-TTTCTGTCCCCATTGCAAAG-3', Fer_Rv_exon_7: 5'-GATTCTGCTGGGTTATTAGC-3', Fer_Fw_exon_6: 5'-GAACCTAATGTAGAATTTGATGC-3', Fer_Fw_exon_8: 5'-CGGAGGCCAAACTCATGGCACA-3' and Fer_Rv_exon_10: 5'-CGCACCAGAAAGTCTCCCTG-3'. Gadph was used as a loading control for the RT-PCR reaction.

Mass spectrometry

Digest Preparation.

Embryos were injected at the 1-cell stage with 150 pg wild type Shp2, 150pg Shp2-D61G or 50pg Shp2-A462T RNA, respectively. Shp2 RNA injected embryos were co-injected with enhanced green fluorescent protein (GFP) RNA used for screening of injection efficiency. Embryos expressing GFP were selected, manually dechorionated and collected at 26hpf to 28hpf. Embryos were then deyolked and washed using deyolking buffer (1/2 Ginzburg Fish Ringer) without calcium (2x10µl/embryo) snap frozen and stored at -80 °C for further usage [11,13]. Embryo pellets corresponding to a total of approximately 2000 embryos per condition were resuspended and lysed in 8 M Urea, 50 mM ammoniumbicarbonate, 1 PhosSTOP tablet per 10 ml plus 1mM vanadate and ethylenediaminetetraacetic acid-free protease inhibitor cocktail (Sigma). Embryo lysates were sonicated for 4x 30 seconds and then centrifuged at 14 500 rpm for 30 minutes at 4°C. Lysate supernatants equivalent to 3 to 4mg total protein per condition were generated in principle as described previously [14,15]. Briefly, the lysates were reduced with dithiothreitol (10mM) for 1 hour at 56°C and alkylated with iodoacetamide (55mM) at room temperature, in the dark for 45 minutes and digested for four hours with the protease Lys-C (1:100 enzyme/substrate) at 37°C. Samples were then diluted 4 fold with 50mM Ammoniumbicarbonate to 2M Urea and trypsin (1:100) was added and digestion was performed overnight at 37°C. The peptide mixtures were acidified to pH 3 by adding acetic acid to a final concentration of 2.5%. The individual peptide solutions were then desalted, dimethyl labelled on-column as described previously [16]. Wild type Shp2 injected embryos were labeled "light" whereas D61G (Noonan) Shp2 and A462T (LEOPARD) Shp2 injected embryos were labeled "intermediate" and "heavy", respectively.

Immunoprecipitation (IP)

IP was performed as described [17]. In principle, labeled peptide solutions were mixed in equal concentrations, vacuum dried and resuspended in IP Buffer (50mM Tris, pH 7.4, 150 mM sodium cloride, 1% n-octyl-β-D-glucopyranoside and a Complete Mini protease inhibitor tablet per 10 ml IP buffer (Roche Diagnostics)). PY99-agarose beads (Santa Cruz Biotechnology) were washed five times with IP buffer prior to IP. The labeled peptide mixture was mixed with the PY99-agarose beads, and incubation was performed overnight at 4 °C under constant rotation. After peptide immunoprecipitation, the beads were washed three times with IP buffer and two times with

ultrapure water. Peptides were eluted by adding two times 50 µl of 0.15% trifluoroacetic acid for 20 min at room temperature. Eluted peptides were then desalted and concentrated on C18 tips and resuspended in 10% formic acid prior to MS analysis.
On-line Nanoflow Liquid Chromatography—As described in [17]: Nanoflow LC-MS/MS was performed on an Linear Trap Quadrupole-Orbitrap XL mass spectrometer (Thermo Electron, Bremen, Germany) coupled to an Agilent 1100 HPLC system (Agilent Technologies, Waldbronn, Germany). Dried peptides were trapped at 5µl/min in 100% solvent A (0.1 M acetic acid in water). Subsequently, peptides were transferred to an analytical column (ReproSil-Pur C18- AQ, 3 µm (Dr. Maisch GmbH, Ammerbuch, Germany); 40 cm * 50 µm inner diameter, packed in house) at ~100 nl/min and eluted using a 3-h gradient from 0 to 40% solvent B (0.1 M acetic acid in 8:2 (v/v) acetonitrile/water). The eluent was sprayed via distal coated emitter tips (New Objective) butt-connected to the analytical column. The LTQ Orbitrap XL was operated in data-dependent mode, automatically switching between MS and MS/MS. Full-scan MS spectra (from m/z 350 to 1500) were acquired in the Orbitrap with a resolution of 60,000 at m/z 400 after accumulation to target value of 500,000. The three most intense ions at a threshold above 500 were selected for collision-induced fragmentation in the linear ion trap at a normalized collision energy of 35% after accumulation to a target value of 10,000.

Data Analysis

All MS2 spectra were processed and quantified with Proteome Discoverer (version 1.3.0.399). Runs were searched against a concatenated forward-decoy version of the Zebrafish Uniprot database (version 20130916, 81920 sequences) with Mascot (version 2.3.02, Matrix Science). The database search was performed with the following parameters: a mass tolerance of ±50 ppm for precursor masses and ±0.6 Da for CID fragment ions, allowing two missed cleavages, cysteine carbamidomethylation as fixed modification. Light, intermediate and heavy dimethylation of peptide N-termini and lysine residues; methionine oxidation; phosphorylation on serine, threonine and tyrosine were set as variable modifications. The enzyme was specified as trypsin. The phosphorylation site localization of the identified phosphopeptides was performed by the phosphoRS algorithm 3.1 implemented in Proteome Discoverer using a 75% cut-off. For phosphopeptides that did not have a phosphorylation site with a pRS score above 75%, the site was counted as “ambiguous”. The dimethyl-based quantitation method was chosen in Proteome Discoverer, with mass precision requirement of 2 ppm for consecutive precursor mass measurements. A 0.5 min retention time tolerance was applied for isotope pattern multiplets and allowed spectra with maximum 1 missing channels to be quantified. Mascot results were further filtered with the following criteria: (i) mass deviations of ±10 ppm; (ii) Mascot ion score of at least 20; (iii) a minimum of 6 amino-acid residues per peptide; and (iv) position rank 1, which results in a peptide FDR <1%. Phosphopeptides that were found to be differentially phosphorylated were manually validated.

Quantification

Quantified phosphopeptides were normalized against the median of all non-phosphopeptides. For peptides with phosphorylation sites with a pRS score above 75%, only these phosphopeptides were used for quantification. For peptides with only pRS scores below 75% all phosphopeptides were used for quantification, but the phosphorylation site was counted as “ambiguous”. Log_2 ratios of heavy/light and medium/light of more than 1 or less than -1 were accepted as significant changes in phosphorylation levels.

Annotation

Phosphorylation sites of each peptide were compared to the total protein sequence of the corresponding zebrafish protein to identify the phosphorylation site. These sites were then compared to human protein in Phosphosite.org. For ambiguous phosphorylation sites (pRS<75) the sequence was compared to Phosphosite.org to identify the most commonly identified site. Non-annotated peptides were BLASTed against the zebrafish proteome to identify the protein.

References

1. Gelb BD, Tartaglia M (2006) Noonan syndrome and related disorders: dysregulated RAS-mitogen activated protein kinase signal transduction. Hum Mol Genet 15 Spec No 2: R220-226.
2. Neel BG, Gu H, Pao L (2003) The 'Shp'ing news: SH2 domain-containing tyrosine phosphatases in cell signaling. Trends Biochem Sci 28: 284-293.
3. Kontaridis MI, Swanson KD, David FS, Barford D, Neel BG (2006) PTPN11 (Shp2) mutations in LEOPARD syndrome have dominant negative, not activating, effects. J Biol Chem 281: 6785-6792.
4. Oishi K, Zhang H, Gault WJ, Wang CJ, Tan CC, et al. (2009) Phosphatase-defective LEOPARD syndrome mutations in PTPN11 gene have gain-of-function effects during Drosophila development. Hum Mol Genet 18: 193-201.
5. Hof P, Pluskey S, Dhe-Paganon S, Eck MJ, Shoelson SE (1998) Crystal structure of the tyrosine phosphatase SHP-2. Cell 92: 441-450.
6. Saxton TM, Henkemeyer M, Gasca S, Shen R, Rossi DJ, et al. (1997) Abnormal mesoderm patterning in mouse embryos mutant for the SH2 tyrosine phosphatase Shp-2. EMBO J 16: 2352-2364.
7. Saxton TM, Pawson T (1999) Morphogenetic movements at gastrulation require the SH2 tyrosine phosphatase Shp2. Proc Natl Acad Sci U S A 96: 3790-3795.
8. Saxton TM, Ciruna BG, Holmyard D, Kulkarni S, Harpal K, et al. (2000) The SH2 tyrosine phosphatase shp2 is required for mammalian limb development. Nat Genet 24: 420-423.
9. Jopling C, van Geemen D, den Hertog J (2007) Shp2 knockdown and Noonan/LEOPARD mutant Shp2-induced gastrulation defects. PLoS Genet 3: e225.
10. Roszko I, Sawada A, Solnica-Krezel L (2009) Regulation of convergence and extension movements during vertebrate gastrulation by the Wnt/PCP pathway. Semin Cell Dev Biol 20: 986-997.
11. Westerfield M (1995) The Zebrafish Book. Eugene, Oregon: University of Oregon Press.
12. Robu ME, Larson JD, Nasevicius A, Beiraghi S, Brenner C, et al. (2007) p53 activation by knockdown technologies. PLoS Genet 3: e78.
13. Link V, Shevchenko A, Heisenberg CP (2006) Proteomics of early zebrafish embryos. BMC Dev Biol 6: 1.
14. Ding VM, Boersema PJ, Foong LY, Preisinger C, Koh G, et al. (2011) Tyrosine phosphorylation profiling in FGF-2 stimulated human embryonic stem cells. PLoS One 6: e17538.
15. Preisinger C, Schwarz JP, Bleijerveld OB, Corradini E, Muller PJ, et al. (2013) Imatinib-dependent tyrosine phosphorylation profiling of Bcr-Abl-positive chronic myeloid leukemia cells. Leukemia 27: 743-746.
16. Boersema PJ, Raijmakers R, Lemeer S, Mohammed S, Heck AJ (2009) Multiplex peptide stable isotope dimethyl labeling for quantitative proteomics. Nat Protoc 4: 484-494.
17. Boersema PJ, Foong LY, Ding VM, Lemeer S, van Breukelen B, et al. (2010) In-depth qualitative and quantitative profiling of tyrosine phosphorylation using a combination of phosphopeptide immunoaffinity purification and stable isotope dimethyl labeling. Mol Cell Proteomics 9: 84-99.
18. Lemeer S, Jopling C, Gouw J, Mohammed S, Heck AJ, et al. (2008) Comparative phosphoproteomics of zebrafish Fyn/Yes morpholino knockdown embryos. Mol Cell Proteomics 7: 2176-2187.
19. Zhao ZJ, Zhao R (1998) Purification and cloning of PZR, a binding protein and putative physiological substrate of tyrosine phosphatase SHP-2. J Biol Chem 273: 29367-29372.
20. Eminaga S, Bennett AM (2008) Noonan syndrome-associated SHP-2/Ptpn11 mutants enhance SIRPalpha and PZR tyrosyl phosphorylation and promote adhesion-mediated ERK activation. J Biol Chem 283: 15328-15338.
21. Paardekooper Overman J, Yi JS, Bonetti M, Soulsby M, Preisinger C, et al. (2014) PZR coordinates Noonan and LEOPARD syndrome signaling in zebrafish and mice. Mol Cell Biol: (in press).
22. Greer P (2002) Closing in on the biological functions of Fps/Fes and Fer. Nat Rev Mol Cell Biol 3: 278-289.
23. Pawson T, Letwin K, Lee T, Hao QL, Heisterkamp N, et al. (1989) The FER gene is evolutionarily conserved and encodes a widely expressed member of the FPS/FES protein-tyrosine kinase family. Mol Cell Biol 9: 5722-5725.
24. Feldman RA, Tam JP, Hanafusa H (1986) Antipeptide antiserum identifies a widely distributed cellular tyrosine kinase related to but distinct from the c-fps/fes-encoded protein. Mol Cell Biol 6: 1065-1073.
25. Lee SH, Peng IF, Ng YG, Yanagisawa M, Bamji SX, et al. (2008) Synapses are regulated by the cytoplasmic tyrosine kinase Fer in a pathway mediated by p120catenin, Fer, SHP-2, and beta-catenin. J Cell Biol 183: 893-908.
26. Ben-Dor I, Bern O, Tennenbaum T, Nir U (1999) Cell cycle-dependent nuclear accumulation of the p94fer tyrosine kinase is regulated by its NH2 terminus and is affected by kinase domain integrity and ATP binding. Cell Growth Differ 10: 113-129.
27. Lemeer S, Jopling C, Naji F, Ruijtenbeek R, Slijper M, et al. (2007) Protein-tyrosine kinase activity profiling in knock down zebrafish embryos. PLoS One 2: e581.
28. Stewart RA, Sanda T, Widlund HR, Zhu S, Swanson KD, et al. (2010) Phosphatase-dependent and -independent functions of Shp2 in neural crest cells underlie LEOPARD syndrome pathogenesis. Dev Cell 18: 750-762.
29. Carney TJ, Dutton KA, Greenhill E, Delfino-Machin M, Dufourcq P, et al. (2006) A direct role for Sox10 in specification of neural crest-derived sensory neurons. Development 133: 4619-4630.
30. Li C, Inglis PN, Leitch CC, Efimenko E, Zaghloul NA, et al. (2008) An essential role for DYF-11/MIP-T3 in assembling functional intraflagellar transport complexes. PLoS Genet 4: e1000044.
31. Runtuwene V, van Eekelen M, Overvoorde J, Rehmann H, Yntema HG, et al. (2011) Noonan syndrome gain-of-function mutations in NRAS cause zebrafish gastrulation defects. Dis Model Mech 4: 393-399.

32. Singh SK, Sundaram CS, Shanbhag S, Idris MM (2010) Proteomic profile of zebrafish brain based on two-dimensional gel electrophoresis matrix-assisted laser desorption/ionization MS/MS analysis. Zebrafish 7: 169-177.
33. Gebriel M, Prabhudesai S, Uleberg KE, Larssen E, Piston D, et al. (2014) Zebrafish brain proteomics reveals central proteins involved in neurodegeneration. J Neurosci Res 92: 104-115.
34. Kessels MY, Huitema LF, Boeren S, Kranenbarg S, Schulte-Merker S, et al. (2014) Proteomics analysis of the zebrafish skeletal extracellular matrix. PLoS One 9: e90568.
35. Muller PJ, Rigbolt KT, Paterok D, Piehler J, Vanselow J, et al. (2013) Protein tyrosine phosphatase SHP2/PTPN11 mistargeting as a consequence of SH2-domain point mutations associated with Noonan Syndrome and leukemia. J Proteomics 84: 132-147.
36. Yu ZH, Xu J, Walls CD, Chen L, Zhang S, et al. (2013) Structural and mechanistic insights into LEOPARD syndrome-associated SHP2 mutations. J Biol Chem 288: 10472-10482.
37. Darian E, Guvench O, Yu B, Qu CK, MacKerell AD, Jr. (2011) Structural mechanism associated with domain opening in gain-of-function mutations in SHP2 phosphatase. Proteins 79: 1573-1588.
38. Katzen AL, Montarras D, Jackson J, Paulson RF, Kornberg T, et al. (1991) A gene related to the proto-oncogene fps/fes is expressed at diverse times during the life cycle of Drosophila melanogaster. Mol Cell Biol 11: 226-239.
39. Putzke AP, Hikita ST, Clegg DO, Rothman JH (2005) Essential kinase-independent role of a Fer-like non-receptor tyrosine kinase in Caenorhabditis elegans morphogenesis. Development 132: 3185-3195.
40. Murray MJ, Davidson CM, Hayward NM, Brand AH (2006) The Fes/Fer non-receptor tyrosine kinase cooperates with Src42A to regulate dorsal closure in Drosophila. Development 133: 3063-3073.
41. Craig AW, Zirngibl R, Williams K, Cole LA, Greer PA (2001) Mice devoid of fer protein-tyrosine kinase activity are viable and fertile but display reduced cortactin phosphorylation. Mol Cell Biol 21: 603-613.
42. Aoki Y, Niihori T, Banjo T, Okamoto N, Mizuno S, et al. (2013) Gain-of-function mutations in RIT1 cause Noonan syndrome, a RAS/MAPK pathway syndrome. Am J Hum Genet 93: 173-180.
43. Craig AW, Greer PA (2002) Fer kinase is required for sustained p38 kinase activation and maximal chemotaxis of activated mast cells. Mol Cell Biol 22: 6363-6374.
44. Salem Y, Shpungin S, Pasder O, Pomp O, Taler M, et al. (2005) Fer kinase sustains the activation level of ERK1/2 and increases the production of VEGF in hypoxic cells. Cell Signal 17: 341-353.
45. Xu G, Craig AW, Greer P, Miller M, Anastasiadis PZ, et al. (2004) Continuous association of cadherin with beta-catenin requires the non-receptor tyrosine-kinase Fer. J Cell Sci 117: 3207-3219.
46. Kogata N, Masuda M, Kamioka Y, Yamagishi A, Endo A, et al. (2003) Identification of Fer tyrosine kinase localized on microtubules as a platelet endothelial cell adhesion molecule-1 phosphorylating kinase in vascular endothelial cells. Mol Biol Cell 14: 3553-3564.
47. Kim L, Wong TW (1995) The cytoplasmic tyrosine kinase FER is associated with the catenin-like substrate pp120 and is activated by growth factors. Mol Cell Biol 15: 4553-4561.
48. Ronnstrand L, Arvidsson AK, Kallin A, Rorsman C, Hellman U, et al. (1999) SHP-2 binds to Tyr763 and Tyr1009 in the PDGF beta-receptor and mediates PDGF-induced activation of the Ras/MAP kinase pathway and chemotaxis. Oncogene 18: 3696-3702.
49. Jia D, Jing Y, Zhang Z, Liu L, Ding J, et al. (2014) Amplification of MPZL1/PZR promotes tumor cell migration through Src-mediated phosphorylation of cortactin in hepatocellular carcinoma. Cell Res 24: 204-217.
50. Bonetti M, Paardekooper Overman J, Tessadori F, Noel E, Bakkers J, et al. (2014) Noonan and LEOPARD syndrome Shp2 variants induce heart displacement defects in zebrafish. Development 141: 1961-1970.

Additional information

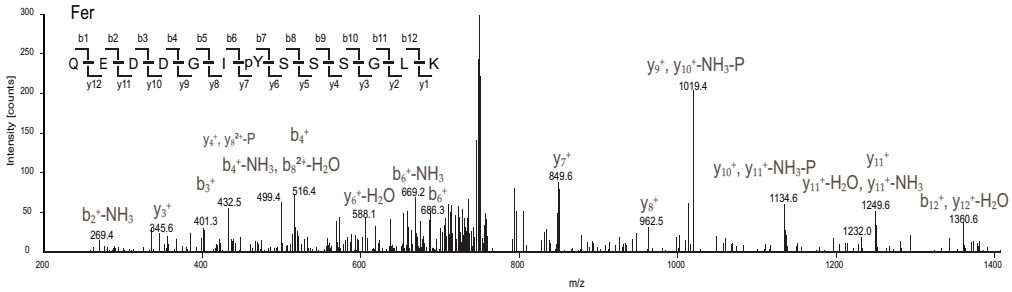

Figure S1. MS2 spectrum of the identified Fer peptide. Fer peptide sequence is shown in the upper left corner indicating the y- and b-ions. Annotated ions are indicated with their respective m/z values.

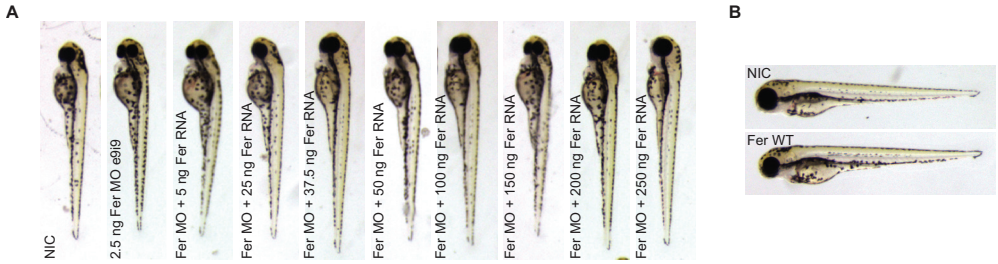

Figure S2. Attempted rescue of Fer MO and overexpression of Fer . Embryos were injected at the 1-cell stage with 2.5 ng Fer MO e9i9 either alone or in combination with increasing amounts of synthetic Fer mRNA (5 ng, 25 ng, 37.5 ng, 50 ng, 100 ng, 150 ng, 200 ng, 250 ng). Co-injection of Fer mRNA did not rescue the Fer knockdown phenotype. B. embryos were injected at the 1-cell stage with Fer WT mRNA. Injection of Fer mRNA by itself induced craniofacial defects, shorter length and heart edema.

Table S1. Raw MS data. Tab1 "PD_Output" shows raw, non-normalized data from Proteome Discoverer, which is used for normalization on all nonphosphopeptides. "numberOFphospho": number of phosphoresidues present in the peptide. "numberOFlocalized": number of localized phosphoresidue (pRS >75). "peptideSite": localized site. Tab2 "Aggregation" shows data averaged per rows based on the following values (protein group accession, sequences, description, numberofphospho, numer of localized, peptide sites). "SITES" tab shows all normalized, quantified, localized, protein assigned peptides. "SITES with lacking protein" tab shows all normalized, quantified, localized, peptides, including non-protein assigned peptides. "quantified only pRS <75" shows all normalized quantified peptides for which no phosphosite could be assigned. "all quant phosphopepts combined" shows a combination of "SITES with lacking protein" and "quantified only pRS<75" with duplicate peptides for which one site is assigned and the other is not removed. "Table 1" shows "all quant phosphopepts combined" where non-assigned peptides are BLASTed against the zebrafish proteome to identify the protein, phosporylation site in zebrafish and the phosphosite is compared to human homologs from PhosphoSite.org to identify the site. Sites without a human homolog were removed from the analysis. Available on request.

PZR coordinates Noonan and LEOPARD syndrome signaling in zebrafish and mice

Jeroen Paardekooper Overman[1,#], Jae-Sung Yi[2,#], Monica Bonetti[1], Matthew Soulsby[2], Christian Preisinger[3,4], Matthew P. Stokes[5], Li Hui[5], Jeffrey C. Silva[5], John Overvoorde[1], Piero Giansanti[3], Albert J.R. Heck[3], Maria I. Kontaridis[6], Jeroen den Hertog[1,7,*] and Anton M. Bennett[2,8,*]

1. Hubrecht Institute-KNAW and University Medical Center Utrecht, Utrecht, Netherlands 2. Department of Pharmacology, Yale University School of Medicine, New Haven, Connecticut 06520, USA 3. Department of Biomolecular Mass Spectrometry and Proteomics, Utrecht, The Netherlands 4. Current address: Proteomics Facility, Interdisciplinary Centre for Clinical Research (IZKF) Aachen, Pauwelsstraße 30, Aachen Germany 52074 5. Cell Signaling Technology, Danvers, MA 01923, USA 6. Harvard Medical School, Department of Cardiology, Beth Israel Deaconess Medical Center, 3 Blackfan Circle, Boston, MA 02115 7. Institute Biology Leiden, Leiden, Netherlands 8. Program in Integrative Cell Signaling and Neurobiology of Metabolism, Yale University School of Medicine, New Haven, Connecticut 06520, USA #; Equal contributing authors. *These authors directed jointly the work

Molecular and Cellular Biology, 2014, August 34(15): 2874-2889

Abstract

Noonan syndrome (NS) is an autosomal dominant disorder caused by activating mutations in the *PTPN11* gene encoding for Shp2, which manifests in congenital heart disease, short stature and facial dysmorphia. The complexity of Shp2 signaling is exemplified by the observation that LEOPARD syndrome (LS) patients possess inactivating *PTPN11* mutations yet exhibit similar symptoms to NS. Here, we identify protein zero-related (PZR), a transmembrane glycoprotein, which interfaces with the extracellular matrix to promote cell migration, as a major hypertyrosyl phosphorylated protein in mouse and zebrafish models of NS and LS. PZR hypertyrosyl phosphorylation is facilitated in a phosphatase-independent manner by enhanced Src recruitment to NS and LS Shp2. In zebrafish, PZR overexpression recapitulated NS and LS phenotypes. PZR was required for zebrafish gastrulation in a manner dependent upon PZR tyrosyl phosphorylation. Hence, we identify PZR as a NS and LS target. Enhanced PZR-mediated membrane recruitment of Shp2 serves as a common mechanism to direct overlapping pathophysiological characteristics of these *PTPN11* mutations.

Introduction

The Src homology 2 (SH2) domain-containing protein tyrosine phosphatase-2 (Shp2) is an ubiquitously expressed non-transmembrane protein tyrosine phosphatase (PTP) encoded by the *PTPN11* gene [1]. Shp2 comprises of two SH2 domains, a PTP domain and a C-terminal tail that contains a proline rich region flanked by two tyrosine phosphorylation sites. The SH2 domains of Shp2 serve to direct protein-protein interactions with its upstream phosphotyrosyl target in a sequence-specific context and the SH2 domains participate in maintaining a closed conformation by establishing contacts with the PTP domain [2]. The phosphatase domain of Shp2 catalyzes substrate-specific dephosphorylation and is tightly regulated. In the basal state, the catalytic activity of Shp2 is suppressed by Shp2 assuming a "closed" conformation maintained through the NH2-terminal SH2 (N-SH2) domain forming surface contacts with the PTP domain, which occludes the catalytic site. SH2 domain engagement disrupts this "closed" conformation leading to allosteric modulation and exposure of the catalytic site in to an "open" state that is now substrate accessible [2]. Engagement of the SH2 domains provides an elegant molecular switch mechanism to activate the phosphatase that allows for targeted substrate dephosphorylation within a precise micro-environment. As such, the repertoire of Shp2-binding proteins plays a major role in dictating Shp2 signaling complexity and specificity. Consistent with this, interference of Shp2's SH2 domains abrogates both physiological and pathophysiological signaling [3]. Thus, the integrity of the SH2 domains of Shp2 plays a critical role in its ability to signal.

A wealth of biochemical, cellular and genetic evidence in mice, *Drosophila* and zebrafish has established that Shp2 plays a positive signaling role downstream of numerous receptor tyrosine kinases, cytokine receptors, G protein-coupled receptor and integrins [1]. The repertoire of Shp2-interacting proteins in combination with a wide variety of substrates [4] endows this phosphatase the capability of engaging a complex array of signaling molecules and pathways such as the Ras/MAPK, PI3K/Akt, JAK/STAT, RhoA/Rac and Src family kinases (SFKs). Shp2 has been shown to promote a number of cellular functions including cell growth, cell survival and differentiation, hence affecting organismal functions such as development in mice [5,6], *Drosophila* [7] and zebrafish [8]. The highly conserved nature of Shp2 signaling in lower organisms has provided powerful model systems for the genetic dissection of Shp2 function in development. The realization that Shp2 plays an important role in human development arose through the discovery that germline mutations in the *PTPN11* gene encoding for Shp2 cause two similar types of autosomal dominant disorders [9,10]. More than 50% of Noonan syndrome (NS) (NIM163950) cases are caused by mutations in *PTPN11* that result in increased Shp2 catalysis. In contrast, as much as 90% of LEOPARD syndrome (LS) (NIM151100) mutations are caused by inactivating *PTPN11* mutations that gives rise to impaired Shp2 activity.

NS and LS are autosomal dominant disorders that manifest in short stature, ocular hypertelorism, cardiac defects, webbed neck and increased incidence of mental retardation [11-13]. NS and LS comprise part of a larger series of disorders that have thus far been characterized by mutations in components of the Ras/MAPK pathway and are collectively referred to as "RASopathies" [14]. As such, NS and LS exhibit overlapping clinical presentations such as proportionate short stature, facial dysmorphia, musculoskeletal anomalies and to a lesser extent congenital heart disease. Despite the similarities between NS and LS, these "RASopathies" are caused by opposite effects on Shp2 activity [9,15-18]. These observations suggest that NS and LS may utilize common signaling components in the pathogenesis of these developmental disorders. Interestingly, one common feature of both NS and LS mutants is that both forms of Shp2 exhibit an increased

propensity to adopt an "open" conformation, leading to increased affinity to upstream target binding through the SH2 domains and target substrates [2,8,19,20]. Hence, the "open" conformation of NS and LS disease mutants may underlie the molecular pathogenesis of these syndromes rather than altered substrate dephosphorylation by the PTP domain. Despite these highly plausible explanations it remains unclear how activating and inactivating mutants of Shp2 liberate overlapping disease outcomes. Moreover, identification of the target(s) for both NS and LS that must presumably be shared in order for them to elicit overlapping clinical outcomes is unknown.

PZR is a transmembrane glycoprotein with an extracellular immunoglobulin (Ig) domain and an intracellular domain containing two immunoreceptor tyrosine-based inhibitory motifs (ITIMs) [21-23]. The ITIMs, when tyrosyl phosphorylated, serve as Shp2 binding sites [21]. We had identified previously that NS-associated Shp2 mutants induce PZR hypertyrosyl phosphorylation and recruit increased Shp2. Moreover, in *Ptpn11*$^{D61G/+}$ mouse embryos PZR is hypertyrosyl phosphorylated demonstrating that it is aberrantly regulated in NS mice during development. Interestingly, PZR is upregulated during blastocyst formation [24]. Moreover, in mouse embryo fibroblasts derived from NS mice, adhesion-dependent ERK1/2 activation is abrogated upon loss of PZR expression [25].

To gain further insight in to how NS and LS might liberate similar phenotypes we performed an unbiased phosphotyrosine proteomics screen in a mouse model of NS and a zebrafish model of NS and LS. We identified protein zero-related (PZR) as a major hypertyrosyl phosphorylated protein in both NS and LS in mice and zebrafish. The role of PZR in development remains unclear and the pathophysiological significance of PZR/Shp2 interactions in NS and LS is also unknown. NS and LS are linked to defects in gastrulation cell movements and Shp2 is essential for gastrulation movements in mouse and zebrafish [11,26]. We show that PZR/Shp2 interactions are required for gastrulation in zebrafish. These results define a functional role for PZR in an intact organism. Moreover, they suggest that PZR is a common target that contributes to altered development in cases of both NS and LS.

Results

PZR is a major hypertyrosyl phosphorylated protein in NS.

Since NS and LS exhibit overlapping clinical outcomes we set out to identify target proteins that are affected by both syndromes. We hypothesized that targets similarly altered in their levels of tyrosyl phosphorylation in both NS and LS likely represent molecules of convergence in these diseases. Given that NS and LS mutants exhibit opposite catalytic activities we reasoned that a phosphatase-independent mechanism likely represents a common pathway for these two syndromes. Therefore, we focused on the identification of hypertyrosyl phosphorylated proteins in a mouse model of NS rather than hypotyrosyl phosphorylated ones, since the latter likely represents phosphatase-dependent Shp2 substrates.

We performed a phosphotyrosyl proteomics screen in mice harboring a knock-in of a NS-associated Shp2 mutant [27]. Mice containing an Asp61 to Gly61 (D61G) mutation within the NH2-terminal SH2 domain of Shp2 (Shp2^{D61G}) generates a NS mutation found in humans [9]. Heterozygous progeny of these mice (*Ptpn11*$^{D61G/+}$) recapitulate several NS features observed in humans such as cardiovascular and skeletal abnormalities [27]. Since both NS and LS exhibit

significant clinical defects in the heart we focused on this tissue. We performed a global survey of the levels of tyrosyl phosphorylated proteins in the hearts of 5 day-old wild type and *Ptpn11*$^{D61G/+}$ mice using an immunoaffinity phosphoproteomics approach [28]. The relative abundance of tyrosyl phosphorylated proteins was assessed by quantitating the frequency of phosphopeptides derived from wild type and *Ptpn11*$^{D61G/+}$ mice [28]. We identified an approximately equal

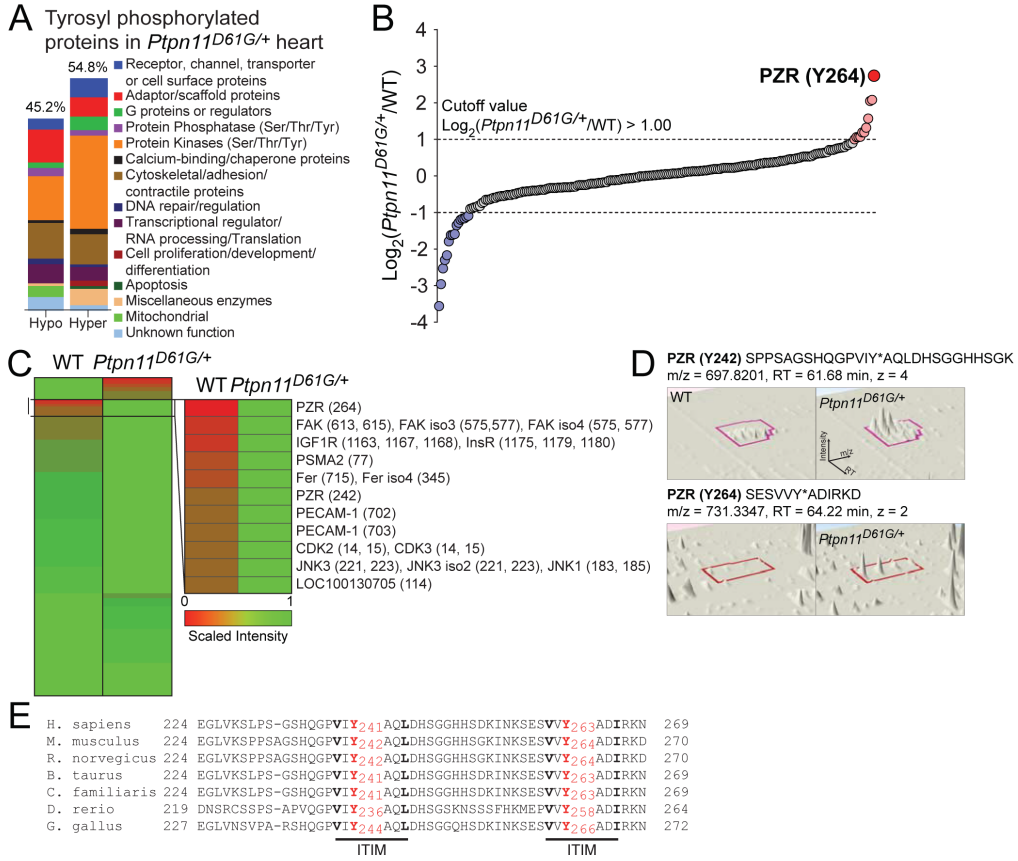

Figure 1 Proteomic analysis of differentially tyrosyl phosphorylated proteins in hearts of *Ptpn11*$^{D61G/+}$ mice. (A) Classification of hypo and hyper-tyrosyl phosphorylated proteins in the hearts of *Ptpn11*$^{D61G/+}$ mice. (B) Log_2-transformed values for the ratio of each phosphotyrosine-containing peptide in wild type and *Ptpn11*$^{D61G/+}$ mouse hearts. (C) Heat map of differentially tyrosyl phosphorylated peptides. (D) Extracted ion chromatogram and peptide sequence of PZR-containing tyrosine 242 (upper panels) and tyrosine 264 (lower panels) by differential proteomics. (E) Amino acid sequences of PZR C-terminus in different vertebrates. Consensus sequences for ITIM (S/I/V/LxYxxI/V/L) are indicated in bold and tyrosine residues are marked red with their appropriate amino acid numbering.

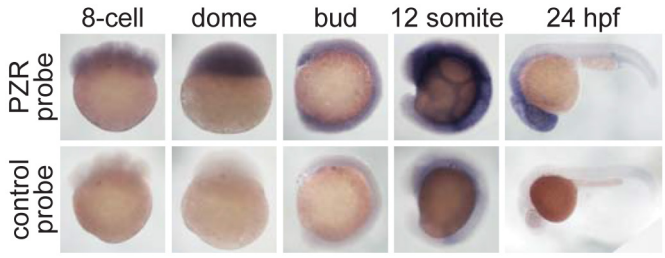

Figure 2 Expression pattern of PZR in developing zebrafish. *In situ* hybridization for PZR was performed on developing zebrafish embryos at 8-cell, dome, bud, 12-somite stage and at 24 hpf. The PZR sense probe was used as a control

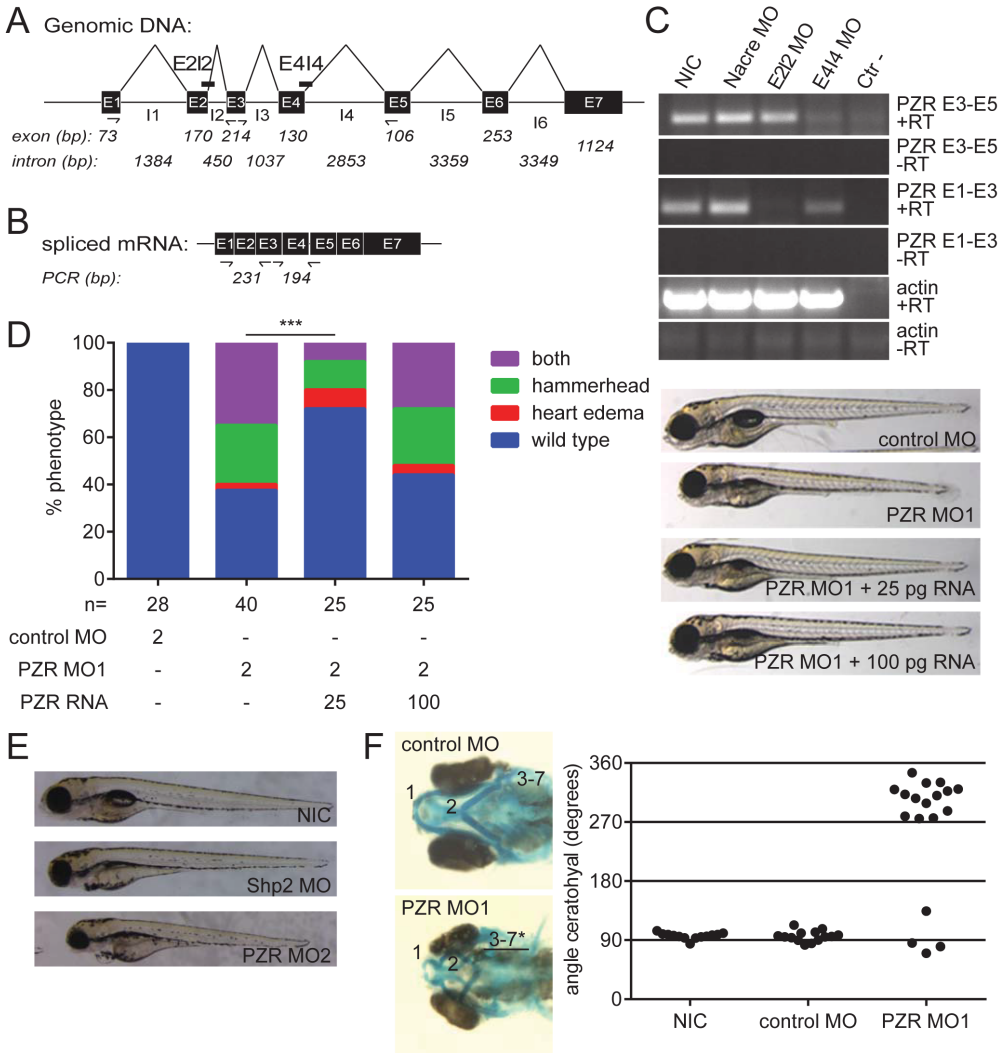

Figure 3 PZR is required for zebrafish development. (A) Genomic organization of zebrafish *mpzl1* gene encoding PZR. The target sites of E4I4MO (PZR-MO1) and E2I2 MO (PZR-MO2) are indicated as well as the positions of the oligonucleotides used for amplification of E3/E5 and E1/E3. (B) PZR mRNA and the positions of the oligos used for RT-PCR are depicted; the size of the PCR products is shown (bp). (C) Embryos were untreated (non-injected control, NIC) or injected at the one-cell stage with control MO (Nacre MO), PZR E2I2MO (PZR-MO2) or E4I4 MO (PZR MO1). PCR was performed for E3/E5, or E1/E3. (ctr-) indicates water control. (D) Embryos were injected (1-cell stage) with 2 pg control MO, 2 pg PZR MO or co-injected with 25 pg or 100 pg PZR mRNA. Embryos were scored at 4 dpf. (E) Zebrafish embryos were injected at the 1-cell stage with 2 ng Shp2 MO or 2 ng PZR MO2 or 2 ng control morpholino and photographed at 3 dpf. (F) Embryos were injected at the 1-cell stage with 2 pg PZR MO, 2 pg control MO or non-injected as a control, fixed at 4 dpf and stained with alcian blue. Meckel's cartilage (1), the ceratohyal (2) and branchial arches (3-7) are indicated. The angle of the ceratohyal was measured.

repertoire of differentially hypo and hypertyrosyl phosphorylated peptides in the hearts of *Ptpn11*$^{D61G/+}$ mice (Figure 1A and B). The limited number of differentially tyrosyl phosphorylated peptides suggests that the NS mutant induces a discrete influence on global tyrosyl phosphorylation levels in the heart (Figure 1B). The highest induced hypertyrosyl phosphorylated peptide represented Y264, which is present in the transmembrane glycoprotein, protein zero-related (PZR) and was induced by 6.7-fold as compared to wild type controls (Figure 1C and D). The sequence surrounding Y264 was identified to be part of the immunoreceptor tyrosine inhibitory motif (ITIMs) of PZR [23]. PZR contains two ITIMs both of which are highly conserved among vertebrates and when phosphorylated binds directly to the SH2 domains of Shp2 [23]. Notably, the other tyrosine-containing ITIM on PZR represented by Y242 was also detected to be hypertyrosyl phosphorylated by 2.2-fold (Figure 1C and D). For clarity, we will use the human amino acid numbering of PZR (Figure 1E - mouse Y242 and Y264 correspond to human Y241 and Y263, respectively). Previously, we found that PZR was hypertyrosyl phosphorylated during embryogenesis in *Ptpn11*$^{D61G/+}$ mice [25]. These results identify Y242 and Y264 as sites of PZR hypertyrosyl phosphorylation in this mouse model of NS.

Zebrafish have been shown to recapitulate both NS and LS phenotypes [11]. Therefore, phosphotyrosyl proteomics screens were performed in developing (26 hours post-fertilization) embryos to identify differentially tyrosyl phosphorylated peptides between zebrafish embryos expressing either NS or LS mutants as compared with controls. When injected with the Shp2^{D61G} NS mutant, peptides representing the ITIMs of zebrafish PZR containing Y241 and Y263 were identified to be amongst the highest induced phosphotyrosyl-containing peptides (7.7 and 4.7-fold increase for Y241 and Y263, respectively as compared with controls). In addition, LS-injected embryos also were found to contain PZR hypertyrosyl phosphorylated peptides at both Y241 and Y263 representing increases of 3.4- and 3.1-fold relative to wild type controls. These results identify PZR as a major hypertyrosyl phosphorylated target in zebrafish embryos expressing either NS or LS mutations.

PZR is expressed ubiquitously and functions in the Shp2 pathway in zebrafish.

Our data demonstrate that PZR tyrosyl phosphorylation is aberrantly regulated in NS mouse embryos and post-developmentally in NS hearts ([25] and Figure 1) and during development of NS/LS expressing zebrafish embryos. These results suggest that altered PZR tyrosyl phosphorylation may play a role in NS and LS pathogenesis. To further examine the role of PZR during zebrafish development we determined the expression of *mpzl1*, the gene encoding zebrafish PZR. Zebrafish PZR was cloned and was used to generate an *mpzl1*-specific probe. *In situ* hybridization of *mpzl1* expression was apparent from the 8-cell stage onwards, indicating maternal expression. *Mpzl1* expression was ubiquitous until bud stage and at later stages *mpzl1* expression appeared to be enhanced anteriorly (Figure 2). The specificity of the antisense *mpzl1* probe was confirmed by the lack of signal of the sense control probe in parallel experiments (Figure 2). Thus, PZR is maternally contributed and expressed at embryonic stages during and after zebrafish gastrulation.

PZR knockdown phenocopies NS and LS expression in zebrafish embryos.

Next, PZR was knocked down in order to investigate the role of PZR in zebrafish signaling. The specificity of the PZR MO to block PZR splicing was confirmed (Figure 3A - C). Knockdown of PZR, but not a control morpholino (MO), induced a phenotype characterized by reduced body axis length (4.9 ± 1.1 % reduction compared with control) and heart edema and this phenotype was confirmed using a second non-overlapping MO (Figure 3D and E). Interestingly, similar phenotypes are observed upon Shp2 knockdown in zebrafish [29]. Co-injection of a moderate

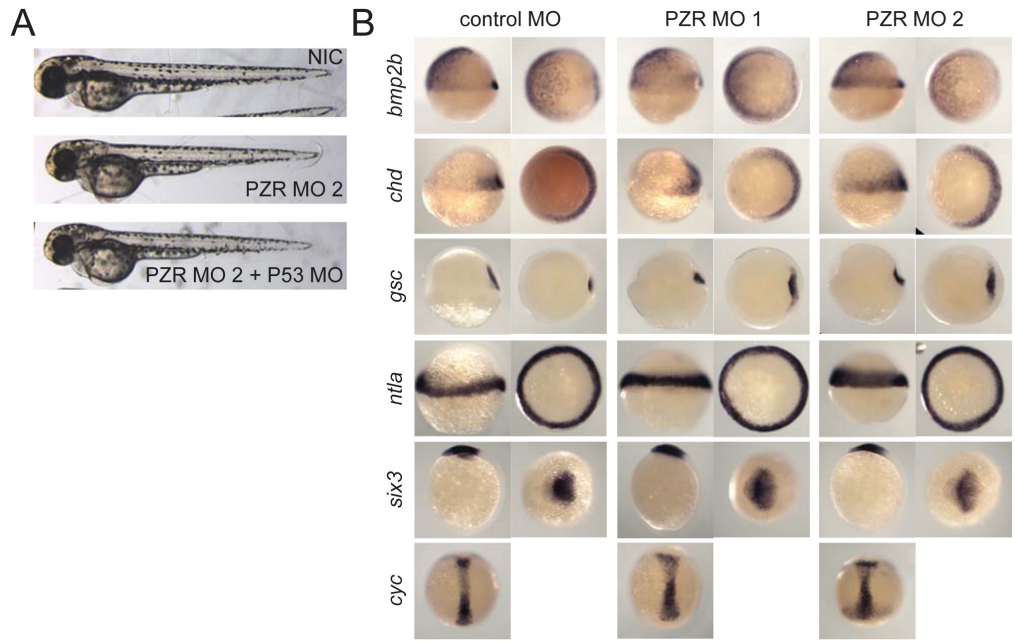

Figure 4. PZR knockdown is specific and does not affect cell specification (A) Zebrafish embryos were injected at the 1-cell stage with 2ng PZR MO alone or co-injected with p53 morpholino and photographed at 2 dpf. (B) Zebrafish embryos were injected at the 1-cell stage with 2 ng PZR MO1 or PZR MO2 or 2ng control morpholino, and fixed at shield stage (*bmp2b*, *chd*, *gsc*, *ntla*), 70% epiboly (*cyc*), and bud stage (*six3*) and probed for cell fate markers using *in situ* hybridization.

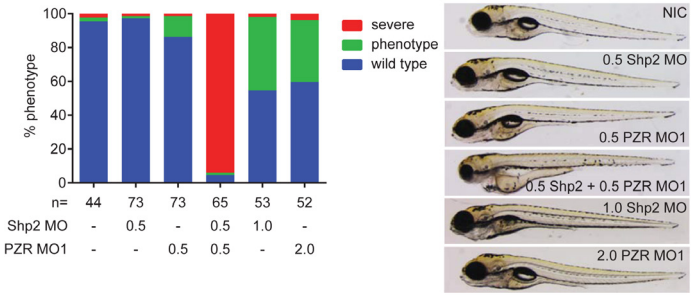

Figure 5. Genetic interaction between Shp2 and PZR. Embryos were injected at the 1-cell stage with Shp2 MO (0.5 pg) or PZR MO (0.5 pg), a combination thereof or Shp2 MO (1.0 pg) and PZR MO (2.0 pg). Embryos were imaged at 4 dpf. The stacked histogram in the left panel indicates quantitation of the phenotypes shown in representative photographs in the right panel.

dose of PZR mRNA (25 pg) rescued the PZR-MO-induced defects, whereas a higher dose of PZR mRNA (100 pg) failed to rescue (Figure 3D). To quantify the craniofacial defects in PZR knockdowns, embryos were fixed at 4 dpf and the cartilage was stained with alcian blue. The cartilage was greatly malformed and the angle of the ceratohyal displayed a significant increase, supporting the notion that PZR knockdown induced craniofacial defects, reminiscent of Shp2 knockdown [11] (Figure 3F).

The use of knockdown approaches by itself may lead to non-specific activation of p53 and subsequent apoptosis, thereby giving rise to developmental defects [30]. To rule-out this possibility we performed a co-knockdown of p53 and PZR, which did not attenuate the phenotype (Figure 4A). We subjected PZR knockdown embryos to *in situ* hybridization using a panel of cell

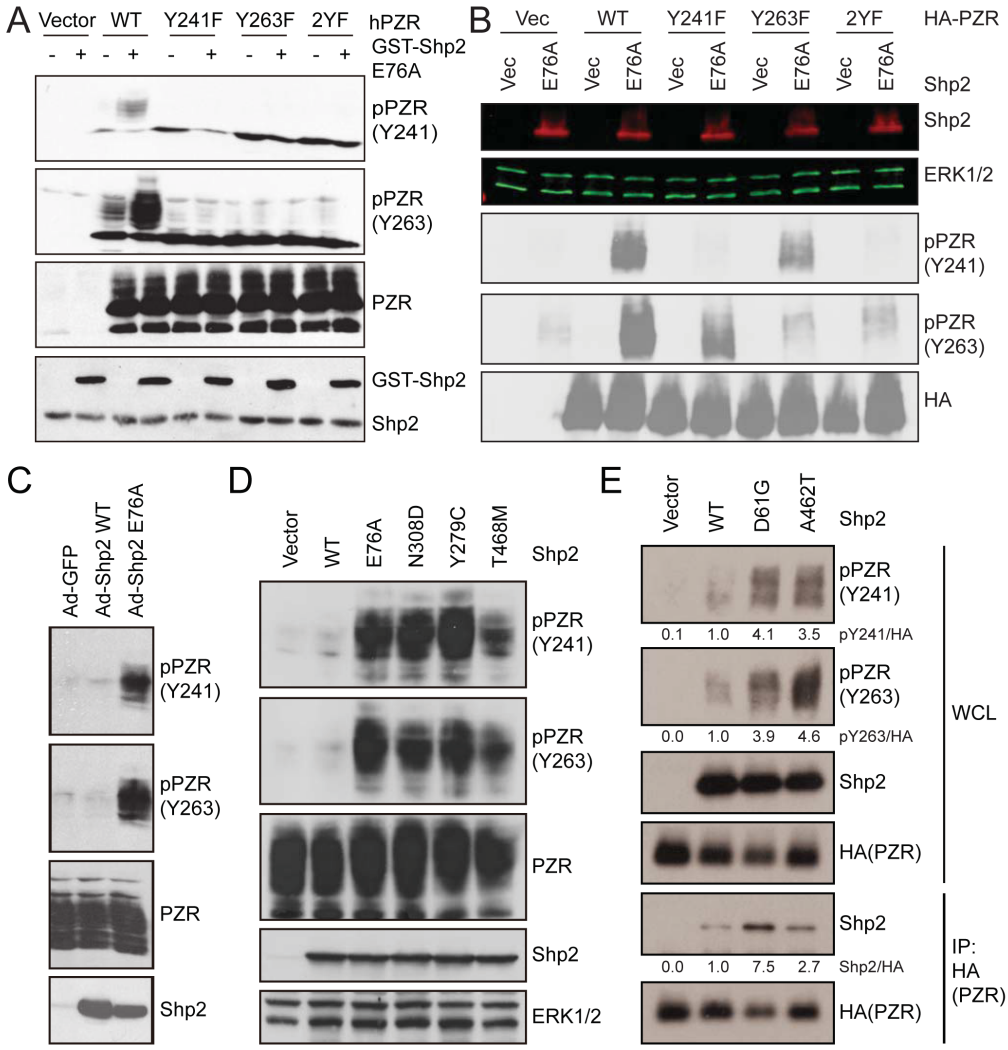

Figure 6. Characterization of PZR tyrosyl phosphorylation. (A) C2C12 cells were co-transfected with empty vector or activated GST-Shp2^{E76A} and either empty vector (vector), wild type human PZR (WT), PZR mutated at tyrosine 242 (Y241F), tyrosine 264 (Y263F), or both (2YF). Cell lysates were immunoblotted with anti-pPZR (Y241 or Y263), PZR or Shp2 antibodies. (B) HEK 293 cells were co-transfected with empty vector or activated Shp2E76A and either empty vector (vector), wild type zebrafish PZR (WT), PZR mutated at tyrosine 236 (Y241F), tyrosine 258 (Y263F), or both (2YF). Cell lysates were immunoblotted with anti-pPZR (Y241 or Y263), PZR or Shp2 antibodies. ERK1/2 was used as a loading control. (C) HUVEC cells were infected with adenoviruses expressing either GFP as a control, wild type Shp2 or Shp2E76A. Cell lysates were immunoblotted with anti-pPZR (Y241 or Y263), total PZR and Shp2 antibodies. (D) HEK 293 cells were transiently transfected with empty vector, wild type Shp2 (WT) or the indicated mutants of Shp2 (Activated Shp2; E76A, NS mutant; N308D or LS mutants; Y279C and T468M). Cell lysates were immunoblotted with anti-pPZR (Y241 or Y263), PZR and Shp2 antibodies. ERK1/2 was used as a loading control. (E) HEK 293T cells were transfected with HA-tagged zebrafish PZR with empty vector, wild type Shp2, Shp2D61G or Shp2A462T. Cell lysates were immunoprecipitated with anti-HA antibodies and immune complexes were immunoblotted with anti-Shp2 and anti-HA antibodies. Whole cell lysates were blotted with anti-pPZR (Y241 and Y263), Shp2 and HA

fate markers at shield stage (*gsc*, *bmp2b*, *chd, ntl*), 70% epiboly (*cyc*), and bud stage (*six3*). All markers were expressed indicating that cell specification was not affected (Figure 4B). Hence, PZR knockdown induced similar defects to those observed in both NS and LS Shp2 expressing embryos.

To investigate the genetic interaction between Shp2 and PZR, we partially knocked down Shp2 and PZR separately and together. If PZR is essential for Shp2 signaling, partial loss of both Shp2 and PZR should induce developmental defects that are more severe than by loss of each alone [29]. Knocking down Shp2 and PZR at sub-optimal levels did not induce developmental defects (Figure 5). However, partial knockdown of PZR and Shp2 together resulted in developmental defects at 4 dpf (Figure 5). The embryos were scored in three categories: wild type, phenotype and severe and it was evident that co-knockdown of Shp2 and PZR greatly enhanced the percentage of embryos displaying a severe phenotype (Figure 5). PZR knockdown also induced wider set eyes, reminiscent of the phenotype that we, and others, reported in Shp2 knockdowns [11,31]. Together, these results are consistent with the notion that PZR and Shp2 function in a conserved signaling pathway in zebrafish.

NS- and LS-associated Shp2 mutants induce PZR Y241 and Y263 hypertyrosyl phosphorylation.

We investigated the characteristics of PZR hypertyrosyl phosphorylation in further detail. To accomplish this, antibodies against tyrosyl phosphorylated PZR at Y241 (pY241-PZR) and Y263 (pY263-PZR) were generated. When cells were co-transfected with PZR, along with an activating mutant of Shp2 ($Shp2^{E76A}$) that induces PZR hypertyrosyl phosphorylation [25] both anti-pY241 and anti-pY263-PZR antibodies recognized tyrosyl phosphorylated PZR (Figure 6A). When Y263 in PZR was mutated to F263, neither anti-pY241 nor anti-pY263-PZR antibodies detected tyrosyl phosphorylated PZR upon co-expression of $Shp2^{E76A}$ (Figure 6A). Similarly, mutation of Y241 to F241 in PZR, also resulted in the failure of both anti-pY241 and anti-pY263-PZR antibodies to detect tyrosyl phosphorylated PZR (Figure 6A). The explanation for these results is that Y241 is required for Y263 phosphorylation, and conversely, Y263 for Y241 phosphorylation. Similar observations have been made by others [21,32]. Importantly, mutation of Y241 and Y263 to non-phosphorylatable residues abolished the immunoreactivity of both phospho-specific PZR antibodies (Figure 6A). These antibodies also recognized Y241 and Y263 in zebrafish PZR (Figure 6B).

We tested whether activating Shp2 mutants induced either Y241-PZR or Y263-PZR tyrosyl phosphorylation in other cell types. To this end, wild type and activating Shp2E76A mutants were introduced into human umbilical vein endothelial cells. These results indicated that pY241-PZR and pY263-PZR antibodies recognized endogenous tyrosyl phosphorylated PZR at Y241 and Y263, respectively (Figure 6C). The LS mutant from human and zebrafish when expressed in 293 cells were capable of inducing PZR hypertyrosyl phosphorylation at both Y241 and Y263 (Figure 6D and E). As reported previously [33], increased zebrafish PZR tyrosyl phosphorylation correlated with enhanced PZR/Shp2 binding (Figure 6E). Hence, both NS and LS mutants in human and zebrafish enhance PZR tyrosyl phosphorylation.

PZR hypertyrosyl phosphorylation in NS and LS mice.

We determined whether PZR was hypertyrosyl phosphorylated in NS mice. Hearts isolated from 8 week-old wild type and $Ptpn11^{D61G/+}$ mice showed a significant increase in pY263-PZR tyrosyl phosphorylation as compared with wild type controls (Figure 7A). In addition, PZR hypertyrosyl phosphorylation was observed in the cortex of $Ptpn11^{D61G/+}$ mice (Figure 7B), as well as in the

kidney, liver and spleen of these mice (Figure 8A-C). Given that in cultured cells LS induces PZR hypertyrosyl phosphorylation (Figure 6D and E), we tested whether PZR is hypertyrosyl phosphorylated using *Ptpn11*$^{Y279C/+}$ knock-in mutant mice, which represented a human LS mutant [34]. Hearts from *Ptpn11*$^{Y279C/+}$ mice were isolated and, although to a much lesser extent to *Ptpn11*$^{D61G/+}$ mice, PZR was hypertyrosyl phosphorylated on Y263 (Figure 7C). In addition, PZR was robustly hypertyrosyl phosphorylated in the cortex of *Ptpn11*$^{Y279C/+}$ mice (Figure 7D). In agreement with these data, we also observed that when zebrafish embryos were injected to express either the NS or LS mutants, PZR was also hyper tyrosyl phosphorylated at Y241 and Y263 (Figure 7E). No apparent differences were observed in the basal levels of Shp2, phosho-ERK1/2 or phospho-Akt between either NS or LS mice (Figure 9A-D). Collectively, these results show that both NS and LS mutants induce PZR hypertyrosyl phosphorylation within the ITIM Shp2 binding motif of PZR in mice and zebrafish.

NS and LS mutants induce PZR hypertyrosyl phosphorylation by enhancing Src/Shp2/PZR complex.

In order to investigate the mechanisms underlying how both NS and LS mutants induce PZR hypertyrosyl phosphorylation, we examined the dependency of NS and LS mutants to induce PZR hypertyrosyl phosphorylation through the SFKs. ITIMs serve as potent Src family kinase (SFK) substrates and SFKs phosphorylate ITIMs within PZR [35]. Pharmacological inhibition of the SFKs by SU6656 impaired both NS- and LS-induced PZR hypertyrosyl phosphorylation at pY241 and pY263 (Figure 10A). Similar results were also observed with the activated E76A mutant (Figure 10B).

Next, we determined the ability of the activating Shp2 mutant to induce PZR hypertyrosyl phosphorylation in fibroblasts lacking the expression of *Src*, *Fyn* and *Yes* (SYF cells). Here, we found that an activating Shp2 mutant failed to induce PZR hypertyrosyl phosphorylation at Y241 and Y263 (Figure 11A). Consistent with this, a kinase-dead mutant of c-Src blocked the ability of the activated Shp2 mutant to induce PZR hypertyrosyl phosphorylation at these sites (Figure 11B). Both human and zebrafish PZR served as c-Src substrates in vitro (Figure 11C and D) and co-expression of a constitutively activated mutant of c-Src promoted tyrosyl phosphorylation of zebrafish PZR in cells (Figure 11E). Hence, c-Src phosphorylates human and zebrafish PZR at the Shp2 binding sites demonstrating that the SFKs likely mediates PZR hypertyrosyl phosphorylation. It has been previously suggested that the "open" conformations of both NS and LS mutants exhibit properties that increase their propensity to interact with other signaling proteins. Based upon our observations that SFKs may play a role we tested whether the SFKs are NS and/or LS binding targets. To test this, c-Src was immunoprecipitated from cells expressing either wild type Shp2, NS or LS mutants and these immune complexes were immunoblotted to detect for the presence of Shp2. We found that in both NS and LS expressing cells that the amount of NS/LS-Shp2 present in c-Src complexes was significantly greater as compared with wild type Shp2 expressing cells (Figure 12A).

To determine whether Src is present in PZR complexes and whether this is enhanced by the "open" conformation of mutated Shp2 we immunoprecipitated Src and assessed the extent of PZR interactions. We found that when Src was immunoprecipitated, PZR and Shp2 were present in the complex (Figure 12B). However, Src failed to co-immunoprecipitate with the form of PZR that was mutated in both the ITIMs but still exhibited enhanced Shp2 binding to the "open" conformation Shp2 mutants (Figure 12B). Wild type PZR, as expected was found to exist in a complex with Shp2 and this was further enhanced when either the activating or LS Shp2-containing mutation was

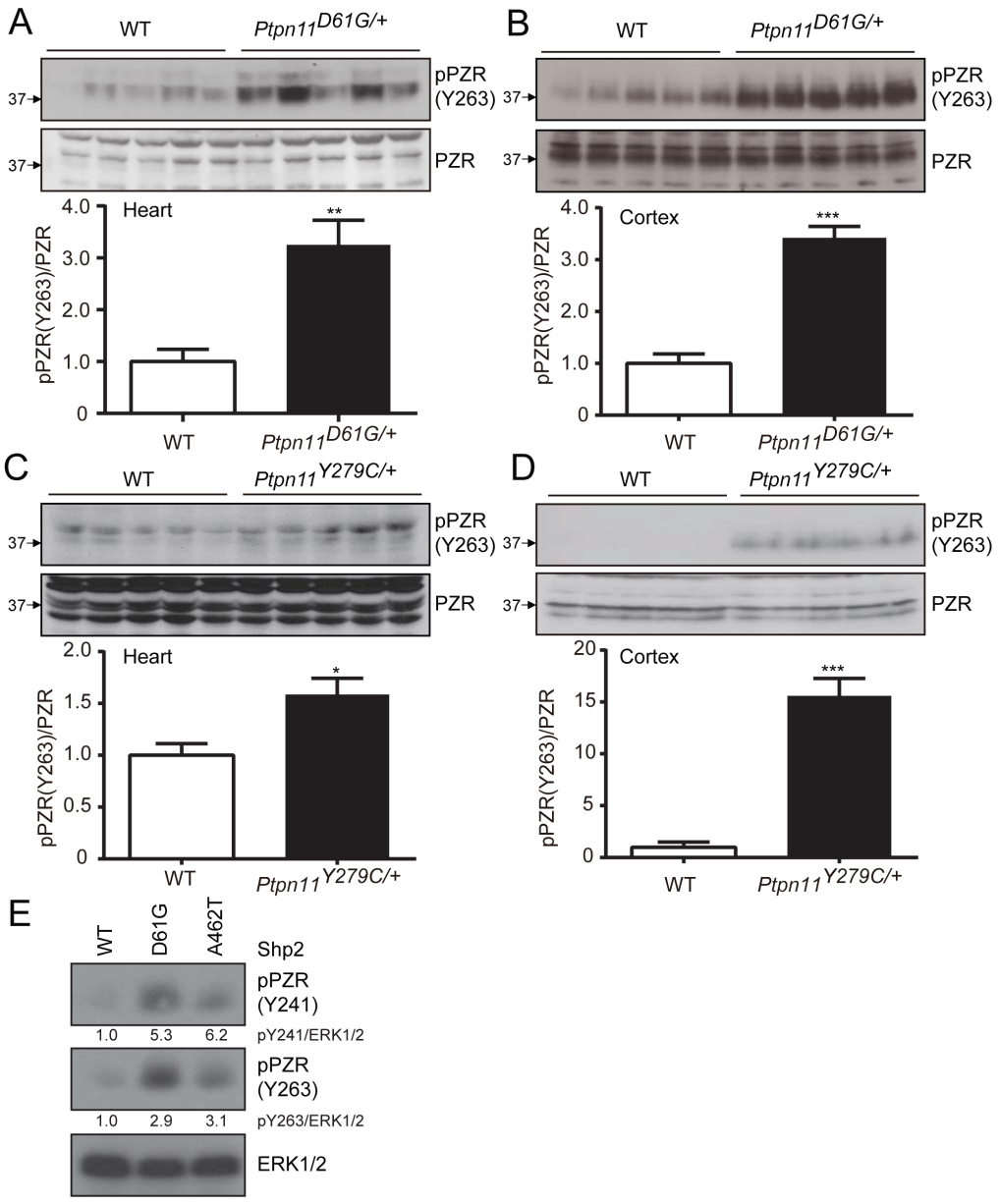

Figure 7. PZR tyrosyl phosphorylation in *Ptpn11*$^{D61G/+}$ and *Ptpn11*$^{Y279C/+}$mice and zebrafish expressing D61G or A462T Shp2. The heart (A and C) and the cortex (B and D) were isolated from 5-week-old WT and *Ptpn11*$^{D61G/+}$ mice (A and B) or 8-week-old WT and *Ptpn11*$^{Y279C/+}$ mice (C and D). Tissue lysates were immunoblotted with pPZR (Y263) and total PZR antibodies. Phosphorylation of tyrosine 264 in PZR represents n=5 per genotype. All data are mean ± S.E.M. *; P < 0.05, **; P < 0.01, ***; P < 0.001. (E) Lysates prepared from zebrafish embryos expressing either wild type, D61G or A462T Shp2 were immunoblotted with anti-PZR (pY241) and PZR pY263 antibodies. Relative quantitation shown below and ERK1/2 expression was used as a loading control.

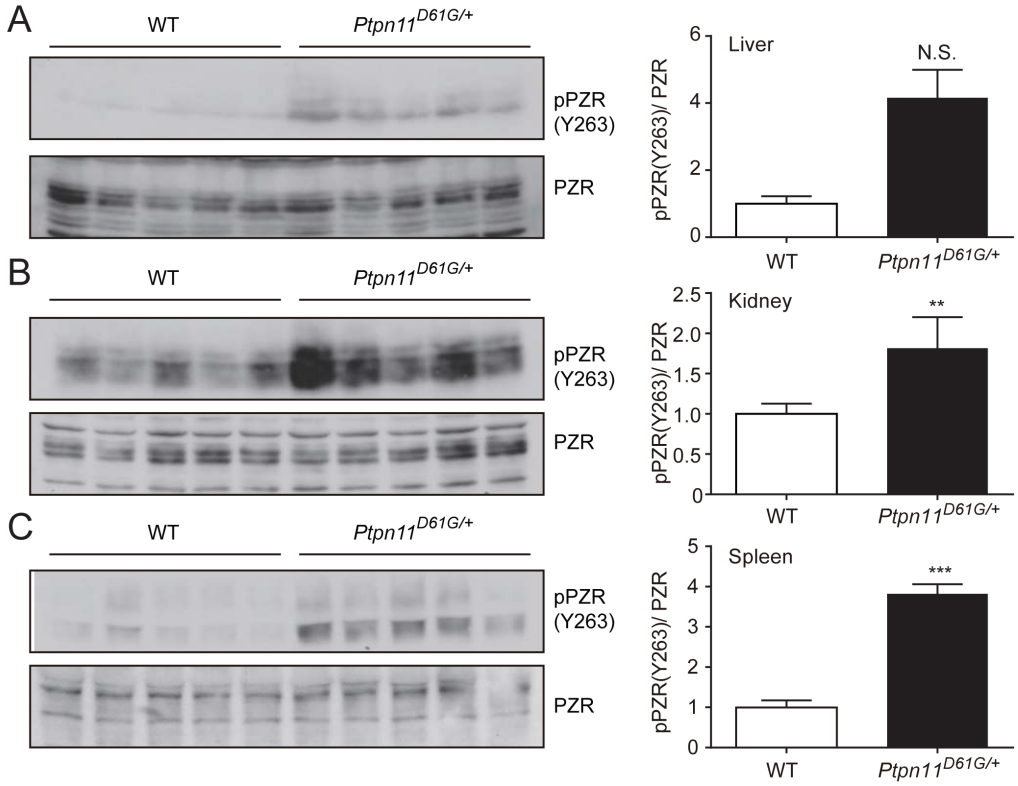

Figure 8 PZR tyrosyl phosphorylation in *Ptpn11*$^{D61G/+}$ mice. (A) liver, (B) kidney and (C) spleen were isolated from 5-week-old wild type and *Ptpn11*$^{D61G/+}$ mice. Tissue lysates were immunoblotted with anti-pPZR (Y263) and total PZR antibodies. Densitometric analysis of the phosphorylation levels of tyrosine 263 in PZR was determined and the results represent the mean ± S.E.M. from 5 mice per genotype. (**; P < 0.01, ***; P < 0.001; WT vs. NS).

expressed (Figure 12B). In contrast, double ITIM-containing mutant PZR, failed to form a complex (Figure 12B). These results suggest that the "open" conformation of Shp2 mutants exhibit an increased propensity to bind c-Src and that the likely explanation for PZR induced hypertyrosyl phosphorylation is causally related to the ability of Src to increase its proximity to PZR through Shp2 binding.

Convergence and extension defects induced by NS and LS are recapitulated by PZR in a phosphotyrosyl-dependent manner.

The similarities between the Shp2 [29] and PZR morphant phenotypes (Figure 3 and 5) indicate common defects during development. Previous results have shown that Shp2 knockdown and NS and LS *PTPN11* mutant overexpression lead to convergence and extension (C/E) cell movement defects during gastrulation resulting in shorter embryos with craniofacial defects and cardiac edema [11]. To test whether PZR knockdown also induces C/E defects, embryos were injected with PZR-, Shp2- or control morpholino, or LS mRNA as a positive control. Embryos were fixed at the 8- to 10-somite stage and subjected to *in situ* hybridization and stained for *krox20* and *myoD*, markers for rhombomeres three and five, and the somites, respectively. Loss of PZR led to shorter and wider embryos compared with controls at the same stage, and these phenotypes were similar

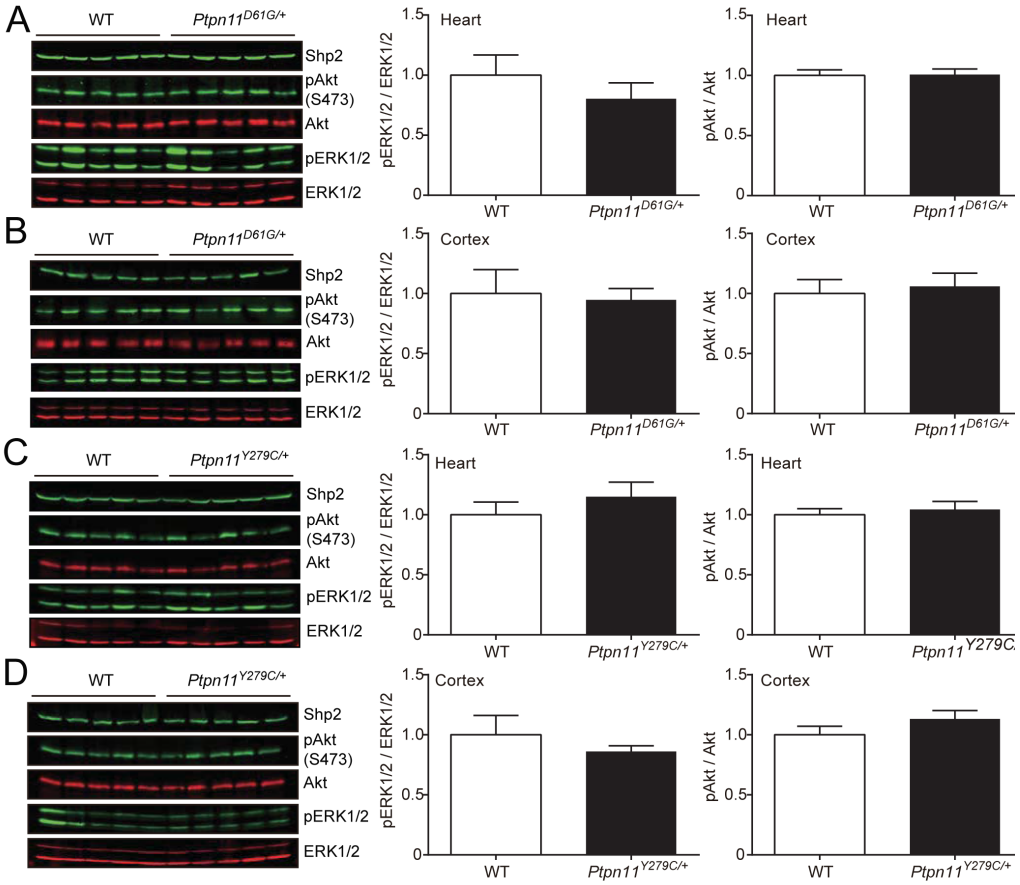

Figure 9. ERK and Akt phosphorylation in *Ptpn11*$^{D61G/+}$ and *Ptpn11*$^{Y279C/+}$ mice. The heart (A and C) and the cortex (B and D) were isolated from 5-week-old wild type and *Ptpn11*$^{D61G/+}$ mice (A and B) or 8-week-old wild type and *Ptpn11*$^{Y279C/+}$ mice (C and D). Tissue lysates were subjected to immunoblotting with anti-Shp2, pERK1/2, total ERK1/2, pAkt and Akt antibodies. Results represent densitometric analyses of the mean ± S.E.M. for pERK1/2 and pAkt from 5 mice per genotype.

to Shp2 knockdown and LS-Shp2 injected embryos (Figure 13A). These results indicated that PZR is essential for C/E cell movements, analogous to that of both NS and LS mutants during zebrafish gastrulation.

To assess whether PZR tyrosyl phosphorylation sites were important for C/E phenotypes we overexpressed wild type PZR and PZR tyrosyl phosphorylation site-deficient mutants and performed *in situ* hybridization at the 8- to 10-somite stage using markers for *krox20* and *myoD*. Overexpression of wild type PZR resulted in shorter and wider embryos (Figure 13B). When mRNA encoding double ITIM tyrosine to phenylalanine mutants (Y241F and Y263F; 2YF) and as a control mRNA encoding GFP were injected into zebrafish embryos the C/E phenotype was inhibited (Figure 13B). As expected, PZR tyrosyl phosphorylation and Shp2 binding to zebrafish PZR is inhibited in the double ITIM Y241F/Y263F mutant (Figure 13C). These data indicate that both tyrosyl phosphorylation sites within each of the ITIMs are required for PZR signaling for the promotion of the C/E phenotype during early development in zebrafish.

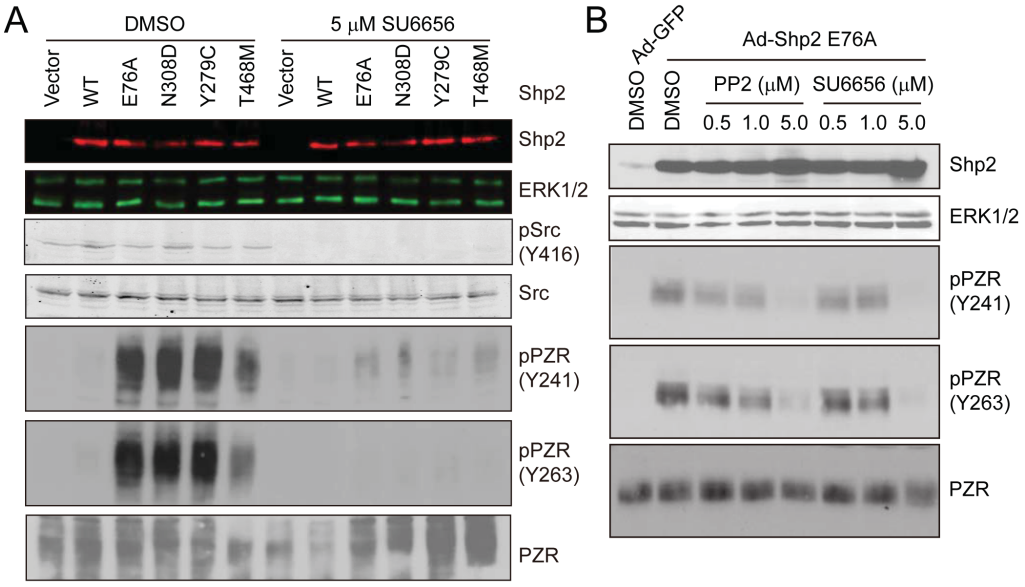

Figure 10. Effect of Src family kinases on PZR Y241 and Y263 phosphorylation. (A) HEK 293 cells were transiently transfected with the indicated Shp2 mutants and treated with either DMSO as a control or 5 μM SU6656. (B) NIH-3T3 cells were infected with the adenoviruses expressing either GFP as a control or a constitutively active Shp2E76A, in the presence of DMSO, PP2 or SU6656 at the indicated concentration. Cell lysates were immunoblotted with anti-Shp2, pSrc (Y416), Src, pPZR (Y241 or Y263) and total PZR antibodies. ERK1/2 was used as a loading control.

Discussion

Here, we identified using non-biased proteomic approaches PZR as a major hypertyrosyl phosphorylated protein in both NS and LS models of mice and zebrafish. Remarkably, disruption of PZR function resulted in similar phenotypes to that observed in NS or LS mutant expressing zebrafish. Mechanistically, NS and LS mutants induce PZR tyrosyl phosphorylation in a Src-dependent manner and these mutants acquire an enhanced Src interaction as compared with wild type Shp2. PZR is required for zebrafish gastrulation and tyrosyl phosphorylation is necessary to promote convergence and extension movements. Thus, NS and LS mutants function in a phosphatase-independent manner to promiscuously promote PZR hypertyrosyl phosphorylation leading to dysfunctional gastrulation. Collectively, these results suggest that PZR is a novel evolutionarily conserved target for NS and LS-associated Shp2 mutants.

The extracellular matrix serves to integrate dynamically processes that govern cell fate, tissue maintenance and homeostasis to outcomes that dictate organ architecture [36]. Growth factor receptors, chemokines and G-protein coupled receptors are either directly or indirectly influenced by the ECM to control cell proliferation, differentiation and cell survival. The "RASopathies" represent mutated components of the SOS/Ras/Raf/Erk and there has been much focus on the role this cascade plays in NS and LS as it relates to cell proliferation and cell survival [10]. PZR has been shown to function in the control of cell adhesion and migration [24,25,32,35,37]. Therefore, our findings imply that aberrant cell migration and adhesion likely play important roles in the pathogenesis of both NS and LS. The development of PZR mutant mice will be necessary to test these conclusions more comprehensively.

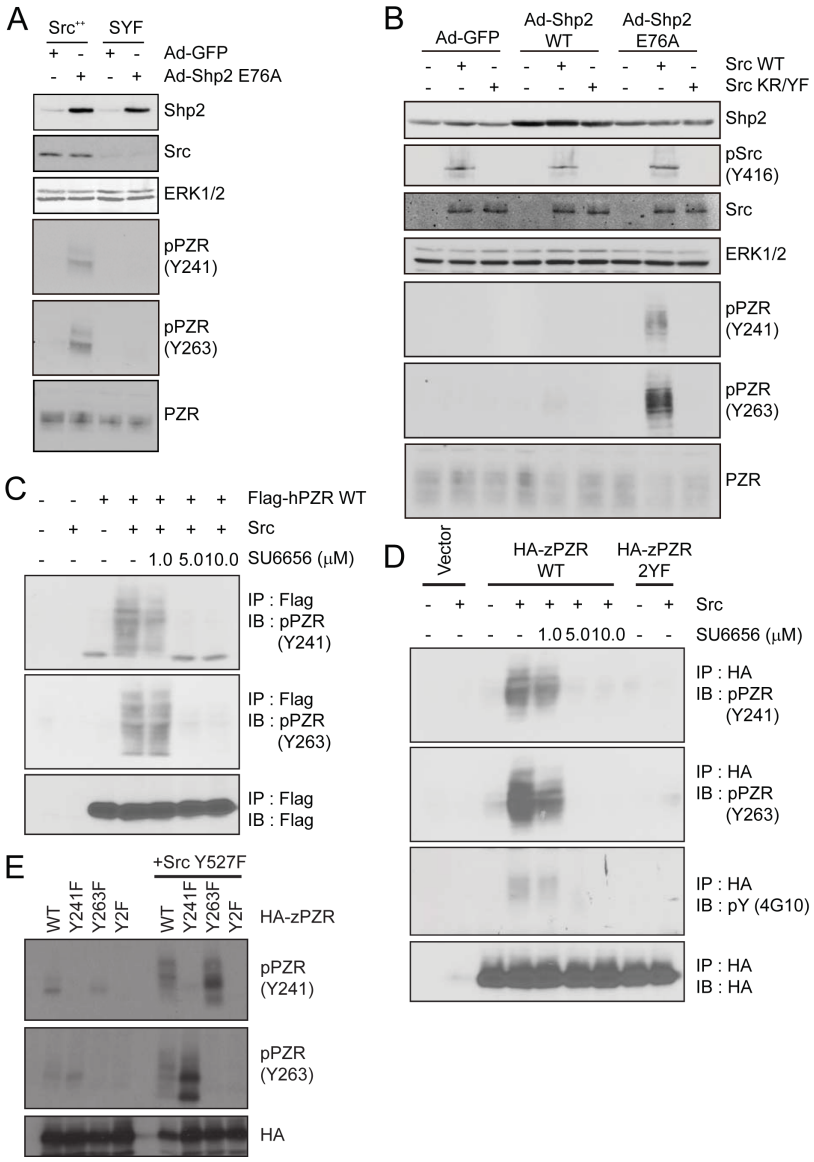

Figure 11. Src family kinases mediate NS/LS-induced PZR hypertyrosyl phosphorylation and increase NS/LS Src binding. (A) SYF (*Src*$^{-/-}$/*Fyn*$^{-/-}$/*Yes*$^{-/-}$ MEFs) and *Src*$^{+/+}$ (SYF-expressing wild type Src) cells were infected with adenoviruses expressing either GFP or Shp2 E76A. (B) SYF cells were transiently transfected with wild type c-Src or kinase-dead c-Src$^{K295R/Y527F\ (KR/YF)}$ and infected with adenoviruses expressing either GFP, wild type Shp2 or Shp2E76A. Cell lysates were immunoblotted with anti-Shp2, pSrc (Y416), pPZR (Y241 or Y263), PZR and Src antibodies. ERK1/2 was used as a loading control. (C and D) HEK-293 cells were transfected with Flag-tagged human PZR (C) or HA-tagged zebrafish PZR (D). The cell lysates were immunoprecipitated with indicated antibody. The immunoprecipitates were subjected to in vitro Src kinase assay with Src recombinant protein. The reaction products were immunoblotted with anti-pPZR (Y241 or Y263) antibodies. (E) HEK-293 cells were co-transfected with constitutively active Src mutant and either HA-tagged wild type zebrafish PZR (WT), PZR mutated at tyrosine 236 (Y241F), tyrosine 258 (Y263F), or both (2YF). Cell lysates were immunoblotted with anti-pPZR (Y241 or Y263) or HA antibodies.

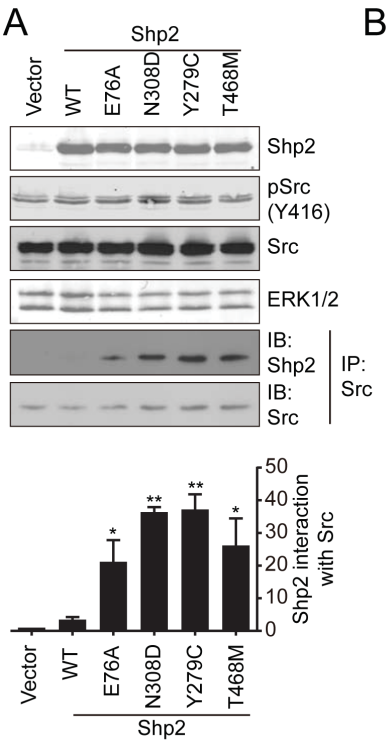

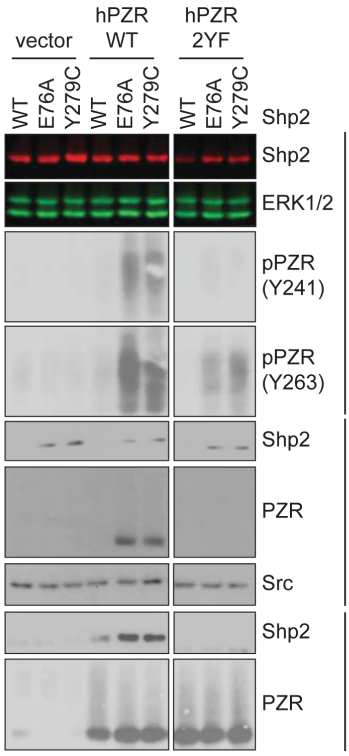

Figure 12. Enhanced Src complex formation with NS/LS-associated Shp2 mutants. (A) HEK 293 cells were transiently transfected either with Shp2 WT and the indicated Shp2 mutants. Cell lysates were immunoprecipitated with anti-c-Src antibodies and immune complexes immunoblotted with anti-Shp2 and anti-Src antibodies. The graph represents the mean ± SEM of the densitometric analysis from three independent experiments. Statistical significance is derived using a Dunnet's test comparing Shp2 mutants with WT. *, $P < 0.05$; **, $P < 0.01$. (B) HEK 293 cells were co-transfected with Shp2 WT, E76A or Y279C and either empty vector (vector), wild type human PZR WT or PZR 2YF mutant. Cell lysates were immunoblotted with anti-pPZR (Y241 or Y263) or Shp2 antibodies. ERK1/2 was used as a loading control. Immune complexes were immunoblotted with anti-Src, Shp2 and PZR antibodies.

Germline mutations in *Ptpn11* that result in either increased or decreased protein tyrosine phosphatase activity leads to developmental defects in zebrafish, mice and humans. Our findings that PZR is a target for *Ptpn11* mutations that exhibit either increased or decreased catalytic activity argue for a central role for PZR in ECM-mediated signaling for both NS and LS mutations. Using a zebrafish model system, we found that PZR is required for development. PZR RNA was apparent at early stages in zebrafish embryos, suggesting a maternal contribution and either knockdown or overexpression of PZR in zebrafish resulted in a gastrulation defect. PZR knock down in zebrafish resulted in similar defects to Shp2 and NS and LS-like phenotypes. In addition, partial knockdown of both PZR and Shp2 resulted in developmental defects. Together, this genetically links PZR to a pathway in which both NS and LS mutations participate. Importantly, we found that the loss of PZR in zebrafish led to convergence and extension defects, which is consistent with deterioration in the fidelity of cell migration. Intriguingly, overexpression of PZR induced gastrulation defects similar to that of both overexpression and reduced expression of Shp2, reported previously [11]. These results suggest a tight balance and interplay exist between PZR and Shp2 signaling, consistent with the biochemical evidence demonstrating that Shp2 binds directly to PZR within its ITIMs [11]. Collectively, these observations argue that PZR-mediated tyrosyl phosphorylation in zebrafish and mice serves as a mechanism to promote NS and LS signaling.

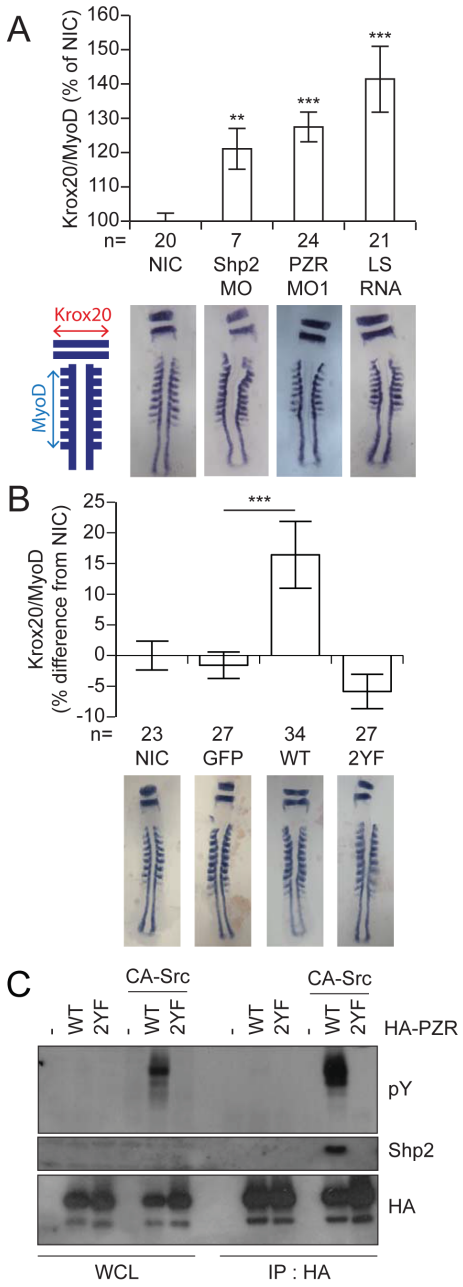

Figure 13. PZR tyrosyl phosphorylation is necessary for zebrafish convergence and extension phenotype. (A) Embryos were injected with Shp2 MO, PZR MO or LS mRNA at the 1-cell stage and fixed at the 8-10 somite stage. *In situ* hybridization was performed using *krox20* and *myoD* staining for rhombomeres 3 and 5, and somites, respectively. Quantification of the width of the rhombomeres (red) and the length of the first 8 somites (light blue) is shown schematically. *Krox20/myoD* ratios are plotted compared to non-injected controls (NIC). Data represent the mean ± S.E.M. **; P < 0.01, ***; P < 0.001. (B) Embryos were injected at the 1-cell stage with mRNA encoding GFP, wild type (WT) PZR or PZR with the indicated mutations. Ratios of *krox20/myoD* were calculated and compared to NIC. All data represent the mean ± S.E.M. ***; P < 0.001. (C) HEK-293 cells were co-transfected with either HA-tagged zebrafish PZR WT or 2YF mutant and constituvely active Src. Cell lysates were immunoprecipitated with HA antibody and blotted with anti-pY, Shp2 and HA antibodies.

What are the consequences of increased PZR tyrosyl phosphorylation? PZR acts as an adhesion-responsive glycoprotein where upon engagement to the extracellular matrix it becomes rapidly tyrosyl phosphorylated within its ITIMs. Upon tyrosyl phosphorylation Shp2 is recruited to PZR and it has been shown that this event is responsible for promoting the pro-migratory and cell adhesive effects in a variety of cell types [24,25,32,35,37]. Given the importance of cell migration and cell adhesion in developmental processes such as gastrulation it is conceivable that aberrant PZR tyrosyl phosphorylation induced by both NS and LS mutants disrupts this process. In mice, PZR is expressed during early development and we have demonstrated that PZR is hypertyrosyl phosphorylated in the developing embryo of *Ptpn11*$^{D61G/+}$ mice [25]. These observations support the notion that altered PZR tyrosyl phosphorylation and hence downstream signaling are associated with developmental defects. The significance of PZR tyrosyl phosphorylation was demonstrated in experiments in which overexpression of the ITIM mutants of PZR failed to induce gastrulation defects. These results define PZR tyrosyl phosphorylation as critical for development.

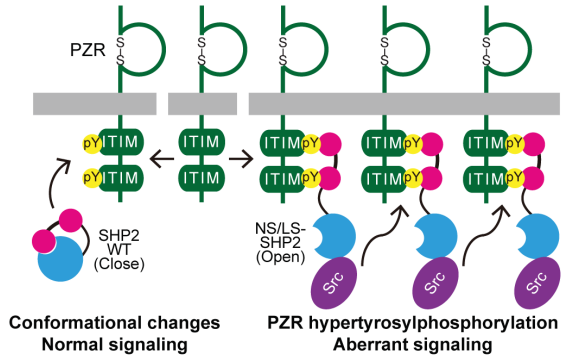

Figure 14. Model for the effects of NS and LS mutants on PZR tyrosyl phosphorylation. See text for details.

A provocative finding from our study is that these results implicate the actions of a tyrosine kinase that promotes PZR tyrosyl phosphorylation by both NS and LS mutants. The observation that PZR is hypertyrosyl phosphorylated in both NS and LS indicates that the ability of the kinase to phosphorylate PZR occurs in an Shp2 catalytically-independent manner. We had shown previously that enhanced PZR tyrosyl phosphorylation caused by NS mutants does not occur as a result of SH2 domain protection [25]. Rather, the data here supports a Src family kinase as responsible for NS and LS-induced PZR hypertyrosyl phosphorylation. Previous work had initially suggested a lack of SFK involvement in NS-mediated PZR hypertyrosyl phosphorylation [25]. In the Eminaga *et al.* study we immunoprecipitated Shp2 and analyzed total tyrosyl phosphorylation of Shp2-associated proteins. The Shp2-associated tyrosyl phosphorylated complex that migrated with a molecular weight of ~40kDa was found to contain at least PZR. It is likely that in this p40 complex that "site-specific" PZR tyrosyl phosphorylation was obscured by other co-migrating tyrosyl phosphorylated proteins. Whereas, in the experiments presented here, PZR tyrosyl phosphorylation is assessed directly using site-specific phospho-antibodies.

We found that both NS and LS mutants contain increased levels of c-Src complexes as compared with wild type Shp2. In addition, we showed increased PZR in Src complexes from activating and LS-associated Shp2 mutants and this was abolished in cells expressing the PZR tyrosyl phosphorylation-deficient mutant. The nature of this increased association with c-Src correlates with the common underlying property that both NS and LS mutants exhibit an "open" conformation [19,38]. Other groups have suggested that the "open" conformation of NS and LS may represent an important molecular mechanism for the pathogenesis of these mutant forms of Shp2 [19,20,31,38]. The open conformation of NS and LS mutants exposes the PTP and SH2 domains, presumably this presents binding surfaces for Src that are otherwise inaccessible. Indeed, it has been shown previously that Shp2 binds to Src through its SH3 domains [39,40]. Our findings support this observation, and extend it by providing a mechanism that reconciles the behavior of both NS and LS in their capacity to promote similar phenotypic outcomes.

The results from our proteomic screen are consistent with activation of a SFK-mediated pathway as we identified the Src substrate, focal adhesion kinase (FAK) and PECAM as hypertyrosyl phosphorylated in the hearts of NS mice. JNK was increased in its level of tyrosyl phosphorylation at one of its activating phosphorylation sites in NS hearts. Interestingly, Marin *et al.* showed that JNK and FAK were hypertyrosyl phosphorylated in LS mice suggesting a catalytic-independent mechanism for the activation of these molecules through the effects of enhanced Src function [34]. Whether or not PZR/Shp2/Src pathway accounts for the entirety of either NS or LS-like phenotypes will need to be determined. However, Jopling *et al.* have shown that Shp2 lies upstream of the SFKs in zebrafish development and the Shp2/SFK pathway is required for convergence and extension cell movements [11]. An integrated interpretation of our results support a model in which we invoke the actions of enhanced Src-mediated PZR tyrosyl

phosphorylation that results in altered development. An important aspect of Shp2-mediated signaling is that it is required to be appropriately localized to its upstream target. Disruption of the SH2 domains of Shp2 results in the abrogation of its ability to signal [1]. Therefore, enhanced PZR tyrosyl phosphorylation results in increased recruitment of Shp2 to PZR to promote further PZR tyrosyl phosphorylation and presumably other Src substrates that are in close proximity (Figure 14). It should also be noted that Src couples to Ras, and in some cases does so through Shp2 [41]. It is formally possible that both NS and LS engage Ras via this mechanism. However, the contribution of Ras signaling specifically for the manifestation of NS- or LS-related pathologies has yet to be determined. Collectively, these observations go some way towards providing an explanation as to how both the NS and LS mutants, which have enhanced and inactive PTP activities, respectively result in overlapping phenotypes.

In summary, we have identified PZR as a proximal target of both NS and LS mutants. PZR functions to regulate cell adhesion and cell migration. Therefore, in NS and LS the augmentation of PZR's interaction with Shp2 when it is hypertyrosyl phosphorylated presumably disrupts key developmental events that rely on the appropriate delivery of migratory ques. This mechanism occurs through enhanced binding of NS and LS mutants to Src. The implications of our findings clinically are that they suggest that the magnitude of PZR tyrosyl phosphorylation may reflect the "openness" of *Ptpn11* mutants and hence the severity of NS and LS-related diseases. As such, it would be instructive to assess the clinical genotype-phenotype relationship in context of PZR tyrosyl phosphorylation in NS and LS patients.

Materials and Methods

DNA constructs and cloning

Ptpn11 was cloned previously [11]. *Mpzl1* was cloned by nested PCR from zebrafish embryos (bud to 48hpf) cDNA with Phusion DNA polymerase (Finnzymes, Vantaa, Finland) using fwPZRout: 5'-GGGCGTTATTCATGAAATCTAAA-3', rvPZRout: 5'- CTCAGGTTGGCAGAGATGT-3', fwPZRstart: 5'- GCGGATCCATGGAAATAAGGCTT -3' and rvPZRstop: 5'-GCCGAATTCTCAGTTCTTGCGGATG-3'. PCR product was cloned into pCS2+ using BamHI and EcoRI. PZR ITIM mutants Y236F, Y258F and Y236F/Y258F were made using site-directed mutagenesis with the following primers:
Fw_Y>F236_PZR:5'-GGACCGGTGATTTTCGCTCAGCTCGAT-3'
Rv_Y>F236_PZR: 5'ATCGAGCTGAGCGAAAATCACCGGTCC-3'
RvstopY258F: 5'- CCGAATTCTCAGTTCTTGCGGATGTCTGCGAACACCACCGGCTC-3' PZR was then sub-cloned using BamHI and XhoI restriction enzymes into pSG5 vector encoding an RPTPa signal sequence and HA tag [42] using the following primers:
FwBamHI AGVSDPZR: 5'-GCCGGATCCGCCGGGGTCTCAGAT-3'
RvXhoI stopPZR: 5'-GCCCTCGAGTCAGTTCTTGCGGAT-3'.

Antibodies, chemicals, cell lines and expression reagents

Rabbit monoclonal phospho-PZR(Y241) and rabbit monoclonal phospho-PZR(Y263) antibodies were generated in collaboration with Cell Signaling. Mouse monoclonal Src antibody, rabbit polyclonal Src antibody, rabbit polyclonal phospho-ERK1/2(T202/Y204), mouse monoclonal ERK1/2 antibody, rabbit polyclonal phospho-Akt(S473) Ab and mouse monoclonal Akt antibodies were purchased from Cell Signaling. Rabbit polyclonal Shp2 antibodies and rabbit polyclonal ERK1/2 antibody were purchased from Santacruz Biotechnology. Mouse monoclonal Shp2 antibody was purchased from BD bioscience. Rabbit polyclonal PZR (105-6) was generously

provided by Dr. Z. J. Zhao. Src family kinase inhibitors, PP2 and SU6656, were purchased from Calbiochem. HEK-293, NIH-3T3, SYF (*Src*$^{-/-}$/*Yes*$^{-/-}$/*Fyn*$^{-/-}$ MEFs) and Src++ (Src overexpressing SYF) cells were purchased from ATCC and grown in growth medium (Dulbecco's modified Eagle's medium supplemented with 1% penicillin/streptomycin and 10% feral bovine serum) in a 5% CO2 incubator at 37°C. Replication-deficient adenoviral constructs harboring Shp2 WT (Ad-Shp2 WT), gain-of-function Shp2 mutant (Ad-Shp2 E76A) and GFP (Ad-GFP) were prepared as previously described [25,43]. NIH-3T3 and SYF cells were infected with by adenovirus at a dosage of 50 MOI. The pJ3 vectors containing Src WT and dominant negative Src mutant (Src K295R/Y527F) have been described in previously [44]. The pIRES-GFP plasmids encoding Shp2 WT, gain-of-function/Noonan syndrome mutants of Shp2 (Shp2 E76A and Shp2 N308D) and LEOPARD syndrome mutants of Shp2 (Shp2 Y279C and Shp2 T468M) have been described in previously [15,25]. DNA transfection into HEK-293 and SYF cells was performed using Lipofectamine 2000 according to the manufacturer's protocol. Mouse anti-phosphotyrosine antibody 4G10 (#05-321) from Merck Millipore, rabbit anti GFP (TP401) from Acris and mouse anti HA.11 clone 16B12 was from Covance.

Animal handling

Ptpn11$^{D61G/+}$ mice were provided from Dr. Benjamin Neel (University of Toronto, Toronto) and were genotyped as described previously [27]. Briefly, *Ptpn11*$^{D61G/+}$ male mice were crossed with WT C75BL/6 X SV129 female mice and their offspring were genotyped by PCR and digestion with AgeI for D61G allele. Animal handling was approved by The Yale University Institutional Animal Care and Use Committee. Tissues from *Ptpn11*$^{Y279C/+}$ mice were provided by Dr. Maria Kontaridis (Harvard University, MA).

In situ *hybridization*

Zebrafish were kept and embryos were staged as described (Westerfield 1995). *In situ* hybridizations were performed as described in Thisse *et al*., 1993. *Bmp2b*, *chd*, *gsc*, *ntla*, *dlx3*, *hgg, krox20* and *myod* probes were as described [11,45]. Antisense and sense *Mpzl1* probe was synthesized by T7 and SP6 mRNA polymerase (Promega), from pCS2+PZR, respectively.

Morpholino's RNA and injections – Zebrafish were kept and embryos were injected at the 1-cell stage. PZR morpholino 5'-CAGAGACCCTTACTGTGGTGGGACGC-3', Shp2 morpholino 5'-GGTGGAACCACCTTCGGGATGTCAT-3', nacre morpholino 5'-CATGTTCAACTATGTGTTAGCTTCA-3' and standard P53 morpholino were from Genetools (Philomath, OR). 5'- capped sense synthetic mRNA was synthesized with SP6 or T7 mRNA polymerase using mMessage mMachine kit from Ambion . The amount of RNA that was injected at the 1-cell stage was optimized for each synthetic RNA. Morpholino's were titrated down to give a specific phenotype without inducing increased apoptosis as co-injection of 1nmol p53 morpholino did not attenuate the phenotype. Likewise, mRNA was titrated down to either induce a phenotype or to rescue a morpholino induced phenotype.

Immunoprecipitation and immunoblotting

Cells were lysed on ice in lysis buffer (20 mM Tris-HCl, 150 mM NaCl, 1 mM CaCl2, 1 mM MgCl2, 1% Nonidet P-40, 1 mM Na3VO4, 10 mM NaF, 1 mM benzamidine, 1 mM PMSF, 1 μg/ml pepstatin A, 5 μg/ml aprotinin, and 5 μg/ml leupeptin. Tissues from Noonan (NS) and LEOPARD (LS) mice were lysed by homogenizing with lysis buffer. Cell or tissue lysates were incubated at 4 °C for 30 min and clarified by centrifugation at 14,000 rpm at 4 °C for 10 min. Protein concentration was determine using the BCA reagent according to the manufacturer's instructions (Pierce). For

immunoprecipitations, 500 μg of lysate was incubated with 1 μg of indicated antibodies at 4 °C for overnight. Immune complexes were collected on either protein A- or protein G-Sepharose beads for 4 hr at 4 °C, washed three times with same lysis buffer and then heated to 95 °C in sample buffer for 5 min. Total cell or tissue lysates and immune complexes were subjected to SDS-PAGE and immunoblotting. The sites of antibody binding were visualized using enhanced chemiluminescence detection or Odyssey Imaging System.

Transfected cells were lysed in RIPA buffer (150 mM NaCl, 20 mM Tris pH 8.0, 10 mM Na_2HPO_4, 5 mM EDTA, 1 mM Na-orthovanadate, 10% glycerol, 1% NP-40, 1% Sodium deoxycholate, 0,1% SDS, sodium fluoride 2.5 mM, β-glycerolphosphate 5 μM, aproptinin 1 μg/ml, leupeptin 1 μg/ml) for 15 minutes on ice with 1 ml per 10 cm dish. Samples were centrifuged for 30 min at 14,000 rpm 4°C. Then samples were pre-cleared using protein A agarose beads for 1 hr, an aliquot of whole cell lysate was immunoprecipitated with 1 μg antibody against HA for approximately 1hr on ice. Samples were precipitated using 25 μl protein A agarose slurry for approximately 1 hr at 4°C. Samples were boiled in 2x laemmli buffer and SDS-PAGE was performed.

For zebrafish, bud stage embryos were snap frozen in liquid nitrogen and stored in -80°C. Subsequently embryos were ground in cell lysis buffer containing 50 mM Tris, pH 7.5, 150 mM NaCl, 1 mM EDTA, 1 mM sodium orthovanadate, 1% Nonidet P-40, 0.1% sodium deoxycholate , sodium fluoride 2.5 mM, β-glycerolphosphate 5mM, aproptinin 1μg/ml, leupeptin 1μg/ml . Samples were then boiled in Laemmli sample buffer containing 4% SDS and β-mercaptoethanol. Proteins equivalent to 4 embryos per lane were subjected to SDS-PAGE and blotted onto a PVDF membrane. After blotting, membranes were stained using coomassie blue to verify equal loading. 293T cells were maintained in DMEM/F12 medium containing penicillin streptomycin and 10% and 7.5% FCS, resspetively. For serum starvation experiments non-essential amino acids were added. 293T and COS7 cells were passed twice a week at 1:20 and 1:7 before transfection. Transfection of zebrafish PZR was performed using polyethyleneimide (PEI) from Sigma with 20 μg DNA. After transfection overnight, medium was replaced with serum and harvested 40 hr after transfection.

Mass Spectrometric Analysis

The PhosphoScan method was performed as previously described [28,46-48]. Wild type and Shp2 mutant (Noonan Syndrome) mouse hearts were homogenized, sonicated, and centrifuged to remove cellular debris. Total protein for each tissue was normalized using the ProteinPlus Coomassie Reagent (Pierce), and proteins were reduced, alkylated, and digested overnight using trypsin (Worthington). Resulting peptides were separated from non-peptide material by solid-phase extraction with Sep-Pak Classic C18 cartridges (Waters). Lyophilized peptides were re-dissolved, and phosphopeptides were enriched by immunoaffinity purification using pY-100 phosphotyrosine antibody (#9411, Cell Signaling Technology). Peptides were eluted with 0.15% TFA and concentrated with C18 spin tips immediately prior to LC-MS analysis.

Duplicate injections of each sample were run to generate analytical replicates and increase the number of MS/MS identifications from each sample. Peptides were loaded directly onto a 10 cm x 75 μm PicoFrit capillary column packed with Magic C18 AQ reversed-phase resin. The column was developed with a 45-minute linear gradient of acetonitrile in 0.125% formic acid delivered at 280 nL/min. Tandem mass spectra were collected with an LTQ-Orbitrap XL mass spectrometer running XCalibur using a top 10 method, a dynamic exclusion repeat count of 1 and a repeat duration of 30 seconds. MS spectra were collected in the Orbitrap component of the mass

spectrometer, and MS/MS spectra were collected in the LTQ.
MS/MS spectra were processed using SEQUEST and the Core platform (Gygi Lab, Harvard University) [49-52]. Searches were performed against the mouse NCBI database with reverse decoy databases included for all searches to estimate false positive rates. Peptide assignments were obtained using a .98 precision cut-off in the linear discriminant analysis module of Core. Cysteine carboxamidomethylation was specified as a static modification, and methionine oxidation and serine, threonine, and tyrosine phosphorylation was allowed. Results were further narrowed using mass accuracy (–/+ 5ppm) filters and the presence of a phosphotyrosine in the peptide. Label-free quantitation was performed using Progenesis v4.1 (Nonlinear Dynamics). Peptide abundance data was manually reviewed in Progenesis for all peptides with at least a 2.0-fold change to ensure accuracy of results.

Global phosphotyrosine differential proteomic analysis in the heart

Heart tissue was lysed in urea buffer (20 mM Hepes, pH 8.0, 9 M Urea, 1 mM sodium vanadate, 2.5 mM sodium pyrophosphate, 1 mM β-glycerophosphate). The lysate was sonicated and clarified by centrifugation. Tissue lysate was reduced by DTT and alkylated with iodoacetamide. Samples were then diluted 4 times with 20 mM Hepes to reduce Urea concentration to 2M, and digested by trypsin overnight at room temperature with gentle shaking. Phosphotyrosine-containing peptides were isolated using immobilized phospho-tyrosine specific antibody PY100 (PhosphoScan Kit; Cell Signaling Technology). Following immuno-purification, phosphotyrosine-containing peptides were analyzed by LC-MS/MS as described previously [48].

Acknowledgements

This work was supported by NIH grant R01 GM099801 (A.M.B.) and in part, by a grant from the Research Council for Earth and Life Sciences (ALW 819.02.021) with financial aid from the Netherlands Organization for Scientific Research (NWO) (to J.d.H.).

References

1. Neel BG, Guo H, Pao L (2009) SH2 Domain-Containing Protein Tyrosine Phosphatases. In: Bradshaw RA, Dennis EA, editors. Handbook in Cell Signaling. 2 ed. San diego: Elsevier. pp. 707-728.
2. Hof P, Pluskey S, Dhe-Pagganon S, Eck MJ, Shoelson SE (1998) Crystal Structure of the Tyrosine Phosphatase SHP-2. Cell 92: 441-450.
3. Mohi MG, Williams IR, Dearolf CR, Chan G, Kutok JL, et al. (2005) Prognostic, therapeutic, and mechanistic implications of a mouse model of leukemia evoked by Shp2 (*PTPN11*) mutations. Cancer Cell 7: 179-191.
4. Tiganis T, Bennett AM (2007) Protein tyrosine phosphatase function: the substrate perspective. Biochem J 402: 1-15.
5. Saxton TM, Henkemeyer M, Gasca S, Shen R, Rossi DJ, et al. (1997) Abnormal mesoderm patterning in mouse embryos mutant for the SH2 tyrosine phosphatase Shp-2. EMBO J 16: 2352-2364.
6. Yang W, Klaman LD, Chen B, Araki T, Harada H, et al. (2006) A Shp2/SFK/Ras/Erk Signaling Pathway Controls Trophoblast Stem Cell Survival. Dev Cell 10: 1-11.
7. Perkins LA, Larsen I, Perrimon N (1992) corkscrew encodes a putative protein tyrosine phosphatase that functions to transduce the terminal signal from the receptor tyrosine kinase torso. Cell 70: 225-236.
8. Neel BG, Gu H, Pao L (2003) The 'Shp'ing news: SH2 domain-containing tyrosine phosphatases in cell signaling. Trends Biochem Sci 28: 284-293.
9. Tartaglia M, Mehler EL, Goldberg R, Zampino G, Brunner HG, et al. (2001) Mutations in *PTPN11*, encoding the protein tyrosine phosphatase SHP-2, cause Noonan syndrome. Nat Genet 29: 465-468.
10. Tartaglia M, Gelb BD (2005) Noonan syndrome and related disorders: genetics and pathogenesis. Annu Rev Genomics Hum Genet 6: 45-68.
11. Jopling C, van Geemen D, den Hertog J (2007) Shp2 knockdown and Noonan/LEOPARD mutant Shp2-induced gastrulation defects. PLoS Genet 3: e225.
12. Runtuwene V, van Eekelen M, Overvoorde J, Rehmann H, Yntema HG, et al. (2011) Noonan syndrome gain-of-function mutations in *NRAS* cause zebrafish gastrulation defects. Dis Model Mech 4: 393-399.
13. Tidyman WE, Rauen KA (2008) Noonan, Costello and cardio-facio-cutaneous syndromes: dysregulation of the Ras-MAPK pathway. Expert Rev Mol Med 10: e37.
14. Gelb BD, Tartaglia M (2011) RAS signaling pathway mutations and hypertrophic cardiomyopathy: getting into and out of the thick of it. J Clin Invest 121: 844-847.
15. Kontaridis MI, Swanson KD, David FS, Barford D, Neel BG (2006) PTPN11 (Shp2) mutations in LEOPARD syndrome have dominant negative, not activating, effects. J Biol Chem 281: 6785-6792.
16. Tartaglia M, Martinelli S, Stella L, Bocchinfuso G, Flex E, et al. (2005) Diversity and Functional Consequences of Germline and Somatic PTPN11 Mutations in Human Disease. Am J Hum Genet 78: 279-290.
17. Hanna N, Montagner A, Lee WH, Miteva M, Vidal M, et al. (2006) Reduced phosphatase activity of SHP-2 in LEOPARD syndrome: consequences for PI3K binding on Gab1. FEBS Lett 580: 2477-2482.
18. Gelb BD, Tartaglia M (2006) Noonan syndrome and related disorders: dysregulated RAS-mitogen activated protein kinase signal transduction. Hum Mol Genet 15 Spec No 2: R220-226.
19. Yu ZH, Xu J, Walls CD, Chen L, Zhang S, et al. (2013) Structural and mechanistic insights into LEOPARD syndrome-associated SHP2 mutations. J Biol Chem 288: 10472-10482.
20. Qiu W, Wang X, Romanov V, Hutchinson A, Lin A, et al. (2014) Structural insights into Noonan/LEOPARD syndrome-related mutants of protein-tyrosine phosphatase SHP2 (*PTPN11*). BMC Struct Biol 14: 10.
21. Zhao R, Zhao ZJ (2000) Dissecting the interaction of SHP-2 with PZR, an immunoglobulin family protein containing immunoreceptor tyrosine-based inhibitory motifs. J Biol Chem 275: 5453-5459.
22. Zhao R, Zhao ZJ (2003) Identification of a variant form of PZR lacking immunoreceptor tyrosine-based inhibitory motifs. Biochem Biophys Res Commun 303: 1028-1033.
23. Zhao ZJ, Zhao R (1998) Purification and cloning of PZR, a binding protein and putative physiological substrate of tyrosine phosphatase SHP-2. J Biol Chem 273: 29367-29372.
24. Roubelakis MG, Martin-Rendon E, Tsaknakis G, Stavropoulos A, Watt SM (2007) The murine ortholog of the SHP-2 binding molecule, PZR accelerates cell migration on fibronectin and is expressed in early embryo formation. J Cell Biochem: [Epub ahead of print].
25. Eminaga S, Bennett AM (2008) Noonan syndrome-associated SHP-2/*Ptpn11* mutants enhance SIRPalpha and PZR tyrosyl phosphorylation and promote adhesion-mediated ERK activation. J Biol Chem 283: 15328-15338.
26. Saxton TM, Pawson T (1999) Morphogenetic movements at gastrulation require the SH2 tyrosine phosphatase Shp2. Proc Natl Acad Sci U S A 96: 3790-3795.
27. Araki T, Mohi MG, Ismat FA, Bronson RT, Williams IR, et al. (2004) Mouse model of Noonan syndrome reveals cell type- and gene dosage-dependent effects of *Ptpn11* mutation. Nat Med 10: 849-857.
28. Rikova K, Guo A, Zeng Q, Possemato A, Yu J, et al. (2007) Global survey of phosphotyrosine signaling identifies oncogenic kinases in lung cancer. Cell 131: 1190-1203.
29. Jopling C, den Hertog J (2005) Fyn/Yes and non-canonical Wnt signalling converge on RhoA in vertebrate gastrulation cell movements. EMBO Rep 6: 426-431.
30. Robu ME, Larson JD, Nasevicius A, Beiraghi S, Brenner C, et al. (2007) p53 activation by knockdown technologies. PLoS Genet 3: e78.
31. Stewart RA, Sanda T, Widlund HR, Zhu S, Swanson KD, et al. (2010) Phosphatase-dependent and -independent

functions of Shp2 in neural crest cells underlie LEOPARD syndrome pathogenesis. Dev Cell 18: 750-762.
32. Zhao R, Guerrah A, Tang H, Zhao ZJ (2002) Cell surface glycoprotein PZR is a major mediator of concanavalin A-induced cell signaling. J Biol Chem 277: 7882-7888.
33. Eminaga S, Bennett AM (2008) Noonan syndrome-associated SHP-2/*PTPN11* mutants enhance SIRPalpha and PZR tyrosyl phosphorylation and promote adhesion-mediated Erk activation. J Biol Chem 283: 15328-15338.
34. Marin TM, Keith K, Davies B, Conner DA, Guha P, et al. (2011) Rapamycin reverses hypertrophic cardiomyopathy in a mouse model of LEOPARD syndrome-associated *PTPN11* mutation. J Clin Invest 121: 1026-1043.
35. Kusano K, Thomas TN, Fujiwara K (2008) Phosphorylation and localization of protein-zero related (PZR) in cultured endothelial cells. Endothelium 15: 127-136.
36. Wickstrom SA, Radovanac K, Fassler R (2011) Genetic analyses of integrin signaling. Cold Spring Harb Perspect Biol 3.
37. Zannettino AC, Roubelakis M, Welldon KJ, Jackson DE, Simmons PJ, et al. (2003) Novel mesenchymal and haematopoietic cell isoforms of the SHP-2 docking receptor, PZR: identification, molecular cloning and effects on cell migration. Biochem J 370: 537-549.
38. Bocchinfuso G, Stella L, Martinelli S, Flex E, Carta C, et al. (2007) Structural and functional effects of disease-causing amino acid substitutions affecting residues Ala72 and Glu76 of the protein tyrosine phosphatase SHP-2. Proteins 66: 963-974.
39. Walter AO, Peng ZY, Cartwright CA (1999) The Shp-2 tyrosine phosphatase activates the Src tyrosine kinase by a non-enzymatic mechanism. Oncogene 18: 1911-1920.
40. Peng Z-Y, Cartwright CA (1995) Regulation of the Src tyrosine kinase and Syp tyrosine phosphatase by their cellular association. Oncogene 11: 1955-1962.
41. Zhang SQ, Yang W, Kontaridis MI, Bivona TG, Wen G, et al. (2004) Shp2 regulates SRC family kinase activity and Ras/Erk activation by controlling Csk recruitment. Mol Cell 13: 341-355.
42. van der Wijk T, Blanchetot C, Overvoorde J, den Hertog J (2003) Redox-regulated rotational coupling of receptor protein-tyrosine phosphatase alpha dimers. J Biol Chem 278: 13968-13974.
43. Kontaridis MI, Eminaga S, Fornaro M, Zito CI, Sordella R, et al. (2004) SHP-2 positively regulates myogenesis by coupling to the Rho GTPase signaling pathway. Mol Cell Biol 24: 5340-5352.
44. Fornaro M, Burch PM, Yang W, Zhang L, Hamilton CE, et al. (2006) SHP-2 activates signaling of the nuclear factor of activated T cells to promote skeletal muscle growth. J Cell Biol 175: 87-97.
45. van Eekelen M, Runtuwene V, Overvoorde J, den Hertog J (2010) RPTPalpha and PTPepsilon signaling via Fyn/Yes and RhoA is essential for zebrafish convergence and extension cell movements during gastrulation. Dev Biol 340: 626-639.
46. Guo A, Villén J, Kornhauser J, Lee KA, Stokes MP, et al. (2008) Signaling networks assembled by oncogenic EGFR and c-Met. Proceedings of the National Academy of Sciences 105: 692-697.
47. Rush J, Moritz A, Lee KA, Guo A, Goss VL, et al. (2005) Immunoaffinity profiling of tyrosine phosphorylation in cancer cells. Nat Biotechnol 23: 94-101.
48. Stokes MP, Farnsworth CL, Moritz A, Silva JC, Jia X, et al. (2012) PTMScan direct: identification and quantification of peptides from critical signaling proteins by immunoaffinity enrichment coupled with LC-MS/MS. Mol Cell Proteomics 11: 187-201.
49. Beausoleil SA, Villen J, Gerber SA, Rush J, Gygi SP (2006) A probability-based approach for high-throughput protein phosphorylation analysis and site localization. Nat Biotechnol 24: 1285-1292.
50. Elias JE, Gygi SP (2007) Target-decoy search strategy for increased confidence in large-scale protein identifications by mass spectrometry. Nat Methods 4: 207-214.
51. Huttlin EL, Jedrychowski MP, Elias JE, Goswami T, Rad R, et al. (2010) A tissue-specific atlas of mouse protein phosphorylation and expression. Cell 143: 1174-1189.
52. Yates JR, 3rd, Eng JK, McCormack AL, Schieltz D (1995) Method to correlate tandem mass spectra of modified peptides to amino acid sequences in the protein database. Anal Chem 67: 1426-1436.

Noonan and LEOPARD syndrome Shp2 variants induce heart displacement defects in zebrafish

Monica Bonetti[1], Jeroen Paardekooper Overman[1], Federico Tessadori[1], Emily Noël[1], Jeroen Bakkers[1] and Jeroen den Hertog[1,2]

1 Hubrecht Institute-KNAW and University Medical Center Utrecht, 3584 CT Utrecht, The Netherlands
2 Institute of Biology 2333 CC, Leiden, The Netherlands

Development 2014, May; 141(9):1961-1970

Abstract

Germline mutations in *PTPN11*, encoding Shp2, cause Noonan syndrome (NS) and LEOPARD syndrome (LS), two developmental disorders that are characterized by multiple overlapping symptoms. Interestingly, Shp2 catalytic activity is enhanced by NS mutations and reduced by LS mutations. Defective cardiac development is a prominent symptom of both NS and LS, but how the Shp2 variants affect cardiac development is unclear. Here, we expressed the most common NS and LS Shp2-variants in zebrafish embryos to investigate their role in cardiac development in vivo. Heart function was impaired in embryos expressing NS and LS variants of Shp2. The cardiac anomalies first occurred during elongation of the heart tube and consisted of reduced cardiomyocyte migration, coupled with impaired leftward heart displacement. Expression of specific laterality markers was randomized in embryos expressing NS and LS variants of Shp2. Ciliogenesis and cilia function in Kupffer's vesicle was impaired, likely accounting for the left/right asymmetry defects. Mitogen activated protein kinase (MAPK) signaling was activated to a similar extent in embryos expressing NS and LS Shp2-variants. Interestingly, inhibition of MAPK signaling prior to gastrulation rescued cilia length and heart laterality defects. These results suggest that NS and LS Shp2-variant mediated hyperactivation of MAPK signaling leads to impaired cilia function in Kupffer's vesicle, causing left-right asymmetry defects and defective early cardiac development.

Introduction

PTPN11 encodes Shp2, a ubiquitously expressed non-receptor protein-tyrosine phosphatase (PTP) with two Src homology 2 (SH2) domains [1-3], that is involved in a variety of signal transduction processes, such as the Ras-Raf-MAP kinase [4], Jak-Stat [2,5], and Phosphatidylinositol-3 kinase (PI-3K) pathways [6]. Shp2 plays a critical role in the transduction of the signal from Receptor Tyrosine Kinases (RTKs), including the receptors of platelet-derived growth factor (PDGFR) [7], fibroblast growth factor (FGFR) [8] and the epidermal growth factor (EGFR) [9,10] as well as from cytokine receptors and Integrins [8,9].

Missense germline mutations in *PTPN11* are associated with Noonan syndrome (NS) (OMIM: 163950) and LEOPARD syndrome (LS) (OMIM: 151100), two autosomal dominant disorders. NS is a relatively common disorder that affects 1 in 1,000-2,000 live births. NS patients are characterized by congenital heart defects, including atrial and ventricular septal defects, pulmonary stenosis and hypertrophic cardiomyopathy (HCM) [11,12]. In addition, NS patients display short stature and facial abnormalities. LS is a more rare disorder (1:3,500 live births) that shows a substantial overlap with the various symptoms of NS patients with two more clinical manifestations that are specific for LS patients: deafness and "café-au-lait" spots on the skin [13,14]. The congenital heart defects among patients with *PTPN11* mutations differ between NS and LS patients, in that pulmonary stenosis is most common in NS, while HCM prevails in LS patients [15,16].

Interestingly, the biochemical properties of NS-Shp2 and LS-Shp2 are distinct, in that NS mutations enhance catalytic activity and LS mutations strongly reduce PTP activity [17,18]. The crystal structure of Shp2 shows that in the absence of a binding partner, the N-SH2 domain interacts with the PTP domain and blocks the catalytic site [19]. NS mutations predominantly reside in the interface between the N-SH2 domain and the PTP domain, resulting in the disruption of the closed conformation and enhanced catalytic activity of NS-Shp2 [17,20]. In contrast, most LS mutations reside close to the active site and result in strongly reduced, yet detectable catalytic activity [17,21,22]. How two mutations with opposite effects on catalytic activity result in syndromes with similar clinical symptoms is a conundrum that still needs to be resolved.

NS-Shp2 causes up-regulation of the MAPK pathway [6]. Whereas several studies show that LS mutations down-regulate the level of phosphorylated ERK [18,23], the role of LS-Shp2 mutation on the MAPK pathway is still controversial [24-26]. Increased RAS/MAPK signaling is implicated in the gain-of-function phenotypes that are caused by expression of the LS *Drosophila* orthologue of *PTPN11*, *corkscrew* (*csw*) [26], suggesting a mechanism by which NS and LS variants may result in similar phenotypes. However, NS- and LS-signaling is distinct, because it is well established that LS-mutations, but not NS mutations [27], enhance PI3K/AKT signaling in hearts of LS/+ knock-in mice [18] as well as in fibroblasts isolated from LS patients [24]. The similarities in RAS/MAPK signaling of NS and LS variants may underlie the overlapping symptoms in NS and LS, whereas the differences in PI3K/Akt signaling may cause the differences in NS- and LS-induced developmental defects.

Shp2 knock-out, knock-down and gain-of function studies in a variety of organisms have begun to reveal the roles of Shp2 in embryonic development. Shp2 null mouse embryos die pre-implantation due to defective Erk activation and trophoblast stem cell death [28]. Dominant-negative Shp2 mutants disrupt gastrulation in *Xenopus* [29]. Moreover, mouse models have been generated for

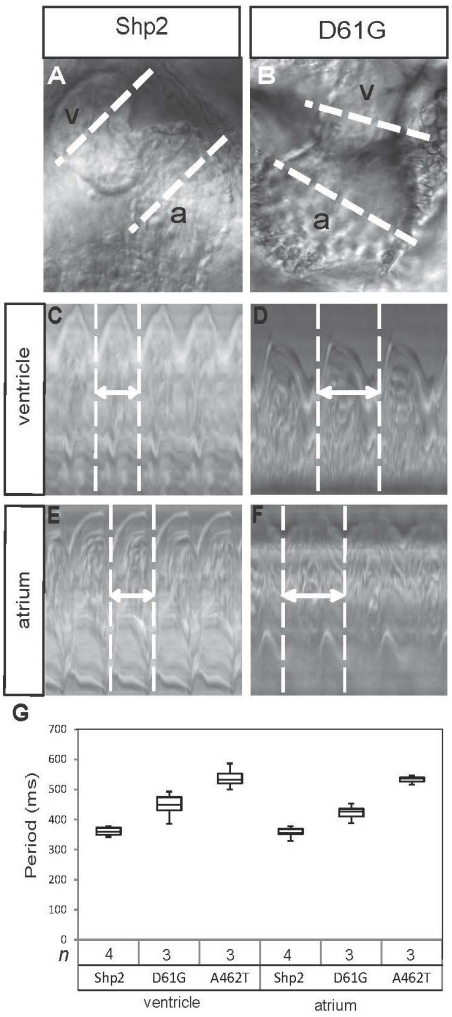

Figure 1. Impaired cardiac function in embryos expressing Shp2-D61G and Shp2-A462T. (A-B) The hearts of WT-Shp2 (Shp2) and Shp2-D61G expressing zebrafish embryos were imaged by high speed video recording microscopy at 2 dpf. White dotted lines through the atrium (a) and the ventricle (v) are indicated. (C-F) Ventricular (C,D) and atrial (E,F) kymographs from 2 dpf embryonic hearts. Note the longer period of the Shp2-D61G expressing heart, compared to the WT-Shp2 expressing heart (double arrow and white dotted vertical lines). (G) Quantitative analysis of the heart period in the ventricle or atrium of WT-Shp2, Shp2-D61G and Shp2-A462T expressing embryos. Whisker plots are depicted.

the two most prevalent NS and LS mutations, *Ptpn11*$^{D61G/+}$ and *Ptpn11*$^{Y279C/+}$, respectively. These mice exhibit developmental defects, including reduced length, cranio-facial abnormalities and congenital heart defects, reminiscent of the clinical characteristics of the human disorders [30,31]. In particular pulmonary stenosis and HCM are evident in the NS and LS mice, respectively. Shp2 is conserved in zebrafish and we previously generated the most common human NS and LS mutations in a cDNA encoding full length zebrafish Shp2. Micro-injection of mRNA encoding mutant Shp2 variants into zebrafish embryos at the one-cell stage induces gastrulation cell movement defects as well as craniofacial and cardiac defects [32]. Furthermore, Stewart *et al.* used zebrafish embryos to show that the function of Shp2 in neural crest cells underlies LS pathogenesis [23].

The role of NS and LS Shp2 variants in the development of cardiac defects is still unclear. Zebrafish has become a powerful model to study cardiac development in recent years [33,34]. We set out to study early heart development in zebrafish embryos expressing NS and LS variants of Shp2, taking advantage of the transparency of zebrafish embryos, which facilitates time-lapse analysis of the onset and nature of the cardiac defects *in vivo*. Our analyses revealed impaired heart function and morphogenesis, which were highly similar in NS- and LS-Shp2 expressing embryos. Furthermore, the heart defects were accompanied by randomization of left-right asymmetry, which was likely due to impaired ciliogenesis and defective cilia function in Kupffer's vesicle that we observed in early embryos. Treatment with a MEK-inhibitor, CI-1040, prior to gastrulation rescued defective leftward heart displacement and the laterality defects in NS- and LS-Shp2 expressing embryos. Taken together, our results provide insight into the mechanism by which NS and LS Shp2-variants induced laterality defects through hyperactivation of MAPK signaling, resulting in cardiac defects during early development.

Results

Expression of NS and LS Shp2-variants caused defects in cardiac function

To investigate the role of Shp2 variants in cardiac function, Shp2-D61G and Shp2-A462T mRNAs were injected at the 1-cell stage. In order to monitor expression of mutant Shp2, we fused a green fluorescent protein (GFP)-peptide 2A sequence to the NH2-terminus of Shp2, which is cleaved off autoproteolytically [35] (Supplemental Figure 1). Following expression of (mutant) Shp2, the developing heart was analyzed at 55 hpf by high-speed video recording. Kymographs of the atrium and ventricle were generated, allowing quantification of heart function as described before [36]. Representative examples of kymographs of embryos expressing WT-Shp2 and Shp2-D61G are depicted (Figure 1A-F). Quantification of the kymographs of WT-Shp2, Shp2-D61G and Shp2-A462T injected embryos revealed significantly longer cardiac cycles in the Shp2-variant expressing embryos, reflecting a reduced but regular heart rate (Figure 1G). Other functional defects, such as an atrio-ventricular block or uncoupling of the two chambers were not detected in Shp2-D61G and Shp2-A462T expressing embryos. These results illustrate functional cardiac defects, particularly a reduced heart rate, in embryos expressing NS and LS variants of Shp2.

Impaired heart asymmetry in embryos expressing NS and LS Shp2-variants

To further characterize the cardiac phenotype in response to expressing of NS and LS variants of Shp2, we first examined the overall morphology and regionalization of the heart at 55 hpf by *in situ* hybridization (ISH), using a panel of cardiac markers. At this stage, the heart chambers are completely formed in wild type embryos and the heart undergoes looping morphogenesis. Analysis of heart shape using a *myl7*-specific probe (formerly known as *cmlc2*) revealed that the hearts of Shp2-D61G and Shp2-A462T expressing embryos exhibited either inverted looping (14%

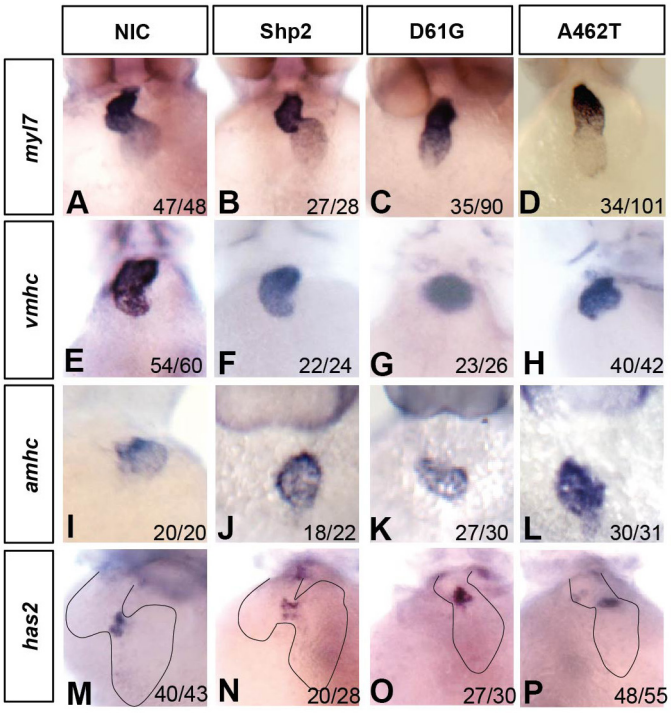

Figure 2. Heart defects in embryos expressing Shp2-D61G and Shp2-A462T. Non-injected control embryos (NIC) and embryos injected at the one-cell stage with mRNA encoding WT-Shp2 (Shp2), Shp2-D61G, or Shp2-A462T were fixed at 48 hpf and *in situ* hybridization was performed using probes for the myosin genes *myl7* (A-D, cardiomyocytes), *vmhc* (E-H, ventricle), *amhc* (I-L, atrium), and for *has2* (M-P, endocardial cushions). Representative pictures are shown and the number of embryos showing this pattern as well as the total number of embryos that were analyzed is indicated in the bottom right corner of each panel. The outline of the heart is indicated with a dashed line in panels M-P.

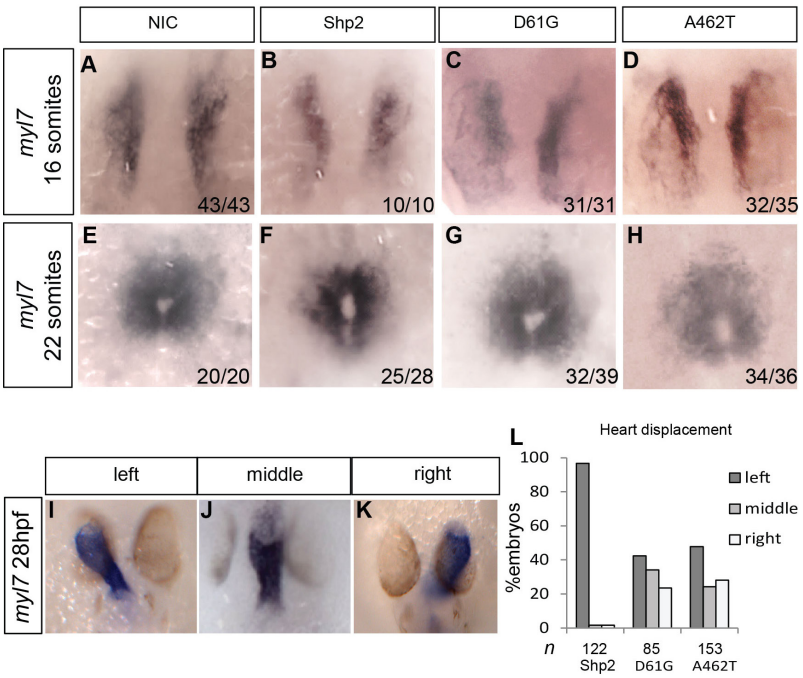

Figure 3. Randomized heart displacement in response to expression of Shp2-D61G and Shp2-A462T. Embryos were injected at the one-cell stage with mRNA encoding WT-Shp2, Shp2-D61G or Shp2-A462T and fixed at the 16-somite stage, the 22-somite stage or at 28 hpf. *In situ* hybridization was done using a *myl7*-specific probe to mark cardiomyocytes. (A-H) The ratio of the number of embryos displaying the depicted pattern and the total number of embryos that were analyzed for each condition is indicated in the bottom right of each panel. (I-K) Representative pictures are shown displaying heart displacement to the left (I), middle (J) and right (K). (L) Percentages of left, middle and right cardiac displacement are depicted.

and 11%, respectively) or non-looped heart (39% and 25%, respectively) in contrast to non-injected control and WT-Shp2 injected embryos, (Figure 2A-D). Myocardial chamber specification was not affected in NS-Shp2 and LS-Shp2 injected embryos as determined by expression of ventricular myosin heavy chain (*vmhc*) (Figure 2E-H) and atrium myosin heavy chain (*amhc*) (Figure 2I-L). Next, the formation of the endocardial cushions, from which the atrioventriclar valves will develop, was assessed by *has2* expression. In Shp2-D61G and Shp2-A462T expressing embryos, *has2* expression was not affected, compared to non-injected control and WT-Shp2 expressing embryos (Figure 2M-P). Expression of this panel of markers was also assessed in embryos expressing Shp2-T73I (NS) and Shp2-G465A (LS) with similar results (Supplemental Figure 2), indicating that all NS and LS variants induced similar defects. Taken together, these data indicate that expression of NS- and LS-variants of Shp2 led to a failure to undergo heart looping in a large proportion of the embryos without inducing defects in cardiac chamber specification or endocardial cushion formation. In addition, the NS- and LS-variants of Shp2 induced cardiac defects to a similar extent during early development.

To investigate at which stage the cardiac defects arise in embryos expressing NS and LS variants of Shp2, *myl7* expression was analyzed at different time points of heart development, particularly during cardiac fusion and heart tube elongation. Zebrafish heart formation is initiated by fusion

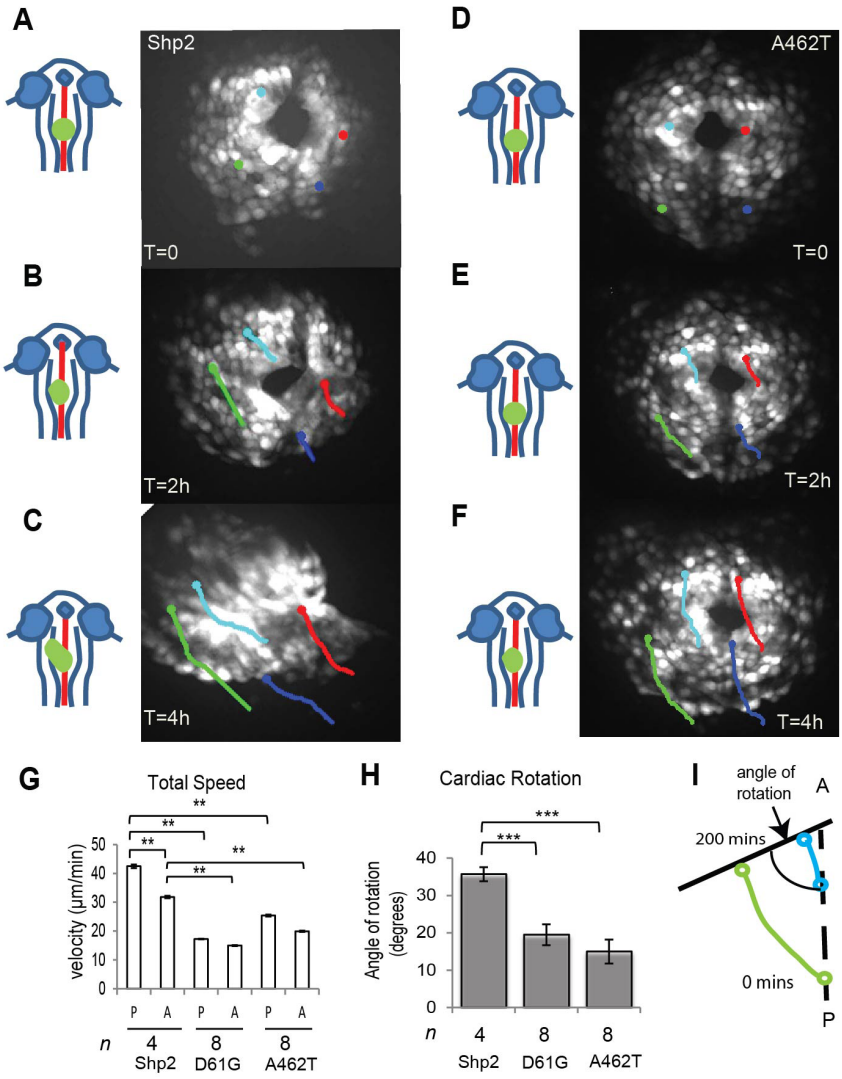

Figure 4. Impaired cardiomyocyte migration in embryos expressing Shp2-D61G and Shp2-A462T. Embryos from the *tg(myl7:GFP)* line were injected with mRNA encoding WT-Shp2, Shp2-D61G or Shp2-A462T lacking eGFP-peptide 2A sequences to allow imaging of GFP-positive cardiomyocytes from the 22-somite stage onwards. **(A-F)** Representative individual GFP-positive cells were color-coded according to their location within the cardiac field at the 22-somite stage and tracked over a 200 min period. The resulting cell tracks are indicated. Dorsal view with the anterior to the top. Schematic representations of the embryos on the left indicate the position and shape of the heart in green. (A-C) WT-Shp2; (D-F) Shp2-A462T **(G)** Quantification of the total speed of posterior (P) and anterior (A) cardiac progenitor cells. Following imaging, heart displacement was assessed in the embryos. WT-Shp2 expressing embryos displayed normal leftward heart displacement; embryos expressing Shp2-D61G and Shp2-A462T that did not display normal heart displacement were selected for further analysis. **(H)** Clockwise cardiomyocyte rotation was determined of the same embryos as in (G). Rotation was quantified as depicted in (I). In (G) and (H), averages are indicated and error bars indicate standard error of the mean. Statistical significance was determined using Student's t-test and is indicated with **, $p < 0.01$ and ***, $p<0.001$.

of two bilateral pools of cardiomyocytes at the 16-somite stage (16 hpf) into a cardiac disc at the midline of the embryo at 22 somites (20 hpf) [33,37]. No obvious defects were detected in *myl7* expression or cardiac fusion between non-injected control, WT-Shp2, Shp2-D61G and Shp2-A462T expressing embryos up to 22 somites (Fig 3A-H). At 28 hpf, the heart in WT-Shp2 expressing embryos formed a tube that extended from the midline to the area under the left eye (Figure 3I), which resembled normal heart displacement. In contrast, in Shp2-D61G and Shp2-A462T expressing embryos the displacement of the heart is randomized: 23% of Shp2-D61G expressing embryos and 28% of Shp2-A462T expressing embryos showed the heart on the right, while 34% of Shp2-D61G expressing embryos and 24% of Shp2-A462T expressing embryos displayed positioning of the heart tube at the midline (Figure 3J-L). Taken together, these results indicate that the first signs of cardiac abnormality in embryos expressing Shp2 variants are observed during asymmetric displacement of the heart tube.

Decreased cardiomyocyte migration speed and rotation in embryos expressing NS and LS Shp2-variants

Randomization of heart displacement may be caused by compromized cardiomyocyte migration [38]. *Tg(myl7:GFP)* embryos express eGFP in cardiomyocytes and were used for high-resolution confocal time-lapse imaging to assess cardiomyocyte migration. Since WT-Shp2 expressing embryos were indistinguishable from non-injected control embryos in *in situ* hybridization experiments (Figure 2, 3), we used WT-Shp2 expressing embryos as a control for the embryos expressing NS and LS variants of Shp2 from here on after. Single cells were tracked in WT-Shp2, Shp2-D61G and Shp2-A462T expressing embryos from cardiac disc stage (21 somites, 19.5 hpf) for 4 hours and their velocities and directions were determined. Consistent with observations of heart morphogenesis in wild type embryos [39,40], cardiac cells moved towards the left and anterior part of the embryo in WT-Shp2 expressing embryos (n=4). Cardiomyocytes in the posterior part of the cardiac disc moved faster than anterior cells (Figure 4A-C). The Shp2-D61G and Shp2-A462T expressing embryos were imaged at 19.5 hpf, like the WT-Shp2 expressing embryos and subsequently, heart displacement was assessed at 24 hpf, allowing correlation between early migration defects and heart displacement. Embryos that displayed impaired heart displacement were selected for further analysis. It is noteworthy that none of the selected embryos displayed heart displacement to the right (Shp2-D61G, n=8; Shp2-A462T, n=8), which may be due to low penetrance of rightward heart displacement. Although cardiomyocytes in the selected embryos formed a cardiac tube, they showed reduced migration to the left. Representative images of an embryo expressing Shp2-A462T are depicted in Figure 4D-F. Quantification of the speed of cardiomyocytes confirmed slower migration of cells in embryos expressing Shp2-D61G and Shp2-A462T, compared to WT-Shp2 (Figure 4G). Cardiomyocytes in selected embryos expressing Shp2-D61G and Shp2-A462T did not cross the midline, but instead migrated anteriorly, which is consistent with defective heart displacement to the left. Rotation of the heart tube was quantified as described before and the observed 30° clockwise rotation of the cardiac cone in WT-Shp2 expressing embryos was consistent with the previously reported clockwise rotation in control embryos [39]. Clockwise rotation was significantly decreased in embryos expressing Shp2-D61G and Shp2-A462T with impaired leftward heart displacement, compared to control WT-Shp2 (Figure 4H). Our results indicate that directional cardiomyocyte migration and heart tube rotation is reduced in embryos expressing NS and LS Shp2-variants, which is consistent with the observed defects in heart tube displacement.

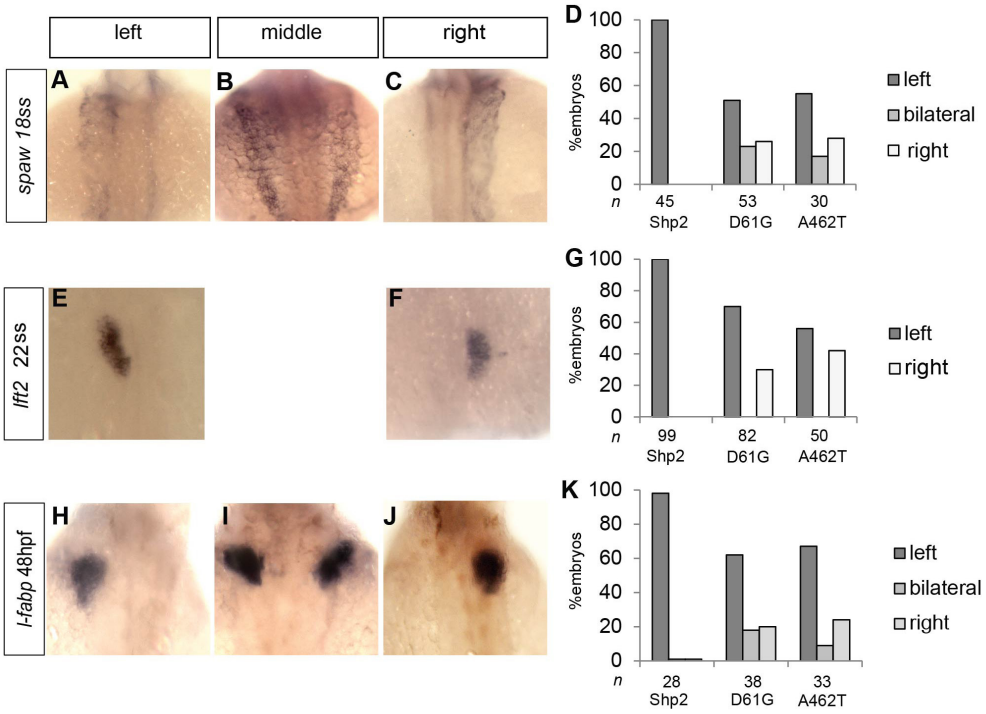

Figure 5. Expression of Shp2-D61G and Shp2-A462T induced L/R asymmetry defects. Embryos were injected at the one-cell stage with mRNA encoding WT-Shp2 (Shp2), Shp2-D61G or Shp2-A462T and fixed at the stage indicated in the panel. *In situ* hybridization was done using probes specific for *spaw* (A-D, *southpaw*), *lft2* (E-G, *lefty2*), and *fabp* (H-K, fatty acid binding protein, marking the liver). Representative pictures are shown of Shp2-D61G expressing embryos. Note that *lft2* expression was only observed on the left side or on the right side. Organ asymmetry as assessed using the different markers was scored for embryos injected with WT-Shp2, Shp2-D61G and Shp2-A462T. Percentages of left, middle/bilateral and right expression of the markers are depicted.

NS and LS Shp2-variants disrupt left/right asymmetry

To determine if the loss of asymmetry in the hearts of embryos expressing NS and LS Shp2-variants is associated with disruption of overall L/R asymmetry, we analyzed the expression of a number of laterality markers. *Southpaw* (*spaw*) is one of the earliest markers displaying asymmetric expression in development [41]. *Spaw* was predominantly expressed in the left lateral plate mesoderm (LPM) in WT-Shp2 expressing embryos (Figure 5A). *Spaw* expression was affected in embryos expressing Shp2-D61G and Shp2-A462T, compared to WT-Shp2, in that 23% of Shp2-D61G and 17% of Shp2-A462T expressing embryos displayed bilateral *spaw* expression and 26% of Shp2-D61G and 28% of Shp2-A462T expressing embryos expressed *spaw* exclusively in the right LPM (Figure 5B-D). Next, expression of *Lefty2* (*lft2*), a downstream target of *spaw,* was investigated at the 22 somite stage (20 hpf). In WT-Shp2 expressing embryos, *lft2* was detected in the left cardiac field in all cases (Figure 5E). In contrast, expression of *lft2* in Shp2-D61G and Shp2-A462T expressing embryos was randomized. 30% of the Shp2-D61G expressing embryos expressed *lft2* on the right side (Figure 5E-G). Similarly, in Shp2-A462T expressing embryos, *lft2* expression was detected at the right side in 42% of the embryos. *Southpaw* is required for visceral organ L/R asymmetry [41], suggesting that defects in L/R asymmetry may not be limited to the heart in embryos expressing Shp2 variants. To investigate this, the position of the liver was

assessed by analysis of the expression of *fabp*. *Fabp* expression was randomized at 48 hpf in embryos expressing Shp2-D61G and Shp2-A462T, in that the liver developed on the opposite side in 20% of the Shp2-D61G expressing embryos and 24% of the Shp2-A462T expressing embryos, or on both sides in 18% of the Shp2-D61G and 9% of the Shp2-A462T expressing embryos (Figure 5H-K). In control WT-Shp2 expressing embryos, the liver always developed on the left side of the embryos. Analysis of the embryonic midline using the sonic hedgehog marker [42] indicated that expression of Shp2-D61G and Shp2-A462T altered left-right patterning without disrupting the

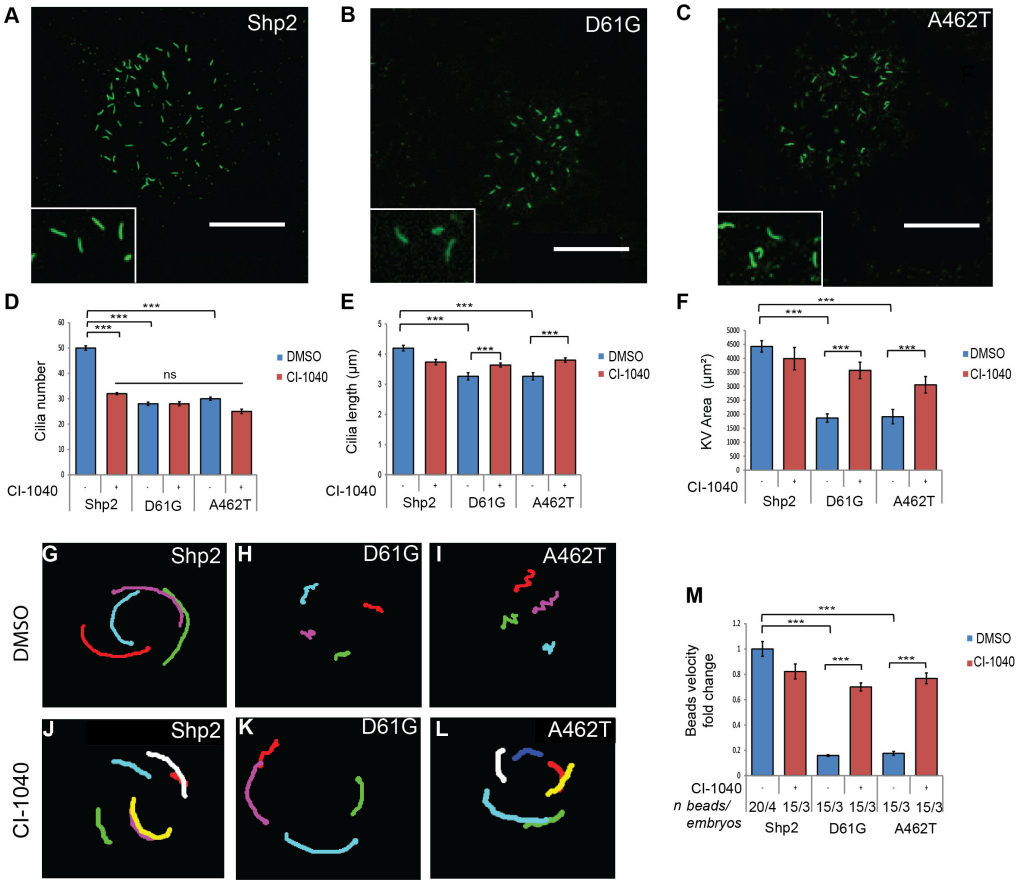

Figure 6. Impaired ciliogenesis and cilia function in Kupffer's vesicle in embryos expressing Shp2-D61G and Shp2-A462T. (A-C) Immunohistochemistry was done using anti-acetylated tubulin on WT-Shp2, Shp2-D61G or Shp2-A462T expressing embryos that were fixed at the 10-somite stage. Representative confocal images are depicted here. Scale bar indicates 50 µm. (D-F) Quantification of the cilia number, cilia length and KV area in WT-Shp2, Shp2-D61G and Shp2-A462T expressing embryos that were treated with 0.5% DMSO (control) or 0.25 µM CI-1040 at 4.5 hpf for 1 h and fixed at the 10-somite stage (n=10 for each condition). Averages are depicted with error bars indicating standard error of the mean. Statistical significance was determined using Student's t-test: ***, $p<0.001$; **, $p<0.01$. (G-L) Tracks of fluorescent beads injected in KV. (G–L) Maximum projections of fluorescent bead movements injected in the KV of WT-Shp2, Shp2-D61G or Shp2-A462T expressing embryo, respectively that were treated with 0.5% DMSO or 0.25 µM CI-1040 at 4.5 hpf for 1 h and fixed at the 10-somite stage. (M) Average flow velocity of beads in KV of embryos expressing WT-Shp2, Shp2-D61G and Shp2-A462T for the DMSO treatment and for the CI-1040 treatment. Averages are depicted with error bars indicating standard error of the mean. Statistical significance was determined using Student's t-test: ***, $p<0.001$.

midline that provides a barrier between the left and the right side (Supplemental Figure 4). These results show that L/R patterning in the LPM is impaired in embryos expressing NS and LS Shp2-variants, which may lead to randomization of heart and gut laterality.

Ciliogenesis and cilia function in Kupffer's vesicle are impaired in embryos expressing NS and LS Shp2-variants

It is well established that Kupffer's vesicle (KV), a fluid-filled ciliated organ, is involved in the establishment of L/R asymmetry in zebrafish [43,44]. Through the oriented rotation of the cilia inside the KV, asymmetric expression of genes such as *spaw* and *lft2* is established. Immunohistochemistry was done using an acetylated tubulin antibody to detect cilia in the KV of 10 somite-stage embryos (14 hpf) (Figure 6A-C). The mean number of cilia was 51.4 ± 0.5 in WT-Shp2 expressing embryos, whereas in embryos expressing Shp2-D61G and Shp2-A462T, the number of cilia was significantly reduced to 30.4 ± 0.7 and 28.5 ± 0.4, respectively (n=10 embryos each) (Figure 6D). Also, the cilia length was significantly reduced in embryos expressing NS and LS Shp2-variants (both 3.2 µm ± 0.1, n cilia=241 for Shp2-D61G and n cilia=172 for Shp2-A462T, respectively) compared to control (4.2 ± 0.1 µm, n cilia=379 for WT-Shp2) (Figure 6E). Measurements of the area of KV indicated significant differences in lumen size among wild-type (4517 ± 355 μm^2, n=10), Shp2-D61G (2243 ± 190 μm^2, n=10) and Shp2-A462T (1914 ± 256 μm^2, n=10) embryos (Figure 6F). These results suggest that disruption of L/R asymmetry in embryos expressing NS and LS variants of Shp2 was a consequence of defective KV function, resulting from impaired ciliogenesis in the KV. To determine the KV functionality directly, we analyzed the fluid flow in embryos expressing NS and LS variants of Shp2. Tracking of fluorescent beads injected into the KV lumen of wild-type Shp2 expressing embryos showed counterclockwise rotation of the beads (Fig 6G). By contrast, tracking of the beads in Shp2-D61G and Shp2-A462T expressing embryos showed that the beads moved about randomly (Fig6 H-I), indicating a loss of coordinated flow. In addition, beads tracked in Shp2-D61G and Shp2-A462T expressing embryos showed a strongly reduced average flow velocity relative to wild-type Shp2 expressing embryos (Figure 6M). These results indicate that ciliogenesis and cilia function is impaired in the KV of embryos expressing NS and LS variants of Shp2, resulting in defective KV function.

Early treatment with the MEK-inhibitor, CI-1040, rescued L/R asymmetry, heart asymmetry and KV function in embryos expressing NS and LS Shp2-variants

Shp2 variants enhance RAS/MAPK signaling [6]. Previously, we and others showed that inhibition of MEK rescued developmental defects in zebrafish embryos that were caused by expression of activators of the RAS/MAPK pathway [45,46]. We investigated whether inhibition of MEK would also rescue the cardiac defects in embryos expressing NS and LS Shp2-variants. First, the efficacy of the MEK inhibitor, CI-1040, to rescue early developmental defects was assessed. Expression of Shp2-D61G or Shp2-A462T in zebrafish embryos induced cell movement defects, resulting in elongated embryos at bud stage (10 hpf) (Figure 7A-C). Treatment with 0.25 µM CI-1040 at 4.5 hpf for 1 h rescued development at 10.5 hpf of embryos expressing Shp2-D61G and Shp2-A462T (Figure 7D-F). Quantification of the epiboly defects confirmed the rescue of the embryos expressing NS and LS Shp2-variants (Figure 7G). In addition, we confirmed that elevated pERK levels in embryos expressing Shp2-D61G and Shp2-A462T were reduced by CI-1040-mediated inhibition of MEK at 10 hpf (Figure 7H).

Next, the effect of CI-1040 treatment was assessed on asymmetry of the heart in embryos expressing Shp2-D61G and Shp2-A462T. Treatment with 0.25 µM CI-1040 at 4.5 hpf for 1 h rescued

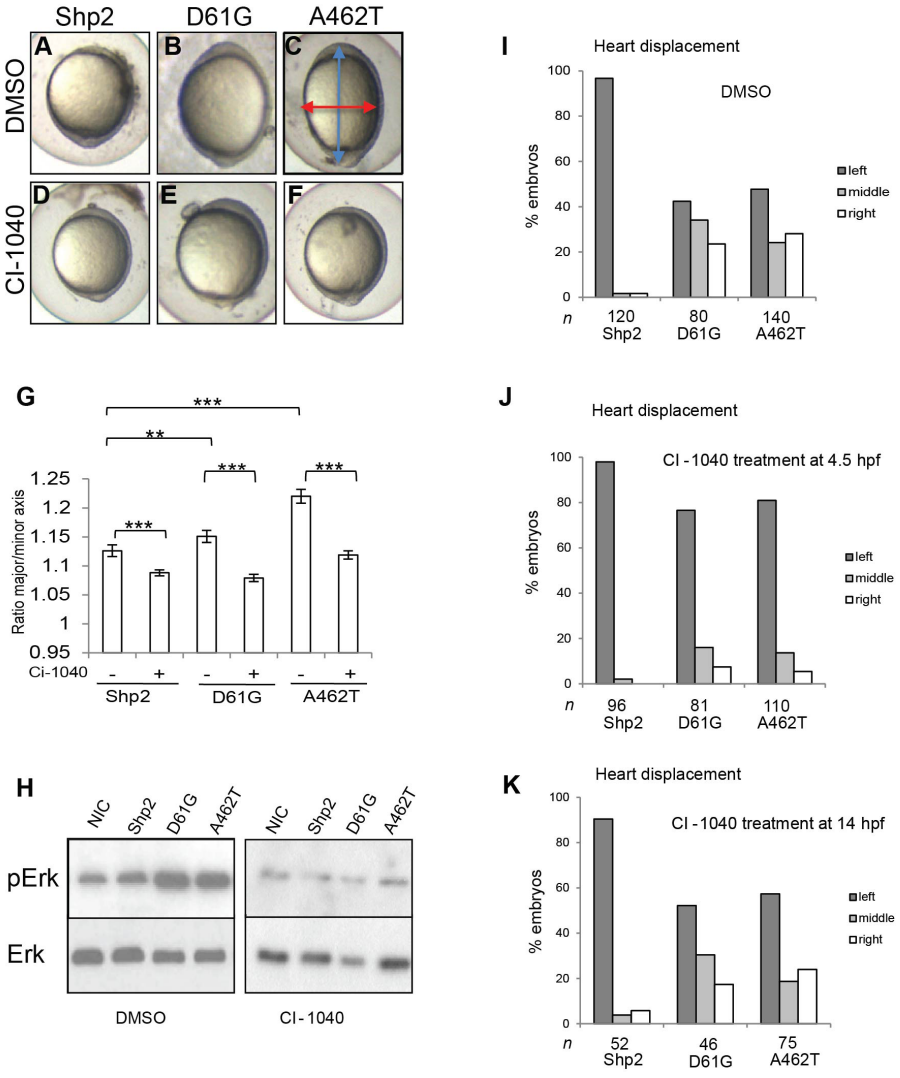

Figure 7. Early treatment with the MEK-inhibitor CI-1040 rescued leftward heart displacement and cilia length in embryos expressing NS and LS Shp2-variants. Embryos were injected with mRNA encoding WT-Shp2 (Shp2), Shp2-D61G and Shp2-A462T at the one cell stage. **(A-F)** Representative images of bud stage embryos are depicted. The shape of the NS- and LS-Shp2 expressing embryos is restored by treatment with 0.25 µM CI-1040 at 4.5 hpf for 1h. **(G)** The ratio between the length of the major and minor axis was determined as quantitative measure of the epiboly defects in NS- and LS-Shp2 expressing embryos. Averages are depicted with error bars indicating standard error of the mean. Statistical significance was determined using Student's t-test (**, p<0.01; ***, p<0.001). **(H)** Embryos were treated with MEK inhibitor CI-1040 (0.25 µM) for 1 h at 4.5 hpf or mock-treated with DMSO and lysed at 10 hpf. Immunoblots of the zebrafish lysates were stained using antibodies specific for pErk and Erk. The experiment was repeated three times and representative blots are depicted here. **(I-K)** Embryos were mock-treated with DMSO (I) or with CI-1040 for 1h at 4.5 hpf (J) or at 10 hpf (K). Heart displacement was determined in embryos following in situ hybridization with a myl7-specific probe as in Figure 4. Histograms represent the percentage of embryos with heart displacement to the left, middle or right.

leftward displacement of the heart at 24 hpf of Shp2-D61G and Shp2-A462T expressing embryos (Figure 7I,J). However, treatment of these embryos for 1 h with CI-1040 at the 10-somites stage (14 hpf) did not restore normal heart displacement in embryos expressing NS and LS Shp2-variants (Figure 7K). Treatment with 0.25 μM CI-1040 at 4.5 hpf for 1 h largely rescued randomization of the left-right asymmetry markers and of the liver (Supplemental Figure 5). These results indicate that inhibition of MEK at early stages rescues L/R asymmetry in embryos expressing NS and LS Shp2-variants.

Finally, the effect of CI-1040 treatment on ciliogenesis and cilia function in KV was assessed. The cilia number was not rescued upon treatment with 0.25 μM CI-1040 at 4.5 hpf for 1 h. In fact, the cilia number in CI-1040-treated WT-Shp2 expressing embryos was significantly reduced to similar levels as in CI-1040 treated embryos expressing NS or LS variants of Shp2 (Figure 6D). Yet, CI-1040 treatment rescued cilia length in embryos expressing Shp2 variants (3.6 ± 0.1 μm in Shp2-D61G and 3.8 ± 0.1 μm in Shp2-A462T expressing embryos, compared to 3.2 ± 0.1 μm in untreated embryos) (cf. Figure 6E). Cilia length in WT-Shp2 expressing embryos was reduced somewhat in response to CI-1040 treatment (from 4.2 ± 0.1 μm to 3.7 ± 0.1 μm; cf. Figure 6E,) and hence, CI-1040 treatment abolished the difference in cilia length between embryos expressing WT-Shp2 and Shp2 variants. Moreover, CI-1040 treatment rescued KV area (3736 ± 373 μm^2 in Shp2-D61G and 3055 ± 294 μm^2 in Shp2-A462T expressing embryos, compared to 3986 ± 398 μm^2 in WT-Shp2 expressing embryos; cf. Figure 6F). Importantly, treatment with 0.25 μM CI-1040 at 4.5 hpf rescued the counterclockwise rotation of the fluorescent beads in Shp2-D61G and Shp2-A462T expressing embryos to levels that were comparable to WT-Shp2 expressing embryos (Figure 6 J-M). Taken together, these results suggest that the cardiac defects in zebrafish embryos expressing NS and LS Shp2-variants are due to hyperactivate MAPK-induced laterality defects originating from impaired cilia function in KV.

Discussion

In this paper, we used zebrafish to investigate defects in cardiac development in response to expression of NS and LS variants of Shp2. We found that NS- and LS-Shp2 expressing embryos showed impaired leftward heart displacement. Our results are consistent with a report that Noonan-associated mutations induce a cardiac looping defect in *Xenopus* [47]. Here, we provide insight into the underlying mechanism. The cardiac defects that we observed in zebrafish embryos are associated with L/R laterality defects and with defects in ciliogenesis. Expression of NS and LS variants of Shp2 in zebrafish embryos enhanced MAPK activation. The laterality defects were rescued by early treatment with CI-1040, a MEK inhibitor, indicating that the defects in heart asymmetry were caused by enhanced MAPK signaling before gastrulation.

Here, we focused on the cardiac defects in embryos expressing NS and LS Shp2-variants. The heart defects only became evident during cardiac tube formation, the first asymmetric process that occurs in the zebrafish heart [33]. Normally, the cardiac tube is displaced to the left, but in embryos expressing NS and LS Shp2 variants, heart displacement was randomized (Figure 3). Cell movement analyses revealed a delay in cell movements, coupled with reduced cardiac tube rotation, resulting in morphologically abnormal hearts at 28 hpf (Figure 4). Cell tracking studies showed that loss of Nodal or BMP signaling leads to similar defects [39,40]. Nodal mutant embryos show reduced speed and directional movement of the cardiomyocytes, resulting in disruption of the leftward morphogenesis and cardiac cone rotation. Asymmetric *spaw* expression in the LPM is responsible for the correct displacement of the heart tube to the left [40,41]. In line with these

findings, we found that expression of *spaw* was randomized in embryos expressing NS and LS Shp2-variants, concomitantly with its downstream gene target *lft2*. As a consequence, left/right asymmetry was lost and leftward displacement of the heart in embryos expressing Shp2-D61G and Shp2-A462T was compromised. In addition, randomized *fabp* expression suggested that not only asymmetry of the heart, but also of the liver was impaired.

Left-right asymmetry is conserved across species and defects in left-right asymmetry are collectively called laterality disease [48]. The phenotype we observed in zebrafish embryos expressing NS and LS Shp2-variants was characterized by randomization of left/right asymmetry. It is noteworthy that laterality disease is frequently associated with congenital heart defects (CHD) [38]. Impaired left-right patterning can affect cardiac morphogenesis, resulting in defective septation and/or double outlet right ventricle (DORV) [38]. Cardiac defects associated with laterality diseases are also reported in Shp2-D61G knock-in mice. A proportion of the heterozygous Shp2-D61G mice displays septal defects and DORV [30]. However, laterality defects are not the only cause of septation defects or DORV. Other laterality defects were not reported in NS or LS Shp2 knock-in mice and laterality defects have not been commonly reported in human individuals with NS and LS. Hence, it remains to be determined whether laterality defects have a role in human NS and LS.

In zebrafish expressing NS and LS variants of Shp2, we found that the underlying mechanism for randomization of L/R asymmetry is likely impaired cilia function in the KV. Particularly cilia length and KV area were associated with Shp2 variant induced impaired fluid flow in KV and subsequent loss of asymmetry (Figure 6). It is well established that L/R asymmetry is mediated by cilia that generate fluid flow within the KV, resulting in expression of *spaw* in the left side of the LPM [49,50]. Laser-mediated ablation of KV randomises expression of *spaw* and *lft2* [50]. Moreover, shorter cilia result in perturbed intravesicular fluid flow, leading to loss of asymmetry in the heart, brain and viscera [51]. KV formation is completed by the 6-somites stage (12 hpf) [52,53] and the generation of the KV depends on the dorsal forerunner cells (DFCs) that are induced during the blastula period [54]. Defects in the specification, clustering or organisation of DFCs induce defective KV organogenesis and/or ciliogenesis [50,53]. Therefore, it will be interesting to investigate the role of the NS and LS Shp2 variants in DFC biology.

Shp2 is a well-known downstream factor in FGFR signaling [8]. It has been reported that FGFR1 signaling regulates cilia length in zebrafish. Morpholino (MO)-mediated knockdown of FGFR1 in zebrafish reduces cilia length in KV and perturbs directional fluid flow, thus impairing L/R patterning of the embryo [43]. That knockdown of FGFR1, a positive regulator of MAPK signaling, has similar effects as mutant Shp2-induced hyperactivation of MAPK appears to be contradictive. However, it is not uncommon that attenuation and activation of a signaling pathway have the same effect on developmental processes. Apparently, FGFR1 knockdown on the one hand and Shp2 variant mediated enhanced MAPK activation on the other have similar effects on cilia function in KV and both impair L/R asymmetry. Our results predict that ectopic activation of MAPK signaling for instance by overexpression of (activated) MAPK around gastrulation would induce laterality defects as well.

Defective ciliogenesis was observed in the KV of NS and LS-Shp2 expressing embryos. It remains to be determined whether ciliogenesis in other organs is affected in these embryos as well. It is noteworthy that deafness is associated with LS in human patients. Deafness is typically associated with defective cilia in the inner ear and future work should focus on ciliogenesis in organs other than KV in NS and LS Shp2-variant expressing zebrafish embryos.

The cardiac defects that were induced by expression of NS and LS Shp2-variants in zebrafish embryos were indistinguishable. MAPK activation was elevated at bud stage in response to expression of both Shp2-D61G (NS) as well as Shp2-A462T (LS) (Figure 7H), which might explain why we observed similar developmental defects at early stages. It is well established that NS-Shp2 mutations enhance MAPK activation, but LS-Shp2 often does not activate MAPK signaling. Nevertheless, it is not unprecedented that LS mutations induce defects that are associated with activation of MAPK signaling. Expression of LS-Shp2 mutants in *Drosophila* results in ectopic wing veins and a rough eye phenotype, characteristics of increased Erk activation. This gain-of-function phenotype is similar to that of NS-Shp2 transgenic flies [25,26]. Moreover, a recent study shows that induced pluripotent stem cells (iPSCs) from LS patient-derived fibroblasts display higher basal pERK levels compared to those of control iPSCs [55]. How the NS and LS variants of Shp2 would both activate MAPK signaling remains to be determined. Whereas catalytic activity of Shp2 is enhanced by the NS mutations, it is reduced by the LS mutations, indicating that MAPK activation is not directly affected by alterations in Shp2 catalytic activity. Rather, the NS and LS Shp2-variant induced defects may result from a phosphatase-independent function of Shp2. Alternatively, as suggested in a recent report, the LS-variants of SHP2 retain some catalytic activity and mediate GOF phenotypes, because they have an increased propensity for the open conformation. Thus, the LS variants bind upstream activators preferentially and stay in complex with their scaffolding adapters longer, thus prolonging specific substrate turnover [22], which in turn may lead to MAPK activation.

Whereas MAPK activation may be elevated by both NS and LS variants of Shp2, elevated PI3K/AKT signaling is exclusively associated with LS. Hyperactivation of AKT signaling in response to LS-Shp2 is responsible for HCM in mouse hearts [31,56,57]. We also observed elevated pAkt levels in response to LS-Shp2 in zebrafish embryos (Supplemental Figure 3), but we did not observe HCM in these embryos. The cardiac defects in embryos expressing NS and LS Shp2-variants were indistinguishable. Moreover, these heart defects were rescued by early treatment with the MEK inhibitor to a similar extent, indicating a causal role for elevated MAPK activation in the observed cardiac defects, independently of Akt signaling.

In summary, our data provide new insights into the role of pathogenic Shp2 variants in cardiac development. Expression of NS and LS Shp2-variants led to similar cardiac defects in zebrafish that were associated with impaired L/R asymmetry, resulting from impaired cilia function in KV. Treatment with a MEK inhibitor prior to gastrulation rescued cilia function, L/R asymmetry and heart displacement, suggesting a causal relation with enhanced MAPK signaling. No studies to date have examined the effect of NS and LS Shp2-variants on L/R asymmetry. Our paper opens a new prospective to understand how pathogenic SHP2 and downstream MAPK activation relates to cardiac development through its effects on L/R asymmetry.

Materials and Methods

Fish line

Zebrafish were maintained and the embryos were staged as previously described [58]. The *tg(myl7:GFP)* line was previously described [59]. All procedures involving experimental animals were approved by the local animal experiments committee and performed in compliance with local animal welfare laws, guidelines and policies, according to national and European law.

Constructs, RNA and injections.

The eGFP-peptide 2A-Shp2 construct was derived by PCR. 5′ capped sense mRNAs were synthesized using the mMessage mMachine kit (Ambion) and linearized plasmid DNA. mRNA injections were performed at the one-cell stage as described [60] using optimized amounts of mRNA (D61G=150pg, A465T=50pg, T73I=80pg G465A=100pg, WT-Shp2=150pg).

Immunoblotting

Zebrafish embryos (10hpf) were lysed in buffer containing 50 mM Tris, pH 7.5, 150 mM NaCl, 1 mM EDTA, 1 mM sodium orthovanadate, 1% Nonidet P-40, 0.1% sodium deoxycholate, protease inhibitor mixture (Complete Mini, Roche Diagnostics) and vanadate. Samples were run on SDS-PAGE gel (10%), transferred to PVDF membrane and stained with Coomassie Blue to verify equal loading. The blots were probed with antibodies specific for SHP2, Actin, pERK, ERK, pAKT, AKT (all Cell Signaling) and GFP (Torrey Pines). Detection was done using enhanced chemiluminescence (Thermo Scientific kit).

In situ Hybridization and Immunofluorescence Microscopy

In situ hybridizations were done essentially as described [61] using probes specific for, *myl7* [37], *vmhc* [62], *amhc* [63], *has2* [64], *lefty-2* [65], *southpaw* [41], *fabp*, *shh* [42].
For zebrafish immunohistochemistry, embryos were fixed in 4% DENT'S solution at 4°C, and subsequently blocked for 1 hour in PBS containing 5% lamb serum, 1% BSA, 1% DMSO, and 0.1% Triton-X. Embryos were incubated in mouse anti-acetylated Tubulin (1:500, Sigma) for 3 hours at RT. After extensive washing, embryos were incubated in goat anti-mouse Alexa Fluor 488. Embryos were flat-mounted in glycerol. Images were acquired using an SPE laser scanning confocal microscope. Confocal z-series images were assembled to present the sum of the focal planes; cilia length, cilia number and KV lumen area were manually measured using Image J software (http://rsb.info.nih.gov/ij/).

Pharmacological inhibition of MAPK signaling

To test the prevention of the NS/LS Shp2 mRNA phenotype, embryos injected with NS/LS Shp2 mRNA were incubated with 0,25 µM CI-1040 at 4.5 hpf or 10 hpf for 1 hour at 28.5°C in the dark.

Time-Lapse Imaging and Analysis

Embryos at the 22-somite stage were dechorionated and mounted in glass-bottom 6-well plates using 0.25% agarose in E3 embryo medium containing 16 mg/ml 3-amino benzoic acid ethylester to block contractile movements. Confocal imaging was performed using a spinning disc confocal laser scanning microscope with 20x magnification, acquiring stacks every 5 min. Embryos were kept at 28.5°C during recordings. ImageJ software (http://rsb.info.nih.gov/ij/) was used to generate time-lapse movies and for cell counting. Cell tracking was done using Volocity software (Improvision) followed by manual inspection of individual tracks generating quantification of

total speed (track length/time). Rotation was calculated by measuring the angle with the LR axis of four imaginary lines connecting four individual cells at the start and the end of the time-lapse (200 min). All statistical analyses were performed in Excel (Microsoft) using the two-tailed student's T-test.

KV fluid flow and cilia motility

Fluorescent beads (Polysciences) were injected into KV to visualize flow as described [50]. Bead flow was imaged at the 8- to 10-somite stage (SS) on a Leica AF7000 microscope (Leica Microsystems GmbH, Wetzlar, Germany) using a 63× water dipping objective and an Hamamatsu C9300-221 high speed CCD camera (Hamamatsu Photonics, Hamamatsu City, Japan) at 80 fps to record a 10 sec movie. Movies were generated using ImageJ software. Bead tracking was done using Volocity software (Improvision). For each embryo, four to five beads were tracked for a minimum of 50 frames of the movie and the average bead velocity was calculated.

High-speed imaging and analysis

2 dpf embryos were mounted in 0.25% agarose prepared in E3 medium embryonic medium with 16 mg/ml 3-amino benzoic acid ethylester. Embryonic hearts were imaged with a Hamamatsu C9300-221 high speed CCD camera (Hamamatsu Photonics, Hamamatsu City, Japan) at 150 fps mounted on a Leica AF7000 microscope (Leica Microsystems GmbH, Wetzlar, Germany) in a controlled temperature chamber (28.5°C) using Hokawo 2.1 imaging software (Hamamatsu Photonics GmbH, Herrsching am Ammersee, Germany). Image analysis was carried out with ImageJ (http://rsbweb.nih.gov/ij/). Statistical analysis and drawing of the box-whisker plot were carried out in Excel 2007 (Microsoft, Redmond, WA, USA).

Statistics

Cilia measurements were analyzed using the two-tailed student's t-test. Averages for controls and experimental were compared within each clutch of embryos. Results were considered significant when $p<0.05$ and results are expressed as mean ± standard error of the mean (p values * $p<0.05$, ** $p<0.01$, *** $p<0.001$).

Acknowledgements

This work was funded, in part, by a grant from the Research Council for Earth and Life Sciences (ALW 819.02.021) with financial aid from the Netherlands Organisation for Scientific Research (NWO) (to J.d.H.).

Author contributions

JdH conceived the project; MB and JdH designed the approach with help from FT, EN and JB; MB, JPO, FT and EN performed experiments; MB and JdH prepared the manuscript, which was edited by JPO, FT, EN and JB prior to submission.

References

1. Feng GS, Hui CC, Pawson T (1993) SH2-containing phosphotyrosine phosphatase as a target of protein-tyrosine kinases. Science 259: 1607-1611.
2. Freeman RM, Jr., Plutzky J, Neel BG (1992) Identification of a human src homology 2-containing protein-tyrosine-phosphatase: a putative homolog of Drosophila corkscrew. Proc Natl Acad Sci U S A 89: 11239-11243.
3. Chan RJ, Feng GS (2007) PTPN11 is the first identified proto-oncogene that encodes a tyrosine phosphatase. Blood 109: 862-867.
4. Tidyman WE, Rauen KA (2009) The RASopathies: developmental syndromes of Ras/MAPK pathway dysregulation. Curr Opin Genet Dev 19: 230-236.
5. Neel BG, Gu H, Pao L (2003) The 'Shp'ing news: SH2 domain-containing tyrosine phosphatases in cell signaling. Trends Biochem Sci 28: 284-293.
6. Feng GS (1999) Shp-2 tyrosine phosphatase: signaling one cell or many. Exp Cell Res 253: 47-54.
7. Van Vactor D, O'Reilly AM, Neel BG (1998) Genetic analysis of protein tyrosine phosphatases. Curr Opin Genet Dev 8: 112-126.
8. Neel BG, Tonks NK (1997) Protein tyrosine phosphatases in signal transduction. Curr Opin Cell Biol 9: 193-204.
9. Huyer G, Alexander DR (1999) Immune signalling: SHP-2 docks at multiple ports. Curr Biol 9: R129-132.
10. Qu CK (2000) The SHP-2 tyrosine phosphatase: signaling mechanisms and biological functions. Cell Res 10: 279-288.
11. Tartaglia M, Mehler EL, Goldberg R, Zampino G, Brunner HG, et al. (2001) Mutations in PTPN11, encoding the protein tyrosine phosphatase SHP-2, cause Noonan syndrome. Nat Genet 29: 465-468.
12. Digilio MC, Conti E, Sarkozy A, Mingarelli R, Dottorini T, et al. (2002) Grouping of multiple-lentigines/ LEOPARD and Noonan syndromes on the PTPN11 gene. Am J Hum Genet 71: 389-394.
13. Mendez HM, Opitz JM (1985) Noonan syndrome: a review. Am J Med Genet 21: 493-506.
14. Legius E, Schrander-Stumpel C, Schollen E, Pulles-Heintzberger C, Gewillig M, et al. (2002) PTPN11 mutations in LEOPARD syndrome. J Med Genet 39: 571-574.
15. Sarkozy A, Digilio MC, Dallapiccola B (2008) Leopard syndrome. Orphanet J Rare Dis 3: 13.
16. Allanson JE, Roberts AE (1993) Noonan Syndrome. In: Pagon RA, Adam MP, Bird TD, Dolan CR, Fong CT et al., editors. GeneReviews. Seattle (WA).
17. Keilhack H, David FS, McGregor M, Cantley LC, Neel BG (2005) Diverse biochemical properties of Shp2 mutants. Implications for disease phenotypes. J Biol Chem 280: 30984-30993.
18. Kontaridis MI, Swanson KD, David FS, Barford D, Neel BG (2006) PTPN11 (Shp2) mutations in LEOPARD syndrome have dominant negative, not activating, effects. J Biol Chem 281: 6785-6792.
19. Hof P, Pluskey S, Dhe-Paganon S, Eck MJ, Shoelson SE (1998) Crystal structure of the tyrosine phosphatase SHP-2. Cell 92: 441-450.
20. Nakamura T, Gulick J, Pratt R, Robbins J (2009) Noonan syndrome is associated with enhanced pERK activity, the repression of which can prevent craniofacial malformations. Proc Natl Acad Sci U S A 106: 15436-15441.
21. Hanna N, Montagner A, Lee WH, Miteva M, Vidal M, et al. (2006) Reduced phosphatase activity of SHP-2 in LEOPARD syndrome: consequences for PI3K binding on Gab1. FEBS Lett 580: 2477-2482.
22. Yu ZH, Xu J, Walls CD, Chen L, Zhang S, et al. (2013) Structural and mechanistic insights into LEOPARD syndrome-associated SHP2 mutations. J Biol Chem 288: 10472-10482.
23. Stewart RA, Sanda T, Widlund HR, Zhu S, Swanson KD, et al. (2010) Phosphatase-dependent and -independent functions of Shp2 in neural crest cells underlie LEOPARD syndrome pathogenesis. Dev Cell 18: 750-762.
24. Edouard T, Combier JP, Nedelec A, Bel-Vialar S, Metrich M, et al. (2010) Functional effects of PTPN11 (SHP2) mutations causing LEOPARD syndrome on epidermal growth factor-induced phosphoinositide 3-kinase/AKT/ glycogen synthase kinase 3beta signaling. Mol Cell Biol 30: 2498-2507.
25. Oishi K, Gaengel K, Krishnamoorthy S, Kamiya K, Kim IK, et al. (2006) Transgenic Drosophila models of Noonan syndrome causing PTPN11 gain-of-function mutations. Hum Mol Genet 15: 543-553.
26. Oishi K, Zhang H, Gault WJ, Wang CJ, Tan CC, et al. (2009) Phosphatase-defective LEOPARD syndrome mutations in PTPN11 gene have gain-of-function effects during Drosophila development. Hum Mol Genet 18: 193-201.
27. De Rocca Serra-Nedelec A, Edouard T, Treguer K, Tajan M, Araki T, et al. (2012) Noonan syndrome-causing SHP2 mutants inhibit insulin-like growth factor 1 release via growth hormone-induced ERK hyperactivation, which contributes to short stature. Proc Natl Acad Sci U S A 109: 4257-4262.
28. Yang W, Klaman LD, Chen B, Araki T, Harada H, et al. (2006) An Shp2/SFK/Ras/Erk signaling pathway controls trophoblast stem cell survival. Dev Cell 10: 317-327.
29. Tang TL, Freeman RM, Jr., O'Reilly AM, Neel BG, Sokol SY (1995) The SH2-containing protein-tyrosine phosphatase SH-PTP2 is required upstream of MAP kinase for early Xenopus development. Cell 80: 473-483.
30. Araki T, Mohi MG, Ismat FA, Bronson RT, Williams IR, et al. (2004) Mouse model of Noonan syndrome reveals cell type- and gene dosage-dependent effects of Ptpn11 mutation. Nat Med 10: 849-857.
31. Marin TM, Keith K, Davies B, Conner DA, Guha P, et al. (2011) Rapamycin reverses hypertrophic cardiomyopathy in a mouse model of LEOPARD syndrome-associated PTPN11 mutation. J Clin Invest 121: 1026-1043.
32. Jopling C, van Geemen D, den Hertog J (2007) Shp2 knockdown and Noonan/LEOPARD mutant Shp2-induced

gastrulation defects. PLoS Genet 3: e225.
33. Bakkers J (2011) Zebrafish as a model to study cardiac development and human cardiac disease. Cardiovasc Res 91: 279-288.
34. Lien CL, Harrison MR, Tuan TL, Starnes VA (2012) Heart repair and regeneration: recent insights from zebrafish studies. Wound Repair Regen 20: 638-646.
35. Kim JH, Lee SR, Li LH, Park HJ, Park JH, et al. (2011) High cleavage efficiency of a 2A peptide derived from porcine teschovirus-1 in human cell lines, zebrafish and mice. PLoS One 6: e18556.
36. Tessadori F, van Weerd JH, Burkhard SB, Verkerk AO, de Pater E, et al. (2012) Identification and functional characterization of cardiac pacemaker cells in zebrafish. PLoS One 7: e47644.
37. Yelon D, Horne SA, Stainier DY (1999) Restricted expression of cardiac myosin genes reveals regulated aspects of heart tube assembly in zebrafish. Dev Biol 214: 23-37.
38. Ramsdell AF (2005) Left-right asymmetry and congenital cardiac defects: getting to the heart of the matter in vertebrate left-right axis determination. Dev Biol 288: 1-20.
39. Smith KA, Chocron S, von der Hardt S, de Pater E, Soufan A, et al. (2008) Rotation and asymmetric development of the zebrafish heart requires directed migration of cardiac progenitor cells. Dev Cell 14: 287-297.
40. de Campos-Baptista MI, Holtzman NG, Yelon D, Schier AF (2008) Nodal signaling promotes the speed and directional movement of cardiomyocytes in zebrafish. Dev Dyn 237: 3624-3633.
41. Long S, Ahmad N, Rebagliati M (2003) The zebrafish nodal-related gene southpaw is required for visceral and diencephalic left-right asymmetry. Development 130: 2303-2316.
42. Krauss S, Concordet JP, Ingham PW (1993) A functionally conserved homolog of the Drosophila segment polarity gene hh is expressed in tissues with polarizing activity in zebrafish embryos. Cell 75: 1431-1444.
43. Neugebauer JM, Amack JD, Peterson AG, Bisgrove BW, Yost HJ (2009) FGF signalling during embryo development regulates cilia length in diverse epithelia. Nature 458: 651-654.
44. Liu DW, Hsu CH, Tsai SM, Hsiao CD, Wang WP (2011) A variant of fibroblast growth factor receptor 2 (Fgfr2) regulates left-right asymmetry in zebrafish. PLoS One 6: e21793.
45. Runtuwene V, van Eekelen M, Overvoorde J, Rehmann H, Yntema HG, et al. (2011) Noonan syndrome gain-of-function mutations in NRAS cause zebrafish gastrulation defects. Dis Model Mech 4: 393-399.
46. Anastasaki C, Estep AL, Marais R, Rauen KA, Patton EE (2009) Kinase-activating and kinase-impaired cardio-facio-cutaneous syndrome alleles have activity during zebrafish development and are sensitive to small molecule inhibitors. Hum Mol Genet 18: 2543-2554.
47. Langdon Y, Tandon P, Paden E, Duddy J, Taylor JM, et al. (2012) SHP-2 acts via ROCK to regulate the cardiac actin cytoskeleton. Development 139: 948-957.
48. Mercola M, Levin M (2001) Left-right asymmetry determination in vertebrates. Annu Rev Cell Dev Biol 17: 779-805.
49. Nonaka S, Tanaka Y, Okada Y, Takeda S, Harada A, et al. (1998) Randomization of left-right asymmetry due to loss of nodal cilia generating leftward flow of extraembryonic fluid in mice lacking KIF3B motor protein. Cell 95: 829-837.
50. Essner JJ, Amack JD, Nyholm MK, Harris EB, Yost HJ (2005) Kupffer's vesicle is a ciliated organ of asymmetry in the zebrafish embryo that initiates left-right development of the brain, heart and gut. Development 132: 1247-1260.
51. Ferrante MI, Romio L, Castro S, Collins JE, Goulding DA, et al. (2009) Convergent extension movements and ciliary function are mediated by ofd1, a zebrafish orthologue of the human oral-facial-digital type 1 syndrome gene. Hum Mol Genet 18: 289-303.
52. Oteiza P, Koppen M, Concha ML, Heisenberg CP (2008) Origin and shaping of the laterality organ in zebrafish. Development 135: 2807-2813.
53. Oteiza P, Koppen M, Krieg M, Pulgar E, Farias C, et al. (2010) Planar cell polarity signalling regulates cell adhesion properties in progenitors of the zebrafish laterality organ. Development 137: 3459-3468.
54. Alexander J, Rothenberg M, Henry GL, Stainier DY (1999) casanova plays an early and essential role in endoderm formation in zebrafish. Dev Biol 215: 343-357.
55. Carvajal-Vergara X, Sevilla A, D'Souza SL, Ang YS, Schaniel C, et al. (2010) Patient-specific induced pluripotent stem-cell-derived models of LEOPARD syndrome. Nature 465: 808-812.
56. Schramm C, Fine DM, Edwards MA, Reeb AN, Krenz M (2012) The PTPN11 loss-of-function mutation Q510E-Shp2 causes hypertrophic cardiomyopathy by dysregulating mTOR signaling. Am J Physiol Heart Circ Physiol 302: H231-243.
57. Ishida H, Kogaki S, Narita J, Ichimori H, Nawa N, et al. (2011) LEOPARD-type SHP2 mutant Gln510Glu attenuates cardiomyocyte differentiation and promotes cardiac hypertrophy via dysregulation of Akt/GSK-3beta/beta-catenin signaling. Am J Physiol Heart Circ Physiol 301: H1531-1539.
58. Kimmel CB, Ballard WW, Kimmel SR, Ullmann B, Schilling TF (1995) Stages of embryonic development of the zebrafish. Dev Dyn 203: 253-310.
59. Chocron S, Verhoeven MC, Rentzsch F, Hammerschmidt M, Bakkers J (2007) Zebrafish Bmp4 regulates left-right asymmetry at two distinct developmental time points. Dev Biol 305: 577-588.
60. Hyatt TM, Ekker SC (1999) Vectors and techniques for ectopic gene expression in zebrafish. Methods Cell Biol 59: 117-126.
61. Thisse C, Thisse B, Schilling TF, Postlethwait JH (1993) Structure of the zebrafish snail1 gene and its expression in

wild-type, spadetail and no tail mutant embryos. Development 119: 1203-1215.
62. Yelon D (2001) Cardiac patterning and morphogenesis in zebrafish. Dev Dyn 222: 552-563.
63. Smith KA, Joziasse IC, Chocron S, van Dinther M, Guryev V, et al. (2009) Dominant-negative ALK2 allele associates with congenital heart defects. Circulation 119: 3062-3069.
64. Bakkers J, Kramer C, Pothof J, Quaedvlieg NE, Spaink HP, et al. (2004) Has2 is required upstream of Rac1 to govern dorsal migration of lateral cells during zebrafish gastrulation. Development 131: 525-537.
65. Bisgrove BW, Essner JJ, Yost HJ (1999) Regulation of midline development by antagonism of lefty and nodal signaling. Development 126: 3253-3262.

Supplemental data

eGFP- peptide 2A- Shp2 fusions allow monitoring of expression of (mutant) Shp2.

In order to monitor injection efficiency, we fused an eGFP-peptide 2A sequence to the NH2-terminus of Shp2. The peptide 2A sequence in the fusion protein is cleaved autoproteolytically [35], producing eGFP and (mutant) Shp2 (Figure S1A), which was confirmed by immunoblotting (Figure S1B). Moreover, eGFP was readily visualized in the injected embryos at 48 hpf (Figure S1C,D). Injection of wild type Shp2 was used as a control and throughout this study Shp2-D61G was used as prototypical NS-variant and Shp2-A462T as LS-variant. Some of the experiments were done with additional variants with similar results. Morphological analysis of the embryos at 48 hpf indicated that injections of the GFP-peptide 2A-Shp2 fusions phenocopied the previously published phenotypes of NS-Shp2 and LS-Shp2, including short stature, craniofacial defects and cardiac defects [32]. (Figure S1C-D). Therefore, we used the GFP-peptide 2A-Shp2 fusions, monitored GFP expression and selected efficiently injected embryos for further analysis unless indicated otherwise.

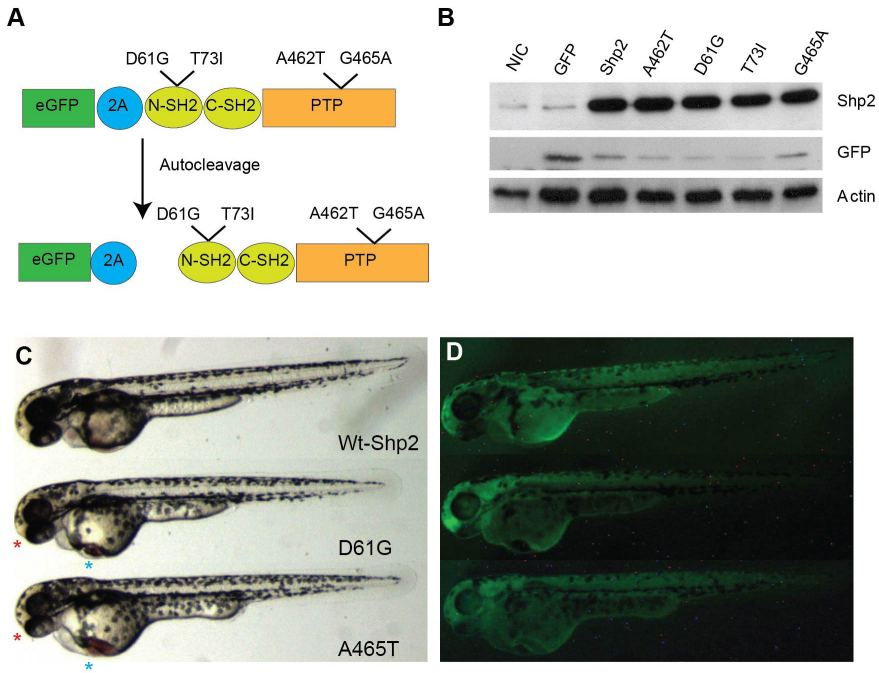

Supplemental Figure S1. EGFP-Peptide 2A-Shp2 fusions induced defects in zebrafish embryos. (A) Schematic representation of eGFP-Peptide 2A-Shp2 with D61G, T73I (NS) and A462T, G465A (LS) mutations indicated. The full length fusion protein is produced and is then cleaved autoproteolytically, resulting in eGFP and (mutant) Shp2. (B) One- or two-cell stage embryos were injected with in vitro transcribed mRNAs encoding the indicated proteins. Immunoblotting analysis reveals that autoproteolytic cleavage of the fusion proteins is highly efficient in zebrafish embryos. The injected embryos were lyzed at 10 hpf, proteins were separated on SDS-polyacrylamide gels, blotted and probed with antibodies specific for Shp2, GFP and β-actin as a loading control. (C-D) Two representative injected embryos (D61G and A462T) show craniofacial defects (red asterisks), a decrease in body length and cardiac edema (blue asterisks). These defects are absent in WT-Shp2 injected control embryos. Injection efficiency was checked by fluorescence microscopy with a GFP filter.

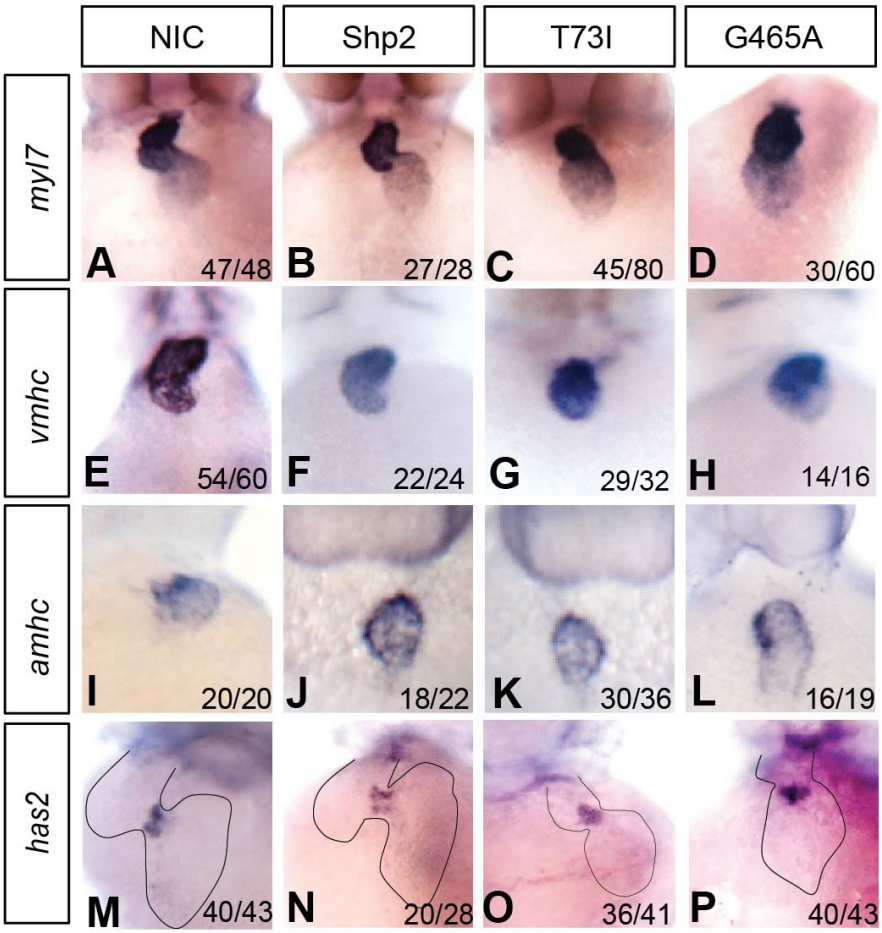

Supplemental Figure S2. Heart looping defects in embryos expressing Shp2-T73I (NS) and Shp2-G465A (LS). Non-injected control embryos (NIC) and embryos injected at the one-cell stage with mRNA encoding WT-Shp2, Shp2-T73I (NS) or Shp2-G465A (LS) were fixed at 48 hpf and *in situ* hybridization was performed using probes for the myosin genes *myl7* (A-D, cardiomyocytes), *vmhc* (E-H, ventricle), *amhc* (I-L, atrium), and for *has2* (M-P, endocardial cushions). Representative pictures are shown and the number of embryos showing this pattern as well as the total number of embryos that were analyzed is indicated in the bottom right corner of each panel. The outline of the heart is indicated with a dashed line in panels M-P.

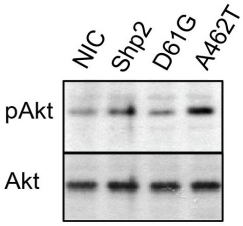

Supplemental Figure S3. Enhanced Akt signaling in Shp2-A462T (LS), but not Shp2-D61G (NS) expressing embryos. Zebrafish embryos were injected with WT-Shp2, Shp2-D61G (NS) or Shp2-A462T (LS) at the one-cell stage. Embryos were lysed at 10 hpf. Immunoblots of the zebrafish lysates were stained using antibodies specific for pAkt and Akt.

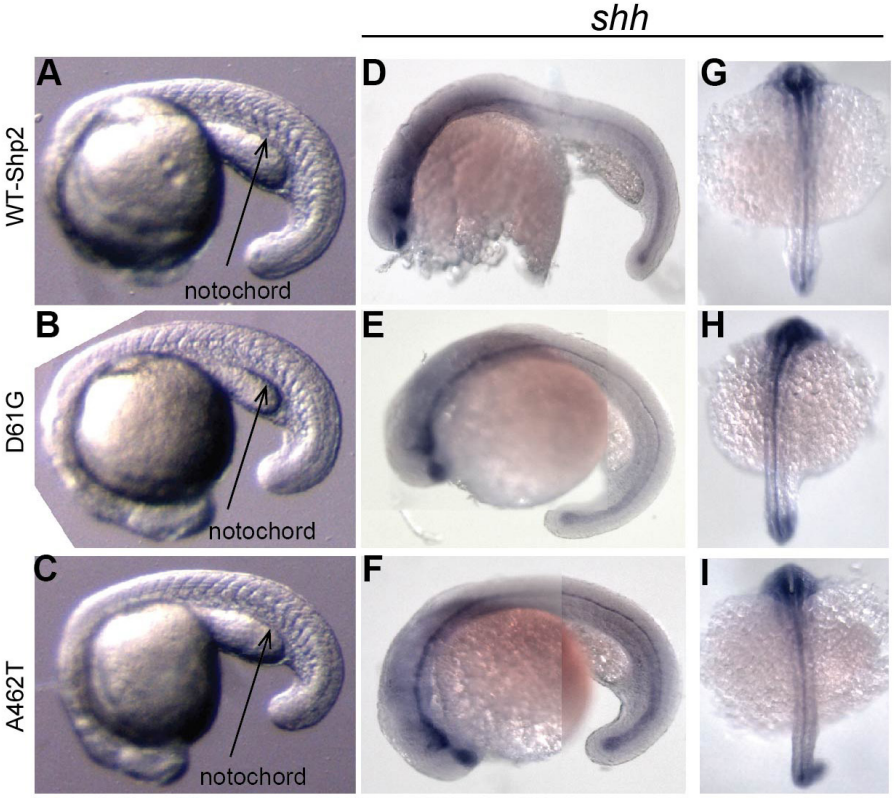

Supplemental Figure S4. Midline structures are intact in NS and LS Shp2-variants. Bright-field images of WT-Shp2 control (A) D61G (B) and A462T (C) embryos, showing normal notochord formation. (D-I) *In situ* hybridization analysis showed contiguous *shh* expression in the floorplate. The total number of embryos analyzed is: WT-Shp2, n=20/20; Shp2-D61G, n=30/30; Shp2-A462T, n=30/30.

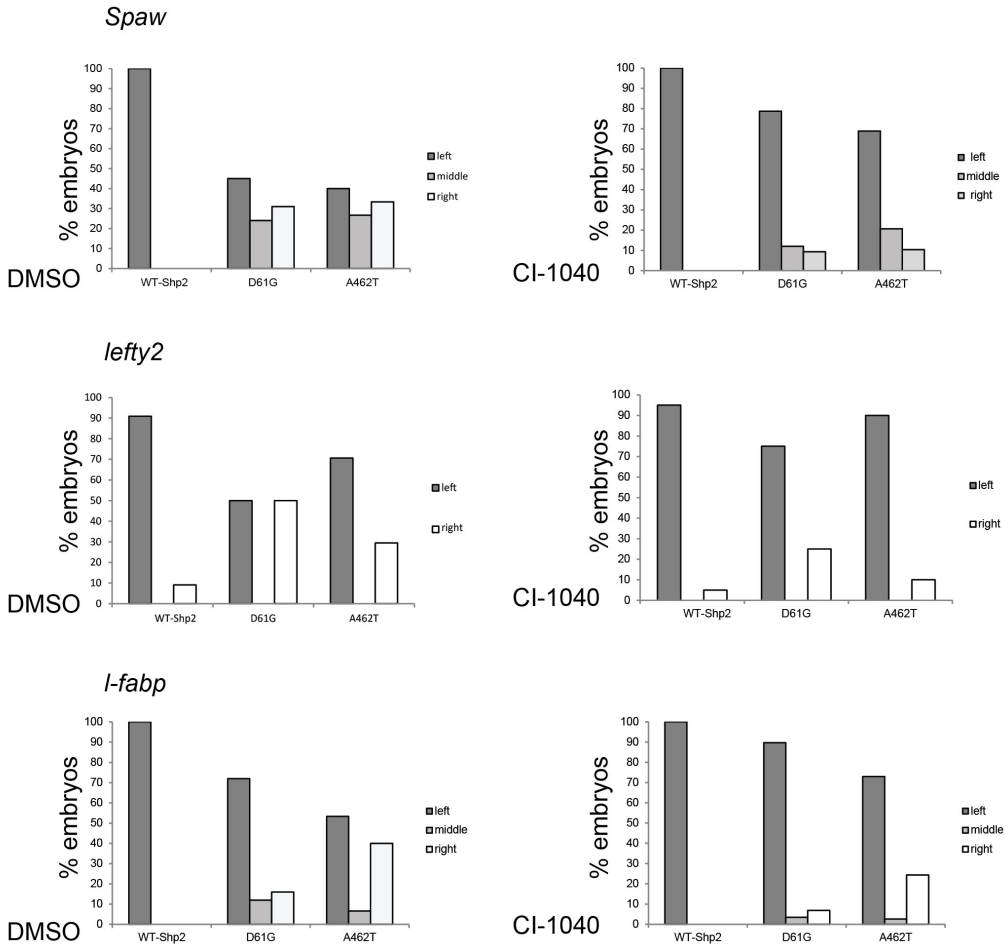

Supplemental Figure S5. Early treatment with the MEK-inhibitor, CI-1040, rescued L/R asymmetry in embryos expressing NS and LS Shp2-variants. Embryos were injected at the one-cell stage with mRNA encoding WT-Shp2 (Shp2), Shp2-D61G (NS) or Shp2-A462T (LS). Embryos were treated with MEK inhibitor CI-1040 (0.25 μM) for 1 h at 4.5 hpf or mock-treated with DMSO and fixed at the stage indicated in the panel. *In situ* hybridization was done using probes specific for *spaw* (A-B, *southpaw*), *lft2* (C-D, *lefty2*), and *fabp* (E-F, fatty acid binding protein, marking the liver). Markers asymmetry was scored for embryos injected with WT-Shp2, Shp2-D61G and Shp2-A462T. Percentages of left, middle/bilateral and right expression of the markers are depicted. The total number of embryos analyzed is: *spaw* (WT-Shp2 n=40, Shp2-D61G n=50, Shp2-A462T n=35); *lft2* (WT-Shp2 n=50, Shp2-D61G n=42, Shp2-A462T n=34) and *fabp* (WT-Shp2 n=26, Shp2-D61G n=28, Shp2-A462T n=35).

Heterozygous germline mutations in A2ML1 are associated with a disorder clinically related to Noonan syndrome

Lisenka E.L.M.Vissers[1,2,3,11,] Monica Bonetti[4,11], Jeroen Paardekooper Overman[4,11], Willy M. Nillesen[1], Suzanna G.M. Frints[5], Joep de Ligt[1,2,3], Giuseppe Zampino[6], Ana Justino[7], José C.Machado[7], Marga Schepens[1], Han G. Brunner[1,2,3], Joris A. Veltman[1,2,3], Hans Scheffer[1], Piet Gros[8], José L. Costa[7], Marco Tartaglia[9], Ineke van der Burgt[1,12], Helger G Yntema[1,2,12,*], and Jeroen den Hertog[4,10,12]

1Department of Human Genetics, Radboud university medical center, Nijmegen, The Netherlands; 2Radboud Institute for Molecular Life Sciences, Radboud university medical center, Nijmegen, The Netherlands; 3Donders Centre for Neuroscience, Radboud university medical center, Nijmegen, The Netherlands; 4Hubrecht Institute-KNAW and University Medical Center, Utrecht, The Netherlands; 5Department of Clinical Genetics, Maastricht University Medical Centre, Maastricht, The Netherlands; 6Dipartimento di Pediatria, Università Cattolica del Sacro Cuore, Rome, Italy; 7IPATIMUP - Institute of Molecular Pathology and Immunology of the University of Porto, Porto, Portugal; 8Crystal and Structural Chemistry, Bijvoet Center for Biomolecular Research, Department of Chemistry, Faculty of Science, Utrecht University, Utrecht, the Netherlands; 9Dipartimento di Ematologia, Oncologia e Medicina Molecolare, Istituto Superiore di Sanità, Rome, Italy; 10Institute of Biology, Leiden, The Netherlands; 11These authors contributed equally to this work; 12These authors jointly directed this work

European Journal of Human Genetics, 2014 Jun 18

Abstract

Noonan syndrome (NS) is a developmental disorder characterized by short stature, facial dysmorphisms and congenital heart defects. To date, all mutations known to cause NS are dominant, activating mutations in signal transducers of the RAS/MAPK pathway. In 25% of cases, however, the genetic cause of NS remains elusive, suggesting that factors other than those involved in the canonical RAS/MAPK pathway may also play a role. Here, we used family-based whole exome sequencing of a case-parent trio and identified a *de novo* mutation, p.(Arg802His), in *A2ML1* which encodes the secreted protease inhibitor Alpha-2-Macroglobulin-Like-1. Subsequent resequencing of *A2ML1* in 155 cases with a clinical diagnosis of NS led to the identification of additional mutations in two families, p.(Arg802Leu) and p.(Arg592Leu). Functional characterization of these human *A2ML1* mutations in zebrafish showed NS-like developmental defects, including a broad head, blunted face and cardiac malformations. Using the crystal structure of A2M, which is highly homologous to A2ML1, we identified the intramolecular interaction partner of p.Arg802. Mutation of this residue, p.Glu906, induced similar developmental defects in zebrafish, strengthening our conclusion that mutations in *A2ML1* cause a disorder clinically related to NS. This is the first report of the involvement of an extracellular factor in a disorder clinically related to RASopathies, providing potential new leads for better understanding of the molecular basis of this family of developmental diseases.

Introduction

Noonan syndrome (NS) is an autosomal dominant, clinically variable condition, with an estimated prevalence of 1 in 1,000-2,500.[1] NS patients are characterized by facial dysmorphism, a wide spectrum of cardiac disease, reduced postnatal growth, variable cognitive deficits, ectodermal and skeletal defects.[2-4] Congenital heart defects are observed in a large proportion of NS patients, in particular pulmonary stenosis (66%), and hypertrophic cardiomyopathy (14%).[5] Other relatively frequent clinical features of NS patients include webbed neck, cryptorchidism, bleeding tendency, and hydrops fetalis. NS is genetically heterogeneous and mutations in *PTPN11, SOS1*, *KRAS*, *NRAS*, *RAF1*, *BRAF*, *SHOC2*, *CBL* and *RIT1* account for approximately 75% of affected individuals.[4,6] To date, all mutations causing NS result in enhanced activation of signal transducers belonging to the RAS-mitogen activated protein kinase (MAPK) pathway.[7]

To identify new genetic causes of NS, we used a family-based whole-exome-sequencing approach in a patient-parent trio with sporadic disease to detect *de novo* changes in the proband. Genetic testing had previously excluded mutations in known NS genes. We identified a *de novo* mutation in *A2ML1*, which encodes the secreted protease inhibitor Alpha-2-Macroglobulin-Like-1 (A2ML1). *A2ML1* was re-sequenced in a cohort of cases with a clinical diagnosis of NS. Moreover, to provide more evidence for the involvement of the gene in this disorder resembling NS, protein modeling was performed and A2ML1 mutants were functionally characterized in zebrafish.

Results

Exome sequencing in a NS case-parent trio

Exome sequencing in case 1 (Figure 1A) and her parents revealed four potential *de novo* mutations, two of which were validated by Sanger sequencing and confirmed to be of *de novo* origin (Supplementary Table 1). The first mutation is predicted to lead to p.(Arg129Pro) in *OR12D3* (NM_030959.2:c.386G>C), encoding an olfactory receptor. Based on the function of the gene product (odor perception) combined with the low evolutionary conservation at base pair level (PhyloP 0.55), we do not consider this variant to be relevant for the phenotype of the patient, but assume that this *de novo* mutation reflects the human per-generation background mutation rate. [16] The second *de novo* mutation was detected in *A2ML1* (NM_144670.3:c.2405G>A) and is predicted to lead to p.(Arg802His). This *de novo* mutation occurred at a highly conserved nucleotide (PhyloP 3.41) and affects a residue within the alpha-2-macroglobulin domain (Figure 2A). It is noteworthy that the c.2405G>A variant in *A2ML1* is also reported in 4/12,194 alleles in the NHLBI Exome Sequencing Project (ESP) (http://evs.gs.washington.edu/EVS/). Further analysis of the ESP database indicated that several frequently reported causal mutations in known NS genes, including *PTPN11*, are described in this database at similar frequency (Table 2).

Mutation analysis of the A2ML1 gene in a NS cohort

Next, 155 individuals with a clinical diagnosis of NS were analyzed for mutations in *A2ML1* by direct Sanger sequencing and Ion PGM system. This screen led to the identification of two additional likely causal missense mutations in two unrelated individuals (Figure 1B-C, Table 2). The mutation identified in case 2, c.2405G>T, affects the same residue as identified in family 1 but is predicted to result in a different substitution, p.(Arg802Leu). Segregation analysis showed that the mutation is transmitted to his son (case 3), who is also diagnosed with the same disorder resembling NS. His mother (case 4), who does not show typical features of NS, also carries the

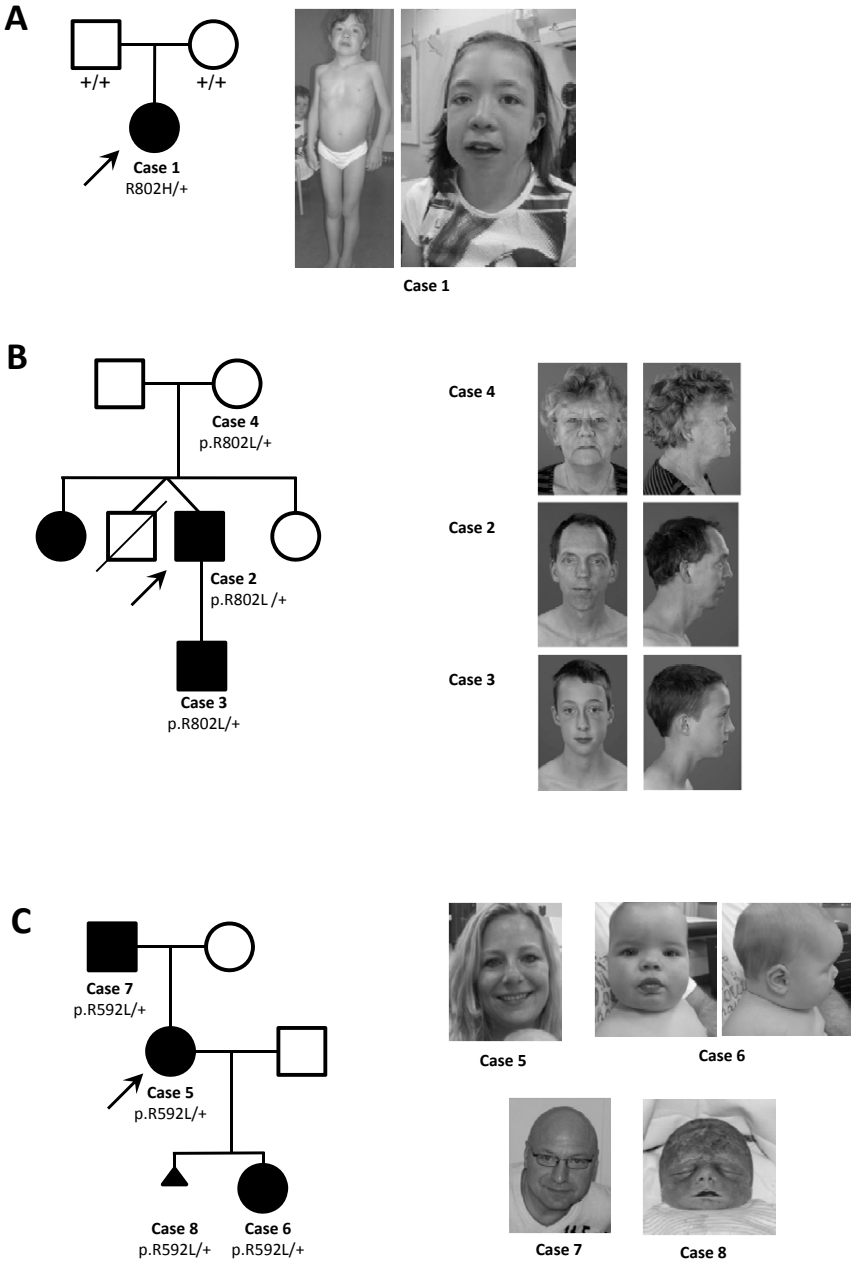

Figure 1. Photographs and pedigrees of families diagnosed with Noonan(-like) syndrome with likely pathogenic mutations in *A2ML1*. (A) Family 1 – case 1. *De novo* mutation p.(Arg802His); (B) Family 2 – cases 2, 3 and 4. Familial p.(Arg802Leu). The sister of case 2 is reported upon heteroanamnesis to have the same clinical phenotype. However, DNA nor detailed clinical information were available for this study. (C) Family 3 – cases 5, 6, 7 and 8. Familial p.(Arg592Leu). Clinical details of all cases are presented in Table 3. Note, the absence of genotypes for (un)affected family members indicates that DNA samples of these individuals were not available for testing. Black solid squares/circles represent clinically affected individuals, whereas as open squares/circles represent healthy individuals.

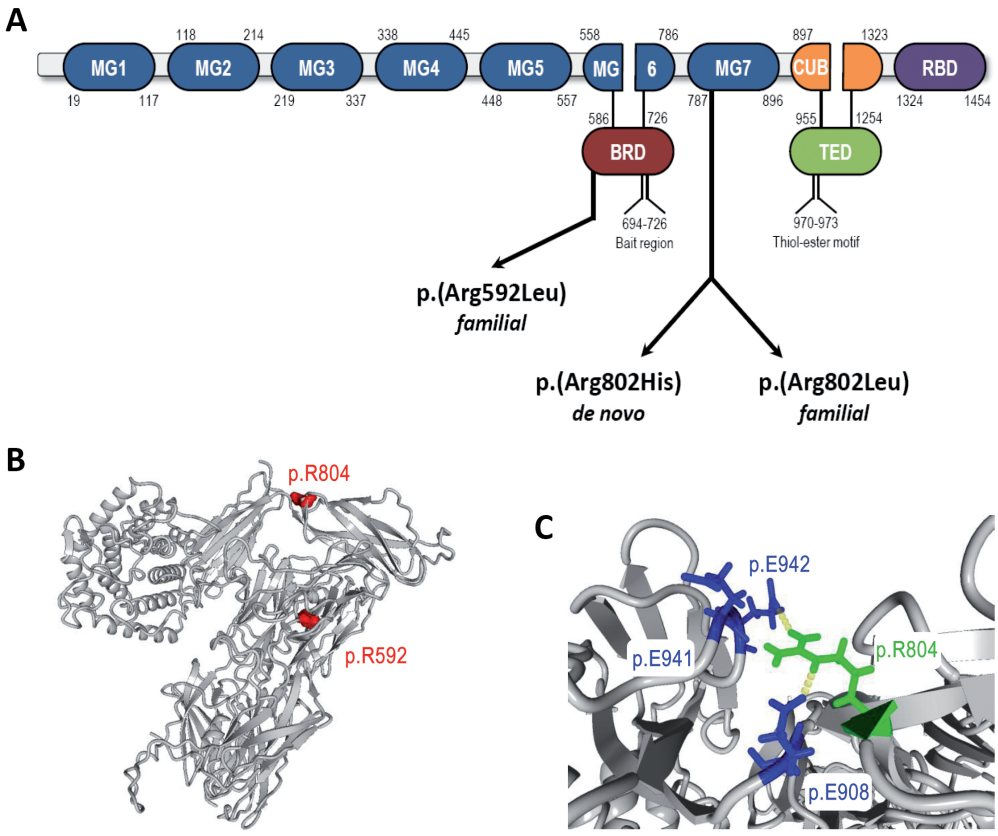

Figure 2. A2ML1 domain structure and modeling of the intramolecular interactions involving p.Arg802. (A) Schematic representation of A2ML1 protein domain structure and mutations in individuals with Noonan syndrome-like disorder. Numbers correspond to amino acid positions of A2ML1. MG: macroglobulin-like domain; BRD: bait region domain; CUB: complement C1r/C1s, Uegf, Bmp1 domain; TED: trioester domain; RBD: receptor binding domain. (B) Crystal structure of A2M (pdb code 4ACQ). Overall structure with p.Arg598 and p.Arg804 highlighted, corresponding to p.Arg592 and p.Arg802 in A2ML1, respectively. (C) Close-up of A2M-R804, corresponding to A2ML1-R802 (in green), which interacts with A2M-E908 (A2ML1-E906) (in blue) through hydrogen bonds (yellow dashed lines) and electrostatic interactions. A2M-E941 and A2M-E942 (in blue) may also interact with A2M-R802, but are not conserved in A2ML1 (p.P939 and p.D940, respectively).

mutation (Figure 1B). In the proband of family 3 (case 5), a c.1775G>T mutation (p.(Arg592Leu)) was detected. Familial segregation studies revealed the same mutation in her daughter (case 6) and her father (case 7), who were both clinically diagnosed with a disorder resembling NS (Figure 1C). Strikingly, the patient's first pregnancy resulted in intra-uterine fetal death at 29 weeks of gestation because of hydrops foetalis (case 8, Figure 1C). Pathological examination of the fetus showed facial features suggestive for NS. Molecular analysis of fetal DNA indicates maternal inheritance of the A2ML1 mutation p.(Arg592Leu). The clinical features of all individuals with an A2ML1 mutation are summarized in Table 3. A full description of the clinical data is provided in the supplement. Screening of selected exons of *A2ML1* in an additional cohort of 140 individuals with a clinical phenotype fitting or suggestive for NS did not reveal any pathogenic mutations. All variants detected are shown in Supplementary Table 2.

Protein modeling of mutations detected in A2ML1

All three *A2ML1* mutations, p.(Arg592Leu), p.(Arg802His) and p.(Arg802Leu), affect highly conserved residues among orthologs (Supplementary Figure 2). For protein modeling of the mutation locations and their predicted effect, the crystal structure of alpha-2-macroglobulin (A2M; pdb 4ACQ) was used (Figure 2, Table 1). A2ML1 is highly homologous to A2M and it is highly likely that protein folding of the two related proteins is similar (Supplementary Figure 1). Arginine 592, corresponding to A2M p.Arg598, is located at the edge of the Bait Region Domain and is buried in a large cavity on the back face of the A2ML1 monomer[17] whereas Arginine 802, corresponding to A2M p.Arg804, is located within macroglobulin-like domain 7 and is positioned more at the surface of the protein (Figure 2B). Mutations of either residue likely lead to conformational changes in A2ML1 by loss of hydrogen bonds or charge interactions. In more detail, within the intramolecular binding network, disease-associated mutations of p.Arg802 were predicted to disrupts the interaction with p.Glu906 (Figure 2C).

Functional consequences of A2ML1 mutations

A2ml1 is relative highly conserved in zebrafish (38% identity) and we investigated the functional consequences of expression of mutant A2ml1 on zebrafish development. *A2ml1* is predominantly expressed in the liver during embryonic development and morpholino-mediated knockdown of A2ml1 has previously been shown to induce defective liver development.[18] We introduced human A2ML1 mutations (p.R802H, p.R802L and p.S592L, human numbering for clarity, see Table 1) in zebrafish A2ml1, C-terminally fused with GFP, allowing to monitor (mutant) A2ml1 expression in tissue culture cells and during development (Supplementary Figure 3, 4).

Expression of most mutant NS-associated genes in tissue culture cells augments activation of the RAS/MAPK pathway, measurable by excessive ERK/MAPK phosphorylation in cycling cells. To investigate the effect of mutant A2ml1 on the RAS/MAPK pathway, we expressed mutant *A2ml1-gfp* fusion proteins in HEK-293T and COS7 cells to determine the levels of ERK/MAPK phosphorylation. Expression of *A2ml1* mutants in normally growing HEK-293T cells or in serum-stimulated COS7 cells did not significantly enhance ERK/MAPK phosphorylation (Supplementary Figure 3). These results suggest either that (mutant) A2ml1 does not modulate ERK/MAPK signaling, or that HEK-293T cells and COS7 cells are not responsive to (mutant) A2ml1. The effect of (mutant) A2ml1 on embryonic development was investigated by microinjection of CMV-promoter-driven expression vectors for wildtype or mutant A2ml1 in zebrafish embryos at the one-cell stage. Exogenous A2ml1-GFP was detected throughout the zebrafish embryo, despite mosaicism of the transgene, which is consistent with A2ml1-GFP being a secreted factor (Supplementary Figure 4).

Expression of mutant A2ml1 resulted in developmental defects in zebrafish embryos that involved the heart and craniofacial structures, whereas expression of GFP alone or wildtype A2ml1 did not affect zebrafish development (Figure 3). The morphological defects elicited by mutant A2ml1 resembled those induced by NS-associated Shp2-D61G and N-Ras-I24N.[12,19] Of note, A2ml1-mutation-induced morphological defects appeared later in development (apparent from 3dpf onwards) and were less severe than those observed for Shp2-D61G-induced defects (from 6hpf onwards). Alcian blue staining of cartilaginous structures in 4dpf zebrafish embryos revealed craniofacial defects that are characteristic of NS. Morphometric analysis showed statistically significant broadening of the head and blunting of the faces in embryos expressing mutant A2ml1 (Figure 3B). Also, *in situ* hybridization using the heart-specific probe *myl7* (formerly known as

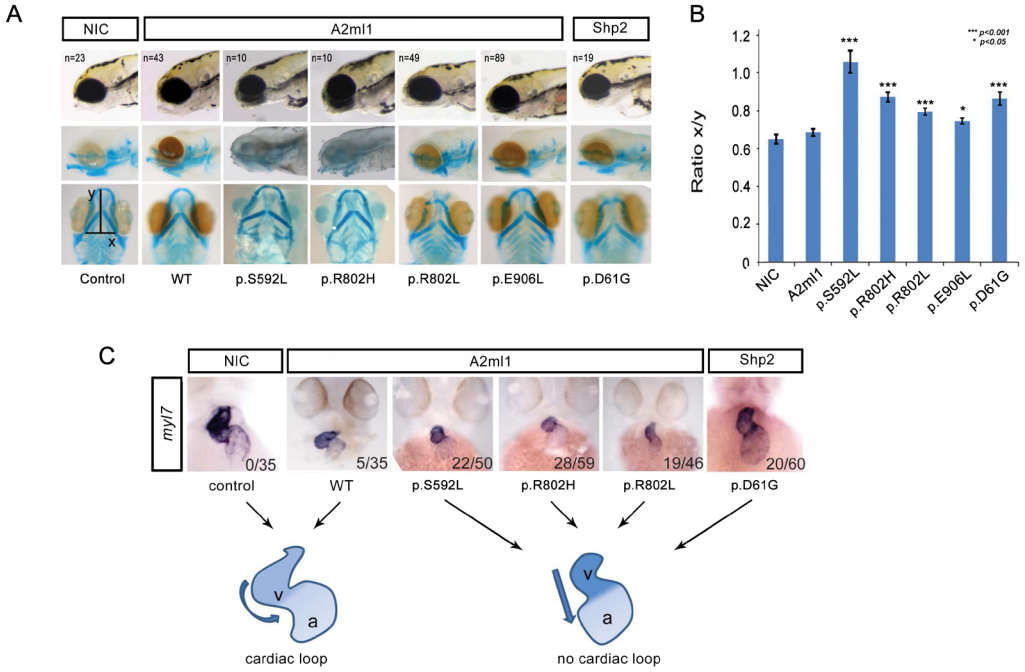

Figure 3. Mutant A2ml1 causes a developmental disorder resembling NS. (A) Expression of mutant A2ml1 results in developmental defects in zebrafish embryos at 4dpf. The craniofacial defects were highlighted by cartilage staining using alcian blue. The heads are broader and the faces blunted. 'n' refers to the number of embryos examined for x/y ratio. (B) To quantify the craniofacial defects, the ratio of the width of the ceratohyal and the distance to Meckel's cartilage (x and y, respectively in bottom left panel of A) was determined. The averages are plotted, error bars indicate standard error of the mean. Student t-test to compare ratios with non-injected control (NIC) indicate that wild type A2ml1 is not significantly different, but mutant A2ml1 and mutant Shp2 are significantly enhanced compared to NIC as indicated. Note that human numbering of residues was used for A2ml1 mutants. (C) *In situ* hybridization of 55hpf embryos using a heart-specific probe (*myl7*) which stains cardiomyocytes. Cardiac looping was assessed as normal looping (loop) or impaired looping (no loop) as indicated schematically. The number of no loop hearts in embryos expressing mutant A2ml1 or mutant Shp2 / total number of embryos is indicated in the bottom right corner of each panel.

cmlc2) indicated that cardiac looping was impaired in mutant *a2ml1*-injected embryos in a similar manner as in Shp2-D61G expressing embryos (Figure 3C). Protein modeling suggested that the p.(Arg802His) and p.(Arg802Leu) mutations would lead to a loss of the interaction between p. Arg802 and p.Glu906. Therefore, p.Glu906 was mutated to leucine and this mutant was expressed in zebrafish embryos to study the functional defect. Expression of mutant A2ml1-E906L induced developmental defects to a similar extent as NS-associated A2ml1-R802L mutants (Figure 3B), further supporting a causal role of A2ml1 mutations involving substitution of p.Arg802.

Discussion

Analysis of a case-parent trio with a clinical suspicion of NS revealed a *de novo* mutation in *A2ML1* (c.2405G>A; p.(Arg802His)). A2ML1 encodes the protease inhibitor A2ML1, which is a member of the alpha-macroglobulin superfamily of proteins that contains both complement components and protease inhibitors. These proteins display a unique trap mechanism of inhibition, by which the alpha-2-macroglobulin inhibitor undergoes a major conformational change upon its cleavage by a protease, thereby trapping the protease and blocking it from subsequent substrate binding.[20]

Moreover, A2ML1 binds to the lipoprotein receptor-related protein 1 (LRP1) receptor[21], an upstream activator of the MAPK/Extracellular signal-regulated kinase (ERK) cascade.[22] Additionally, LRP1 directly interacts with CBL.[23] Together, these reports suggest that A2ML1 may act upstream of signaling pathways known to be involved in NS.

Two additional missense mutations in families with a disorder clinically resembling NS were identified by Sanger sequencing of the entire coding region of the gene (c.2405G>T; p.(Arg802Leu), and c.1775G>T; (p.(Arg592Leu)). The frequency of *A2ML1* mutations in the cohort tested in this study is therefore approximately 1%. However, since mutations in the major NS genes had already been excluded, the contribution of A2ML1 mutations to the total population clinically diagnosed with NS is expected to be less than 0.5%. The fact that two of the three A2ML1 mutations have been reported in the EVS database with a frequency comparable to that in the NS patients, could either mean that the A2ML1 mutations are not pathogenic, or that the phenotypic features of people with an *A2ML1* mutation is milder and they are unrecognized in the general population (making *A2ML1* a relatively high frequency gene in mild NS). The fact that case 4 does not show phenotypic features of NS would fit both of these theories, since cases with non-penetrance, which albeit very rare, have previously been described in NS.[24] Evidence for the pathogenicity of the *A2ML1* mutations therefore had to be provided by functional studies.
Whereas most NS-associated mutations have an effect on RAS/MAPK signaling, we did not detect RAS/MAPK activation in response to expression of *A2ml1* mutations in HEK293T cells or COS7 cells. Cell type specific MAPK activation by NS-associated genes is not unprecedented; NS-associated mutant SHOC2 enhances stimulus-induced MAPK activation in Neuro2A cells, but not in Cos-1 or 293T cells.[25] Hence, our results do not exclude involvement of A2ML1 in NS, but either suggest that A2ML1 does not modulate ERK/MAPK signaling, or that COS7 and HEK-293T cells are irresponsive to A2ML1. Future studies of A2ML1 variants in cell systems expressing LRP1 receptor might shed more light on the role of A2ML1 in ERK/MAPK signaling.

Expression of mutant A2ml1 in zebrafish embryos resulted in developmental defects that were characterized by craniofacial and cardiac defects, resembling those induced by expression of mutant Shp2. The A2ml1-mutation-induced morphological defects appear however later in development (apparent from 3dpf onwards) and are less severe than those observed for Shp2-D61G-induced defects (from 6hpf onwards). In line with this notion, the affected individuals in families 2 and 3, who transmitted the *A2ML1* mutation to their offspring, do not fulfill all classical van der Burgt criteria for NS[3], but present with a less severe phenotype suggestive of the disorder. Of note, phenotypic variability is well known for NS, and more explicitly, not all patients with NS have a cardiac malformation.[5,26] Also, the affected individuals in the two families with an *A2ML1* mutation do not have a heart defect, while the same mutations in zebrafish cause cardiac malformation. Zebrafish mutants of the most recently described NS gene, RIT1, show incomplete looping of the heart and hypoplastic heart chambers, while the heart phenotype was variable or even absent in patients with *RIT1* mutations.[6]

Finally, we hypothesized that a conformational change in A2ML1 is the underlying mechanism leading to the developmental defects resembling NS. This conformational change may lead to destabilization of A2ML1, or it may interfere with its trap mechanism of inhibition. Since both intragenic deletions of *A2ML1* (reported in the Database of Genomic Variants[27]), as well as frameshift mutations are detected in healthy controls (Supplementary Table 2), haploinsufficiency is highly unlikely as a the underlying disease mechanism. Given that the A2M family of proteins acts in multimeric complexes, it is expected that conformational changes might have a dominant

negative effect or lead to gain of function of the complex. Since mutation of p.Arg802 likely disrupts the interaction with p.Glu906, we reasoned that mutation of p.Glu906 should have the same effect on A2ML1 function as mutation of p.Arg802. Indeed, expression of mutant A2ml1-E906L induced developmental defects to a similar extent as NS-associated A2ml1-R802L mutants, providing additional support that A2ML1 is involved in NS.

In summary, our results provide evidence that mutations in *A2ML1* are a cause of Noonan-like syndrome, with a variable phenotype ranging from severe (resulting in intra-uterine fetal death) to very mild (or even non-penetrance). Although mutations in this gene did not lead to detectable enhanced activation of the RAS/MAPK pathway in HEK293T cells or COS7 cells, expression of A2ml1 mutants in zebrafish embryos induced developmental defects that are comparable to mutations of other NS genes. Thus, we identified a causal role of an extracellular factor in NS for the first time and our results pave the way for further exploration of the function of A2ML1, its binding partners/receptors, and other relevant extracellular cascades in the pathogenicity of NS.

Materials and Methods

Patients

The individual (case 1) selected for exome sequencing had a clinical diagnosis of NS based on the criteria defined by Van der Burgt *et al*. (2007)[3]. For Sanger sequencing of the *A2ML1* gene we obtained a total of 295 DNA samples from unrelated individuals with NS or a clinically related phenotype. All patients, including patient 1, had been tested negative for mutations in previously identified disease genes (*PTPN11*, *KRAS*, *SOS1*, *NRAS*, *SHOC2*, *CBL*, *RAF1*, *BRAF*, *MAP2K1*, *MAP2K2*, *HRAS*, and *RIT1*). These samples were collected from three genetic centers (35 patients selected by IPATIMUP, Porto, Portugal, 120 patients from the Department of Human Genetics, RUNMC, Nijmegen, the Netherlands and 140 patients from the Department of Pediatrics, Università Cattolica del Sacro Cuore (UCSC), and Department of Hematology, Oncology and Molecular Medicine, Istituto Superiore di Sanità (ISS), Rome, Italy). The clinical diagnosis for NS or suggestive of a related trait was made on the basis of standardized clinical criteria assessed by experienced clinical geneticists.

Genomic DNA from whole blood was extracted using standard protocols. This study was approved by the Review Boards of all participating institutions. Informed consent to participate in the study was obtained for all individuals as well as permission to publish photographs of individuals shown in Figure 1.

Exome sequencing for de novo variants

Exome sequencing was performed as described before.[8] In brief, exome enrichment was performed using a SOLiD optimized SureSelect Human Exome Kit (v1, 37Mb; Agilent), subsequently followed by SOLiDv3 PLUS sequencing. Read mapping and variant calling for the patient-parent trio was performed as described before.[8] All candidate *de novo* mutations present in the individual with NS were independently validated using Sanger sequencing.

Mutation analysis

For 120 individuals with NS from the department of Human Genetics, Nijmegen, the Netherlands and 35 individuals with NS from IPATIMUP, Porto, Portugal, all coding exons and flanking intronic sequences of A2ML1 were PCR amplified and analyzed by Sanger sequencing or the Ion PGM

system, respectively, using standardized protocols. All variants and protein codons are referred to according to NM_144670.3 using HGVS nomenclature. Mutations identified were checked for *de novo* occurrence whenever parental DNAs were available. For the 140 individuals with NS or a clinically related phenotype selected from the ISS and UCSC, Rome, Italy, exons 15, 16, 19, 24, 25, 26, 29, 31 and 32 and flanking intronic sequences were considered, based on the identification of possible pathogenic mutations in the first cohort. For all variants detected, an *in-silico*-based method was used to assess the effect of the mutation (Alamut software, version 2.1; http://www.interactive-biosoftware.com/) in addition to an assessment of variant pathogenicity according to guidelines by the CMGS and VKGL, for the British and Dutch Molecular Genetic Societies respectively.[9]

Protein modeling of mutations identified in A2ML1

Pathogenic mutations were modeled for their effect on protein function. Because the three-dimensional structure of A2ML1 (Uniprot entry A8K2U0) is unknown, protein modeling was performed using PDB entry 4ACQ which represents the crystal structure of A2M. Overall, A2M and A2ML1 share 40% sequence identity. Mutations used for modeling occur within a sequence stretch that is highly conserved (Supplementary Figure 1). Graphical representations for mutations modeled on 4ACQ were generated and analyzed through project HOPE and YASARA.[10,11] Residue numbers in the paper are based on residues in A2ML1 (not 4ACQ). The residues in A2ML1 and their counterparts in 4ACQ and zebrafish (see section below) are listed in Table 1.

Cell culture, transfection and immunoblotting

COS7 cells and 293T cells were maintained using standard protocols and transfected using polyethyleneimine (PEI) (Sigma). Cells were lysed directly in 2x SDS sample buffer (125mM Tris-HCl pH 6.8, 20% glycerol, 4% SDS, 2% β-mercatoethanol and 0.04% bromophenol blue) and boiled. Lysates were separated on a 10% SDS-polyacrylamide gel and blotted using mouse anti-pERK, rabbit anti-ERK (Cell Signalling Technologies) and rabbit anti-GFP (Torrey Pines Biolabs). Enhanced chemiluminescence was used to detect signal from HRP conjugated secondary antibodies (BD Bioscience).

Zebrafish injections and in situ hybridization

Zebrafish were kept and embryos were raised under standard conditions. Zebrafish *a2ml1* (GenBank: BC125959.1) was cloned into pCS2+. Mutants were derived by PCR and verified by sequencing. The gene encoding *eGFP* was fused in frame to the 3'end of (mutant) *a2ml1* which allows monitoring of expression of (mutant) A2ml1 protein in zebrafish embryos. Cytomegalovirus (CMV)-driven expression vectors for (mutant) A2ml1, *CMV:a2ml1-egfp*, were injected into zebrafish embryos at the one-cell stage. Synthetic RNA encoding mutant Shp2-D61G was injected at the one cell stage as a control.[12] Morphological phenotypes were assessed at 4 days post fertilization (dpf). Embryos were anesthesized at 4 dpf with MS-222 (Sigma), fixed in 4% PFA and the cartilage was stained with alcian blue. The width of the ceratohyal and the distance to the tip of Meckel's cartilage were determined using Image J software[13] and the ratio was determined as a direct measure for craniofacial defects. Averages were determined and a student t-test was done to determine whether the differences between the different conditions were statistically significant. To investigate cardiac defects, embryos were fixed at 55 hpf and *in situ* hybridizations were done essentially as described[14] using probes specific for *myl7*.[15]

Deposition of genetic data

The data obtained in this study are submitted to LOVD, an online gene-centered collection and display of DNA variations (http://databases.lovd.nl/shared/genes).

Acknowledgements

We thank Hanka Venselaar for bioinformatics support in protein modeling and Martina Ruiterkamp-Versteeg, Petra de Vries, Suzanne Keijzers-Vloet, and Martine van Zweeden for technical assistance. This work was funded, in part, by a grant from the Research Council for Earth and Life Sciences (ALW 819.02.021) with financial aid from the Netherlands Organisation for Scientific Research (NWO) (to J.d.H.), Telethon-Italy (GGP13107; to M.T.), Fundação para a Ciência e Tecnologia (PTDC/BIM-MEC/0650/2012; to JLC), and PPS5 Consórcio DoIT (ADI–Agência de Inovação; to JLC). IPATIMUP is an Associate Laboratory of the Portuguese Ministry of Education and Science and is partially supported by FCT, the Portuguese Foundation for Science and Technology.

References

1. Mendez HM, Opitz JM (1985) Noonan syndrome: a review. Am J Med Genet 21: 493-506.
2. Allanson JE (1987) Noonan syndrome. J Med Genet 24: 9-13.
3. van der Burgt I (2007) Noonan syndrome. Orphanet J Rare Dis 2: 4.
4. Roberts AE, Allanson JE, Tartaglia M, Gelb BD (2013) Noonan syndrome. Lancet 381: 333-342.
5. Colquitt JL, Noonan JA (2013) Cardiac Findings in Noonan Syndrome on Long-term Follow-up. Congenit Heart Dis.
6. Aoki Y, Niihori T, Banjo T, Okamoto N, Mizuno S, et al. (2013) Gain-of-Function Mutations in RIT1 Cause Noonan Syndrome, a RAS/MAPK Pathway Syndrome. Am J Hum Genet 93: 173-180.
7. Tartaglia M, Gelb BD, Zenker M (2011) Noonan syndrome and clinically related disorders. Best Pract Res Clin Endocrinol Metab 25: 161-179.
8. de Ligt J, Willemsen MH, van Bon BW, Kleefstra T, Yntema HG, et al. (2012) Diagnostic exome sequencing in persons with severe intellectual disability. N Engl J Med 367: 1921-1929.
9. Bell JB, D.; Sistermans, E.; Ramsden, S.C. (2007) Practice guidelines for the Interpretation and Reporting of Unclassified Variants (UVs) in Clinical Molecular Genetics. Guidelines ratified by the UK Clinical Molecular Genetics Society (11th January, 2008) and the Dutch Society of Clinical Genetic Laboratory Specialists (Vereniging Klinisch Genetische Laboratoriumspecialisten; VKGL) (22nd October, 2007) http://www.cmgs.org/bpgs/pdfs%20current%20bpgs/UV%20GUIDELINES%20ratified.pdf.
10. Krieger E, Vriend G (2002) Models@Home: distributed computing in bioinformatics using a screensaver based approach. Bioinformatics 18: 315-318.
11. Venselaar H, Te Beek TA, Kuipers RK, Hekkelman ML, Vriend G (2010) Protein structure analysis of mutations causing inheritable diseases. An e-Science approach with life scientist friendly interfaces. BMC Bioinformatics 11: 548.
12. Jopling C, van Geemen D, den Hertog J (2007) Shp2 knockdown and Noonan/LEOPARD mutant Shp2-induced gastrulation defects. PLoS Genet 3: e225.
13. Software IJ http://rsb.info.nih.gov/ij/.
14. Thisse C, Thisse B (2008) High-resolution in situ hybridization to whole-mount zebrafish embryos. Nat Protoc 3: 59-69.
15. Yelon D, Horne SA, Stainier DY (1999) Restricted expression of cardiac myosin genes reveals regulated aspects of heart tube assembly in zebrafish. Dev Biol 214: 23-37.
16. Roach JC, Glusman G, Smit AF, Huff CD, Hubley R, et al. (2010) Analysis of genetic inheritance in a family quartet by whole-genome sequencing. Science 328: 636-639.
17. Marrero A, Duquerroy S, Trapani S, Goulas T, Guevara T, et al. (2012) The crystal structure of human alpha2-macroglobulin reveals a unique molecular cage. Angew Chem Int Ed Engl 51: 3340-3344.
18. Hong SK, Dawid IB (2008) Alpha2 macroglobulin-like is essential for liver development in zebrafish. PLoS One 3: e3736.
19. Runtuwene V, van Eekelen M, Overvoorde J, Rehmann H, Yntema HG, et al. (2011) Noonan syndrome gain-of-function mutations in NRAS cause zebrafish gastrulation defects. Dis Model Mech 4: 393-399.
20. Galliano MF, Toulza E, Gallinaro H, Jonca N, Ishida-Yamamoto A, et al. (2006) A novel protease inhibitor of the alpha2-macroglobulin family expressed in the human epidermis. J Biol Chem 281: 5780-5789.
21. Galliano MF, Toulza E, Jonca N, Gonias SL, Serre G, et al. (2008) Binding of alpha2ML1 to the low density lipoprotein receptor-related protein 1 (LRP1) reveals a new role for LRP1 in the human epidermis. PLoS One 3: e2729.
22. Geetha N, Mihaly J, Stockenhuber A, Blasi F, Uhrin P, et al. (2011) Signal integration and coincidence detection in the mitogen-activated protein kinase/extracellular signal-regulated kinase (ERK) cascade: concomitant activation of receptor tyrosine kinases and of LRP-1 leads to sustained ERK phosphorylation via down-regulation of dual specificity phosphatases (DUSP1 and -6). J Biol Chem 286: 25663-25674.
23. Takayama Y, May P, Anderson RG, Herz J (2005) Low density lipoprotein receptor-related protein 1 (LRP1) controls endocytosis and c-CBL-mediated ubiquitination of the platelet-derived growth factor receptor beta (PDGFR beta). J Biol Chem 280: 18504-18510.
24. Tartaglia M, Kalidas K, Shaw A, Song X, Musat DL, et al. (2002) PTPN11 mutations in Noonan syndrome: molecular spectrum, genotype-phenotype correlation, and phenotypic heterogeneity. Am J Hum Genet 70: 1555-1563.
25. Cordeddu V, Di Schiavi E, Pennacchio LA, Ma'ayan A, Sarkozy A, et al. (2009) Mutation of SHOC2 promotes aberrant protein N-myristoylation and causes Noonan-like syndrome with loose anagen hair. Nat Genet 41: 1022-1026.
26. Zenker M, Voss E, Reis A (2007) Mild variable Noonan syndrome in a family with a novel PTPN11 mutation. Eur J Med Genet 50: 43-47.
27. Variants DoG http://projects.tcag.ca/variation/.

Supplementary Information

Supplementary Clinical Descriptions of families with A2ML1 *mutations*

Family 1: c.2405G>A, p.(Arg802His), *de novo*

Case 1 This individual was referred because of hypotonia and facial dysmorphisms noticed directly after birth. Her parents were non-consanguineous, apparently healthy, and had no features suggestive for Noonan syndrome (NS). During pregnancy hygroma colli and polyhydramnion were noticed. Birth weight was 4005 gr. (+2 SD), length 49 cm (-0.5 SD). Clinical examination after birth showed short stature, developmental delay, typical Noonan syndrome facial features: a broad and high forehead, hypertelorism, low-set posteriorely rotated ears and webbed neck (Figure 1A). She had a broad thorax with widely spaced nipples (10,5 cm at 6 months of age) and pectus excavatum. Cardiologic evaluation revealed no structural heart defect. At 2 years the clinical diagnosis of NS was made. Her OFC at 12 years was 55 cm (+0,5 SD), at 15yrs and 9 months puberty stage : MIII,PIII-IV,A0. At16 years of age her height is 156 cm (-2 SD).
Of note, in this individual another *de novo* mutation was identified using exome sequencing being a missense change in *OR12D3* (NM_030959.2:c.386G>C). Evaluation of its pathogenicity in the context of the patients phenotype, however, excluded this variant as a likely cause.

Family 2: c.2405G>T, p.(Arg802Leu)

Case 2 The patient was referred together with his son. Clinical examination at the age of 48 years revealed general mild central hypotonia, height 181 cm (0 SD), weight 69,2 kg (0 SD), head circumference 58.1 cm (0SD). He had Noonan-like facial features with a high forehead, prominent eyes, slightly hypertelorism (intercanthal distance 3,6 cm at adult age , and thick hooded eyelids (Figure. 1B). Multiple pigmented nevi were noticed. The inter-nipple distance was 22cm at adult age. No heart abnormalities were seen. The patient was born prematurely at 34 weeks of gestation and stayed in an incubator for three months. He was part of a twin; His twin brother died at birth unexplained. He has social fears, performance anxiety and poor concentration.

Case 3 This individual is the son of case 2. He was born with a pulmonary valve stenosis. Physical examination at 11 years 9 months showed facial hypotonia with Noonan-like features (Figure 1B). His height was 155 cm (+0.5 SD), head circumference 54.5 cm (0SD), and intercanthal distance (2,9 cm) and genitalia were normal. The inter-nipple distance was 15,7 cm. Puberty was at Tannerstage 1-2 with no axillary hair. He walked clumsy with pes planus. His psychomotor development was mildly delayed. At the age of 6 years he was diagnosed with autistic-like behavior with attention deficit.

Case 4 This individual is the mother of case 2. She was healthy and had normal basic education. Examination at 73 years of age showed normal height and no facial dysmorphisms (Figure 1B). Cardiac evaluation revealed no abnormalities. No typical Noonan-like features were recognized.
Family 3: c.1775G>T, p.(Arg592Leu)

Case 5 This individual was referred in her second pregnancy. She has short stature with adult height of 157 cm (<-2 SD), facial features suggestive for Noonan syndrome and easy bruising (Figure 1C). The intercanthal distance was 3,4 cm at adult age. She had severe neonatal feeding problems, was clumsy and had an anxiety disorder at adult age. Her first menarche was at 12 years of age.

Case 6 This individual is the second child of case 5, and was born after 37 weeks of gestation with a birth weight of 3,195 gram and length of 50 cm. The intercanthal distance was 3,0 at 9 months (>+2SD). She had facial features suggestive for Noonan syndrome and bilateral hearing loss (30/40 dB) (Figure 1C). Cardiac evaluation revealed no abnormalities.

Case 7 This individual is the father of case 5. He has an adult height of 172 cm (-1,5 SD), relatively large head (OFC 59,5 cm (+ 1 SD)), hypertelorism (intercanthal distance 3,5 cm at adult age), a short broad neck. The inter-nipple distance was 25 cm at adult age. Cardiac evaluation revealed no abnormalities.

Case 8 This individual is the first child of case 5. The first pregnancy of case 5 ended at 29 weeks of gestation in an intra-uterine fetal death because of severe hydrops. There was polyhydramnios. The presence of MPS or a viral infection during pregnancy was excluded. Karyotyping and SNP array analysis on amniotic cells revealed no abnormalities. After birth, no pathologic examination has been done. The child had facial features compatible with Noonan syndrome. Analysis of fetal DNA material showed the same mutation as identified in his mother. There was insufficient amount of DNA left to exclude mutations in the other NS associated genes.

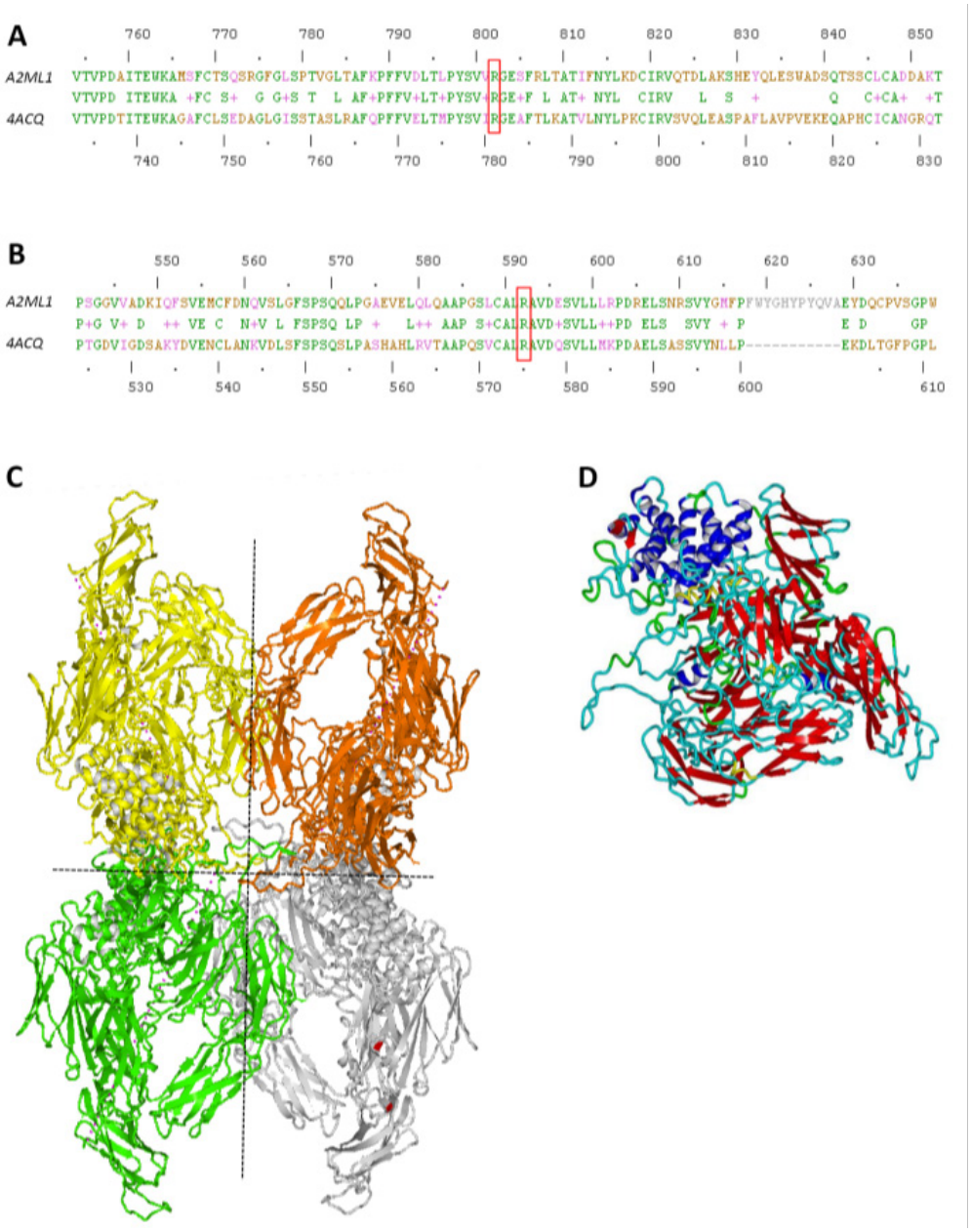

Supplementary Figure 1: Protein modeling of A2ML1 mutations
For protein modeling pdb file 4ACQ (representing A2M) was used, which shares 40% identity with A2ML1, and has positive scores for 57% and gaps for only 3% of sequence. Local protein alignments indicate that both affected amino acids are conserved in A2M (A,B, with the mutated residues highlighted in red boxes). A2ML1 proteins form a homotetrameric complex (C, with each monomer indicated by a different colour and dashed lines indicating planes of symmetry). The secondary structure of each of its monomers contains β-barrels (in red), that twist and coil to form a closed structure in which the beta-strands are arranged in an antiparallel fashion (D).

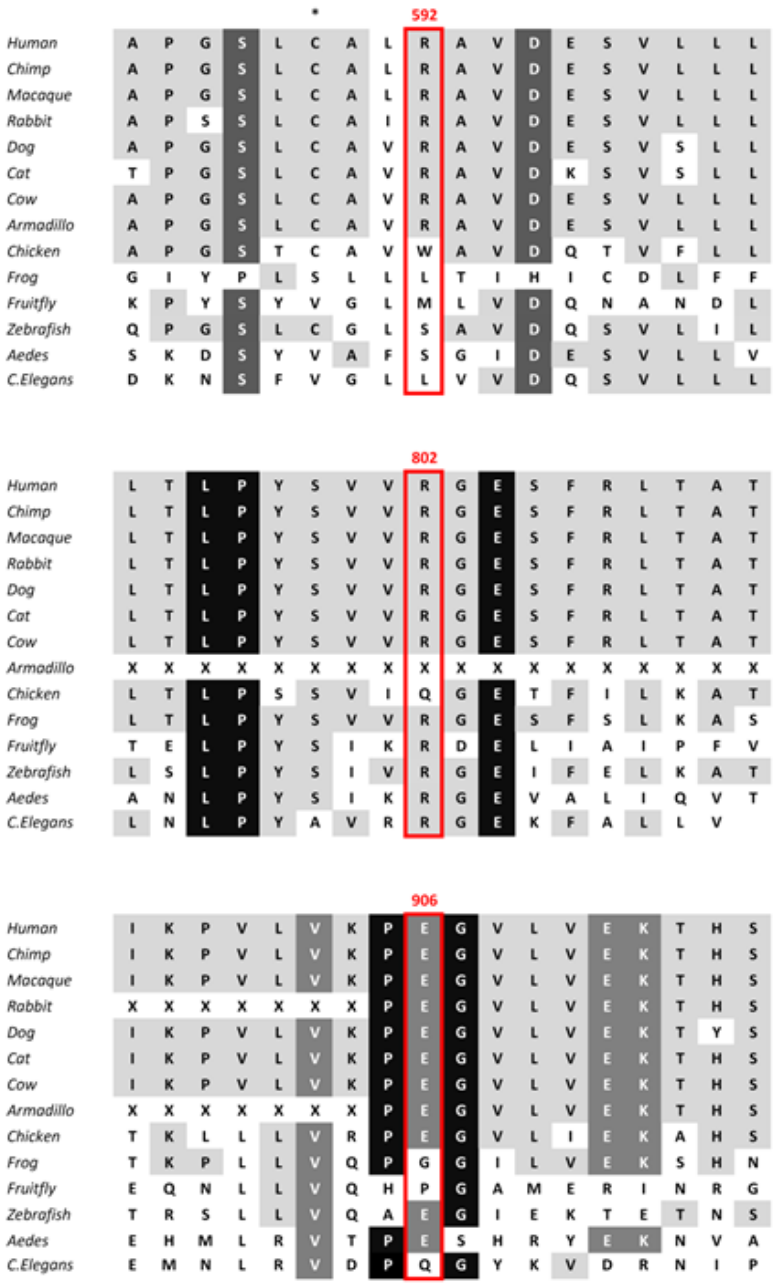

Supplementary Figure 2: Regional conservation of residues affected by mutations A2ML1 amino acid conservation across various species (listed on the left) for the residues affected by mutations. (A) Region surrounding p.Arg592 (highlighted in red box); note that p.Arg592 is not conserved in zebrafish A2ml1. (B) Region surrounding p.Arg802 (highlighted in red box), with full conservation in zebrafish. (C) Region surrounding p.Glu906, which is predicted to interact with p.Arg802 in wildtype A2ML1. This residue is conserved in Zebrafish. Asterisk in (A) represents cysteine involved in disulfide bridge formation.

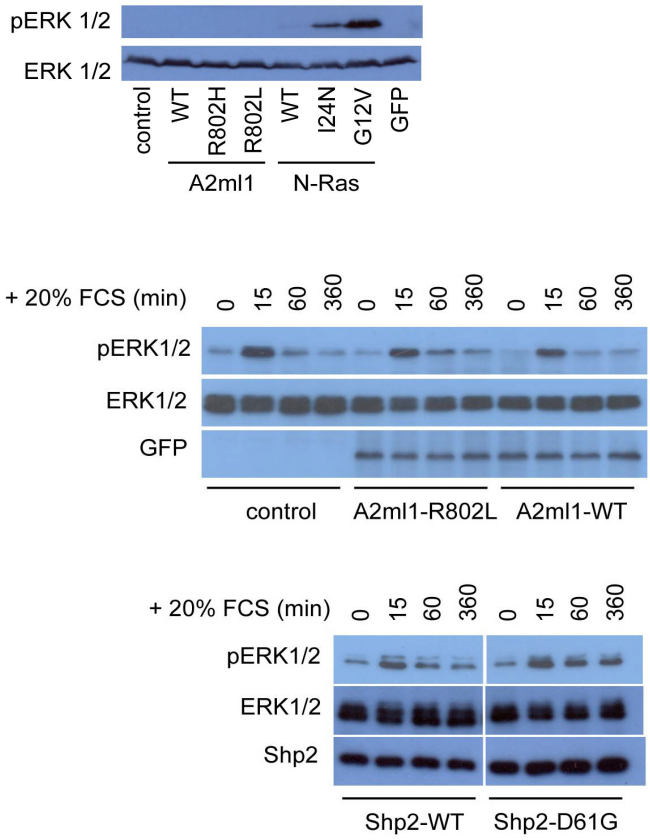

Supplementary Figure 3. Expression of mutant A2ml1 does not induce MAPK activation
(A) Human embryonic kidney HEK-293T cells were transfected with CMV-promoter-driven expression vectors for (mutant) A2ml1 or (mutant) N-Ras (known to induce MAPK activation). Cells were cultured in the presence of 10% fetal calf serum, lysed and the whole cell lysates were processed for immunoblotting using pERK1/2 specific antibodies and ERK1/2 specific antibodies to monitor protein levels. Expression of wild type (WT) and mutant A2ml1 (p.R802H or p.R802L) did not induce phosphorylation of ERK1/2, whereas NS-associated N-Ras-I24N induced mild activation and oncogenic N-Ras-G12V induced strong activation of ERK1/2. (B) Serum stimulation of COS7 cells expressing mutant A2ml1 did not affect ERK1/2 phosphorylation. COS7 cells were transfected with expression vectors encoding (mutant) A2ml1 or Shp2-D61G. Serum-starved cells were treated with 20% FCS for the indicated periods of time and subsequently, the cells were lysed and processed for immunoblotting using pERK1/2- and ERK1/2-specific antibodies. Expression of (mutant) A2ml1-GFP and (mutant) Shp2 was monitored using antibodies specific for GFP and Shp2, respectively. The ERK phosphorylation levels of wildtype (WT) and mutant A2ml1 expressing cells were indistinguishable, whereas ERK phosphorylation was enhanced in Shp2-D61G expressing cells. These results suggest either that A2ml1 does not modulate ERK/MAPK signaling, or that HEK-293T cells and COS7 cells are not responsive to A2ml1.

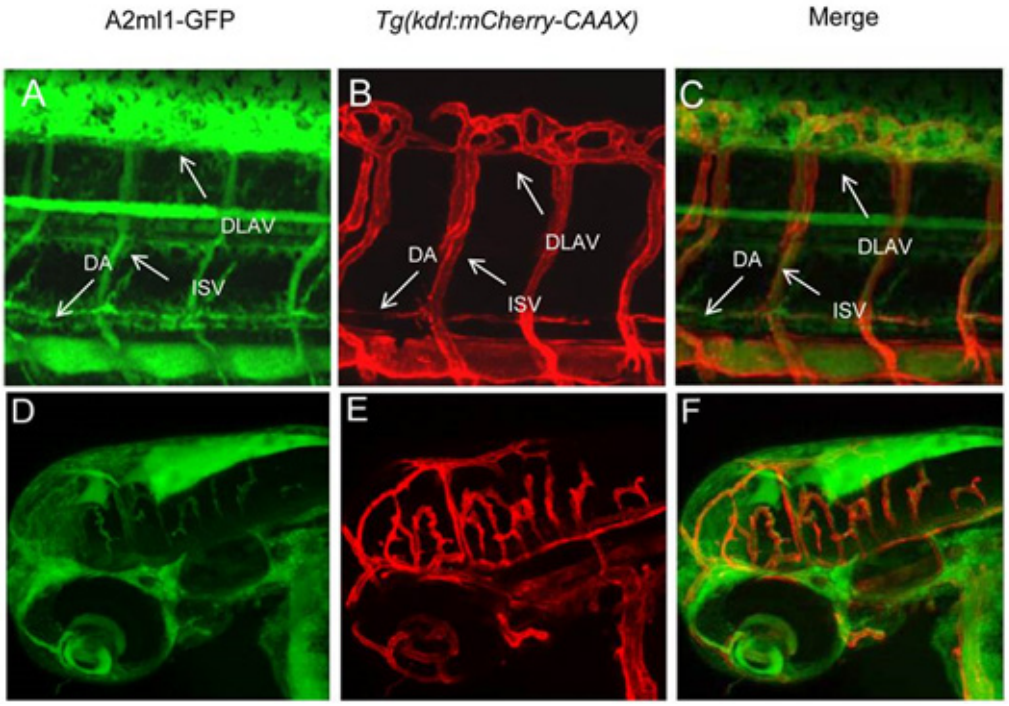

Supplementary Figure 4: A2ml1-GFP expression in zebrafish Expression of A2ml1-GFP was monitored in the transgenic reporter line Tg(kdrl:mcherry-CAAX) with expression of mCherry in all endothelial cells, thus highlighting vasculature. Zebrafish embryos were injected with plasmid DNA encoding a CMV-promoter-driven expression vector for A2ml1-GFP at the one-cell stage and imaged at 2 dpf. Lateral view of the trunk (A-C) and the head (D-F) are depicted. The dorsal aorta (DA), the Dorsal Longitudinal Anastomotic Vessel (DLAV) and intersegmental vessels (ISV) are indicated.

The expression patterns of A2ml1-GFP and mCherry were largely overlapping. A2ml1 is a secreted factor and these results confirm A2ml1-GFP localization throughout the vasculature system, even though not all cells express A2ml1-GFP due to mosaicism of the injected plasmid DNA.

Confocal imaging

Embryos at 48 hpf were dechorionated and mounted in glass-bottom 6-well plates using 0.25% agarose in E3 embryo medium containing 16 mg/ml 3-amino benzoic acid ethylester to block movements. Confocal imaging was performed using a SPE live confocal laser scanning microscope with 20x magnification for the head and 40x magnification for the trunk.

Raw sequencing statistics	**Case 1**	**Father**	**Mother**
Total number of mapped reads (Million)	56.02	79.73	59.88
Total number of bases mapped (Gb)	2.63	3.87	2.83
Total bases mapping to targets (Gb)	1.87	3.02	2.12
% mapping to target	71.10	78.04	74.91
% targets with 10x coverage	85.96	93.55	88.42
Mean target coverage	32.20	52.83	35.33
Median target coverage	39.14	66.87	45.28

Variant prioritization	**Case 1**
Total variants	23,021
*QC**	19,771
Located in coding sequence/canonical splice site	10,887
Leading to nonsynonymous change	5,063
*Excluding variants in controls***	124
Excluding variants inherited from healthy parent (possible de novo variants)	4

* ≥ 5 variant reads, ≥ 20% variantion reads
** dbSNPv130; in-house exome database

Supplementary Table 1: Raw sequencing statistics and variant prioritization

Exon	Variant (mRNA level)	Predicted protein effect	rs-number	Allele count over all populations (ESP)	Minor Allele Frequency 100%
*A. Presumable non-pathogenic variants**					
11	c.1123C>T	p.(=)	-	-	-
11	c.1215A>G	p.(=)	-	-	-
16	c.1918G>A	p.(Asp640Asn)	-	-	-
27	c.3287C>T	p.(Ser1096Phe)	-	-	-
B. Non-pathogenic variants					
2	c.105C>A	p.(=)	rs201185025	T=9/C=11923	0.08
2	c.186C>T	p.(=)	rs17792974	T=550/C=11532	4.55
3	c.289C>G	p.(Arg97Gly)	rs199701571	G=10/C=11922	0.08
5	c.463-9C>G	p.(?)	rs11047493	G=317/ C=11591	2.66
6	c.619G>C	p.(Gly207Arg)	rs11047499	C=329/G=12037	2.66
9	c.861C>A	p.(Asp287Glu)	rs61921916	A=124/C=12108	1.01
11	c.1101T>C	p.(=)	rs61744222	C=313/T=11763	2.59
11	c.1109T>C	p.(Phe370Ser)	rs61744220	C=310/T=11762	2.57
12	c.1275A>G	p.(=)	rs7308106	G=932/A=11214	7.67
12	c.1476+9G>A	p.(?)	rs7136813	A=3383/G=6475	34.32
15	c.1686T>G	p.(=)	rs12296765	G=102/T=9772	1.01
15	c.1777del**	p.(Ala593fs)	-	-	-
16	c.2026C>T	p.(Arg676Trp)	rs200503836	T=1/C=12065	0.09
18	c.2197T>C	p.(Phe733Leu)	rs117213221	C=3/T=11915	0.03
19	c.2367G>A	p.(=)	rs1860927	A=9912/G=2358	80.78
20	c.2550A>C	p.(Glu850Asp)	rs1860926	A=9644/C=372	96.29
22	c.2749T>C	p.(=)	rs200462659	C=7/T=12181	0.06
24	c.2868C>T	p.(=)	rs56179521	T=438/C=11740	27.24
24	c.2909G>A	p.(Cys970Tyr)	rs1558526	A=2356/G=10066	18.97
26	c.3237G>A	p.(=)	rs11612600	A=3769/G=8527	30.65
26	c.3252C>T	p.(=)	rs61745125	T=41/C=12247	0.33
27	c.3269G>A	p.(Gly1090Asp)	rs200964353	A=16/G=12812	0.12
27	c.3272T>C	p.(Val1091Ala)	rs61736726	C=172/T=12648	1.34
28	c.3364C>T	p.(Arg1122Trp)	rs1860967	T=3694/C=8552	30.16
29	c.3569C>T	p.(Ala1190Val)	rs73040625	T=742/C=11430	6.10
29	c.3676_3677del	p.(Ala1226fs)	rs144686314	-	2.1***
30	c.3686G>T	p.(Arg1229Leu)	rs10219561	G=11720/A=386	96.81
30	c.3769A>C/G	p.(Met1257Leu)	rs7308811	G=9457/A=2707	77.75
30	c.3843T>C	p.(=)	rs61749073	C=1326/T=10942	10.81
31	c.3878A>G	p.(Asn1293Ser)	rs201478459	G=10/A=12246	0.08
31	c.4020A>G	p.(=)	rs1476910	G=9125/A=3099	74.65
31	c.4061+1G>A****	p.(?)	rs202067416	A=6/G=10106	0.01

Supplementary Table 2: Presumable non-pathogenic variants detected by *A2ML1* sequencing (NM_144670.3)

*Parental DNAs not available for further segregation analysis. Guidelines for variant classification (see section Mutation interpretation) however predicts these variants to be non-pathogenic. As no rs-identifier is known for this variant, nor has been observed in 1000 genomes and/or ESP we cannot formally show its non-pathogenicity.
**Variant also detected in non-affected family members.
*** Minor Allele frequency from 1000 genomes project.
****For this variant segregation analysis was not possible. Since both c.1777del and c.3676_3677del are predicted to result in loss of function of the A2ML1 protein and are considered not pathogenic (see also under**), we hypothesize also the c.4061+1G>A is a rare non-pathogenic loss-of-function variant.

General Discussion

Monica Bonetti[1], Jeroen Paardekooper Overman[1]
and Jeroen den Hertog[1,2]

1. Hubrecht Institute-KNAW and University Medical Centre Utrecht, the Netherlands
2. Institute of Biology Leiden, Leiden University, the Netherlands

Over the past years, several studies described the function of SHP2 in Noonan syndrome (NS) and LEOPARD syndrome (LS) and its crucial role during development. The work described in this thesis contributes to the understanding of the developmental and molecular mechanisms by which Shp2 variants that are associated with NS and LS result in two genetic disorders with similar features. Below, we discuss the major findings of this thesis and in Figure 1 we provide an integrated view of this thesis, with a schematic representation of the main findings of each chapter.

Role of the ptpn11 *gene in zebrafish development.*

Zebrafish has developed into a very powerful model for genetic studies as its genome is fully sequenced and it is annotated as part of the Ensembl project [1]. Moreover, the zebrafish model allows to study gene function *in vivo* and to analyze vertebrate embryogenesis as development occurs externally and the embryos are transparent [2]. We took advantage of the zebrafish model to characterize the phenotype of knock-out zebrafish embryos with impaired *ptpn11* gene function. Our analysis aimed to understand the function of Shp2 in zebrafish development and the mechanism underlying how NS- and LS-variants of Shp2 induce similar defects. In our study, *ptpn11a*$^{-/-}$ and double mutant embryos died during early embryogenesis, indicating that Shp2a was essential during zebrafish embryonic development. Notably the double mutant phenotype was more severe than the *ptpn11a*$^{-/-}$ phenotype, indicating that *ptpn11b* contributes to zebrafish development. Rescue experiments show that *ptpn11a* and *ptpn11b* are partially redundant with *ptpn11a* having a dominant role. At 5 dpf, the *ptpn11a* homozygous single mutant and the double homozygous mutant zebrafish embryos showed craniofacial defects, reduced length and absence of swim bladder (Chapter 4). The phenotype of *ptpn11a*$^{-/-}$ and double mutant embryos resemble the clinical characteristics of NS/LS patients. In fact, the embryos show reduced body length reminiscent of the growth defects in NS/LS patients [3] [4]. Moreover NS/LS patients present visible craniofacial defects, including high forehead, hypertelorism, downslanting palpebral fissures, epicantal folds, ptosis, low-set and/or posteriorly rotated ears [5, 6]. Similarly, *ptpn11a*$^{-/-}$ and double mutant embryos display craniofacial defects. Similar to the double mutant phenotype, also expression of NS/LS Shp2 led to reduced body length and craniofacial defects in zebrafish at 4 dpf [7, 8]. Shp2 acts upstream in the Erk/MAPK signaling pathway [9]. We investigated Erk/MAPK signaling in the double and single *ptpn11* mutant embryos and we found that pErk levels are downregulated only in double mutant embryos. However, we cannot exclude the possibility that the observed developmental defects are independent of Erk/MAPK signaling, since in the *ptpn11a*$^{-/-}$ embryos pERK levels are similar as in the wildtype.

In our study, we also investigated the Erk/MAPK pathway upon NS/LS Shp2 expression. We found hyperactivation of Erk after injections of either NS Shp2 or LS Shp2 at bud stage, which is consistent with a role of Erk in gastrulation cell movements. Importantly, we were able to rescue the elongated shape of the embryos by early treatment with CI-1040, a MEK inhibitor, indicating that the gastrulation defects are caused by enhanced MAPK signaling before gastrulation (Chapter 7). It has already been established in several models that NS associated mutations are gain-of-function (GOF) mutations and they promote sustained activation of ERK [10]. LS mutations reside in the PTP domain and they affect Shp2 catalytic properties. Although biochemical studies show that LS variants of Shp2 are catalytically impaired *in vitro* [11], suggesting these are loss-of-function mutations, genetic models argue against this [12]. Moreover, it has been shown that LS associated-mutations still retain significant phosphatase activity compared to the catalytically dead C460S Shp2 mutant [13]. A more recent study demonstrates that LS mutations weaken the intramolecular interaction between the PTP domain and the N-SH2 domain, leading to a

constitutive open conformation of the protein [14]. As a consequence, LS Shp2 is more prone to bind upstream effectors, compensating for the diminished phosphatase activity. In addition, previous studies in Drosophila report that LS-associated mutations induce developmental defects and hence act as GOF mutations. In our case it is feasible to hypothesize that although LS mutations are catalytically impaired, they affect the conformation of Shp2, leading to an open conformation that is more prone to bind to upstream activators than wildtype Shp2 or the C460S mutant. This is in concordance with our results with PZR (Chapter 6). Expression of catalytically inactive C460S Shp2 in parallel to the NS and LS shp2 variants may provide insight into the role of the catalytic activity of Shp2 in the developmental defects that we observed in NS and LS. Moreover, rescue experiments by expression of catalytically inactive Shp2 in double mutant embryos will provide insight into whether or not catalytic activity is important for Shp2 function and hence whether Shp2 acts as a phosphatase or as an adaptor in embryonic development.

Role of SHP2 in Noonan and LEOPARD heart defects

Congenital heart defects (CHDs) are the most common type of birth defect (~1/100 live births) and the major cause of birth-related deaths [15]. NS is the second most common syndromic cause of CHD, exceeded only by Down-syndrome [16]. A role of SHP2 in human developmental heart defects was established after the finding that missense mutations in the *PTPN11* gene are associated with NS and LS. The heart defects appear to be distinct between NS and LS patients, in that NS patients usually develop valve defects, such as pulmonary stenosis and hypertrophic cardiomyopathy (HCM) is observed more in LS patients. HCM has also been reported in NS patients without *PTPN11* mutations [6] and most cases of LS patients present HCM associated with valve anomalies [17]. However, the exact mechanism that leads to two different heart defects in syndromes with overlapping symptoms, still needs to be addressed. In our study, we used zebrafish as a model to investigate the cardiac development in NS and LS. We showed that NS/LS Shp2 mRNA injections lead to phenotypes similar to the clinical features in human patients, characterized by cranio-facial defects, short body length and cardiac anomalies. Concerning the heart defects, we found that injected embryos show a pericardial edema varying in penetrance from mild to severe. *In situ* hybridization for the heart specific probe *myl7*, reveals that around 50% of NS and LS embryos show a left/right randomization of the heart displacement and an impairment of the cardiac chambers asymmetry at 48 hpf. Consistent with our findings, Langdon *et al*. [18] showed that Noonan-associated mutations lead to failure of the complete looping in *Xenopus*. Notably, even though the cardiac phenotype in humans is quite distinct, we did not detect any difference between NS and LS cardiac defects in zebrafish embryos. Moreover, the first defect that appears in NS/LS injected embryos, consists of an elongation of the embryo at the end of gastrulation, resulting in oval-shaped embryos, rather than the almost perfect sphere of wildtype embryos (Chapter 7). Immunoblotting of NS/LS embryos at bud stage showed hyper-activation of the MAPK pathway both in NS and LS Shp2-associated mutants, which may explain why the early developmental defects were indistinguishable. Furthermore, the development of the endocardial cushions in zebrafish is relatively late (36 hpf) and at that stage, the stability of the NS/LS Shp2 could already be compromised. The formation of the cardiac tube is the first manifestation of L/R asymmetry in the vertebrate heart [19]. Usually, failure in cardiac jogging is a consequence of aberrant expression of southpaw (*spaw*) and *lefty-2*, two genes that are usually expressed on the left side. In NS/LS Shp2 injected embryos, the expression pattern of *spaw* is randomized which also affects the correct expression of the more downstream gene *lefty-2*. Our studies link NS/LS Shp2 with the disruption of L/R asymmetry in zebrafish embryos. The misplacement of *spaw* gene expression is caused by the impairment of the ciliated organ Kupffer's vescicle (KV), which is responsible for L/R asymmetry in zebrafish. Cilia within the vescicle

rotate in counter-clockwise direction, generating a fluid flow that induces leftward expression of *spaw* in the LPM. Laser ablation of the KV leads to randomized expression of *spaw* and *lefty-2*. We demonstrated that ciliogenesis of the KV is impaired in NS and LS embryos. The KV in NS and LS embryos showed reduced cilia length and cilia number; moreover the KV's lumen in NS and LS embryos is smaller compared to the WT-Shp2 injected embryos and cilia function is impaired. This leads to a reduction or absence of fluid-flow in the KV and consequent disruption of laterality in the LPM. Our investigations show that the increased level of pERK was associated with perturbation of KV in NS and LS embryos, in that we were able to rescue the laterality defects and the ciliogenesis impairment by early treatment with CI-1040, a MEK inhibitor. Hence, the defects in heart asymmetry were caused by enhanced MAPK signaling before gastrulation. In summary, our data open a new prospective to understand how Shp2 relates to cardiac development and disease in NS and LS.

A2ML1: an extracellular protein causing Noonan-like syndrome

The genetic cause of some 25% of all Noonan cases still remains to be determined. We identified mutations in *A2ML1* in patients that were diagnosed with NS. Mutations were found in the same codon in two separate families with Noonan-like symptoms, which strengthens the hypothesis that these mutations in *A2ML1* are indeed causative for Noonan syndrome. Alpha-2-macroglobulin like 1 (A2ML1) is a 170 kDa extracellular broad range protease inhibitor of the A2M family, that is present in the epidermis and circulates the bloodstream [20, 21]. Hence, A2ml1 is the first extracellular protein to be associated with NS-like features. Overexpression of mutated A2ml1 caused enhanced Noonan-like phenotypes in developing zebrafish embryos, compared to WT A2ml1. A2ml1 is a ligand for the transmembrane receptor LRP1 [23]. Activation of LRP1 may potentiate growth factor signaling by RTKs like EGFR, FGFR and VEGFR [24, 25]. Concurrent activation of LRP1 by LDL and lactoferrin with RTK activation causes a sustained activation of the MAPK pathway by downregulation of the MAPK targeting phosphatases DUSP-5 and DUSP-6 [24]. Upon activation of PDGFR, the receptor is internalized in LRP1 containing endosomes, where it forms a signaling complex [25]. Shp2 is able to bind both PDGFR and LRP1 directly, and LRP1 competes with PDGFR for Shp2 in endosomes [26]. A MAPK-potentiating LRP1-dependent mechanism may drive A2ml1-induced signaling in NS. Importantly, both NS and LS Shp2 cause sustained MAPK activation upon GF stimulation in cells [14]. As we were not able to show sustained MAPK activation in response to A2ml1, further investigations are essential to elucidate the mechanism by which *A2ML1* mutations cause NS. We cannot exclude the possibility that variation in the genetic landscape between patients affect the response to (mutant) A2ML1. Distinct genetic backgrounds that mildly influence the MAPK activation pathway may contribute differently to (mutant) A2ML1 signaling. Previously, a single Shp2 variant was observed in a family with both NS patients and healthy siblings, underlining the importance of enhancers and suppressors of the phenotype [27]. Other Noonan causing mutations in *MYST4*, *KRAS* and *SOS1* are also known to show heart defects with variable penetrance [27-30]. The patients with mutations in *A2ML1* did not display all symptoms of classical NS and expression of mutant A2ml1 in cells or zebrafish did not induce sustained MAPK activation. For these reasons, we conclude that the mutations we identified in *A2ML1* are associated with Noonan-like syndrome, rather than NS *proper*.

Downregulation of Fer tyrosine kinase in Noonan and LEOPARD syndrome

Noonan and LEOPARD syndromes are complex congenital disorders, and the elucidation of affected pathways may provide key elements for targeted therapies [31, 32]. High throughput methods are useful for the identification of novel target genes and proteins for therapy. Microarray

based phosphoproteomic experiments showed an increase in phosphorylation of several proteins including MEK, caveolin, EGFR and FAK, while other proteins like vinculin and LCK were less phosphorylated [33]. Whereas these data from *in vitro* studies are useful, they may not reflect the phosphorylation status and thus the activity of these proteins *in vivo* and during development. Mass spectrometry based proteomics have been proven feasible in developing zebrafish embryos [34-36]. We combined multiple methods previously pioneered by Lemeer *et al*. and sought out to identify a common mechanism on how activating and inactivating mutations of Shp2 may drive the development of similar phenotypes. We identified the auto-phosphorylation loop of Fer kinase as a major downregulated tyrosyl phosphorylation site. In contrast to 1 dpf zebrafish, 5 day old *Shp2*$^{D61G/+}$ mouse hearts showed an increase in Fer phosphorylation (Chapter 6). The discrepancy may be explained by differences in developmental time points or tissue-specific activation of Fer in NS. Tissue specific expression of NS genes is not unknown [28]. *MYST4*, a Noonan gene discovered in a patient not showing any cardiac defects, showed tissue specific expression. Cell type and growth factor specific roles for Shp2 have also been described [10, 37]. It is therefore not unlikely that tissue-specific activation or inactivation may contribute to clinical signs of NS and LS [28]. Loss of Fer expression leads to convergence and extension (C/E) defects, indicating an essential role in gastrulation. Using epistasis experiments, we showed a genetic interaction between Fer and disease associated Shp2. Partial loss of Fer expression concurrent with either NS or LS Shp2 expression, but not WT Shp2 expression, leads to developmental defects, phenocopying those seen in NS/LS expressing embryos. Epistasis experiments are a powerful tool to show genetic interactions that may cause disease [38]. Fer and Shp2 interact in many ways [39, 40], and the altered binding properties of NS/LS Shp2 may affect the function of interacting proteins like Fer. Indeed, in Chapter 6 we show enhanced complex formation of Shp2, PZR and Src. It is not difficult to imagine signalling pathways other than the canonical MAPK pathway to be affected by the altered properties of NS and LS Shp2. As both Fer and Shp2 share common binding partners [26, 40, 41], it may be that Fer is "quenched off" from its binding partners by the enhanced binding properties of NS/LS Shp2. Further studies are necessary to uncover the mechanism how Fer down regulation may contribute to NS/LS.

Enhanced Src-Shp2-PZR complex formation in Noonan and LEOPARD syndromes

Like Fer, we identified PZR in a mass spectrometric approach to identify novel factors that drive NS and LS. PZR was found hyperphosphorylated in both mouse hearts and zebrafish in NS and LS, compared to WT Shp2. PZR was previously identified as a Shp2 binding protein [42, 43]. PZR is a transmembrane protein with two immunoreceptor tyrosine inhibitory motifs (ITIMs). These ITIMs serve as Shp2 binding sites and Shp2 is able to dephosphorylate these ITIMs, thus acting in a negative feedback loop under normal conditions [42, 43]. In addition to enhanced PZR phosphorylation, we observed enhanced binding of NS/LS Shp2 to Src, compared to WT Shp2, causing a change in the flux of Shp2/Src signaling. We hypothesize a model in which NS/LS Shp2 binds Src, which leads to sustained PZR phosphorylation and binding. This may mediate hyper-activation of cortactin and abnormal cell migration [44]. Previous reports showed that PZR affects cell migration *in vitro* and that PZR is expressed during early mouse embryogenesis, consistent with our results [45]. PZR forms lacking the ITIM sites do not show this effect on cell migration or induce developmental defects [45]. These results indicate that altered signaling of the PZR/Shp2/Src complex, either too little or too much results in disease. This hypothesis is strengthened by the finding that recently, copy number variations of PZR were found to cause cell migration in tumor cells [44]. This was mediated by activation of cortactin. Moreover, duplication of *PTPN11* was identified recently in a NS patient, indicating that not only GOF mutations but also altered protein levels may result in NS [22]. How PZR phosphorylation is affected in this patient

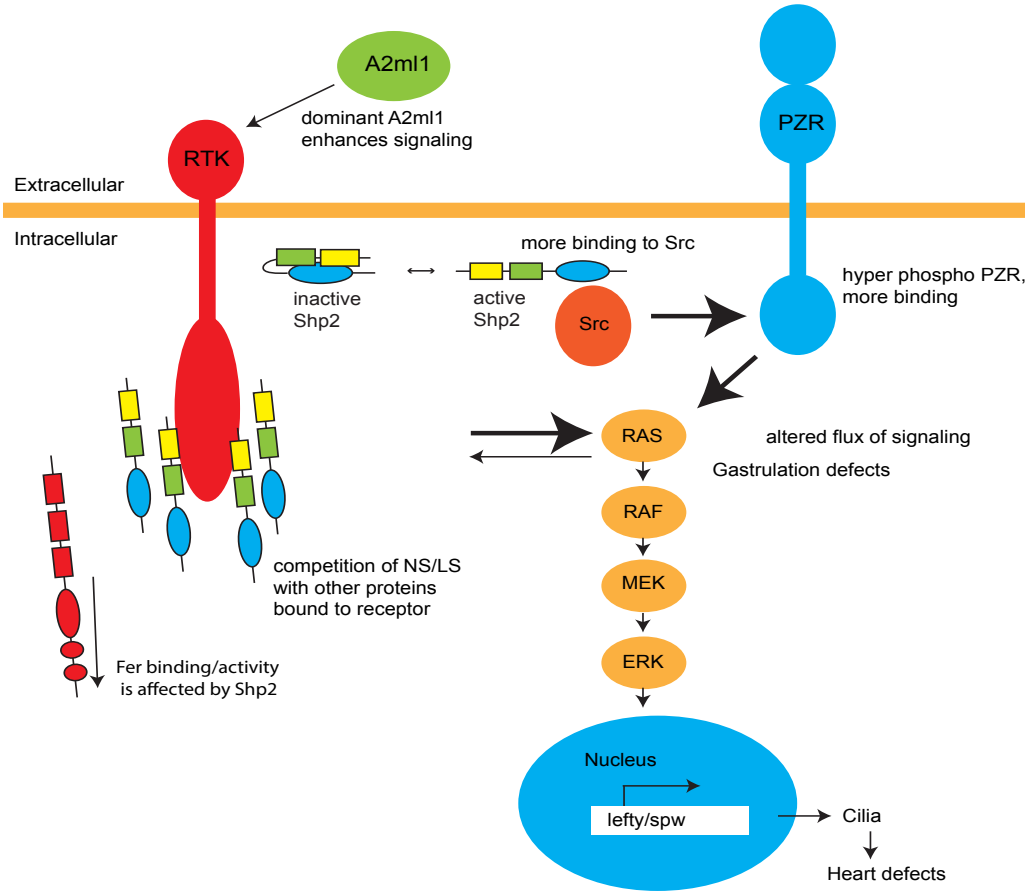

Figure 1. Schematic overview of the highlights of this thesis and proposed mechanisms. Enhanced binding of mutant A2ml1 (green) to LRP1 in combination with RTKs (red) may result in enhanced MAPK activation. Due to the open state of Shp2, it is more prone to bind other proteins like Src (orange) and RTKs. Enhanced binding of NS/LS Shp2 leads to Src recruitment to PZR (blue) and PZR phosphorylation, which in turn results in gastrulation defects and changes in MAPK activation flux. On the other hand, potential "quenching" of Fer from RTKs by Shp2 may lead to inactivation of Fer (red). MAPK activation gives rise to altered gene expression including Spw and lefty-2. This in turn results in changes in ciliogenesis development and heart development. See text for further details.

remains to be investigated. Taken together, our finding that NS/LS mutations leads to an altered flux of signaling, that PZR duplication leads to disease [44] and that Shp2 duplication may cause NS [22], a protein interaction-based view on the etiology of NS an LS would be the next step into identifying novel mutations (or CNVs) that, together may be causative of unexplained NS/LS. The discovery of PZR as a hyperphosphorylated protein in LS, in addition to NS [46], provides insights into the aetiology of both syndromes. Clearly, a common mechanism is shared between activating (NS) and inactivating (LS) forms of Shp2, which leads to PZR phoshorylation. Src binding may be causative for some of the clinical features that are observed in NS and LS . Additionally, this may provide an explanation into how Fer may be downregulated in NS/LS, given the high probability that these proteins may act in a complex. Hyperactivation of cortactin by Shp2 mediated Src activation may possibly lead to a negative feedback signal to Fer [47]. Therapeutically, PZR phosphopeptide might inhibit hyperactivation of Shp2, possibly in both NS and LS [48]. Interestingly, treatment of cells with PZR phosphopeptide caused a remarkable decrease in ERK

activation due to quenching of Shp2 from its physiological substrates [48]. Alternatively, PZR phosphorylation might be used in the clinic to assess the effect of Shp2 mutations in patients.

Conclusion

Overall, we demonstrate that Shp2 plays a crucial role in zebrafish development. Genetic duplication of *ptpn11* allowed us to study gene dosage effects and the role of Shp2a and Shp2b at various stages of development (Chapter 4). Moreover, we show that both NS and LS Shp2 cause hypo- and hyperphosphorylation of Fer and PZR, respectively compared to WT. Genetic interaction studies indicated a role for reduced signaling by Fer in the etiology of NS and LS (Chapter 5). Functional studies showed indications for enhanced signaling complex formation of NS and LS Shp2 with PZR and Src (Chapter 6). Changes in protein-protein interactions are an important contributor to NS and LS. Both NS and LS Shp2 can lead to GOF phenotypes, showing enhanced Erk phosphorylation at the end of gastrulation in zebrafish. Both NS and LS lead to early heart defects in a similar way as well (Chapter 7). In addition, we identified mutations in an extracellular protein, A2ml1, to be associated with Noonan-like phenotypes (Chapter 8). Taken together, our findings show that NS and LS Shp2 share many mechanistic and developmental features, and that these disease associated proteins should not only be viewed as "activating" or "inactivating". Using a versatile *in vivo* model, we show that these proteins should rather be viewed in a network of interacting proteins that gives rise to similar developmental defects. Overall, we used zebrafish embryos as a model to study the etiology of NS and LS at the genetic, molecular, proteomic and organismal level.

References

1. Flicek, P., et al., Ensembl 2013. Nucleic Acids Res, 2013. 41(Database issue): p. D48-55.
2. Lieschke, G.J. and P.D. Currie, Animal models of human disease: zebrafish swim into view. Nat Rev Genet, 2007. 8(5): p. 353-67.
3. Noonan, J.A., R. Raaijmakers, and B.D. Hall, Adult height in Noonan syndrome. Am J Med Genet A, 2003. 123A(1): p. 68-71.
4. Gorlin, R.J., R.C. Anderson, and M. Blaw, Multiple lentigenes syndrome. Am J Dis Child, 1969. 117(6): p. 652-62.
5. Noonan, J.A., Hypertelorism with Turner phenotype. A new syndrome with associated congenital heart disease. Am J Dis Child, 1968. 116(4): p. 373-80.
6. Tartaglia, M., et al., *PTPN11* mutations in Noonan syndrome: molecular spectrum, genotype-phenotype correlation, and phenotypic heterogeneity. Am J Hum Genet, 2002. 70(6): p. 1555-63.
7. Jopling, C., D. van Geemen, and J. den Hertog, Shp2 knockdown and Noonan/LEOPARD mutant Shp2-induced gastrulation defects. PLoS Genet, 2007. 3(12): p. e225.
8. Stewart, R.A., et al., Phosphatase-dependent and -independent functions of Shp2 in neural crest cells underlie LEOPARD syndrome pathogenesis. Dev Cell, 2010. 18(5): p. 750-62.
9. Feng, G.S., Shp-2 tyrosine phosphatase: signaling one cell or many. Exp Cell Res, 1999. 253(1): p. 47-54.
10. Araki, T., et al., Mouse model of Noonan syndrome reveals cell type- and gene dosage-dependent effects of *Ptpn11* mutation. Nat Med, 2004. 10(8): p. 849-57.
11. Kontaridis, M.I., et al., *PTPN11* (Shp2) mutations in LEOPARD syndrome have dominant negative, not activating, effects. J Biol Chem, 2006. 281(10): p. 6785-92.
12. Oishi, K., et al., Phosphatase-defective LEOPARD syndrome mutations in *PTPN11* gene have gain-of-function effects during Drosophila development. Hum Mol Genet, 2009. 18(1): p. 193-201.
13. Hanna, N., et al., Reduced phosphatase activity of SHP-2 in LEOPARD syndrome: consequences for PI3K binding on Gab1. FEBS Lett, 2006. 580(10): p. 2477-82.
14. Yu, Z.H., et al., Structural and mechanistic insights into LEOPARD syndrome-associated SHP2 mutations. J Biol Chem, 2013. 288(15): p. 10472-82.
15. Weismann, C.G. and B.D. Gelb, The genetics of congenital heart disease: a review of recent developments. Curr Opin Cardiol, 2007. 22(3): p. 200-6.
16. Marino, B., et al., Congenital heart diseases in children with Noonan syndrome: An expanded cardiac spectrum with high prevalence of atrioventricular canal. J Pediatr, 1999. 135(6): p. 703-6.
17. Limongelli, G., et al., Prevalence and clinical significance of cardiovascular abnormalities in patients with the LEOPARD syndrome. Am J Cardiol, 2007. 100(4): p. 736-41.
18. Langdon, Y., et al., SHP-2 acts via ROCK to regulate the cardiac actin cytoskeleton. Development, 2012. 139(5): p. 948-57.
19. Ramsdell, A.F., Left-right asymmetry and congenital cardiac defects: getting to the heart of the matter in vertebrate left-right axis determination. Dev Biol, 2005. 288(1): p. 1-20.
20. Galliano, M.F., et al., A novel protease inhibitor of the alpha2-macroglobulin family expressed in the human epidermis. J Biol Chem, 2006. 281(9): p. 5780-9.
21. Hong, S.K. and I.B. Dawid, Alpha2 macroglobulin-like is essential for liver development in zebrafish. PLoS One, 2008. 3(11): p. e3736.
22. Chen, J.L., et al., Rare copy number variations containing genes involved in RASopathies: deletion of SHOC2 and duplication of PTPN11. Mol Cytogenet, 2014. 7(1): p. 28.
23. Galliano, M.F., et al., Binding of alpha2ML1 to the low density lipoprotein receptor-related protein 1 (LRP1) reveals a new role for LRP1 in the human epidermis. PLoS One, 2008. 3(7): p. e2729.
24. Geetha, N., et al., Signal integration and coincidence detection in the mitogen-activated protein kinase/extracellular signal-regulated kinase (ERK) cascade: concomitant activation of receptor tyrosine kinases and of LRP-1 leads to sustained ERK phosphorylation via down-regulation of dual specificity phosphatases (DUSP1 and -6). J Biol Chem, 2011. 286(29): p. 25663-74.
25. Muratoglu, S.C., et al., Low density lipoprotein receptor-related protein 1 (LRP1) forms a signaling complex with platelet-derived growth factor receptor-beta in endosomes and regulates activation of the MAPK pathway. J Biol Chem, 2010. 285(19): p. 14308-17.
26. Craig, J., et al., The LDL receptor-related protein 1 (LRP1) regulates the PDGF signaling pathway by binding the protein phosphatase SHP-2 and modulating SHP-2- mediated PDGF signaling events. PLoS One, 2013. 8(7): p. e70432.
27. Zenker, M., E. Voss, and A. Reis, Mild variable Noonan syndrome in a family with a novel *PTPN11* mutation. Eur J Med Genet, 2007. 50(1): p. 43-7.
28. Kraft, M., et al., Disruption of the histone acetyltransferase MYST4 leads to a Noonan syndrome-like phenotype and hyperactivated MAPK signaling in humans and mice. J Clin Invest, 2011. 121(9): p. 3479-91.
29. Roberts, A.E., et al., Germline gain-of-function mutations in SOS1 cause Noonan syndrome. Nat Genet, 2007. 39(1): p. 70-4.
30. Sznajer, Y., et al., The spectrum of cardiac anomalies in Noonan syndrome as a result of mutations in the *PTPN11* gene. Pediatrics, 2007. 119(6): p. e1325-31.

31. Gelb, B.D. and M. Tartaglia, Noonan syndrome and related disorders: dysregulated RAS-mitogen activated protein kinase signal transduction. Hum Mol Genet, 2006. 15 Spec No 2: p. R220-6.
32. Neel, B.G., H. Gu, and L. Pao, The 'Shp'ing news: SH2 domain-containing tyrosine phosphatases in cell signaling. Trends Biochem Sci, 2003. 28(6): p. 284-93.
33. Carvajal-Vergara, X., et al., Patient-specific induced pluripotent stem-cell-derived models of LEOPARD syndrome. Nature, 2010. 465(7299): p. 808-12.
34. Lemeer, S., et al., Protein-tyrosine kinase activity profiling in knock down zebrafish embryos. PLoS One, 2007. 2(7): p. e581.
35. Lemeer, S., et al., Comparative phosphoproteomics of zebrafish Fyn/Yes morpholino knockdown embryos. Mol Cell Proteomics, 2008. 7(11): p. 2176-87.
36. Lemeer, S., et al., Online automated *in vivo* zebrafish phosphoproteomics: from large-scale analysis down to a single embryo. J Proteome Res, 2008. 7(4): p. 1555-64.
37. Araki, T., H. Nawa, and B.G. Neel, Tyrosyl phosphorylation of Shp2 is required for normal ERK activation in response to some, but not all, growth factors. J Biol Chem, 2003. 278(43): p. 41677-84.
38. Badano, J.L., et al., Dissection of epistasis in oligogenic Bardet-Biedl syndrome. Nature, 2006. 439(7074): p. 326-30.
39. Lee, S.H., et al., Synapses are regulated by the cytoplasmic tyrosine kinase Fer in a pathway mediated by p120catenin, Fer, SHP-2, and beta-catenin. J Cell Biol, 2008. 183(5): p. 893-908.
40. Udell, C.M., et al., Fer and Fps/Fes participate in a Lyn-dependent pathway from FcepsilonRI to platelet-endothelial cell adhesion molecule 1 to limit mast cell activation. J Biol Chem, 2006. 281(30): p. 20949-57.
41. Kogata, N., et al., Identification of Fer tyrosine kinase localized on microtubules as a platelet endothelial cell adhesion molecule-1 phosphorylating kinase in vascular endothelial cells. Mol Biol Cell, 2003. 14(9): p. 3553-64.
42. Zhao, Z.J. and R. Zhao, Purification and cloning of PZR, a binding protein and putative physiological substrate of tyrosine phosphatase SHP-2. J Biol Chem, 1998. 273(45): p. 29367-72.
43. Zhao, R. and Z.J. Zhao, Dissecting the interaction of SHP-2 with PZR, an immunoglobulin family protein containing immunoreceptor tyrosine-based inhibitory motifs. J Biol Chem, 2000. 275(8): p. 5453-9.
44. Jia, D., et al., Amplification of *MPZL1*/PZR promotes tumor cell migration through Src-mediated phosphorylation of cortactin in hepatocellular carcinoma. Cell Res, 2014. 24(2): p. 204-17.
45. Roubelakis, M.G., et al., The murine ortholog of the SHP-2 binding molecule, PZR accelerates cell migration on fibronectin and is expressed in early embryo formation. J Cell Biochem, 2007. 102(4): p. 955-69.
46. Eminaga, S. and A.M. Bennett, Noonan syndrome-associated SHP-2/*Ptpn11* mutants enhance SIRPalpha and PZR tyrosyl phosphorylation and promote adhesion-mediated ERK activation. J Biol Chem, 2008. 283(22): p. 15328-38.
47. Sangrar, W., et al., Fer-mediated cortactin phosphorylation is associated with efficient fibroblast migration and is dependent on reactive oxygen species generation during integrin-mediated cell adhesion. Mol Cell Biol, 2007. 27(17): p. 6140-52.
48. Zhao, R. and Z.J. Zhao, Identification of a variant form of PZR lacking immunoreceptor tyrosine-based inhibitory motifs. Biochem Biophys Res Commun, 2003. 303(4): p. 1028-33.

Appendix

English Summary

Nederlandse Samenvatting

Riassunto Italiano

Curricula Vitae
&
List of Publications

Abbreviations

Summary

This thesis describes the use of zebrafish to study Noonan- (NS) and LEOPARD syndromes (LS). In the first three chapters, we provide a background for the following six chapters. In **Chapter 1**, we briefly discuss zebrafish gastrulation and the associated signaling mechanisms. The use of zebrafish to study protein tyrosine phosphatases (PTP) is discussed in **Chapter 2**. A brief overview of previous studies on PTPs using zebrafish is given and genetic tools available in zebrafish are discussed. As our lab is interested in gastrulation, we further outline the tools we use to study zebrafish gastrulation. Moreover, phosphoproteomics is discussed as a method to study PTPs *in vivo*. **Chapter 3** describes the role of *PTPN11* (protein-tyrosine phosphatase, non-receptor type 11), the gene encoding SHP2, a cytoplasmic PTP that is essential for vertebrate development. Mutations in *PTPN11* are associated with NS and LS, two autosomal dominant disorders with overlapping symptoms. Intriguingly, while NS mutations result in a more 'active' state of Shp2, LS mutations give rise to a PTP defective protein. NS and LS patients display various symptoms, including short stature, craniofacial defects and heart abnormalities. Interestingly, the cardiac phenotype of NS and LS patients is quite distinct; in this sense NS patients present pulmonary stenosis (PS) while hypertrophic cardiomyopathy (HCM) is the most common cardiac defect present in LS.

In **Chapter 4** we have used the zebrafish as a model to investigate the role of Shp2 in embryonic development. We characterized in details the role of the two *ptpn11* zebrafish isoforms (*ptpn11a* and *ptpn11b*). We show that *ptpn11a* is expressed constitutively and *ptpn11b* expression is strongly upregulated during development. In addition, the products of both ptpn11 genes, Shp2a and Shp2b, are functional. Target-selected inactivation of *ptpn11a* and *ptpn11b* revealed that double homozygous mutants are embryonic lethal at 5-6 days post fertilization (dpf). *Ptpn11a*$^{-/-}$ *ptpn11b*$^{-/-}$ embryos showed pleiotropic defects from 4 dpf onwards, including reduced body axis extension and craniofacial defects, which was accompanied by low levels of phosphorylated Erk at 5 dpf. Interestingly, defects in homozygous *ptpn11a*$^{-/-}$ mutants overlapped with defects in the double mutants albeit they were milder, whereas *ptpn11b*$^{-/-}$ single mutants did not show detectable developmental defects and were viable and fertile. *Ptpn11a*$^{-/-}$*ptpn11b*$^{-/-}$ mutants were rescued by expression of exogenous *ptpn11a* and *ptpn11b* alike, indicating functional redundancy of Shp2a and Shp2b.

Using phoshoproteomics, in **Chapter 5** we describe the identification of Fer kinase as a potential downstream protein in the etiology of both NS and LS. Phosphotyrosine immunoprecipitation of lysates from zebrafish injected with wild type, NS or LS Shp2 followed by mass spectrometry showed a decrease in a phosphopeptide corresponding to the tyrosine kinase Fer in both NS and LS. We showed that *fer* is expressed in early embryos and that loss of Fer results in developmental defects, including convergence and extension defects. Partial loss of Fer cooperated with low expression of NS and LS variants of Shp2 but not with wild type Shp2 expression. Thus, the loss of Fer contributed to NS and LS phenotypes in zebrafish.

In **Chapter 6** a similar approach is used in NS mouse hearts to identify Protein zero related (Pzr) as the most hyper phosphorylated protein in NS. Loss of Pzr leads to gastrulation defects in zebrafish and phenotypes reminiscent of loss of Shp2, NS and LS. Pzr is hyper phosphorylated at its immunoreceptor tyrosine inhibitory motifs (ITIMs) in multiple tissues and is shown to be dependent on Src activation. Co-immunoprecipitation studies show that NS and LS Shp2 exhibit enhanced binding to Src and PZR, consisting of a complex. Moreover, the ITIMs, binding sites for

Shp2 are essential for induction of the zebrafish convergence and extension phenotype. Thus, NS and LS Shp2 form a complex with Src and Pzr to induce developmental defects in zebrafish.

In **Chapter 7** we investigated the role of the most common NS and LS Shp2 mutations in zebrafish in cardiac development. Defective heart development is a prominent symptom of both NS and LS, but how the Shp2 variants affect cardiac development is unclear. We showed that the heart function was impaired in embryos expressing NS and LS variants of Shp2. The cardiac anomalies consisted of reduced cardiomyocyte migration, coupled with impaired leftward heart displacement. Expression of specific laterality markers was randomized in embryos expressing NS and LS variants of Shp2. Ciliogenesis and cilia function in Kupffer's vesicle was impaired, likely accounting for the left/right asymmetry defects. Mitogen activated protein kinase (Mapk) signaling was activated in embryos expressing NS and LS Shp2-variants. Interestingly, inhibition of Mapk signaling prior to gastrulation rescued cilia length and heart laterality defects suggesting that NS and LS Shp2-variant mediated hyperactivation of Mapk signaling leads to impaired cilia function in Kupffer's vesicle, causing the heart impairment at later stages.

Finally we investigated the role of Alpha-2-Macroglobulin-Like-1 (A2ML1) in NS in **Chapter 8**. To date, all mutations known to cause NS are dominant and they enhance the RAS/MAPK signaling pathway. However in 25% of cases, the genetic cause of NS remains unknown, suggesting that factors other than those involved in the canonical RAS/MAPK pathway may also play a role. In our study, we used family-based whole exome sequencing of a case-parent trio and identified a *de novo* mutation, p.(Arg802His), in *A2ML1* which encodes the secreted protease inhibitor Alpha-2-Macroglobulin-Like-1. Subsequent resequencing of *A2ML1* in 155 cases with a clinical diagnosis of NS led to the identification of additional mutations in two families, p.(Arg802Leu) and p.(Arg592Leu). Functional characterization of these human *A2ML1* mutations in zebrafish showed NS-like developmental defects, including a craniofacial defects and cardiac malformations. The crystal structure of A2M, which is highly homologous to A2ML1, led us to the identification of the intramolecular interaction partner of p.Arg802. Mutation of this residue, p.Glu906, induced similar developmental defects in zebrafish, strengthening our conclusion that mutations in *A2ML1* cause a disorder clinically related to NS. We showed for the first time, the involvement of an extracellular factor in a disorder clinically related to RASopathies, providing potential new leads for better understanding of the molecular basis of this family of developmental diseases.

In **Chapter 9**, we discuss each previous chapter separately and provide an integrated view on the findings of this thesis.

Nederlandse Samenvatting

Dit proefschrift beschrijft het gebruik van de zebravis bij de studie van Noonan- (NS) en LEOPARD syndromen (LS). In de eerste drie hoofdstukken wordt achtergrondinformatie gegeven voor de zes hoofdstukken die daarop volgen. In **Hoofdstuk 1** worden gastrulatie en de betrokken signaaltransductie mechanismen in de vis besproken. Het gebruik van zebravissen om proteïne tyrosine fosfatasen (PTP) te bestuderen wordt besproken in **Hoofdstuk 2**. Er wordt een kort overzicht gegeven van eerdere studies naar PTPs die gebruik hebben gemaakt van de zebravis en de genetische instrumenten die beschikbaar zijn in de vis worden besproken. Bovendien wordt fosfoproteomica besproken als één van de methodes om PTPs *in vivo* te bestuderen. **Hoofdstuk 3** beschrijft de rol van *PTPN11* (proteïne tyrosine fosfatase, non-receptor type 11), het gen coderend voor SHP2, een cytoplasmatische PTP dat essentieel is voor de ontwikkeling van vertebraten. Mutaties in *PTPN11* worden geassocieerd met NS en LS, twee autosomale syndromen met overlappende symptomen. Verrassend is dat NS mutaties leiden tot een 'actieve' vorm van SHP2 terwijl LS mutaties leiden tot een PTP-defecte vorm van SHP2. NS en LS patiënten vertonen verscheidene symptomen waaronder een kort postuur, craniofaciale defecten en hartafwijkingen. Het hart phenotype van NS en LS patiënten is vrij verschillend; terwijl NS patiënten vooral pulmonaire stenose (PS) vertonen, is hypertrofische cardiomyopathie (HCM) het meest voorkomende defect in LS patiënten.

In **Hoofdstuk 4** hebben wij de zebravis als model gebruikt om de rol van Shp2 tijdens de embryonale ontwikkeling te bestuderen. We hebben in detail de rol van de twee *ptpn11* isovormen (*ptpn11a* en *ptpn11b*) gekarakteriseerd. We laten zien dat *ptpn11a* constitutief tot expressie komt en dat *ptpn11b* sterk wordt opgereguleerd tijdens de ontwikkeling. Bovendien zijn de producten van beide *ptpn11* genen, Shp2a en Shp2b, functioneel. Gerichte inactivatie van *ptpn11a* en *ptpn11b* laat zien dat homozygote mutanten lethaal zijn op dag 5-6 na fertilisatie (dpf). *Ptpn11a-/- ptpn11b-/-* embryo's vertoonden verscheidene defecten vanaf 4dpf, waaronder een kortere lichaamsas en craniofaciale defecten, wat samen ging met verlaagde hoeveelheden gefosforyleerd Erk op 5dpf. Defecten in de homozygote *ptpn11a-/-* mutanten waren vergelijkbaar, hoewel milder, met defecten in de dubbel mutanten, terwijl de *ptpn11b-/-* homozygote mutanten geen zichtbare ontwikkelingsdefecten vertoonden, levensvatbaar waren en vruchtbaar waren. *Ptpn11a-/- ptpn11b-/-* mutanten konden gered worden door expressie van exogeen *ptpn11a* en/of *ptpn11b*, wat impliceert dat Shp2a en Shp2b functioneel gelijk zijn.

In **Hoofdstuk 5** beschrijven wij, met behulp van fosfoproteomica, de identificatie van Fer kinase als een stroomafwaarts eiwit dat betrokken is in de etiologie van NS en LS. Fosfotyrosine immunoprecipitatie van lysaten van zebravissen die geïnjecteerd zijn met wild type-, NS- of LS-Shp2, gevolgd door massa spectrometrie toonde een vermindering aan in NS en LS van een fosfopeptide wat correspondeert met de tyrosine kinase Fer. Wij hebben laten zien dat Fer tot expressie komt in vroege embryo's en dat verlies van Fer zorgt voor ontwikkelingsdefecten, waaronder convergentie en extensie defecten. Gedeeltelijk verlies van Fer samen met lage expressie van NS en LS varianten van Shp2, maar niet met wild type Shp2 zorgde ook voor ontwikkelingsdefecten. In conclusie, het verlies van Fer draagt bij aan de NS en LS fenotypes in zebravissen.

In **Hoofdstuk 6** wordt een vergelijkbare aanpak gebruikt met muizenharten waarbij Protein Zero Related (PZR) als het meest gefosforyleerde eiwit in NS wordt geïdentificeerd. Verlies van PZR leidt tot gastrulatie defecten in zebravissen en fenotypes die vergelijkbaar zijn met verlies van Shp2 en met NS en LS. PZR is meer gefosforyleerd in diens immuunreceptor tyrosine remmende motieven (ITIMs) in verschillende weefsels en wij laten zien dat dit afhankelijk is van Src activering. Co-immuunprecip-

itatie studies laten zien dat NS en LS Shp2 meer binden aan Src en PZR, waarmee een complex wordt gevormd. Bovendien laten wij zien dat de ITIMs, wat bindingsplaatsen zijn voor Shp2, essentieel zijn voor de inductie van het convergentie en extensie phenotype in de zebravis. In conclusie, NS en LS vormen een complex met Src en PZR wat leidt tot ontwikkelingsdefecten in de zebravis.

In **Hoofdstuk 7** hebben wij de rol van de meest voorkomende NS en LS mutaties onderzocht tijdens de hartontwikkeling in de zebravis. Foutieve hartontwikkeling is een prominent symptoom van NS en LS, echter hoe de Shp2 varianten hartontwikkeling beïnvloeden is nog onduidelijk. Wij laten zien dat de hart functie van embryo's die NS en LS varianten van Shp2 tot expressie brengen, aangetast is. De hartafwijkingen bestonden uit verminderde cardiomyocyte migratie, gekoppeld aan verminderde linkswaartse hart verplaatsing. Expressie van lateraliteitsmarkeringen was gerandomiseerd in embryo's die NS en LS varianten van Shp2 tot expressie brachten. Ciliogenese en cilia functie in Kupffer's vesicule was verminderd, wat waarschijnlijk de oorzaak was van de links/rechts asymmetrie defecten. Mitogeen geactiveerd eiwit kinase (Mapk) signalering was geactiveerd in embryo's die NS en LS Shp2 varianten tot expressie brachten. Remming van Mapk signalering voor de aanvang van gastrulatie verminderde de cilia lengte- en hart lateraliteits defecten, wat suggereert dat NS en LS Shp2 varianten zorgen voor hyperactivatie van Mapk wat leidt tot verminderde cilia functie in Kupffer's vesicule wat zorgt voor hartdefecten op latere stadia.

Als laatste hebben wij de rol van Alpha-2-Macroglobulin-Like-1 (A2ML1) in een NS-gerelateerd syndroom bestudeerd in **Hoofdstuk 8**. Tot op heden zijn alle bekende mutaties die NS veroorzaken dominant en activeren de RAS/MAPK signaaltransductie route. Echter, in 25% van de gevallen blijft het genetische defect onbekend, wat suggereert dat andere factoren dan de standaard RAS/MAPK route ook een rol kunnen spelen. In onze studie hebben wij gebruik gemaakt van familie- gebaseerd exoom sequencing van een casus-ouder trio en hebben wij een *de novo* mutatie p.(Arg802His), gevonden in *A2ML1* wat codeert voor de uitgescheiden protease remmer Alpha-2-Macroglobulin-Like-1. Het vervolgens uitlezen van A2ML1 in 155 gevallen met een klinische diagnose van NS leidde tot de identificatie van verdere mutaties in twee families, p.(Arg802Leu) and p.(Arg592Leu). Functionele karakterisatie van deze mutaties in zebravissen toonde NS-achtige ontwikkelingsdefecten aan, waaronder craniofaciale defecten en hartafwijkingen. De kristalstructuur van A2M, wat zeer homoloog is aan A2ML1, leidde ons tot de identificatie van de intramoleculaire interactiepartner van p.Arg802. Het muteren van dit residu, p.Glu906, induceerde vergelijkbare ontwikkelingsdefecten in zebravissen wat onze conclusie bevestigt dat mutaties in A2ML1 een stoornis veroorzaakt die klinisch vergelijkbaar is met NS. Wij laten voor de eerste keer de betrokkenheid van een extracellulaire factor zien in een aandoening die klinisch gerelateerd is aan de RASopathies. Hierbij dragen wij potentiële nieuwe aanwijzingen aan voor een beter begrip van de moleculaire basis van deze familie van ontwikkelingsstoornissen.

In **Hoofdstuk 9** bediscussiëren wij elk vorig hoofdstuk apart en geven wij een overkoepelende blik op basis van de bevindingen van dit proefschrift.

Riassunto in Italiano

Questa tesi descrive l'uso di *Danio Rerio* nello studio della sindrome di Noonan-(NS) e di Leopard (LS). Nei primi tre capitoli, mettiamo a disposizione un background per i seguenti sei capitoli. Nel capitolo 1, discuteremo brevemente e in maniera concisa il processo di gastrulazione in zebrafish e i meccanismi di trasduzione del segnale ad essa associati. L'uso di zebrafish per studiare le proteine tirosina-fosfatasi "protein tyrosine fosfatase" (PTP) sarà discussa nel capitolo 2. In questo capitolo viene fornita una rassegna sulla letteratura esistente riguardo alla definizione del ruolo delle PTP in zebrafish e saranno discusse le diverse metodologie genetiche utilizzate a questo scopo. Inoltre, descriveremo in dettaglio l'analisi fosfoproteomica come metodo per studiare PTP *in vivo*. Nel capitolo 3 descriveremo il ruolo del gene *PTPN11* (proteina tirosina fosfatasi, non-ricettore tipo 11), che codifica SHP2, una PTP citoplasmatica essenziale per lo sviluppo dei vertebrati. Le mutazioni in *PTPN11* sono associate con NS e LS, due patologie autosomiche dominanti con sintomi clinici comuni. Le mutazioni NS comportano uno stato più 'attivo' di Shp2, mentre mutazioni LS danno origine a una proteina con un dominio catalitico difettoso. Pazienti NS e LS presentano vari sintomi, tra cui difetti cranio-facciali e anomalie cardiache. È interessante notare che il fenotipo cardiaco dei pazienti NS e LS è differente; infatti i pazienti NS sono affetti da stenosi polmonare (PS), mentre la cardiomiopatia ipertrofica (HCM) è il difetto cardiaco più comune in LS.

Nel **Capitolo 4** descriveremo l'uso di zebrafish come modello per studiare il ruolo di Shp2 nello sviluppo embrionale. Abbiamo caratterizzato in dettaglio il ruolo delle due isoforme *PTPN11* presenti in zebrafish (*ptpn11a* e *ptpn11b*) dimostrando (concludendo?) che ptpn11a è espresso costitutivamente e che l'espressione *ptpn11b* è più abbondante negli ultimi stadi di sviluppo embrionale. Inoltre, i prodotti di entrambi i geni *PTPN11*, Shp2a e Shp2b, sono funzionanti. L'inattivazione di *ptpn11a* e *ptpn11b* comporta la morte dei doppi mutanti *ptpn11a-/-ptpn11b-/-* entro 5-6 giorni dopo la fecondazione (dpf). Gli embrioni di questi doppi mutanti mostrano difetti pleiotropici da 4 dpf in poi, tra cui ridotta estensione dell'asse corporeo e difetti cranio-facciali, accompagnata da bassi livelli di fosforilazione di Erk a 5 dpf. È interessante notare che i difetti degli omozigoti *ptpn11a-/-* si sovrappongono ai difetti dei doppi mutanti anche se questi difetti sono più lievi, mentre i singoli mutanti *ptpn11b-/-* non mostrano difetti di sviluppo e sono fertili e vitali. L'espressione esogena di *ptpn11a* e *ptpn11b*, riduce la severità del fenotipo dei doppi mutanti, indicando ridondanza funzionale tra Shp2a e Shp2b.

Utilizzando approcci di fosfoproteomica, abbiamo identificato la kinasi ? Fer come proteina potenzialmente coninvolta a valle del signalling di shp2 e nell'eziologia di entrambe le sindromi NS e LS (**capitolo 5**). Lisati proteici di embrioni di zebrafish iniettati con mRNA wild type, NS o LS Shp2, seguita da spettrometria di massa e arricchimento per proteine fosforilate, ha mostrato una riduzione nel picco di un fosfopeptide corrispondente alla tirosina chinasi Fer sia nella NS che nella LS. Abbiamo dimostrato che Fer è espresso negli stadi iniziali dello sviluppo embrionale e che la perdita di Fer si traduce in difetti di sviluppo, inclusi difetti di convergenza e di estensione. La perdita parziale di Fer coopera con la bassa espressione delle varianti NS e LS di Shp2, ma non con l'espressione Shp2 wild-type. Quindi, la perdita di Fer contribuisce allo sviluppo dei fenotipi NS e LS in zebrafish.

Nel **capitolo 6** descriveremo l'uso di un approccio simile a quello poc'anzi descritto ma applicato su cuori di topi NS. L'uso di questa metodologia ci ha portato ad identificare la proteina PZR (protein zero related) come iper-fosforilata nella sindrome di Noonan (NS). Inoltre, la perdita di PZR comporta sia difetti gastrulazione in zebrafish che un fenotipo che ricorda quello risultante dalla mancanza delle proteine Shp2, NS e LS. PZR risulta essere iper-fosforilata sulle sequenze ITIMs in diversi tessuti

e la sua fosforilazione è dipendente dalla attivazione di Src. Studi di co-immunoprecipitazione mostrano che NS e LS Shp2 si legano a Src e PZR, costituendo un complesso. Inoltre abbiamo dimostrato che le ITIMs sono siti di legame per Shp2 e sono essenziali per l'induzione della convergenza zebrafish ed estensione fenotipo. Così, NS e LS Shp2 formano un complesso con Src e PZR per indurre difetti dello sviluppo in zebrafish.

Nel **capitolo 7** abbiamo studiato il ruolo delle mutazioni più comuni nella NS e nella LS in zebrafish, durante lo sviluppo cardiaco. I difetti cardiaci sono un sintomo importante di entrambe le patologie, ma ancora non è chiaro come le varianti Shp2 influenzino lo sviluppo cardiaco. Abbiamo dimostrato che la funzionalità del cuore è compromessa in embrioni che esprimono NS e LS. Le anomalie cardiache durante lo sviluppo di zebrafish consistono nella deregolazione della migrazione dei cardiomiociti, insieme al ridotto movimento del cuore verso sinistra. L'espressione di marcatori specifici di lateralità è randomizzata (casuale?) negli embrioni che esprimono NS e LS Shp2. La funzione delle *cilia* nelle vescicole di Kupffer è compromessa, causando probabilmente i difetti di asimmetria sinistra / destra. Inoltre il signaling delle Mapk risulta iper-attivato negli embrioni che esprimono NS e LS Shp2. È interessante notare che l'inibizione della cascata delle Mapk prima della gastrulazione ripristina la lunghezza delle *cilia* e annulla parzialmente il difetto cardiaco e di lateralità, suggerendo che NS e LS Shp2 possano mediare l' iperattivazione delle Mapk portando a un'alterata funzione ciliare nelle vescicole di Kupffer e al difetto cardiaco successivo.

Infine nel **Capitolo 8**, abbiamo studiato il ruolo di Alpha-2-Macroglobulina-Like-1 (A2ML1) nella NS. Fino ad oggi, tutte le mutazioni note che causano la NS sono dominanti e comportano un'iperattivazione della via di segnalazione RAS/ MAPK. Tuttavia nel 25% dei casi, la causa genetica di NS rimane sconosciuta, suggerendo che altri fattori, oltre quelli coinvolti nella canonica via RAS/MAPK, possano svolgere un ruolo. In questo capitolo, abbiamo utilizzato il sequenziamento dell'esoma (cos'è?) basandoci su un trio (??) familiare e abbiamo identificato una mutazione *de novo*, p. (Arg802His), in *A2ML1* che codifica per l'inibitore della proteasi alfa-2-Macroglobulina-Like-1. Il successivo sequenziamento di *A2ML1* in 155 casi con una diagnosi clinica di NS ha portato all'identificazione di mutazioni aggiuntive in due famiglie, p. (Arg802Leu) e p. (Arg592Leu). La caratterizzazione funzionale di queste mutazioni A2ML1 umani in zebrafish ha mostrato difetti di sviluppo NS-like, tra cui difetti cranio-facciali e malformazioni cardiache. La struttura cristallografica di A2M, altamente omologa ad A2ML1, ci ha portato all'identificazione del partner di interazione intramolecolare p.Arg802. La mutazione di questo residuo, p.Glu906, induce difetti di sviluppo simili in zebrafish, rafforzando la nostra conclusione che le mutazioni in A2ML1 causano una malattia clinicamente correlata alla NS. In questa tesi, abbiamo dimostrato per la prima volta, il coinvolgimento di un fattore extracellulare in un disturbo clinicamente correlato alle RASopatie, fornendo una migliore comprensione della base molecolare di questa famiglia di malattie.

Nel **capitolo 9,** discutiamo ogni capitolo precedente fornendo una visione integrata sui risultati di questa tesi.

Curricula vitae

Monica Bonetti was born the 7th of October 1984 in Italy (RC), where she got her secondary education diploma at the Scientific Liceum, in 2002. From there she went to the University of Messina for her B.Sc in Biology. Her interest in Molecular Biology led her to choose the specialization in Genetics and Molecular Biology in Rome (Università La Sapienza). She got her M.Sc degree *cum laude* in March 2008. In May 2008 she started to work at the CSS-Mendel Institute (Rome) in the Neurogenetics team of Prof. Enza Maria Valente and Prof. Bruno Dallapiccola, where she focused on the correlation between movement disorders and human genetic variations. She started her Ph.D at the Hubrecht Institute (Utrecht) in 2010, under the supervision of Prof. Jeroen den Hertog. The research topic was focus on the characterization of cardiac defects of Noonan and LEOPARD patients, using zebrafish as animal model. The results of these studies are described in this thesis.

List of Publications

1) M Bonetti, A Ferraris, M Petracca, A R Bentivoglio, B Dallapiccola, E M Valente. (2009). GIGYF2 variants are not associated with Parkinson's disease in Italy. *Mov Disord*. 24(12):1867-8

2) M Bonetti*, C Barzaghi*, F Brancati, A Ferraris, E Bellacchio, A Giovanetti,T Ialongo, G Zorzi, C Piano, M Petracca, A Albanese, N Nardocci, B Dallapiccola, A R Bentivoglio, B Garavaglia# and E M Valente#.(2009). Mutation Screening of the DYT6/THAP1 Gene in Italy. *Mov Disord.* 24(16):2424-7

3) M Carecchio, M Magliozzi, M Copetti, A Ferraris, L Bernardini, M Bonetti, G Defazio, M J Edwards, I Torrente, F Pellegrini, C Comi, K P Bhatia, E M Valente. (2013). Defining the Epsilon-Sarcoglycan (SGCE) Gene Phenotypic Signature in Myoclonus-Dystonia: A Reappraisal of Genetic Testing Criteria. *Mov Disord*. 28(6):787-94

4) V Guida*, R Ferese*, M Rocchetti, M Bonetti, A Sarkozy, S Cecchetti, V Gelmetti, F Lepri, M Copetti, G Lamorte, C Digilio, B Marino, A Zaza, J den Hertog, B Dallapiccola, A De Luca. (2013). A variant in the carboxyl-terminus of connexin 40 alters GAP junctions and increases risk for tetralogy of Fallot. *Eur J Hum Genet*. 21(1):69-75

5) M Bonetti, J Paardekooper Overman, F Tessadori, E Noël, J Bakkers, J den Hertog. (2014). Noonan- and Leopard-syndrome Shp2 variants induce cilia-related laterality defects in Zebrafish. *Development*. 141(9):1961-70

6) M Bonetti, V Rodriguez Martinez, J Paardekooper Overman, J Overvoorde, M van Eekelen, C Jopling, J den Hertog. (2014). Distinct and overlapping functions of ptpn11 genes in zebrafish development. *PLoS One*. 9(4):e94884

7) L E L M Vissers*, M Bonetti*, J Paardekooper Overman*, W M Nillesen, S G M Frints, J de Ligt, G Zampino, M Schepens, H G Brunner, J A Veltman, H Scheffer, P Gros, J L Costa, Ma Tartaglia, I van der Burgt, H G Yntema# and J den Hertog#.(2014). Heterozygous germline mutations in A2ML1, encoding the secreted protease Inhibitor Alpha-2-Macroglobulin-Like-1, cause Noonan-like syndrome. *Eur J Hum Genet*. doi: 10.1038

8) J Paardekooper Overman*, J S Yi*, M Bonetti, M Soulsby, C Preisinger, M Stokes , L Hui, J Silva, A J R Heck, M I Kontaridis, J den Hertog# and A M Bennett#.(2014). PZR coordinates Shp2 phosphatase independent Noonan and LEOPARD syndrome signaling in zebrafish and mice. *Mol Cell Biol* 34(15):2874-89

9) J Paardekooper Overman, C Preisinger, K Prummel, M Bonetti, P Giansanti, J Overvoorde, A Heck, J den Hertog. (2014). A role for Fer kinase in the pathogenesis of Noonan and LEOPARD syndrome. *PlosOne*, Accepted

* equal contribution
# These authors jointly directed this work

Jeroen Paardekooper Overman was born on April 13th in Hoorn, the Netherlands. After obtaining his Athenaeum diploma from the Schoter Scholengemeenschap in Haarlem in 2002 he went to the Vrije Universiteit Amsterdam where he studied Biomedical Sciences. After doing his internship at the Molecular and Cellular Neurosciences group he obtained his B.Sc. degree in 2008. During his M.Sc. Biomolecular Sciences at the Vrije Universiteit he studied the role of Notch1 in cervical cancer at the VU Medical center and researched mitchondrial mutations using mass spectrometry at the Leiden University Medical Center. His thesis on microRNAs in the brain was performed in collaboration with the Hubrecht Institute. After obtaining his M.Sc. in 2009, Jeroen started his Ph.D. studies at the Hubrecht Institute under the supervision of Prof. Dr. Jeroen den Hertog. The aim was to study the role of Shp2 and potential downstream factors in Noonan and LEOPARD syndrome using zebrafish and mass spectrometry. The results are described in this thesis. He is currently working as a scientific information specialist at Elsevier in Amsterdam.

List of Publications

1) J Paardekooper Overman, J den Hertog. (2014). Zebrafish as a model to study PTPs during development. *Methods*. 15;65(2):247-53

2) M Bonetti, J Paardekooper Overman, F Tessadori, E Noël, J Bakkers, J den Hertog. (2014). Noonan and Leopard-syndrome Shp2 variants induce cilia-related laterality defects in Zebrafish. *Development.* 141(9):1961-70

3) M Bonetti, V Rodriguez Martinez, J Paardekooper Overman, J Overvoorde, M van Eekelen, C Jopling, J den Hertog. (2014). Distinct and overlapping functions of ptpn11 genes in zebrafish development. *PLoS One*. 9(4):e94884

4) L E L M Vissers*, M Bonetti*, J Paardekooper Overman*, W M Nillesen, S G M Frints, J de Ligt, G Zampino, M Schepens, H G Brunner, J A Veltman, H Scheffer, P Gros, J L Costa, Ma Tartaglia, I van der Burgt, H G Yntema# and J den Hertog#.(2014). Heterozygous germline mutations in A2ML1, encoding the secreted protease Inhibitor Alpha-2-Macroglobulin-Like-1, cause Noonan-like syndrome. *Eur J Hum Genet*. doi: 10.1038

5) J Paardekooper Overman*, J S Yi*, M Bonetti, M Soulsby, C Preisinger, M Stokes , L Hui, J Silva, A J R Heck, M I Kontaridis, J den Hertog# and A M Bennett#.(2014). PZR coordinates Shp2 phosphatase independent Noonan and LEOPARD syndrome signaling in zebrafish and mice. *Mol Cell Biol* 34(15):2874-89

6) J Paardekooper Overman, C Preisinger, K Prummel, M Bonetti, P Giansanti, J Overvoorde, A Heck, J den Hertog. A role for Fer kinase in the pathogenesis of Noonan and LEOPARD syndrome. *PLoS One*, Accepted.

* equal contribution
# These authors jointly directed this work

Abbreviation list

A2ML1	Alpha 2 Macroglobulin like 1
C&E	Convergence and Extension
CRISPR	Clustered Regularly Interspaced Short Palindromic Repeat
DFC	Dorsal Forerunner Cell
DORV	Double Outlet Right Ventricle
DPF	Days Post Fertilization
ECM	Extracellular Matrix
ENU	N-ethyl-N-nitrosourea
EVL	Enveloping Layer Cells
FER	Fps/Fes related
HCM	Hypertrophic Cardiomyopathy
HPF	Hours Post Fertilization
ISH	In Situ Hybridization
ITIM	Immunoreceptor Tyrosine-based Inhibitory Motif
KV	Kupffer's Vesicle
LEOPARD	Lentigines, Electrocardiographic conduction abnormalities, Ocular hypertelorism, Pulmonary stenosis, Abnormal genitalia, Retarded growth, Deafness: Sensorineural
LPM	Lateral Plate Mesoderm
LS	LEOPARD Syndrome
MO	Morpholino
MPZL1	Myelin Protein Zero Like 1
MS	Mass Spectrometry
NIC	Non Injected Control
NS	Noonan Syndrome
PS	Pulmonary Stenosis
PRR	Proline Rich Region
PTK	Protein Tyrosine Kinase
PTP	Protein Tyrosine Phosphatase
PTPN11	Tyrosine-protein phosphatase non-receptor type 11
PZR	Protein Zero Related
RTK	Receptor Tyrosine Kinase
SFK	Src Family Kinase
SH2	Src Homology 2
SHP2	Src Homology 2-containing protein-tyrosine-phosphatase 2
Spaw	Southpaw
TALEN	Transcription Activator Like Effector Nuclease
TSGI	Target Selected Gene Inactivation
VSD	Ventricle Septal Defect
YSL	Yolk Syncytial Layer
ZFN	Zinc Finger Nuclease